The Role of The Oligodendrocyte-enriched Ectonucleotide Pyrophosphatase-6 In Energy Metabolism

WANG RONGLING

王茸灵

Doctor of Philosophy

The University of Edinburgh

2021

Declaration

This thesis has been composed by myself;

This thesis contains my own work except any work was not performed entirely by myself as clearly indicated in the text;

This work has not been submitted for any other degrees or professional qualification.

Rongling Wang, 2021

Abstract

Despite the continuing global rise in obesity prevalence, few effective medicines are available to ameliorate this disease. There remains a need to identify new therapeutic targets. Previously, our genome-wide association studies (GWAS) study in a population isolate identified that variants in and around the human *ENPP6* gene (encoding the ectonucleotide pyrophosphatase-6 enzyme ENPP6) were associated with reduced visceral fat accumulation. Moreover, our preliminary data showed that mice lacking the *Enpp6* gene (*Enpp6*$^{-/-}$) exhibited reduced visceral adiposity and improved glucose tolerance after high-fat-diet (HFD) feeding compared to *Enpp6*$^{+/+}$ littermates. The ENPP6 enzyme belongs to a family of ENPP(1–7) enzymes, which have recently emerged as potential mechanistically distinct therapeutic targets for metabolic and vascular diseases. Of these, ENPP6 is a lysophospholipase C type enzyme. In parallel with our work, ENPP6 deficiency was linked by others to excessive hepatic lipid accumulation as a result of local choline deficiency.

To better understand the role of ENPP6 in nutrient metabolism, we characterised the *Enpp6*$^{-/-}$ mice and tested the hypothesis that choline deficiency was the underlying mechanism for their metabolic phenotype. We showed that HFD-fed mixed-strain B6129F1-*Enpp6*$^{-/-}$ mice exhibited reduced visceral adipocyte size and lower liver fat accumulation. Lower liver choline level was found in HFD-fed B6129F1-*Enpp6*$^{-/-}$ mice compared to the wildtype, consistent with our hypothesis. The improved metabolic phenotype of B6129F1-*Enpp6*$^{-/-}$ mice was reversed by dietary choline supplementation, but it was not further improved by short-term dietary choline deficiency, which unexpectedly caused higher liver fat accumulation in B6129F1-*Enpp6*$^{-/-}$ mice. Additionally, the metabolic benefits of *Enpp6* deficiency were strain dependent. In contrast to B6129F1-*Enpp6*$^{-/-}$ mice, congenic (5 generations back-cross to C57BL/6J strain) C57BL/6J-*Enpp6*$^{-/-}$ mice were more prone to HFD-induced obesity. These mice exhibited worsened metabolic profiles including increased whole-body weight and fat mass, impaired insulin sensitivity, and a trend for

higher liver fat accumulation compared to their littermate controls. This discrepancy may be explained by the significant difference in endogenous *Enpp6* expression in the different background strains.

ENPP6 is highly expressed in brain newly formed oligodendrocytes (NFOs), but the biological function of ENPP6 in NFOs and whether it is involved in energy balance is unknown. To gain insight into this, this thesis also determined the impact of ENPP6 inhibition/deficiency on oligodendrocyte development by tracking oligodendrocyte lineage marker expression and assessed the metabolic consequences of oligodendrocyte-specific knockdown of *Enpp6* in mouse NFOs. No evidence of altered metabolism was found in oligodendrocyte-specific *Enpp6* knockdown (*Pdgfrα-Cre*$^{+}$*Enpp6*$^{fl/fl}$) compared to their littermates (*Pdgfrα-Cre*$^{-}$*Enpp6*$^{fl/fl}$) after HFD feeding. Additionally, a potential risk of demyelination caused by ENPP6 deficiency was ruled out, since there was no difference in myelin basic protein (MBP) expression in the corpus callosum of young or adult B6129F1-*Enpp6*$^{-/-}$ mice brain. *In vitro* data showed that ENPP6 inhibition by the selective ENPP6 inhibitor T11, or genetic ablation of *Enpp6,* resulted in impaired oligodendrocyte differentiation without affecting total MBP expression. Nevertheless, *Enpp6* deficiency did alter expression of key signalling pathways associated with lipid metabolites G-protein coupled receptor 17 (GPR17), suggesting an alternative yet unknown role for ENPP6 in NFO/oligodendrocyte function.

Taken together, the data suggest a strain dependent metabolic role for ENPP6, with some support for ENPP6 inhibition as a potential therapeutic strategy for visceral obesity and diabetes that may relate to individual variation in ENPP6 expression as revealed by mouse strain differences.

Lay Summary

Hundreds of millions of people are suffering from being overweight and obese in the world. Obesity threatens people's health and can cause high blood sugar, blood pressure, heart disease and cancer. The location of fat accumulation is also an important determinant of health outcomes. Those who have upper body (belly) fat or an 'apple-shaped body', are more likely to face health problems than those who have lower body (hip and thigh) fat or a 'pear-shaped body'. Our body shape is determined by our DNA, inherited from our biological parents. My PhD project looks at a newly identified gene, ENPP6, found by studying human DNA patterns that determine fat accumulation and body shape. Medicines that target the active protein made from this gene could help treat apple-shaped obesity and diabetes. Right now, we don't know much about the function of the ENPP6 protein. I am asking whether and how ENPP6 controls body shape. To answer these questions, I studied a laboratory mouse genetically engineered to lack the ENPP6 protein and fed them special high sugar, high fat diets to mimic the most common cause of obesity in humans. Mice lacking ENPP6 gained less belly fat and kept healthy blood sugar compared with normal mice that got fat and became diabetic. I also found that the ENPP6-lacking mice were protected from obesity and diabetes because they make less choline in their livers. Choline is an important nutrient for our body, obtained from certain foods and, importantly, it also made by our own bodies if dietary levels are low. Too much or too little choline can cause health problems. Researchers found that lowering choline levels in food can protect from obesity and diabetes, but increases fat storage in the liver. However, I showed that less choline, caused by lack of ENPP6, can actually improve liver health. These promising results support the idea that medicines that stop ENPP6 protein action (inhibitors) may be a promising new treatment for apple-shaped obesity and diabetes.

It is important to know if the drug is equally functional to different groups of people. Similar to diversity of race in humans, different types (strains) of laboratory mouse (e.g., fur colour) are widely used in research. To consider

this, in the following chapter, I used a different laboratory mouse strain lacking ENPP6 protein in their bodies and repeat the previous experiment to validate my observation. Surprisingly, the second type of ENPP6-lacking mouse suffered from more whole-body fat gain, also showed poorer control of their blood sugar when compared to the normal mice. When I looked at another mouse type, which only lacks ENPP6 in the brain cells that have high levels of ENPP6, their fatness and blood sugar were not different to normal mice of the same strain (the second type of ENPP6-lacking mouse). This tells us that brain ENPP6 must be involved in some aspect of overall body fatness.

In the last chapter, I looked at what ENPP6 does in brain cells. ENPP6 is only found in one specific type of brain cell. The main function of this cell is to ensure the information and signals can be quickly transferred to other parts of brain. I did not find any evidence for differences in brain structure in mice without ENPP6. However, either using drugs to suppress ENPP6 or using cells from ENPP6-lacking mice, I found that stopping ENPP6 action makes the brain cells mature slower, which is likely due to another key protein GPR17. Interestingly, others have shown GPR17 also controls body weight and blood sugar. Together, my findings suggest ENPP6 works at least in one strain of mice to counteract belly-fat obesity and diabetes and links the brain to body weight and fat accumulation through controlling choline and GPR17.

.

Publications

1. McHugh, B.J., **Wang, R.**, Li, H. N., Beaumont, P.E., Kells, R., Stevens, H., Young, L., Rossi, A.G., Gray, R. D., Dorin, J. R., Findlay, E. L., Brough, D., Davidson, D.J. *Cathelicidin is a "fire alarm", generating protective NLRP3-dependent airway epithelial cell inflammatory responses during infection with Pseudomonas aeruginosa.* PLOS Pathogens. 2019 Apr 12;15(4): e1007694.

2. Dillon, S., Suchacki, K., Hsu, S. N., Stephen, L. A., **Wang, R.**, Cawthorn, W. P., Stewart, A. J., Nudelman, F., Morton, M. N. JBMR Plus. 2021; 5(2): e10439.

3. **Wang R**, Schraut K, Carter R, Kentistou K, Wilson J, Michailidou Z, et al., editors. Hepatic choline deficiency underpins amelioration of visceral obesity and diabetes in ectonucleotide pyrophosphatase (*Enpp)-6*$^{-/-}$mice. Endocrine Abstracts. 2021;77; OC3.4.

Oral and poster presentations

Oral presentation

1. The effects of *Enpp6* gene deletion and pharmacological ENPP6 inhibition on oligodendrocyte development.

The 25th Annual Conference of Chinese Life Scientists Society in the UK-London, 2019.

2. Ectonucleotide pyrophosphatase-6 (ENPP6) deficiency selectively ameliorates visceral obesity and diabetes.

Centre for Cardiovascular Science Symposium-Edinburgh, 2021.

3. Hepatic choline deficiency underpins amelioration of visceral obesity and diabetes in ectonucleotide pyrophosphatase (*Enpp*)-*6*$^{-/-}$mice.

Society for Endocrinology BES 2021 Conference-Edinburgh, 2021.

Poster presentations

1. Newly formed oligodendrocyte-ENPP6 is a novel therapeutic target for visceral obesity and diabetes.

Centre for Cardiovascular Science Symposium-Edinburgh, 2019

2. Newly formed oligodendrocyte-ENPP6 is a novel therapeutic target for visceral obesity and diabetes.

Scottish Developmental Biology Group Meeting-Edinburgh, 2019

3. Preclinical validation of a novel anti-diabetic target ENPP6.

Edinburgh Diabetes Day-Edinburgh, 2020.

4. Genetic deficiency of ectonucleotide pyrophopshatease-6 ameliorates high-fat-diet-induced visceral obesity and diabetes.

The 56th European Association for the Study of Diabetes (EASD) Annual Meeting-Virtual Meeting, 2020. Poster A section PS37.

Acknowledgements

Firstly, I would like to express my sincere gratitude to my supervisor Prof. Nik Morton for the continuous support and encouragement of my PhD study and my life in Edinburgh. He is always patient, knowledgeable, professional, kind, humorous and more importantly, unconditionally supporting and helping me in all the time of research, writing, presenting, and communicating in science. He is not just my supervisor, also a good friend during my study in Edinburgh. I did my maxi-master project in Nik's lab in 2016, and since then, I decided to go further in the academic field and chose him to be my mentor for my PhD study. The key words of brave, independent and creative are what I felt deeply during my study under his supervision. I also think these are good qualities to be a scientist in the future. Also, I always keep in mind that he told me a '4-step' to be a good researcher: observe, analysis, distill and teach. During the beginning of my 1st year of study, I would say that was a tough time I have ever experienced during my PhD. I was extremely struggled to setup my cell work. I was upset not just due to the complex and difficulties to learn how to do these cell work, I have never expected that crazy drama happened afterwards. To be honest, it is very hard to take, even since now, I still feel hurt when I think this old story. I still remembered Nik told me about a similar story happened to him when he was doing his PhD, and encouraged me to be brave and be strong. Luckily and certainly, I successfully setup my own cell works finally! Apart from my PhD study, Nik also gave me some "chicken soup for the soul", encourage me to participate in science social networking, which make my PhD life fruitfully and enriched. Nik supports me a lot when I applied PhD position, when I applied the scholarships before starting PhD study; inspires me a lot when I felt stuck in science, when I felt unset in life during my PhD study; advises me a lot when I think about the future plan after the PhD study. I also would like thanks him for the warm invitation for Christmas celebration at his home each year. Time passed quickly, but I always appreciate his supports all the time.

Besides my primary supervisor, I would like to thank my second supervisor Prof. Scott Webster, and the chair of my thesis committee: Prof. David Lyons, for his insightful comments and encouragements, questions, discussion when I had my 10-week, 1st, 2nd year reviews, which incanted me widen my research from various perspectives. Scott is always kind, nice and amiable. Every time I expressed my nervous and concerns for my reviews/talks to him, he always says humorously: “you should not be worried, well, you should be worried, oh no, you should not….” (Webster, 2018-2020). Hilarious! I remembered the first time I met David was during my 10-week review. He did ask me so many hard questions related to my hypothesis, and most of them I could not give answers during that review. However, these hard questions, indeed made me think carefully and deeply about my project, inspired more discussion on the project.

I would also thank Prof. Ruth Andrew who is the chair of CVS symposium/seminars committee, in charge of organising external seminars and annual symposium. In 2018-2019, my 2nd year, I was the PhD student Rep in the committee and organized ‘meet the speaker’ section every week after the seminars. Indeed, it is an excellent opportunity to talk science and careers with senior scientists from around the world. For myself, it is a fantastic, inspiring and motivating opportunity to get involved in the year's activities of seminar programme and the CVS-symposium, also gain more transferable skills and broaden the research. I chaired the ECR oral presentation competition at the annual symposium day and organised the “skittles night” as part of the symposium. It was the first time but an unforgettably lovely memory. Therefore, I would like thank Ruth gave me this precious opportunity during my PhD study.

My sincere thanks also go to Dr. Rod Carter, a senior postdoc in our lab. Rod was in the group since I did my master project. He is always helpful and knowledgeable in the lab. Everytime I cannot process the experiment, find the solution, calculate the stupid dilution factors, take down the incubators, order, clean, organise the lab work, he is always offering his brain, hands and eyes.

He is more likely an engineering, accountant, receptionist, builder, teacher, etc…Ah! Importantly, sweet treats provider in the office!

My sincere thanks also go to Dr. Andrew McBride, who supervised me generating ENPP6-expressing HEK293 cells step by step, applying ENPP6-TG-mPC assay; Dr. Roberta Felici, who supervised me on brain dissection, OPC cultures at the very beginning of learning stages which took me ages to get workable OPCs; Dr Katherine Schraut for supervising me managing mice colony, training me TD-NMR, genotyping, and meetings for the project with her contribution to this project. Dr. Will Ramsy, Dr. Shonna Johnson and Dr. Mari Pattison for helping me setting up the flow cytometry template and training me on this technology, also their professional suggestions for this project; Dr. Calum Rod for training me using the EVOS FL microscopes and discussion for the project and suggestions for my project; All the staff at the LF2 animal unit, especially Will Mungall for training me all the techniques for the project, still remembered there were so many happy moments when you trained me, Duncan, Chris, Sandra Spratt, Hollie, Lorraine, Ami for their kind help, and training me for setting plugs, breeding pairs, editing card on tickatlab, and for their invaluable contribution to the project. Without their endless support, it would not be possible to conduct this research. I would like also to thank Dr. Zoi Michailidou who financially supported me during the last couples of months before this thesis summitted, and it has been a good time working with her and trained her Master students in the lab.

I would also thank my fellow labmates Ciara McDonnell, Iris Prunonosa Cervera, Tanguy Blehaut, Dr. Katherine Kentistou for the stimulating discussions, happy times we were working together, helping each other, and for all the fun we have had in the last 3-4 years (It’s shame I only have you Diana Binti Said and Ahlam Darasi around for such a short time in W3.07). Thanks all for offering suggestions and questions to help me rehearsal my CPR talk, reviews, data discussion.

My sincere thanks go to Dr. Veronique Miron and Prof. Anna Williams for kindly offering the Cre mice for our breeding lines; Dr. Jamieson Craig in the University of Strathclyde Glasgow, for kindly offering T11 for the projects.

I would like to thank Linda Feng. I am glad we met and became friend, sharing happy and unhappy daily life, French, gym, yoga, shopping, dining out etc. Especially during the Covid-19 lockdown, our daily zoom meetings were full of fun and laughter. I would like to express my sincere appreciation to Dr. Feng Li who always unconditionally supports, helps, inspires, encourages, motivates, accompanies, understands me whenever and wherever I need; unlimitedly helps me get through the difficulties.

I also do appreciate that college of medicine and veterinary (CMVM) which funded my PhD stipends and conference travel budget; the principal career development scholarship and global research scholarship from University of Edinburgh to provide the tuition fees for my PhD programme. I would also thank “The Great Britain-China Educational Trust” who financially support me in the writing-up period.

Finally, I would appreciate my wonderful and loving family, my mom Liying Lu 鹿丽英 and my dad Zheng Wang 王峥, my grandma Peixi Liu 刘佩玺, my grandpa 鹿瑞吾, and my cats 小乖和小小, their compassion, strength, and unconditional love are always around me, even though most of time we are separated in the two side of the earth. Thank you for being by my side and supporting me to study PhD abroad for 4 years. Having a family like you makes me feel so deeply loved and gives me strength.

感谢家人和朋友的付出与陪伴。

List of Tables and Figures

Contents

Chapter 1 Introduction

1.1 Obesity is a worldwide heath crisis

Obesity is characterised as an excess of body fat. Obesity prevalence has almost tripled over the past 40 years worldwide. Over 650 million adults are obese in 2016, with more than 1.9 billion are overweight (1). Not only adults are facing the overweight issue, more and more of younger generations are also suffering from being overweight or obese. Over 340 million children and adolescents aged 5-19 years were classified as overweight or obese in 2016 (1). As obesity prevalence is a global issue and increasing dramatically, many countries, especially the low-income nations, are suffering from a significantly increasing burden to obesity-related health care cost. Targeting to reduce obesity prevalence to the level that displayed 10 years ago is included as one of the main targets of the 'global action plan for the prevention and control of non-communicable diseases 2013-2020' (1). Non-communicable diseases (NCDs) include cardiovascular diseases, cancers and diabetes, accounting for over 70% of early mortality in the world (2). Obesity, a leading risk factor for deaths worldwide, drives a parallel increase in mortality-associated diseases such as type 2 diabetes, non-alcoholic fatty liver diseases (NAFLD) and cardiovascular diseases (3). Unfortunately, the epidemic is still growing and there is no sign that the high prevalence of overweight/obesity worldwide is receding (4).

1.2 Importance of body fat distribution

The World Health Organization (WHO) defines body mass index (BMI) as a simple and common way to classify whether people are overweight (BMI is greater than or equal to 25 Kg/m^2) or obese (BMI is greater than or equal to 30 Kg/m^2) (1). An increase of BMI is associated with high risk of complications such as type 2 diabetes, dyslipidaemia, hypertension, cardiovascular disease, gallstones, and cancers (5-8). However, some studies failed to find the significant association between BMI and cardiovascular risks (9-13). Although BMI appears to be a straightforward and quick measurement without requiring expertise, it cannot provide comprehensive and precise information on body fat distribution to distinguish where the fat stored. For example, Odamaki *et al.* observed that non-diabetic patients with lower BMI exhibited increased visceral fat accumulation assessed by abdominal computed tomography (CT) (14). Thus, it is reasonable to conclude that the estimation of obesity content by BMI is not adequate to reflect the distribution of body fat and the amount of visceral fat.

Along with the clinical observations reported in the past half century, the importance of regional fat distribution in determining the health risks associated with obesity, metabolic and cardiovascular abnormalities, has been investigated and highlighted in the past few decades (15-18). Dated back to 1947, Jean Vague firstly proposed two different body shapes: the ‘android obesity’ and ‘gynoid obesity’, commonly referred to as ‘apple shape’ and ‘pear shape’ obesity, respectively (19). ‘Android obesity’ represents that adipose tissue accumulated preferentially in the upper body area, whereas ‘gynoid obesity’ represents that adipose tissue accumulated preferentially in the hips and thighs (19). He also pointed out that ‘android obesity’ was the type of obesity strongly associated with diabetes and cardiovascular diseases (19). Decades later, the development of body fat topography has increasingly contributed support to cardiometabolic health. For example, Krotkiewski *et al.* reported that body shape, and regional accumulation of body fat were key drivers of metabolic abnormalities (20). Lapidus *et al.* showed that an

increased abdominal waistline relative to hip girth carried higher risks of coronary cardiac diseases (9). Ohlson *et al.* reported that an increase abdominal fat was highly correlated with risk of diabetes (21).

Thus, given the fact that obesity is a heterogeneous condition, BMI-based assessment of obesity faced limitations. Two striking examples of the limitation of BMI-based assessment of obesity were reported by Ruderman *et al*. (22, 23) and St-Onge *et al.* (24). In the first study, a group of individuals was characterised as normal weight (normal BMI) but metabolically obese, as these individuals suffered from metabolic complications that are commonly observed in obese individuals. In the second study, the other group of individuals was characterised as metabolically healthy obese, as they were not diagnosed with metabolic complications such as insulin resistance and dyslipidaemia despite having excessive fat accumulation (25, 26).

In addition, given at the time the impossibility of direct measurements of whole-body adiposity as adipose tissue is widespread and inaccessible (27), it was a challenge for researchers and clinicians to 'correctly and precisely' measure the body fat and predict obesity and its-related metabolic complications. To more precisely assess and better understand body fat distribution, several advanced imaging technologies were developed and applied such as CT, dual energy X-ray absorptiometry (DEXA) or magnetic resonance imaging (MRI) (28). For example, CT scans the whole body or specific parts of the body and generates cross-sectional images that facilitate distinction of the adipose, muscle and bone tissues (29, 30). With the advances in these methods, body fat distribution was identified as three main components: subcutaneous (67.1% of adipose tissue compartments), intramuscular (12.2%) and visceral fat (20.7%) (measured subject: adult male with BMI 18–25 Kg/m^2) (31).

1.3 Visceral adiposity as a risk factor of metabolic alterations

Advances in imaging technology led to the discovery that visceral and intramuscular fat depots were important to clarify the extent of visceral obesity, and that visceral adiposity acts as a powerful predictor for metabolic complications (27). This section will focus on reviewing visceral adiposity as a risk factor of four main metabolic alterations including elevated free fatty acid (FA), insulin resistance, glucose intolerance and dyslipidaemia.

1.3.1 Visceral adiposity alters FA metabolism

1.3.1.1 FA metabolism in the liver and adipocytes

FAs circulating in the blood are one of the key metabolites and important energy sources for humans. FAs either comprise the acyl moieties of triglycerides inside the lipoproteins or as circulating free FAs (FFAs) released from triglycerides. In the absorptive state, or the fed state where the glucose concentration in the bloodstream rises, insulin released from the pancreatic β cells initiates the absorption of glucose by the body cells.

De novo FA synthesis (lipogenesis) is the metabolic pathway which synthesises FAs from acetyl-coA from excessive glucose. During the postprandial phase, *de novo* FA synthesis mainly takes place in liver and adipose tissue, making significant contribution to the lipid content in human body (32). In the liver, the excess glucose is converted into glucose-6-phosphate, and ultimately converted to glycogen for storage through glycogenesis. The non-stored circulating glucose converts into pyruvate to produce energy through glycolysis and the tricarboxylic acid (TCA) cycle to form FA synthesis precursors. The precursor is then converted into FAs, esterified to mono-acyl-glycerides, di-acyl-glycerides, triglycerides and ultimately exported in lipoproteins to be taken up in other peripheral tissues. Triglycerides are synthesized by FA esterification and packaged into the lipid droplets in the form of the very-low density lipoprotein (VLDL) releasing into

the blood. Figure 1.1 shows the metabolic pathway of *de novo* FA synthesis in liver.

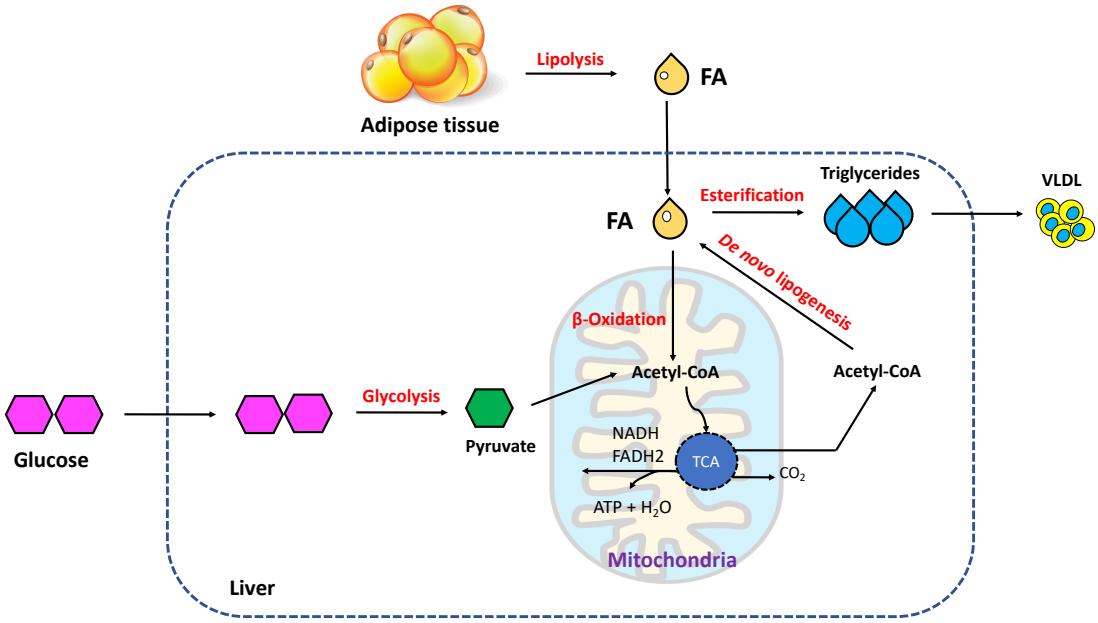

Figure 1.1 Schematic diagram of fatty acid metabolism and *de novo* lipogenesis in the liver in human. FA: fatty acid; VLDL: very-low density lipoprotein. There are two main sources of fatty acid in the liver: 1. Excessive glucose transported from blood stream into liver cells. After the glycolysis and TCA, glucose is then transformed as acetyl-coA, providing substrates for de novo lipogenesis to produce FAs. 2. The liver uptakes FAs released from adipose tissues via lipolysis. In the fed state, the FAs are synthesised into triglycerides and esterified into triglycerides and then packaged into VLDL and secreted into the blood stream. These lipids are then delivered to the peripheral tissues as energy sourse or energy storage. In the fasting state, FAs are transported into the mitochondria to produce acetyl-CoA for the TCA cycle by β-oxidation.

Glucose from the bloodstream can also be taken up into the adipocytes. The glucose converts into glycerol 3-phosphate by glycolysis from the main precursors of glyceroneogensis including pyruvate, lactate, glutamine, and alanine. The glycerol 3-phosphate then converts into adipose triglycerides (33). FAs are released by the adipose triglycerides, known as adipocyte lipolysis which is regulated by several hormones including insulin (34). When the insulin level is low or absent, cells are unable to absorb the glucose and therefore switch to alternative fuels such as FAs to fulfil their energy demands. The main role of insulin on adipocyte metabolism is to suppress lipolysis and promote FA synthesis and triglycerides esterification and storage (Figure 1.2).

1.3.1.2 Elevated FFA level by visceral adiposity

An elevated FFA turnover rate and increased FFA levels were observed in obese patients (35), suggesting that excess adiposity might alter FFA metabolism. Importantly, given the importance of regional fat distribution (as mentioned in chapter 1.2), Jensen *et al.* recognised the influence of body fat distribution on FFA metabolism (36). They reported that the FFA levels from viscerally obese women was higher than subcutaneous obese or non-obese women (36). Smith *et al*. supported this idea, pointing out that adipocyte lipolysis varies in adipocytes from omental, abdominal subcutaneous and gluteal-thigh adipose depots (37). Later on, Björntorp *et al.*, indicated that visceral adipocytes had higher lipolysis that led to more rapid mobilisation of FFAs, than the subcutaneous adipocytes in both non-obese and obese individuals (38). Similarly, Arner found that the lipolytic rate was higher in the human visceral (omental) region than the subcutaneous depots (39). Arner proposed a possible explanation for the different rates of lipolysis in non-obese subjects, which was likely due to the variation in the function of lipolytic and anti-lipolytic activities (39). This study reported that the high activity of lipolytic adrenoceptors contributed to the lipolysis of visceral fat depots, whereas high activity of anti-lipolytic adrenoceptors and adenosine receptors mediated lower subcutaneous lipolysis activity (39). Similarly, Bonadonna and Bonora pointed out that visceral fat displays a higher turnover of lipids than other fat depots,

showing greater sensitivity to catecholamine-induced lipolysis but lower sensitivity to insulin-stimulated anti-lipolysis, in other words, visceral fat exhibits a 'lipolytic mode', whereas subcutaneous fat does an opposite pattern, turning in a 'liposynthetic mode' (40). To conclude, given that visceral adiposity has a distinct metabolic profile that contributes more to elevation of FFAs levels and increase of lipolysis than the subcutaneous adiposity, it has more risks for the metabolic complications, as detailed below.

1.3.2 Visceral adiposity-related insulin resistance

1.3.2.1 The role of Insulin

Insulin has profound effects on carbohydrate and lipid metabolism, which facilitates entry of glucose into peripheral tissues including muscles and adipose tissues. Several key metabolic organs including skeletal muscle and adipose tissue require insulin for enhanced glucose uptake whereas some tissues are insulin-independent such as brain, pancreas, and liver (require other glucose transporters). The insulin-dependent metabolic process is regulated by a major insulin receptor, and an insulin-inducible glucose transporter type 4 (GLUT4) which translocates to the external surface of the plasma membrane upon stimulation of glucose uptake (41, 42).

1.3.2.2 Insulin resistance

Insulin resistance is routinely assessed by the degree of impaired glucose clearance rate responding to a defined insulin concentration in humans and rodents (43). Systemic insulin resistance is caused by impaired insulin action in metabolically active organs and tissues including the liver, skeletal muscle, and adipose tissue. Insulin resistance commonly results in hyperinsulinaemia, and is associated with the development of type 2 diabetes, hypertension and dyslipidaemia (43).

1.3.2.3 Visceral adiposity: a risk factor for insulin resistance

Several studies have recognised and highlighted the location of fat accumulation was strongly correlated with insulin resistance. Preis *et al*.

reported a stronger correlation of insulin resistance with the mass of visceral depots than the subcutaneous depots in obese individuals (44). Similarly, McLaughlin *et al.* showed that predominantly subcutaneous fat mass decreased the risk of insulin resistance whereas visceral fat had the opposite effects, suggesting the body fat distribution was associated with risks of insulin resistance (45). Bergstrom *et al.* (46), Hayashi *et al.* (47) and Sparrow *et al.* (48) also reported that visceral adiposity was independently associated with impaired glucose homeostasis and insulin resistance. The fat distribution effects of insulin resistance can explain why those viscerally obese populations with low BMI were facing high risks of diabetes and insulin resistance (49). More recently, Verboven *et al.* reported that adipocyte hypertrophy in visceral adipose tissue may contribute to insulin resistance, whereas hypertrophic subcutaneous adipose tissue did not independently contribute to insulin resistance (50).

Moreover, as mentioned chapter 1.3.1.2, visceral adiposity is correlated with the elevated FFA levels. Notably, the plasma FFA level can also affect glucose and insulin homeostasis by regulating insulin sensitivity and metabolism in key metabolic organs. Boden *et al.* reported that increased plasma FFAs reduced insulin-dependent glucose uptake in muscle (51). Santomauro *et al.* showed that overnight lowering of FFA improved insulin sensitivity and glucose tolerance in obese diabetic patients (52). Additionally, a negative feedback loop exists that perpetuates elevation of FFA levels in obesity; obesity-induced FFA elevation inhibits insulin-stimulated antilipolytic action, which further promotes FFA release into the circulating blood (36) (Figure 1.2).

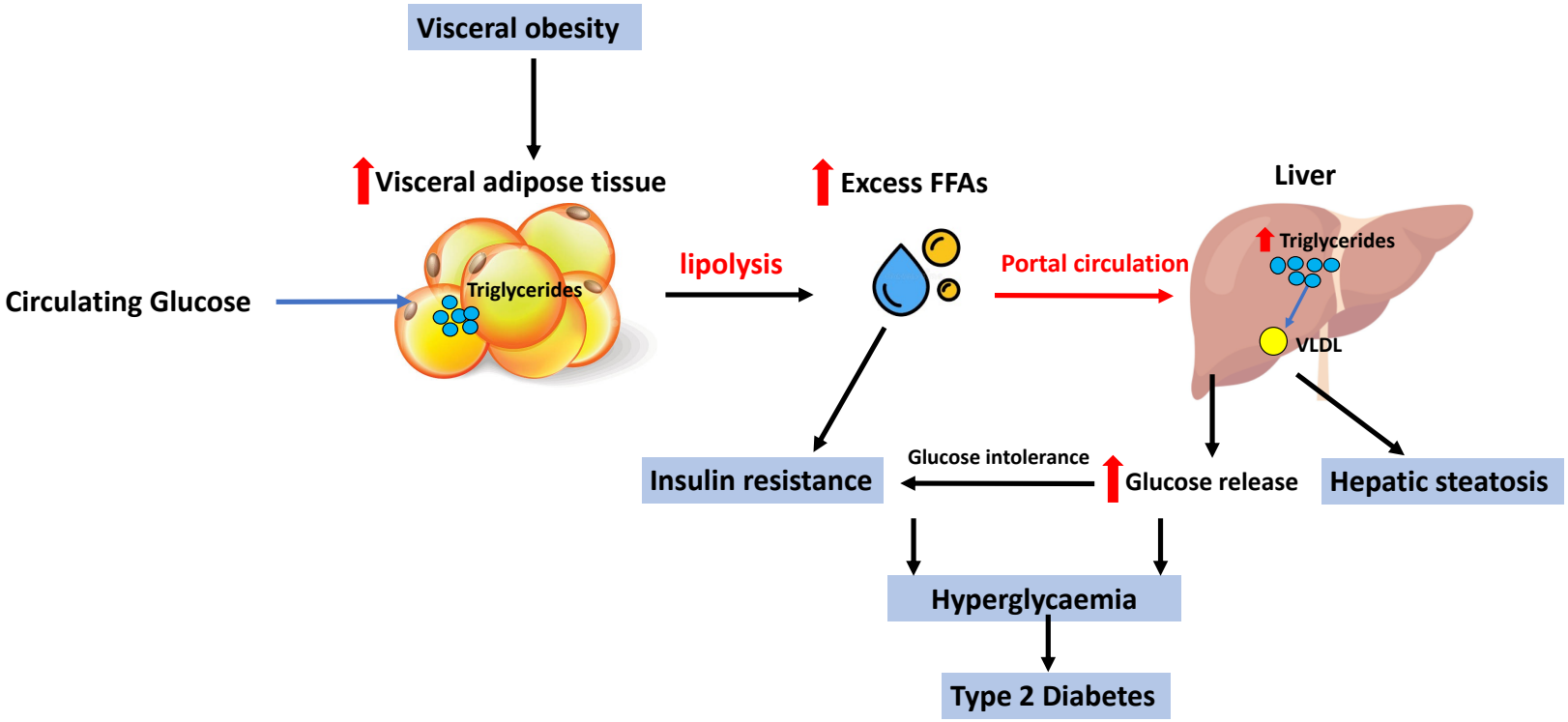

Figure 1.2 Schematic chart of visceral adiposity and its associated insulin resistance, type 2 diabetes, and hepatic steatosis. Circulating glucose is absorbed into the adipose tissue and converted into triglycerides. Adipose triglycerides are released via lipolysis to produce free fatty acid (FFAs). Excess visceral adiposity induced elevated FFAs level results in insulin resistance, and elevated triglycerides level in the liver. Triglycerides in the liver are assembled and packaged into the very-low-density lipoprotein (VLDL), and then exported into the blood. Excess lipid storage in the liver causes hepatic steatosis.

1.3.2.4 The underlying mechanisms of correlation between the visceral adiposity and insulin resistance

Obesity-induced adipocyte hypertrophy can lead to cell death, which may trigger the immune cell to infiltrate into the tissue (53, 54). Thus, the effects of inflammatory adipokines have been proposed as the underlying mechanisms of correlation between the visceral obesity and insulin resistance (55).

Adipokines such as leptin (56) and adiponectin (57), are secreted by the adipocytes within adipose tissues. Apart from the adipose-specific cytokines, a variety of other factors are also released by the adipose tissues including inflammatory cytokines such as tumour necrosis factor (TNF)-α (58), interleukin (IL)-6 (59), and IL-8 (60). These cytokines are often referred to as adipokines because they are released from adipose tissues (61). Adipokines play an important role in a wide range of physiological processes including energy homeostasis by affecting energy expenditure and food consumption, lipid metabolism, blood pressure regulation, angiogenesis, obesity-related metabolic syndromes especially insulin resistance and diabetes (62-65).

TNF-α and insulin resistance are strongly associated in obesity (66, 67). Hotamisligil *et al.* showed TNF-α mRNA and protein levels in adipose tissue were locally and systemically elevated in the obese and diabetic rodents and that neutralization of TNF-α in obese rats promoted glucose uptake and insulin sensitivity (68). Similarly in humans, elevated TNF-α strongly correlated with increasing adiposity and body fat mass (69). Moreover, Kern *et al.* reported that TNF-α and IL-6 expression in adipose tissues were significantly higher in those with obesity-related insulin resistance compared with insulin sensitive subjects (70). Esposito *et al.* also observed that obese women had higher circulating IL-6 and IL-10 than nonobese women (71). In Esposito's study, the obese subjects (BMI is greater than or equal to 30 Kg/m^2) were divided into two groups, obese with high waist circumference group, and obese without high waist circumference group. Interestingly, it was shown that the level of IL-10 was elevated in those obese women with high waist circumference, but

decreased in the other group, suggesting that IL-10 secretion was regulated by fat distribution. Moreover, adipokines released from visceral adiposity may have a pronounced effect on liver dysfunction as visceral adipose tissue drains immediately into the liver via the portal vein. Rytka *et al*. showed that an increase of visceral adipokines draining into the portal vein caused hepatic insulin resistance and impaired glucose tolerance in mice (72). Also, IL-6 level was elevated in the visceral fat-drained portal vein, but under the same circumstance, IL-6 knockout mice exhibited normal glucose homeostasis (72).

Similarly, inflammatory cytokines released from visceral adipose tissue were strongly linked to insulin resistance in human obesity (73). Hardy *et al.* showed that increased inflammatory chemokines (C-C motif ligand 2,3,4 and 18) and cytokines (IL-8) in visceral adipose tissues, along with increased visceral fat depot and adipocyte size were found in insulin-resistant subjects (73). These studies together suggested that inflammatory adipokines secreted from visceral adipose tissue contribute to insulin resistance in visceral obesity.

Aside from the exaggerated release of adipokines from visceral fat, increased 'classical' inflammatory response is also linked to insulin resistance in visceral obesity. For example, nucleotide-binding domain leucine-rich containing pyrin domain containing-3 (Nlrp3) inflammasome is an inflammatory and metabolic sensor that triggers the proinflammatory cytokines IL-1 and IL-18. Stienstra et al. showed that the chow diet-fed *Nlrp3* knockout mice exhibited improved insulin sensitivity (74). The role of Nlrp3 in regulating glucose homeostasis was also reported elsewhere (75, 76). Vansanmagsar *et al.* showed that Nlrp3 inflammasome in the visceral adiposity regulated obesity-induced insulin sensitivity, steatohepatitis and inflammation (77).

1.3.3 Visceral adiposity-related glucose intolerance

1.3.3.1 Type 2 diabetes

Type 2 diabetes is defined as increased insulin resistance, hyperinsulinaemia and with up to 50% pancreatic β cell failure (78, 79). Despite increasing

understanding of risk factors, the incidence and prevalence of type 2 diabetes is still growing rapidly worldwide. More than 90% diabetic patients are living with type 2 diabetes, which almost entirely derives from concurrent obesity. Obese people who have BMI ≥ 30 Kg/m^2, account for 60% of patients with type 2 diabetes (79, 80). Obesity-linked type 2 diabetes has a profound detrimental health impact on both patients and upon national health-care systems (81).

1.3.3.2 Visceral adiposity contributes glucose intolerance

Patients with impaired glucose tolerance preceding diabetes, have a higher incidence of visceral obesity (82-84). This suggests body fat distribution has a more important effect on diabetes risk than total fat accumulation (21, 80, 85, 86). In 1987, Fujioka *et al.* firstly reported that a preferential accumulation of visceral adiposity might cause glucose intolerance and hyperlipidaemia in the obese patients (87). Later on, Despres *et al.* quantified the contribution of visceral adiposity to dyslipidaemia, glucose intolerance, and hyperinsulinaemia in obese patients (88, 89). Ross *et al.* furthered tested the glucose tolerance between two groups of obese individuals with the similar abdominal subcutaneous adiposity but with different levels of visceral adiposity (90, 91). They found that obese individual with higher levels of visceral adiposity exhibited significantly higher glucose values compared to those with lower levels of visceral adiposity (90, 91). Moreover, Pascot *et al.* showed that men with more visceral adipose tissue had impaired glucose tolerance (85). Wang *et al.* reported that waist circumference was a better predictor of type 2 diabetes than BMI, suggesting visceral obesity, rather than the whole-body obesity, is more strongly associated with type 2 diabetes (92). Balkau *et al.* performed a large cohort of human studies in 63 countries and clearly confirmed a stronger correlation between the frequency of diabetes and waist circumference, highlighting the importance of waist circumference over BMI in predicting diabetes across regions and genders (93). A similar observation was found in the study from Boyko *et al.*, in which visceral adiposity assessed by CT revealed a strong correlation with incidence of type 2 diabetes in

Japanese Americans. In their study, they pointed out the importance of visceral adiposity in prediction of type 2 diabetes independently, suggesting excessive visceral adiposity can be a key feature of the development of type 2 diabetes (94).

1.3.4 Visceral adiposity-related dyslipidaemia

1.3.4.1 Dyslipidaemia

Dyslipidaemia is defined as abnormally excessive lipids in the blood. These lipids contain a broad range of lipids involving the most common forms of dyslipidaemia: high levels of low-density lipoproteins (LDL), low levels of high-density lipoproteins (HDL), high levels of triglycerides, and high cholesterol, particularly LDL cholesterol. The physiological role of LDL is primarily to carry the cholesterol synthesised by liver to other cells and organs in the body. However, abnormally high level of LDL causes plaques in the blood vessels. Plaques, also called fatty deposits, are deposited in the artery wall and trigger inflammation, smooth muscle hypertrophy and promote thrombosis resulting in atherosclerosis. In contrast to LDL, HDL particles, which are small and dense, can counteract the detrimental effects of LDL cholesterol levels as they have a high efficiency of cholesterol clearance from tissues (95). Increased HDL level benefits the clearance of excess cholesterol level in healthy humans (96). Apart from low level of HDL and high level of LDL, the typical dyslipidaemia of obesity also consists of high level of triglycerides. The excess FAs that is stored as the form of triglycerides in the liver are packaged into the very-low-density lipoprotein (VLDL) and then exported into the bloodstream. The excess liver triglycerides can result in NAFLD, which is the most common obesity-associated liver diseases and contributes to ectopic lipid accumulation in other metabolic tissues such as skeletal muscle and insulin-secreting pancreatic β cells.

1.3.4.2 Visceral adiposity is associated with dyslipidaemia

Apart from genetic factors that cause dyslipidaemia – high triglycerides and/or high cholesterol levels – dyslipidaemia is recognized as one of the features of

idiopathic visceral obesity, and is a major risk of cardiovascular diseases (89, 97-99) Viscerally obese patients were more likely to present with high levels of triglycerides and low HDL cholesterol (89). To date, numerous studies have also shown that visceral adiposity was independently associated with atherogenic dyslipidaemia, characterised by increased triglycerides and/or decreased HDL cholesterol (100, 101). Moreover, the increased ratio of LDL to HDL cholesterol, a predictor of coronary heart disease (102), was mainly due to the reduced plasma HDL cholesterol levels in the viscerally obese individuals (103). Furthermore, visceral adiposity was associated with higher VLDL and LDL particle number, larger VLDL particle size (104), and reduced HDL particle size (105), whereas excess subcutaneous adiposity was not associated with dyslipidaemia (104). Tchernof *et al*. reported that viscerally obese individuals exhibit an increase in atherogenic small-dense LDL particles and apolipoprotein B (106). Additionally, elsewhere studies showed that reduction of visceral adiposity significantly decreased fasting apolipoprotein B levels, reduced triglycerides and elevated HDL cholesterol (107, 108).

Taken together, these studies provided evidence to support that the obese individuals with higher levels of visceral adiposity are more likely to display alterations in FFA metabolism, glucose-insulin homeostasis, and lipid metabolism, thus increasing the risks of developing metabolic complications.

1.4 Current treatments and pharmacotherapeutics for obesity

1.4.1 Lifestyle management and surgery

Lifestyle management (i.e., eat less and exercise more) is the fundamental approach to attenuate obesity. However, it is always difficult to achieve and maintain the necessary beneficial weight loss (109). Other approaches such as bariatric surgery has been demonstrated among obese patients as an effective treatment to lose weight and ameliorate type 2 diabetes and associated cardiovascular abnormalities (110, 111). Apart from inherent risks of surgical procedures, patients with bariatric surgery also face risks and side-effects such as obstruction of stomach, acid reflux, chronic nausea and vomiting, and possibilities of incident relapse (112).

1.4.2 Current anti-obesity pharmacotherapeutics

Given the limitations of lifestyle management and surgery, pharmacotherapeutic approaches have been applied as an alternative treatment of obesity and its associated metabolic abnormalities. Anti-obesity drugs have been designed for those patients with high BMI (greater than 30 Kg/m^2), and with the presence of least one additional cardiovascular risk factor manifestation (113). The Food and Drug Administration (FDA) deems that an effective anti-obesity medication should produce greater than 5% body weight loss relative to placebo, alternatively, at least 35% of study participants should lose greater than 5% of their initial body weight (114). Currently there are 6 major anti-obesity drugs approved by FDA (Table 1.1): Phentermine (Adipex-P®), Phentermine/topiramate extended release (ER) (Qsymia®), Lorcaserin (Belviq®), Naltrexone sustained release (SR)/bupropion SR (Contrave®), Liraglutide (Saxenda®) and Orlistat (Xenical®). Apart from Orlistat, these drugs exert their anti-obesity effect via reducing appetite and promoting energy expenditure. Orlistat decreases fat absorption instead (115). However, these approved anti-obesity drugs have some serious adverse effects and contra-indications. For example, dry mouth and insomnia (116), palpitations,

tachycardia and hypertension (117) (Adipex-P®); paraesthesia, dizziness, dysgeusia, insomnia, constipation and dry mouth (118) (Qsymia®); the life-threatening serotonin syndrome (119) (Saxenda®); gastrointestinal side-effects including diarrhoea, flatulence, bloating, abdominal pain and dyspepsia (120) (Xenical®).

Table 1.1 Current FDA-approved anti-obesity drugs.

Anti-Obesity Drugs	How to control body weight	Mechanism of Action	Adverse effects
Phentermine (Adipex-P®)	Reducing appetite and promoting energy expenditure	Stimulator of synpatic noradrenaline, dopamine and serotonin release	Dry mouth, insomnia, palpitation, tachycardia and hypertension
Phentermine/topiramate extended release (ER) (Qsymia®)		Stimulator of synpatic noradrenaline, dopamine and serotonin release + augmenting the activity of γ aminobutyrate	Paraesthesia, dizziness, dysgeusia, insomnia, constipation and dry mouth
Lorcaserin (Belviq®)		Serotonin agonist (5-HT2C receptor agonist)	Headache, dizziness, nausea
Naltrexone sustained release (SR)/bupropion SR (Contrave®)		Opioid receptor antagonist and re-uptake inhibitor of dopamine and noradrenaline	Nausea, headache, constipation, dizziness, vomitting and dry mouth
Liraglutide (Saxenda®)		Glucagon-like peptide-1 receptor agonist	Life-threatening serotonin syndrome
Orlistat (Xenical®)	Reducing fat absorption	Lipase inhibitor	Gastrointestinal side-effects

1.4.3 Challenge for anti-visceral obesity

Considering the untoward effects, benchmarks for safety and efficacy, current anti-obesity pharmacotherapeutics are still facing challenges. For example, for efficacy, FDA-approved anti-obesity drugs are mainly based on monotherapy which targets on a single protein. As noted, monotherapy has limited efficacy because of the recruitment of alternative pathways and counter-regulations (115). Thus, instead of monotherapy, multi-target-based combination strategies may facilitate therapeutic outcomes. However, the incidence of adverse effects and risk to benefit ratio may also increase due to the combination of products (115). Moreover, the FDA-approved drugs are mainly designed for the overall weight loss either via controlling food intake or energy expenditure. No such approved drug currently allows selective targeting of adverse fat distribution (visceral obesity). As visceral obesity carries higher risk

for health conditions, it would be advantageous if a novel target could be identified for anti-visceral obesity pharmacotherapeutics.

To conclude, although research has substantially expanded our knowledge of mechanism of underlying energy homeostasis, and has made steps forwards for anti-obesity pharmacotherapeutics, current anti-obesity drugs have faced challenges in untoward effects, low efficacy, and potential safety issues. Moreover, there is no drug for treatment of visceral obesity and visceral obesity-induced metabolic diseases. Therefore, there remains a need to explore novel targets for obesity, especially visceral obesity, and its associated metabolic abnormalities.

1.5 Genetic factors in obesity

Obesity is a complex disease influenced by heritable (genetic) predisposition and environmental exposure (121, 122). The concept of a genetic component for obesity was first described by Von Noorden in 1907 and has been extensively investigated since then (123-125). Silventonien *et al.* (2010) demonstrated that genetic heredity contributes to obesity-related behaviours such as eating habits and exercise, implicating genetic risk factors as an important cause of obesity (126).

1.5.1 Monogenic obesity

The genetic contribution to obesity is classified as monogenic and polygenic, with polygenic being the predominant mode of inheritance in obesity and its related type 2 diabetes (2). Monogenic obesity results from a mutation in a single gene. This type of inheritance comprises only a small percentage (less than 10% of the population) of the heritability of obesity (127), although several genes causing monogenic obesity have been identified. Mutations in leptin (*LEP*) (56), leptin receptor (*LEPR*) (128), pro-opiomelanocortin *(POMC)* (129), proprotein convertase subtilisin/kexin type 1 *(PCSK)* (130), melanocortin 4 receptor *(MC4R)* (131) and single-minded homolog 1 *(SIM1)* (132, 133).

1.5.2 Polygenic obesity

The most common form of idiopathic obesity is polygenic, which can be caused by multiple genetic variants and environmental factors (134). Understanding the mechanisms of polygenic obesity is essential for developing novel targeted therapy and given its complexity, it may require personalised approaches across the diverse underlying genetic basis in populations. However, understanding of the causal genes underlying polygenetic obesity has met with limited success. Precise and high-throughput modern strategies such as genome-wide association studies (GWAS) has advanced the identification of genetically driven causal factors for obesity. GWAS has been widely used to identify the candidate loci, and in some cases genes, associated with major human diseases by analysing association between the single-nucleotide polymorphisms (SNP) and common diseases (135). Researchers have identified hundreds of loci that are associated with BMI (136), body fat mass (137) and body fat distribution (WHR (138-140), hip/waist circumference (139), subcutaneous and visceral adiposity (141). However, a large number of those variants are at low frequency or only have a small effect size, thus lose the potential for justifying further validation and progression to drug development, let alone clinical trials. Despite this, those variants discovered by GWAS provide valuable information and help identify those high-risk individuals and promote the outcome from early intervention with various forms of obesity.

1.5.3 The *ENPP6* gene is linked to reduction in visceral fat

From our previous GWAS performed in the population of isolates of Orkney and Shetland (142), we identified that genetic variants in and around the gene ectonucleotide pyrophosphatase 6 (*ENPP6*) on chromosome 4 were found that associated with reduced android to gynoid fat ratio. In an effort to investigate the translational significance of this finding, we examined the phenotypes of mice lacking the *Enpp6* gene; *Enpp6* knockout ($Enpp6^{-/-}$) mice. $Enpp6^{-/-}$ mice exhibited reduced visceral (epididymal) fat, improved glucose tolerance and resistance to fatty liver fed after 8-week high fat diet (HFD) exposure compared to the wide-type controls, without altering the energy

expenditure, activity or respiratory exchange ratio (142). This suggested an improved metabolic profile is the result of tissue-specific effects of *Enpp6* ablation in mice.

1.6 Ecto-nucleotide pyrophosphatase/phosphodiesterase 6 (ENPP6)

1.6.1 ENPPs enzymes: a novel therapeutic target

The ENPP family of enzymes recently emerged as a novel therapeutic target in a range of diseases as ENPPs function extracellular (143). The ENPP family consists of 7 members with catalytic domains in mammals (ENPP1-7), acting as key regulators of major physiological signalling pathways and also participates in several pathological conditions (143) (Table 1.2). ENPPs are also attractive drug-targets due to their pharmacological accessibility, being cell-surface expressed (144).

Table 1.2 Domain structure and Pathophysiological conditions of ENPPs.

Genes	Domain structure	Substrates and Functions	Pathophysiological conditions	Tissue specificity
ENPP1	Type II transmembrane, N-terminal somatomedin-B like domain, C-terminal Nuclease-like domain	Phosphoanyhydrides	Bone mineralisation, soft tissue calcification, obesity, insulin resistance, type 2 diabetes	Low tissue specificity
ENPP2	Secreted, N-terminal somatomedin-B like domain, C-terminal Nuclease-like domain	Phosphoanyhydrides, Phosphodiesters, Lysophospholipase D	Tunorignesis, angiogenesis, metastasis, obesity, insulin resistance, adipogensis, hypertrophy, hepatic steatosis, liver fibrosis	Brain and placenta
ENPP3	Type II transmembrane, N-terminal somatomedin-B like domain, C-terminal Nuclease-like domain	Phosphoanyhydrides	Allergic inflammation	Ductus deferens, intestine, seminal vesicle
ENPP4	Type I C-terminal Transmembrane, Signal-peptide sequence	Unknown	Vascular coagulation	Low tissue specificity
ENPP5			Unknown	Epididymis
ENPP6		Phosphodiesters, Lysophospholipase C	Bone mineralisation, myelination, hepatic steatosis	Brain and kidney
ENPP7			Digestion	Intestine

In the past decades, ENPPs, mainly ENPP1 and ENPP2, were highlighted as important in the area of metabolic diseases. ENPP1 regulates pyrophosphate levels, functioning in bone mineralisation and soft tissue calcification (145). *ENPP1* variants were associated with childhood and adult obesity, insulin resistance and type 2 diabetes (146), thus ENPP1 has been proposed as a

pathogenic factor predisposing to insulin resistance (147-150). ENPP2, also known as autotaxin, has lysophospholipase D activity that converts lysophosphatidylcholine (LPC) into phospholipid lysophosphatidic acid (LPA). ENPP2 has been largely investigated for its role in tumorigenesis, angiogenesis and metastasis (151). However, several studies have linked ENPP2 to obesity and insulin resistance (152-156), adipogenesis (152, 154, 157), hypertrophy (155, 158), hepatic steatosis (156) and liver fibrosis (159). Although there is no evidence of ENPP3 and ENPP4 playing roles in metabolism, researchers found that ENPP3 (160) and ENPP4 (161, 162) modulated allergic inflammation and vascular coagulation, respectively. ENPP5 (163), ENPP6 (164-166) and ENPP7 (167) have poorly characterised functions and their role, if any, in pathological conditions remains obscure (Table 1.2).

1.6.2 The biological function of ENPP6

ENPP6 shares the same lipid substrate, LPC, as ENPP2. ENPP2 catalyses lysophospholipase D activity which generates lysophosphatidic acid (LPA) and choline (168), whereas ENPP6 has a lysophospholipase C activity on LPC (164) (Figure 1.3). Apart from breakdown of LPC, ENPP6 also shows catalytic activity with other phospholipids such as glycerophosphocholine (GPC), sphingosylphophorylcholine (SPC), platelet-activating factor (PAF) and lysoPAF, but notably not phosphatidylcholine (PC) (165). These physiological substrates of ENPP6 are degradation products of PC, which provides an extracellular source of choline for all living cells. *ENPP6* is highly expressed in brain (oligodendrocytes), kidney (proximal tubule cells), liver (sinusoidal endothelial cells), but not the adipose tissues (165, 169). In the brain, ENPP6 is predominantly expressed in the newly formed oligodendrocytes (NFOs), and less strongly in mature myelinating oligodendrocytes (165, 170). Moreover, ENPP6 was recently described as a marker of NFOs (171).

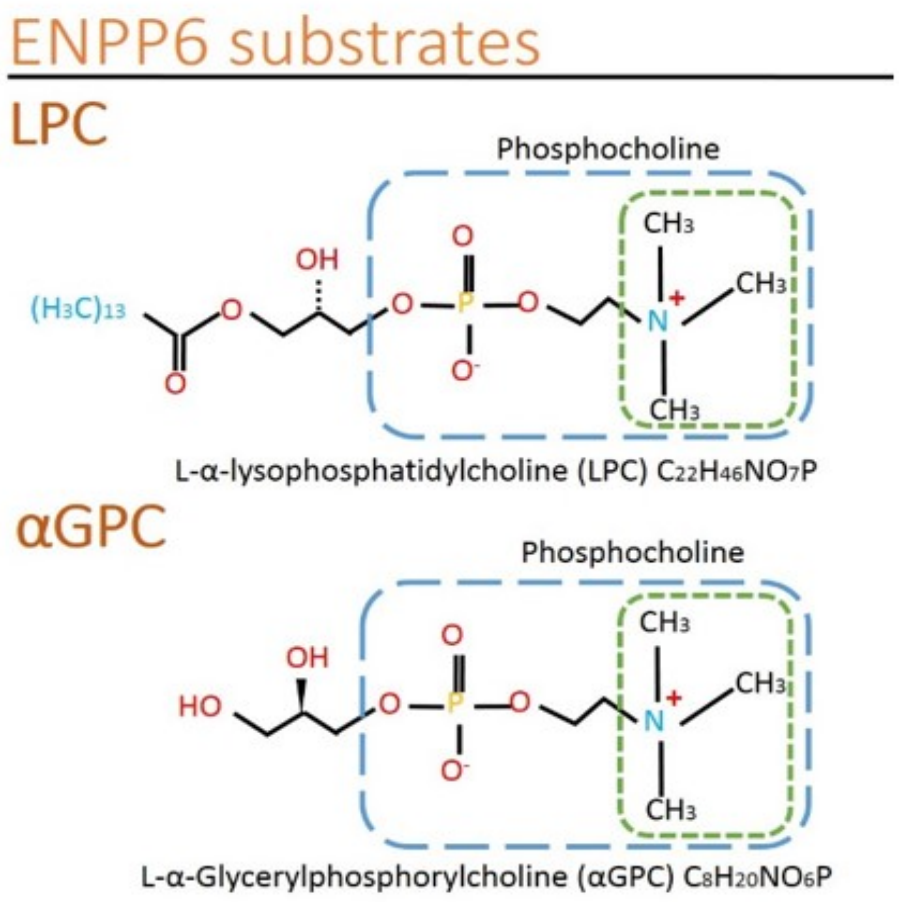

Figure 1.3 ENPP6 has a lysophospholipase C activity. ENPP6 has phosphodiesterase activities. ENPP6 recognizes the choline moiety (charged trimethylamine) as its substrates (e.g., LPC and αGPC) to produce phosphocholine LPC: lysophosphatidylcholine; αGPC: α-glycerophosphocholine.

Morita *et al.* generated C57BL/6J mice lacking *Enpp6* gene and showed that impaired myelin development in the neonatal and adult brain (165). This was explained by endogenous choline deficiency in the newly formed oligodendrocytes. In parallel, this study also showed qualitative histological assessment of liver lipid in *Enpp6*$^{-/-}$ mice, suggesting increased hepatic fat accumulation which was also attributed to choline deficiency. Recently, Dillon *et al.* reported that deletion of ENPP6 resulted in transient bone hypomineralisation (166), linking the ENPP6 to the bone metabolism. However,

the roles of ENPP6, specifically those involved in nutrient metabolism, is largely unexplored. Thus, further investigation is needed for better understanding this enzyme in the context of metabolism and its underlying mechanisms of action.

1.6.3 The function of ENPP6 in the brain

ENPP6 is highly expressed in the brain, predominantly in the NFOs, and less strongly in mature myelinating oligodendrocytes, but not in neurons or other glial cells including oligodendrocyte precursor cells (OPCs), astrocytes or microglial (165, 170). Xiao *et al* showed that ENPP6 was not expressed in the very earliest differentiating oligodendrocytes; instead, there was a time gap between the disappearance of *Pdgfrα* (OPC marker) and appearance of ENPP6 (170). In addition, *Enpp6* expression was not detected in any fetal tissues, but in the neonatal and adult animals through single-cell RNA sequencing (172) More evidence from single-cell RNA sequencing studies confirmed that *Enpp6* is highly expressed in the NFOs (171, 172). The role of oligodendrocyte in the central nervous system (CNS) is well-established, which is to generate lipid-rich myelin surrounding neuronal axons with the purpose of promoting the neurotransmissions of electrical impulses (173-175). Most OPCs myelination take place in the early postnatal period, approximately at 10 weeks of age of mice and 5 to 10 years of humans (170). OPCs myelination can also occur in the adulthood. A recent study also reported that the adult oligodendrocytes participate in the remyelination process, protecting axons from degeneration (176). Thus, it may suggest a potential role of ENPP6 on oligodendrocyte development and myelination. Indeed, Morita *et al.* showed that young *Enpp6*$^{-/-}$ mice (post-partum day 14) developed myelin sheath abnormalities, supporting the idea that ENPP6 plays an important role in oligodendrocyte development and myelination (165). The functional role, if any, of ENPP6 in OPC development and differentiation thus remains unclear.

1.7 The role of ENPP6 in choline metabolism

ENPP6 is a choline-specific phospholipase enzyme, functioning to supply choline via breakdown of its substrates including LPC and GPC (165). This suggests that ENPP6 possibly plays a role in regulating choline supply, as well as generating bioactive lipid metabolites. Choline is an essential dietary component according to the Food and Nutrient Board of the National Academies of Medicine, since 1998 (177). Choline plays a crucial role in supporting functions of liver, muscle, brain development, as well as participating in neurotransmitter synthesis, signalling functions of cell membranes, lipid metabolism, methyl-group metabolism and cell growth (178, 179). Choline is mainly acquired (70% contribution) from the diet and partially (30% contribution) via *de novo* biosynthesis through the methylation of phosphatidylethanolamine (PE) to PC by PE N-methyltransferase (PEMT) enzyme (180). PC serves as the predominant phospholipid in most mammalian cell membranes and subcellular organelles, comprising 50% of total cellular phospholipids (181). PC is an important, and the most abundant, choline species and source of choline relative to dietary choline intake (182).

Choline is phosphorylated to phosphocholine or oxidised to betaine in some cells, e.g., hepatocytes, when it is delivered into the cell body (183). Choline is essential for interconversion to other membrane components via metabolic pathways, such as PC, LPC, GPC, choline plasmalogen, sphingomyelin and betaine (184). As noted, betaine is irreversibly converted from choline via oxidation by the mitochondrial enzyme choline dehydrogenase (185, 186), acting as an important methyl donor in the betaine homocysteine methyltransferase (BHMT) pathway to generate methionine, an essential amino acid (187).

1.7.1 Choline deficiency

Given the wide range of roles choline plays in human metabolism, growing evidence suggests that altered choline levels are associated with a variety of diseases. Choline deficiency causes neural tube defects (188), neonatal brain

dysfunction (182, 189-191), cardiovascular diseases (192, 193), cancer (194, 195), fatty liver or muscle damage (184, 196), and metabolic syndrome (197). The recommended adequate intake for choline has been established in 1998 at 425 mg per day for women aged 19 and over, and 550 mg per day for men aged 19 and over (177). However, it has been argued that the recommendation for choline intake must be considered in relation to other factors, as a number of modifiable and non-modifiable factors have been found to determine the risk of inadequate choline intake. For example, Fischer *et al.* reported that sex and menopausal status had an impact on human dietary requirements for choline intake, evidenced by 77% men and 80% of postmenopausal women exhibited fatty liver or muscle damage after fed nutrients deprived of choline, whereas only 44% of premenopausal women experienced such signs (196). Furthermore, several studies reported that a significant number of common genetic polymorphisms modulate the dietary choline requirements and potentially influence public health (198-200). Polymorphisms in the *PEMT* gene are also associated with the susceptibility for NAFLD (201-203), which may explain the damaged liver phenotype in people deprived of choline intake. In the study from Kohlmeier *et al*., premenopausal women with 5,10-methylenetetrahydrofolate dehydrogenase (*MTHFD1*) 1958A allele (rs2236225), a very common single nucleotide polymorphism, were 15 times more likely to develop the phenotype of choline deficiency when exposed to a diet devoid of choline (198).

1.7.2 The role of choline in metabolic control

Dietary choline has effects on reducing body fat in animal studies (204-206), but the data on humans are limited and controversial across three studies so far. In a community-based study of 7074 middle aged and elderly men and women, choline level was found positively associated with serum triglycerides, glucose, BMI, fat mass percentage, waist circumference and physical activity, suggesting that elevated choline was associated with a high risk of metabolic syndrome including obesity, unfavourable body composition (higher body fat) and glucose homeostasis (197). However, a contrasting conclusion was made

from another observational cross-sectional study with 1081 adult subjects. In this study, high serum choline level was found to associate with a favourable body composition (lower body fat) in males only but not females (207). A third study was conducted among 1996 Chinese adults aged 40-75 years old and showed that serum choline was negatively associated with favourable body composition and fat distribution (208).

It is also controversial in animal studies regarding the effects of choline in metabolic control (204-206). For example, high choline level was observed in the liver of C57BL/6J mice after HFD feeding, in parallel with the development of obesity, hyperglycaemia and hepatic steatosis (209). Wu *et al.* reported that choline deficient diet attenuated the metabolic syndromes in obese and diabetic mice (*ob/ob* mice) through reducing body fat mass and improving glucose tolerance (210). Moreover, choline-supplemented diet promoted body weight gain and adipose depot weight gain, elevated liver fat and resulted in glucose intolerance in diet-induced obese mice, whereas choline-deficient diet protected these diet-induced obese mice from glucose intolerance and insulin resistance (211). Notably, all these studies were consistent with respect to the fatty liver phenotype induced by choline deficiency.

In summary, it is controversial that how nutrient choline afftects body fat and glucose homeostasis either in animal studies or based on human data. However, choline deficiency is consistently harmful to liver, resulting in hepatic steatosis in animals and humans. More solid evidence is needed to study the effect of endogenous choline deficiency on metabolic controls.

1.8 Regulation of energy homeostasis in the CNS

Given the high expression of ENPP6 in the brain, it is plausible that ENPP6 plays a role in whole body metabolism through its effects on the brain. Brain is widely identified as a master regulator of metabolism, particularly, the hypothalamus which plays a crucial role in regulation of energy expenditure and food intake (212-214). Moreover, several hypothalamus-expressing genes are strongly associated with obesity pathogenesis including *POMC* (215)*, MC4R* (216, 217)*, SIM1*(133)*,* Forkhead Box 1 (*FoxO1)* (218)*,* suggesting a direct genetic link between the brain and the obese phenotype. Intriguingly, ENPP6 can hydrolyse LPC to produce 2-AG and phosphocholine. 2-AG is an endogenous ligand for endocannabinoid receptors CB1R and CB2R. Until their withdrawal as an anti-obesity drug due to side effects of increased suicide/depression, cannabinoid antagonists such as rimonabant targeting the CBR1 were approved medication (219). Activating endocannabinoid signalling pathway participates in neural transmissions and activities. Moreover, increased 2-AG level was linked to visceral obesity in humans (220), suggesting that 2-AG involved endocannabinoid signalling in the brain can have influence on metabolic controls. Thus, ENPP6 in brain might also exert its influence through the endocannabinoid system. In this section, I will review the roles of hypothalamus and the endocannabinoid system in regulation of energy homeostasis.

1.8.1 Hypothalamic regulation

In the brain, the hypothalamus plays an important role in receiving signals from the peripheral nervous system and regulates energy homeostasis (221). There are 11 major nuclei in the hypothalamus: lateral preoptic (LP) nucleus, medial preoptic (MP) nucleus, paraventricular (PV) nucleus, anterior hypothalamic (AH) nucleus, suprachiasmatic (SH) nucleus, supraoptic nucleus, dorsomedial (DM) nucleus, ventromedial (VM) nucleus, arcuate (ARC) nucleus, lateral hypothalamic (LH) nucleus and posterior hypothalamic (PH) nucleus (222). Among these nuclei, four of them play critical roles in regulation of neuroendocrine signals: ARC, PV nucleus, VM nucleus and LH nucleus (223,

224). The ARC regulates glucose homeostasis, food intake and energy balance, hyperphagia (overeating due to the impaired hunger satiation) (223, 224) and obesity (225) have been found in the ARC-damaged humans. PVN has essentials roles in metabolism, growth and other autonomic functions including gastrointestinal, renal and cardiovascular (226). Lesion of the VH results in adiposogenital dystrophy, which results in increased appetite, and thus elevated caloric intake whereas damage of LH results in prevention of spontaneous feeding and thereby causes starvation (227).

In the ARC of the hypothalamus, it is well-demonstrated two populations of ARC neurons involved in the energy metabolism: the orexigenic neuropeptide Y/agouti-related peptide (NPY/AgRP) neurons, and the anorexigenic proopiomelanocortin/cocaine-amphetamine related transcript (POMC/CART) neurons (Figure 1.4). The activation of NPY and AgRP neurons regulate energy metabolism in stimulating food intake, increasing body weight and reducing energy expenditure (223, 224, 228-232). Moreover, Gropp *et al.* (233) and Luquet *et al.* (234) supported this concept by showing mice lacking NPY or AgRP neurons resulted in reducing feeding and body weight. In contrast, the activation of POMC and CART neurons inhibited food intake, increased energy expenditure and decreased body weight (223, 229, 230, 232, 235). Furthermore, AgRP neurons inhibit POMC neurons (236).

Apart from the two main neurons, ARC also widely expresses receptors of several hormones, including leptin and adiponectin and insulin, thereby gets involved in the regulation of food intake and energy homeostasis as a metabolic sensor (223, 230, 237-243). POMC neurons produce the neuropeptide precursor POMC, which is cleaved to generate α-melanocyte-stimulating hormone (α-MSH). The *α*-MSH is an agonist of the melanocortin receptors (MC1R, MC3R, MC4R and MC5R) except MC2R which is exclusive receptor for the adrenocorticotropic hormone (ATCH) (another major POMC-derived peptide). Among these MCRs, the *α*-MSH activates MC4R, ultimately resulting in the reduction of food intake. AgRP neurons produce the AgRP and

NPY which can bind to the downstream neuronal receptors and stimulate appetite.

AgRP is inversely functional with *α*-MSH and melanocortin receptors, inhibiting the *α*-MSH to activate MC4R. Mice lacking α-MSH and MC4R exhibited hyperglycaemia, hyperinsulinaemia, obesity, and insulin resistance (216, 244-246). Human with MC4R mutations also display severe obesity and insulin resistance (247-251). Taken together, two major opposing pathways: NPY/AgRP and POMC/CART play an important role in the energy homeostasis by affecting the energy expenditure and food intake.

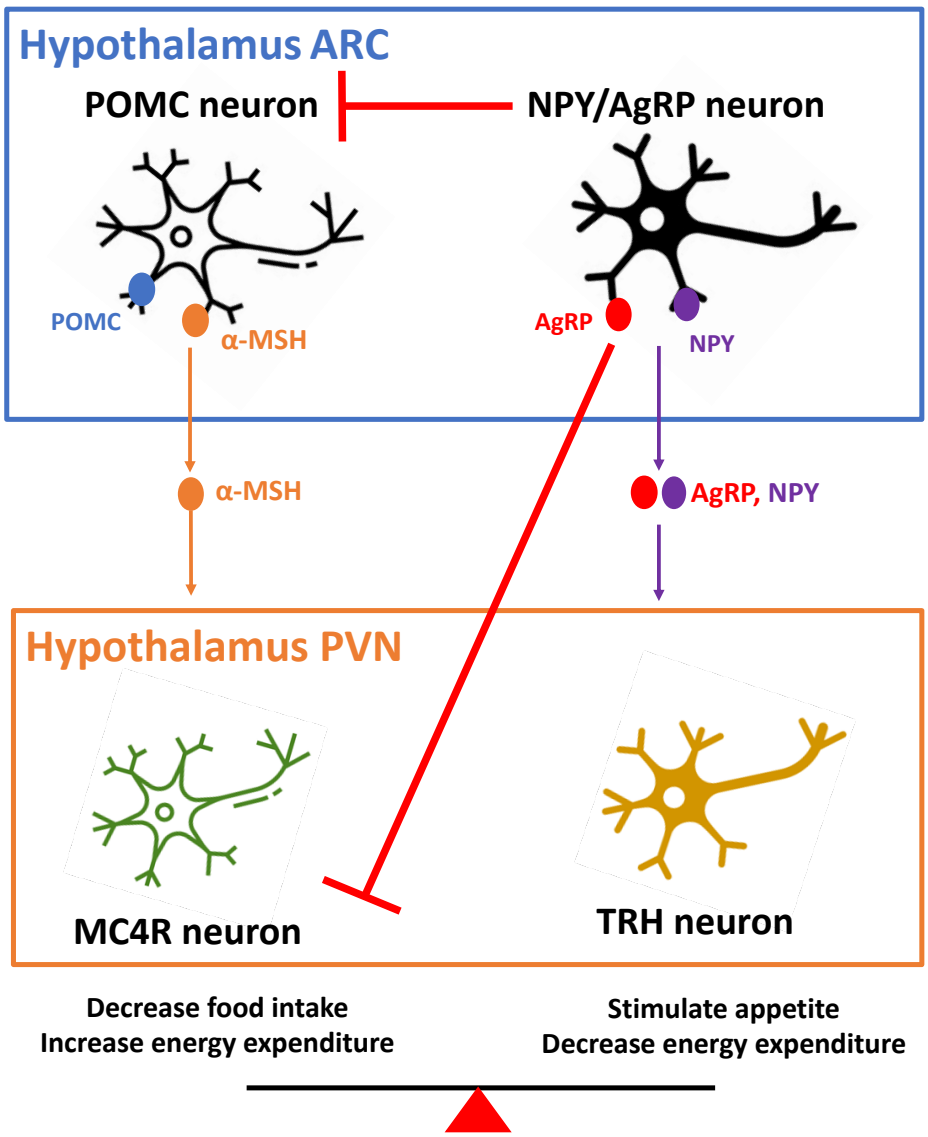

Figure 1.4 Schematic diagram of complementary roles of POMC and NPY/AgRP neurons in food intake and energy expenditure. POMC neurons and NPY/AgRP neurons localised in the hypothalamic ARC are crucial to energy homeostasis. In POMC neurons, POMC polypeptide produce *α*-MSH via cell-specific proteolytic cleavage. In the fed state, POMC neurons send the signal to stop eating and increase energy expenditure. POMC neuron activity is regulated by other neurons. In the fasting state, POMC neuron activity is inhibited by the inputs from NPY/AgRP neurons to stimulate the appetite and reduce the energy expenditure. POMC neurons project to the PVN to increase activity of MC4R neurons to reduce the food intake and increase the energy expenditure, whereas NPY/AgRP neurons send projections to synapse with MC4R neurons and increase the TRH neurons in the PVN. PVN: paraventricular nucleus.

1.8.2 Endocannabinoid system

The endocannabinoid system comprises endocannabinoids, cannabinoid receptors and related enzymes in the regulation of endocannabinoid synthesis and degradation (252). Two major endocannabinoids with a chemical structure of an arachidonic acid moiety, are identified as arachidonoyl ethanolamine (AEA) (253) and 2-arachidonoyl glycerol (2-AG) (254). Cannabinoid receptor type 1 (CBR1) and Cannabinoid receptor type 2 (CBR2) were cloned and subsequent discovery of their ligands was identified in the early 1990s (255, 256). CB1R and CB2R belong to the G-protein coupled receptor (GPCR) family and play an important role in the regulation of neuronal activity in the CNS. CB1R is the one of the most abundant GPCR in the brain (257), thereby it is believed to functionally signal in the CNS. Unlike CB1R, CB2R is rarely present in the brain except from the brainstem or under the physiological conditions (258). CB2R is highly expressed in the periphery (256), particularly in immune cells, thereby it is thought to be modulate cytokines and immune function (259). Since the early discovery of CBRs and their ligands, the endocannabinoid system has received broad interest in its action in the CNS. CB1R levels are enriched in the neuronal plasma membrane, thereby they are closely associated with regulation of neuronal activity and function (260-262). The critical role of the endocannabinoid system in the brain in the control of energy metabolism, including control of appetite, food intake and energy balance has been widely investigated (263). In the hypothalamus, CB1R is present at the membrane of neuronal mitochondria, where it exerts its function on cellular respiration and energy metabolism via inhibition of cyclic adenosine monophosphate (cAMP) and protein kinase A (PKA) activity (262). Levels of 2-AG were elevated during fasting period, but decreased during the fed period, and dropped to normal baseline in satiated animals (264). Increased levels of endocannabinoids was found in the hypothalamus of *ob/ob* and *db/db* obese mice and leptin administration was found to attenuate excessive endocannabinoid production (265), suggesting an interaction between the endocannabinoid and leptin pathways in the hypothalamus.

Endocannabinoids also increase fatty acid synthase gene expression in the hypothalamus (266).

1.8.2.1 ENPP6 and endocannabinoid system

ENPP6 has been shown to have a preference to polysaturated LPC (20:4) to produce monoacylglycerol (MAG): 2-AG (MAG 20:4) and phosphocholine (PhoC), via lysophospholipase C activity (164). Given 2-AG is a specific ligand for the central and peripheral CBRs, and the endocannabinoid system has been involved in the control of energy homeostasis (details described above), it is, hence, likely that the metabolic role of ENPP6 may be associated with CBRs activation. Regarding the visceral obesity, previous studies showed elevated 2-AG level in obese humans, which is positive correlated with body fat distribution (visceral adiposity). Also, given 2-AG and CBRs are expressed in the ENPP6-enriched oligodendrocyte in the CNS (267-269), it is likely that ENPP6 may exert its effects on the regulation of metabolism via 2-AG and CBRs in the CNS (oligodendrocytes).

1.9 Glia: contributors in energy metabolism

ENPP6 is highly expressed in the brain oligodendrocytes but not neurons, suggesting it may play metabolic roles through its effects on the oligodendrocytes. Oligodendrocytes and OPCs are the major glial cell population in the CNS. Glial cells comprise 90% of total brain cells in the CNS, consisting of OPC, oligodendrocyte, astrocyte, and microglia (172). Although glial cells are documented as the ‘supporter’ and ‘protector’ cells for neurons, participating in the neurotransmission activities (270), the metabolic role of glial cell has also been investigated in the past decade. In the study of obesity pathogenesis, most studies focused on astrocyte and microglial. So far, only one recent study by Ou *et al.* identified the role of NFOs in regulation of metabolic control via the oligodendrocyte-neuronal crosstalk (271). Due to the limited research on NFOs’ function in metabolic control, in this section, I will review the function of glial cells and glial-neuronal crosstalk in the regulation

of metabolic control, which will help understand the mechanism of metabolic role of ENPP6 in the CNS.

1.9.1 The function of glial cells in obesity pathogenesis

Several studies showed that glial cells regulate physiological and pathophysiological mechanisms of appetite and energy expenditure (272-274). Theras *et al.* showed that HFD feeding in rodents induced the rapid onset of hypothalamic inflammation and that gliosis (enlarged glial cell size and proliferated glial cells) was found in the hypothalamus of obese humans (273). Valdearcose *et al.* identified hypothalamic microglia as sensors of saturated fat, that mediate the hypothalamic inflammation induced by high dietary saturated fat (274). De Souza *et al*. showed that HFD activated a proinflammatory response that induced insulin resistance in the hypothalamus (272). Together, these studies indicated that obesity is associated with robust glial responses in the hypothalamus that resembles inflammatory response.

Apart from the pathological inflammatory response to obesity, glial cells also participate in physiological mechanism of energy homeostasis through the release of numerous hormones and the expression of metabolic factors. Garcia-Caceres *et al.* found that astrocytes were activated directly by the increased circulating leptin level in the hypothalamus (275). Hscuchou *et al.* found an increase in the expression of leptin receptors in the hypothalamic astrocytes was associated with obesity (276). Gao *et al.* revealed that HFD induced hypothalamic microglia activation (277). Chang *et al.* showed that mice lacking OPCs exhibit obesity due to the disruption of brown adipose tissue-involved energy expenditure (278). The study from Djogo *et al.* supports that OPC-deficiency displays obese phenotype, moreover, their study demonstrated that OPC is sensitive to leptin signalling, thereby regulates body weight control (279). More recently, Ou *et al.* reported that GPR17-null (exclusively expressed in the differentiated oligodendrocytes) mice are resistant to HFD-induced obesity (271). Thus, glial cells, not merely neurons, may participate in metabolic control and could be considered as promising obesity therapeutic targets.

In short, the metabolic role of oligodendrocytes is still largely unclear. ENPP6-expressing NFOs might provide a clue to establish the interaction between the oligodendrocytes and metabolic control. Thus, in my PhD study, I investigated the metabolic role of ENPP6 and its function in oligodendrocyte development, aiming to close the gap in study of oligodendrocyte-involved energy metabolism.

1.10 Hypotheses and aims

Overarching hypothesis:

ENPP6 ablation protects against diet-induced visceral obesity and diabetes via altering choline metabolism.

Aims:

1. To investigate the metabolic phenotype of global knockout of *Enpp6* gene mice and the underlying mechanism (via altering choline metabolism).

2. To assess the metabolic phenotype of oligodendrocyte-specific knockdown of *Enpp6* gene mice.

3. To investigate the effect of genetic deletion and pharmacological inhibition of ENPP6 on oligodendrocyte differentiation *in vitro*.

Chapter 2 Materials and methods

2.1 Experimental animals

Experimental mice were maintained group-housed in standard conventional cages with *ad libitum* access to water and standard chow (CRM, Special Diet Service, Essex, UK) or experimental diets (described below in chapter 2.1.4), at the biological research resources facility in the University of Edinburgh. A 12-hour light/dark cycle (lights on at 7 am and off at 7 pm) and a controlled temperature/humidity (19-21°C/50%) were maintained within the animal facility. For this thesis, only male mice were used for study (for the consideration of the time and budget limitation, the limitation of using male mice only will be discussed in detail in Chapter 6). All experimental protocols were approved after review of the University of Edinburgh Biological Science Services and performed under the Home Office Scientific Procedure (Animals) Act 1983.

2.1.1 B6129F1-*Enpp6*$^{-/-}$ and B6129F1-*Enpp6*$^{+/+}$ mice

B6129F1-*Enpp6*$^{-/-}$ mice (exon-first knockout of *Enpp6*) were purchased from Taconic Bioscience (Hudson, USA). The model was generated through ES-cells of the 129/SvEvTac strain (referred to as 129S6) and maintained subsequently with C57BL/6 strain through random mating. Therefore, all these animals were on a mixed genetic background (C57BL/6J and 129S6: referred as B6129F1).

2.1.2 C57BL/6J-*Enpp6*$^{-/-}$ and C57BL/6J-*Enpp6*$^{+/+}$ mice

Given the time and cost limitation for this study, C57BL/6J-*Enpp6*$^{-/-}$ mice were generated by back-crossing 5 generations onto a C57BL/6J-Crl strain from the original B6129F1-*Enpp6*$^{-/-}$ mixed strain. By the 5th backcross generation, nuclear genomes of B6129F1-*Enpp6*$^{-/-}$ and C57BL/6J-Crl strains are nearly 93.75% identical. Ideally, backcrossing at least 10 generations (>99.9% identical) is required to remove contaminating background heterozygosity (280). These mice were referred to as C57BL/6J-*Enpp6*$^{-/-}$ and C57BL/6J-*Enpp6*$^{+/+}$ mice (Figure 2.1).

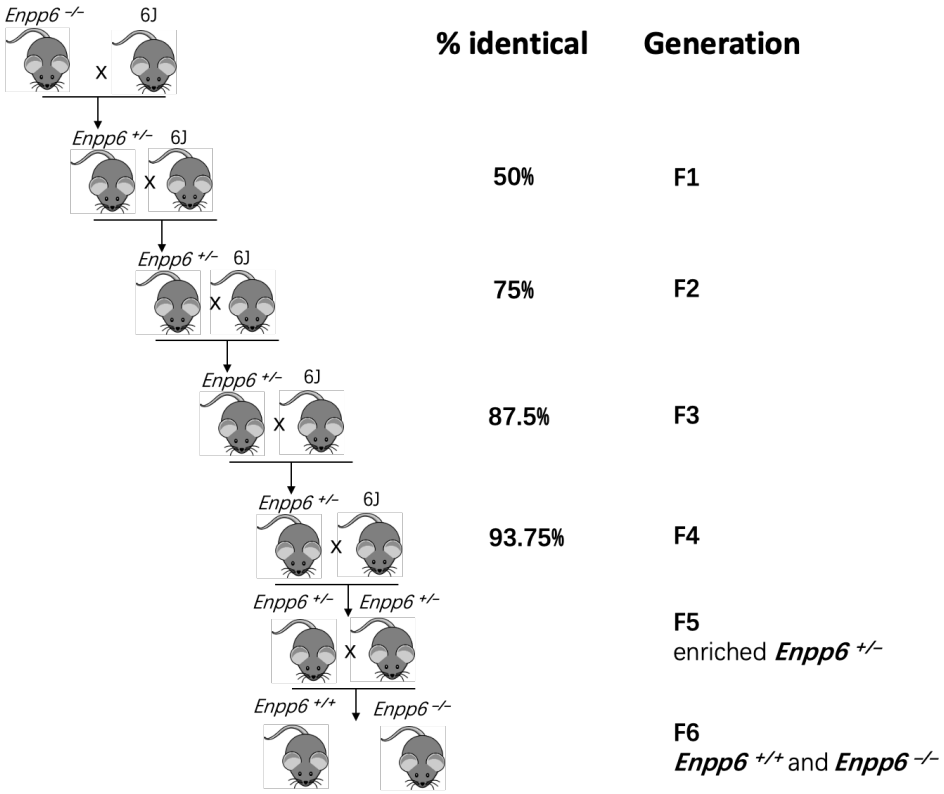

Figure 2.1 Breeding strategy for C57BL/6J-*Enpp6*$^{-/-}$ mice generation. The original B6129F1-*Enpp6*$^{-/-}$ mice were crossed with C57BL/6J (referred to as 6J in the figure) to generate the heterozygous *Enpp6*$^{+/-}$ mice, followed by repeatedly backcrossed with C57BL/6J for 4 generations. The 5th heterozygous *Enpp6*$^{+/-}$ mice were then inter-crossed to obtain the C57BL/6J -*Enpp6*$^{-/-}$ and their *Enpp6*$^{+/+}$ controls. These mice were referred as C57BL/6J -*Enpp6*$^{-/-}$ and C57BL/6J-*Enpp6*$^{+/+}$ mice.

2.1.3 C57BL/6N-*Pdgfrα-Cre*$^{+}$*Enpp6*$^{fl/fl}$ mice

The Cre-recombinase flanked by *loxP* (floxed) recombination system was used to delete *Enpp6* in *Pdgfrα*-expressing cells specifically. Pdgf receptor alpha (*Pdgfrα)* is specially expressed in immature oligodendrocyte precursor cells (OPCs) (281, 282). Figure 2.2 shows the flowchart of breeding strategy for *Pdgfrα-Cre*$^{+}$*Enpp6*$^{flox/flox}$ mice. Heterozygous *Enpp6* floxed (*Enpp6*$^{fl/+}$) mice were designed bespoke and purchased from Cyagen Bioscience (US). These mice are on the C57BL/6N strain background. *Enpp6*$^{fl/+}$ mice were inter-crossed to produce homozygous *Enpp6* floxed (*Enpp6*$^{fl/fl}$) mice. The *Pdgfrα*-

Cre^{+} transgenic (C57BL/6-Tg(*Pdgfrα-Cre*)1Clc/J) mice were provided by Prof. Anna Williams (Centre for Clinical Brain Sciences, University of Edinburgh). The *Enpp6*$^{fl/fl}$ line was crossed with *Pdgfrα-Cre*$^{+}$ line to generate the *Pdgfrα-Cre-Enpp6*$^{fl/+}$ line. Initial colonies of *Pdgfrα-Cre*$^{+}$*Enpp6*$^{fl/fl}$ and their littermates' control *Pdgfrα-Cre*$^{-}$*Enpp6* $^{fl/fl}$ mice were generated by crossing of *Pdgfrα-Cre*$^{+}$*Enpp6*$^{fl/+}$ and *Enpp6*$^{fl/fl}$ mice.

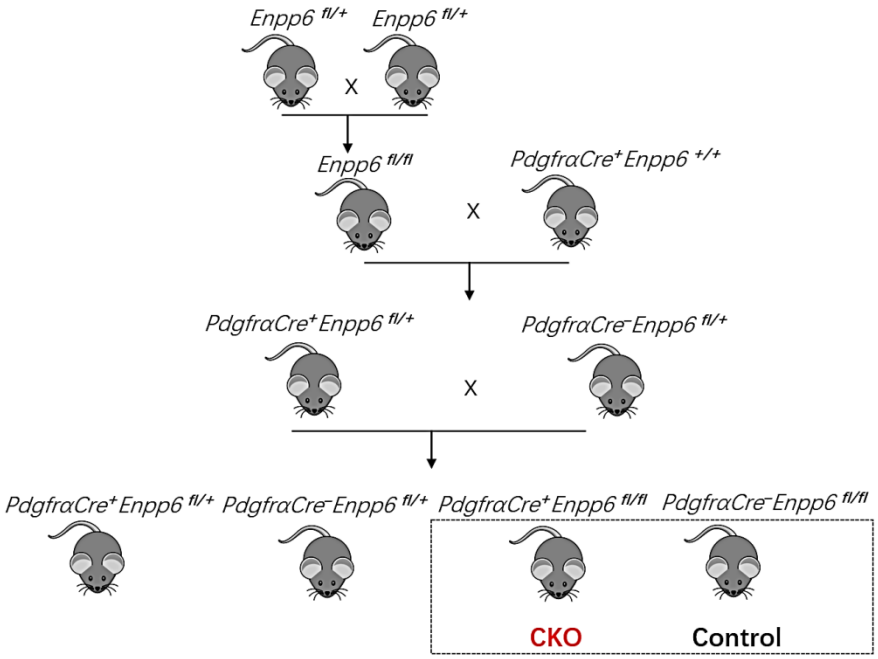

Figure 2.2 Breeding strategy for oligodendrocyte precursor cell (OPC)-specific *Enpp6* knockdown mice (*Pdgfrα-Cre*$^{+}$*Enpp6*$^{fl/fl}$). To generate constitutive conditional knockout (CKO) *Enpp6* mice, heterozygous *Enpp6* floxed (*Enpp6*$^{fl/+}$) mice were inter-crossed to obtain the homozygous *Enpp6* floxed mice (*Enpp6*$^{fl/fl}$). On crossing with *Pdgfrα-Cre*$^{+}$ transgenic mice, the *Cre* recombination led to deletion of *Enpp6* gene in OPCs.

2.1.4 Alteration of diet

All the details of experimental design are described within individual result chapters. Except chow diet (CRM E, Special Diet Service, Essex, UK), all the other diets were obtained from Research Diet Inc (New Brunswick, USA, https://researchdiets.com/). Table 2.1 summarises the contents of all diets used in this project.

Table 2.1 Mouse diets composition

	Chow	**HFD**	**CSHFD**	**CDHFD**
Fat *(kcal %)*	9	58	58	58
Carbohydrate *(kcal %)*	22	26	26	26
Protein *(kcal %)*	17	17	17	17
Choline *(gm %)*	0.1	0.08	2.08	0

HFD: high fat diet; **CSHFD**: choline supplemented HFD; **CDHFD**: choline deficient HFD.

2.1.5 Termination of animals

Animals were culled by decapitation or exposed to CO_2 gas in a rising concentration. Tissues were collected, weighed and immediately frozen under dry ice. Samples including the plasma were stored at -80^{o}C for further investigation. The remaining depot of tissues (kidney, brown adipose, subcutaneous and epididymal fat) were fixed with 10% formalin solution (Sigma, HT5014) and then dehydrated after 24-hour fixation in 75% ethanol. The fixed tissues were stored at 4^{o}C for further histology analysis.

2.2 Metabolic profiling of mice

2.2.1 Diet induced obesity

In the present, using commercial HFDs in small rodents to model the situation of human obesity has been commonly applied in research. Woods *et al.* showed that assessment of body fat is a sensitive criterion for assessing obesity in animals. In our diet-induced obesity model, we used a 7-week HFD which contains 58% fat to accelerate the fattening process and reduce the costs. Our preliminary data showed that after 7-weeks of HFD, the wild-type mice (B6129F1 strain, the mixed genetic background) gained nearly 20% body fat mass, displaying a diet-induced obese model. Thus, in this study, at the age of 11-14 weeks, the mice were exposed to a HFD for a period of 7 weeks to model the diet-induced obesity. Animals were allowed *ad libitum* access to water and diet. The whole-body weight was measured weekly, body fat mass and lean mass were determined by time domain-nuclear magnetic resonance (TD-NMR, Bruker) during the HFD feeding period.

2.2.2 CSHFD

As mentioned in Chapter 2.1.4, this project also used choline supplementation HFD intervention to test the hypothesis that whether choline level is altered by ENPP6 deficiency *in vivo*. The standard chow diet and HFD used in the experiments contains approximately 0.1 gm % of choline of diet (chow: 0.8%, HFD: 0.13%). According to the previous study, where they use 0.4 gm % of choline supplemented HFD to wild-type and *Pemt* knockout mice for 10 weeks, the choline-deficiency phenotype of reduced body weight gain and improved glucose tolerance caused by *Pemt* knockout was eliminated (209). In our experiment, we used 2 gm % of choline added to HFD (In total: 2.08 gm % of choline) for 2 weeks feeding to accelerate the experimental process and reduce the cost.

2.2.3 Glucose tolerance test

The animals were fasted for 4 hours prior to the glucose tolerance test (GTT), with *ad libitum* access to water only. Glucose solution (2 gram/kilogram body

weight, 25% glucose in 0.9% saline) was administered into the intra-peritoneal space by injection. Blood glucose were monitored by using a glucometer (OneTouch Ultra, LifeScan) before the injection at 0, and then after the injection at 15, 30, 60 and 120 minutes. A further blood sample of ~20 µL was collected at each time point into microvette EDTA-coated capillary tubes (Sarsted, 16.444.100) for assessment of the circulating insulin level. Blood was sampled from a single tail-venesection. The blood samples were centrifuged to separate plasma and red blood cells at 3,000 g for 8 minutes at 4°C.

2.2.4 Plasma insulin levels

Plasma insulin levels were analysed by using a mouse insulin ELISA assay kit (Crystal Chem, USA) according to the manufacturer's instruction for wide-range assay. In brief, insulin standards at 0, 0.1, 0.2, 0.4, 1.6, 3.2, 6.4 and 12.8 ng/mL were prepared by a serial dilution from the insulin stock (provided). For the standards, 5 µL of insulin standard per well and 95 µL of sample diluent solution were added. Standard reactions were carried out in duplicate (Individual relative percentage difference (RPD) of duplicate less than 20% was set as the acceptance criteria). For the samples collected before HFD (basal level), 3 µL of plasma sample per well and 97 µL of sample diluent solution were added. Samples from HFD were diluted 1:5 prior to this with the sample diluent solution (0.6 µL of plasma sample per well and 99.4 µL of sample diluent solution). The plate was incubated for 2 hours at 4°C. Well contents were discarded and the assay plate was washed for 5 times with 300 µL wash solution per well. Next, 100 µL of anti-insulin enzyme conjugate was added and incubated for 30 minutes at room temperature. The plate was then washed for 7 times with 300 µL wash solution per well. 100 µL of enzyme substrate was added and the plate incubated for 40 minutes reaction at room temperature avoiding light exposure. 100 µL of stop solution was added to stop the enzyme reaction. Finally, absorbance was measured within 30 minutes at 450 nm and corrected to 630 nm using a plate reader (Tecan Infinite 1000). Insulin levels were calculated from the standard curve.

2.2.5 Liver and plasma triglycerides levels

Liver and plasma triglycerides levels were analysed by using Triglycerides liquid reagent (Sentinel diagnostics, 17624H) according to the manufacturer's instruction. In brief, 50 mg pieces of frozen liver were weighed and homogenized in 20 volumes of isopropanol. The liver homogenate mixture was then shaken in an orbital shaker for 45 minutes with vortexing every 10 minutes. The homogenate was centrifuged at 3,000 g for 10 minutes. The supernatant was collected and assayed in a 96-well plate using triglycerides liquid reagent kit. Standards at 0, 0.25, 0.5, 1, 2, 4, 6 and 8 mmol/L were prepared by a serial dilution with isopropanol (for liver sample) or Phosphate-buffered saline (PBS) (for plasma sample) from the glycerol stock (Sigma, G5516). 3 µL of standards or samples and 300 µL of reagent 1 (provided) were added per well. All the reactions were carried out in duplicate (Individual relative percentage difference (RPD) of duplicate less than 20% was set as the acceptance criteria). The plate was incubated for 10 minutes at 37˚C. Absorbance was measured within 30 minutes at 546 nm and corrected to 700 nm using a plate reader (Tecan Infinite 1000) and a standard curve was generated. Triglycerides levels were calculated from the standard curve.

2.2.6 Total choline level detection

Total choline levels from liver, kidney and brain were analysed by using Total choline detection kit (Abcam, ab219944) according to the manufacturer's instruction. In brief, 20 mg pieces of frozen livers, kidneys and brains were weighed and homogenized in 400 µL (200 µL for brain) of assay buffer using a Dounce homogenizer. The homogenates were centrifuged at 300g rpm for 5 minutes at 4°C and the supernatants collected and transferred to new eppendorf tubes. Choline standards at 0, 1, 3, 10, 30, and 100 µM were prepared by a serial dilution with the assay buffer and assayed in a 96-well solid black plate with clear flat bottom. 50 µL of standards or samples (liver: 1:10 diluted, kidney: 1:20 diluted and brain: neat) and 50 µL of choline reaction mix (mixed by adding 20 µL of 250X red dye stock solution to the choline probe solution) were added per well. All the reactions were carried out in duplicate

(Individual relative percentage difference (RPD) of duplicate less than 20% was set as the acceptance criteria). The plate was incubated for 10 minutes at 37˚C. The amount of choline is proportional to the concentration of hydrogen peroxide which is detected by the increase of fluorescence at a 540 nm of excitation wavelength and 510 nm of emission wavelength within 30 minutes using a plate reader (Tecan Infinite 1000). A standard curve was generated. Total choline levels were calculated from the standard curve.

2.2.7 Histological Analysis

2.2.7.1 Adipocyte size measurement

Adipose tissues were fixed in 10% formalin and embedded in paraffin. 5 μm adipose tissue sections were stained with haematoxylin and eosin (H&E). Images were taken with Eclipse E800 (Nikon) with ProScan II (Prior Scientific) using 40X magnification. Adipocyte size were assessed by calculating the average cross-sectional area of the cells. Histomorphometry of adipose tissue was assessed by ImageJ (version: 1.50d).

2.2.7.2 Liver Oil red O staining

Liver Oil red O staining work was processed by QMRI SURF histology lab (University of Edinburgh). In brief, the right lobe of frozen liver was embedded in cryosections and sliced into a 5–10 μm sections and mounted on slides for staining. Slides were placed in absolute propylene glycol for 2 to 5 minutes, followed by staining in the pre-warmed Oil red O solution (0.5g/100 mL in propylene glycol stock) for 8 minutes in 60°C oven. The slides were differentiated in 85% propylene glycol solution for 2 to 5 minutes and rinsed in distilled H_2O twice. Next, the slides were stained in Gill's or Mayer's haematoxylin for 30 seconds and washed thoroughly in running tap water for 3 minutes. The final step was to place the slides in distilled H_2O, followed by mounting with glycerin jelly. Images were taken with Eclipse E800 (Nikon) with ProScan II (Prior Scientific) using 20X magnification. Histomorphometry of liver fat accumulation was assessed by ImageJ (version: 1.50d).

2.3 Cell culture

2.3.1 Oligodendrocyte precursors cell (OPC) primary cell culture

All primary cell isolation was done in accordance with regulations of the Animal (Scientific Procedures) Act under an issued UK Home Office project license. Primary culture of OPC was isolated from P0-P2 rodent (Sprague-Dawley neonatal rat, C57BL/6J-*Enpp6*$^{-/-}$ and C57BL/6J-*Enpp6*$^{+/+}$ mice) cerebral cortices. This method was optimized from (283-288).

2.3.1.1 Cerebral cortices dissection

Dissection was done immediately when P0-P2 pups were culled using over-dose of anaesthetic by intraperitoneal injection. All pups and dissection tools were autoclaved, sprayed and wiped with 70% ethanol before experiments. Images of dissection steps were shown below. The deceased pup was immobilized (i). Skin and skull were gently cut from the back of neck to the nose using fine small scissors (ii), followed by removing skin and peeling skull using forceps. The whole brain was scooped out (iii) and then transferred to one 60 mm untreated petri-dish containing 10 mL cold Minimum Essential medium (MEM) (Thermo Fisher, 32360026) with 1% Penicillin/streptomycin (Thermo Fisher, 15070063) (iv).

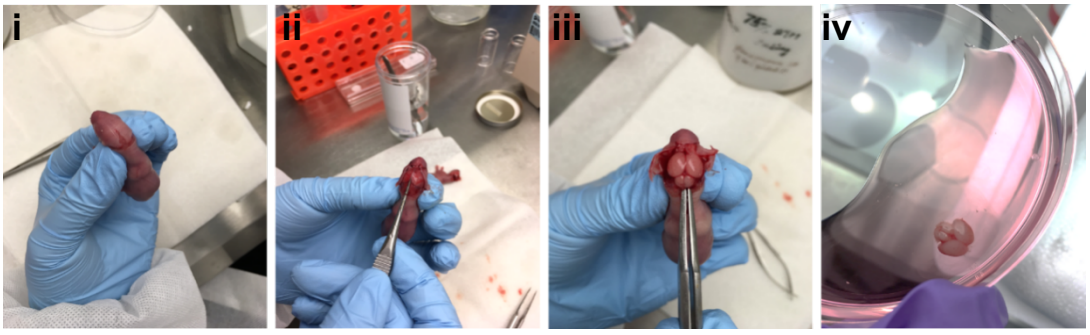

Olfactory bulbs were removed. Cortices were collected for mixed glial culture. The 2 hemispheres of the cerebrum were isolated from the midbrain. Finally, all meninges were completely removed from the cortices (Figure 2.3). Figure 2.4 shows the dorsal and ventral view of rat pup brain including the

representative region of the brain. For rat cortices, 1 brain was transferred to a bijou with 1 mL of cold MEM with 1% Penicillin/streptomycin. For mouse cortices, 2 brains were mixed into 1 bijou with 750 mL of cold MEM solution.

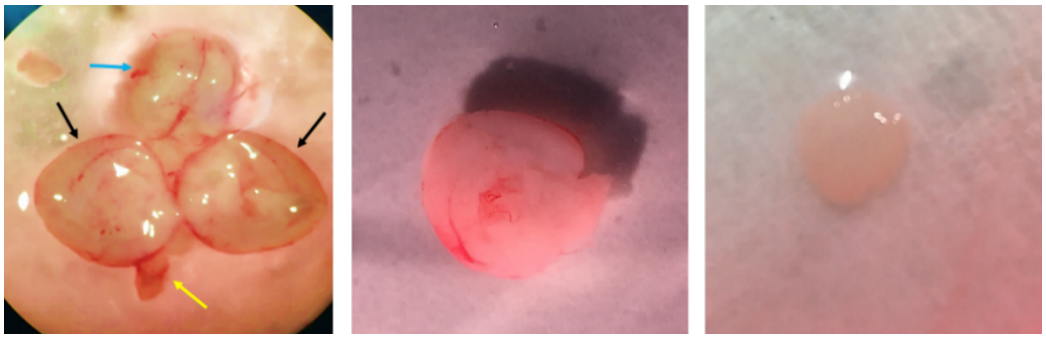

Figure 2.3 Dissection microscope images of cortices. (**left**) Ventral view of rat brain including cerebellum (blue arrow), cerebrum (black arrow) and olfactory bulbs (yellow arrow). Dorsal view of one-half cerebral cortex before meninges removing (**middle**) and after removing (**right**).

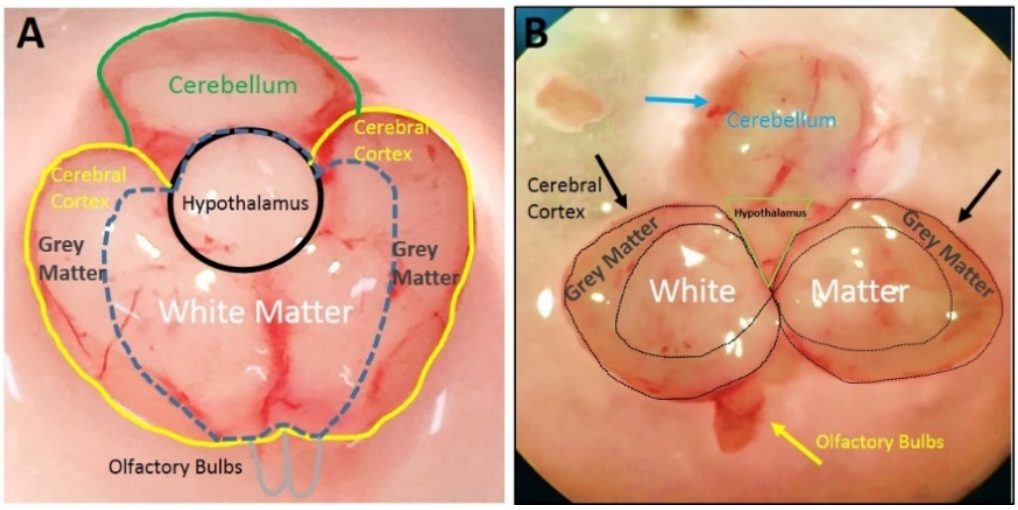

Figure 2.4 Schematic representation of dissection microscope images of P1 rat brain. (**A**) Dorsal view of rat brain including cerebellum (green area), cerebral cortex (grey matter) (areas between the yellow lines and blue dashed lines), white matter (non-cortical part of cerebral) (blue dashed area), hypothalamus (black circle) and olfactory bulbs (grey). (**B**) Ventral view of rat brain including cerebellum, cerebral cortex, white matter (including hypothalamus), and olfactory bulbs.

2.3.1.2 Tissue digestion and the mixed glial culture

Primary cells were dissociated for 1 hour for rat and 20 minutes for mouse at 37°C using a 0.22 μm-filtered papain solution. Papain solution was activated at 37°C for 20 minutes before adding to the tissues. To make up papain solution (75 μL per brain), 1 mL MEM containing 1% Penicillin/streptomycin, 0.24 mg/mL L-Cysteine (Sigma-Aldrich, C-7477), 40 μL papain (Worthington, LS003126) and 0.4 mg/mL DNase I (Sigma-Aldrich, D5025) were mixed well. To deactivate the digestion solution, 2 mL of pre-warmed mixed glial culture medium (Dulbecco's Modified Eagle's Medium (DMEM) (Invitrogen 41966029) with 20% fetal bovine serum (HyClone, sv30180.03) and 1% Penicillin/streptomycin) was added into the cell suspension and placed for 10 minutes at room temperature. Then the cell suspension was mixed well by pipetting and triturating for 4 times gently with 19 gauge needle, followed by 4 times of trituration with a 23 gauge needle (needles are not necessary for processing mouse cortices). Next, the cell mixture was centrifuged at 300 g for 5 minutes. The supernatant was discarded, and 5 mL of mixed glial culture medium was added into cell mixtures and mixed well. Followed by passing through a 70 μm nylon cell strainer, cells were then plated onto 0.1 mg/mL poly-D-lysine (PDL) (Sigma-Aldrich, P0899) coated T-75 flasks (1h-incubation at 37°C, followed by rinsing with distilled H_2O twice (288). The mixed glial cells were cultured at 37°C in 8.0% CO_2 incubator with 2-3 days medium change for 9 days.

2.3.1.3 OPC isolation

After 9 days mixed glial cells were confluent, and phase-dark cells (OPCs) appear on the top of phase-grey bed layers of the astrocytes. The cells were firstly shaken on the orbital shaker for 1 hour at 210 rpm (rat) or 45 minutes at 50 rpm (mouse); at 37°C to remove loosely adherent microglia, followed by additional 18 hour- shaking at 250 rpm to separate OPCs (283, 284). One flask of cell suspension was transferred onto one 60 mm untreated petri-dish and then incubated at 37°C in 8.0% CO_2 incubator for 30 minutes, in order to remove remaining microglia and astrocytes. All the supernatant was harvested

and centrifuged at 100 g for 5 minutes to obtain pure OPCs. 95% OPCs were obtained and validated by flow cytometry ($A2B5^+$ cells % of total cell number; Figure 2.6).

2.3.1.4 OPC counting and differentiation

To count the OPC number,10 µL of the cell suspension was mixed well with 10 µL 0.4% trypan blue solution. The mixture was transferred to a cell counter slide (Bio-Rad, 1450011) and analysed by TC20 cell counter (Bio-Rad). After counting, OPCs were then seeded into PDL-coated plates (500,000 cells/well onto 6-well plate, 150,000 cells/well onto 24-well plate) in OPC differentiation medium, which contains DMEM, 1% Pen/strep, 0.5% fetal bovine serum, 100X Insulin-Transferrin selenium (Sigma-Aldrich, I3146) and 100X Sato stock (289) including 100 µg/mL BSA fraction V, 60 ng/mL progesterone, 16.1 µg/mL putrescine, 400 ng/mL Triiodothyroxine and 400 ng/mL L-thyroxine (all from Sigma-Aldrich, A7030, P8783, P5780, T2752, T1775) (288). Figure 2.5 shows the flowchart of rat OPC isolation and culture.

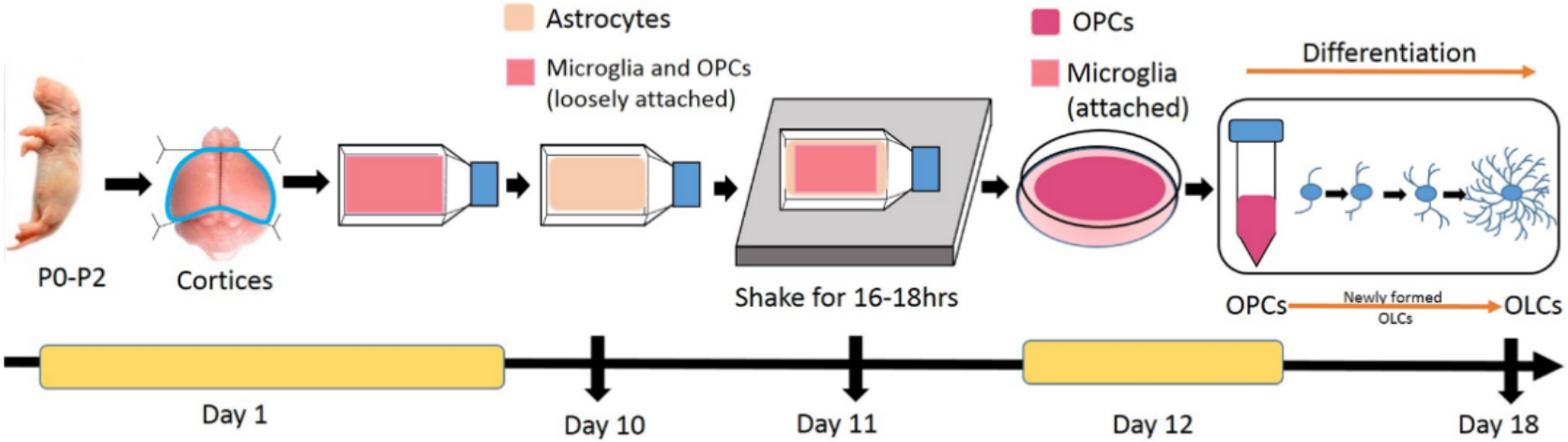

Figure 2.5 Schematic flowchart of the process of rat OPC isolation and culture. The method was adapted and optimised from (283). On day 1, cortices were collected and processed to obtain mixed glial culture. On day 11, attached astrocytes were removed by an overnight shaking process. On day 12, suspended OPCs were collected from petri-dish and differentiated for the following days. 95% OPCs were obtained and validated by flow cytometry (Figure 2.6).

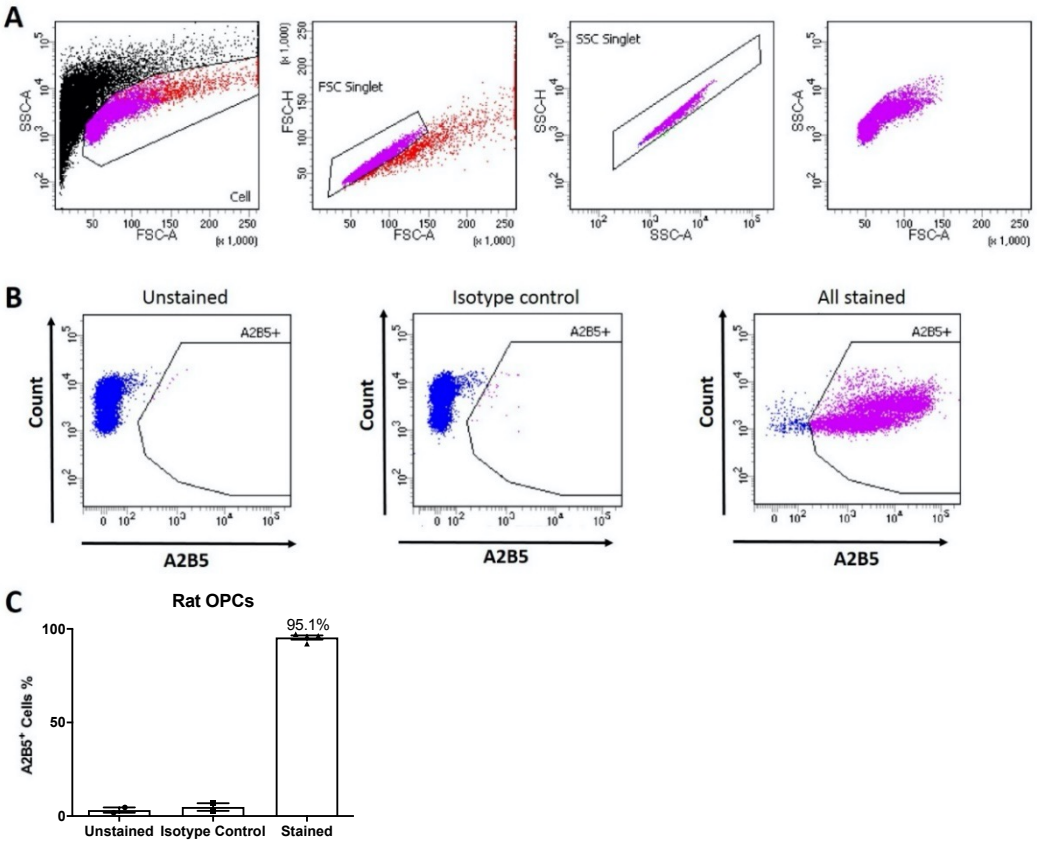

Figure 2.6 Validation of the purity of rat OPC population. Cells were gated using forward scatter (FSC) and side scatter (SSC); Singlets were gated by FSC-A (area) and FSC-H (Height), followed by SSC-A and SSC-H (**A**). A2B5-negative cells were gated out using unstained and isotype control cells through the red laser (633 nm) (**B**). A2B5-positive cell number percentages in unstained, isotype and all stained groups are shown (n=4).

2.3.2 ENPP6 expressing human embryonic kidney (HEK) 293 cells

To obtain stable ENPP6-overexpressing HEK293 transfected cell line, the cDNA open reading frame (ORF) clone for the full-length human *ENPP6* (Genscript®, untagged pcDNA3.1+ vector) was transfected into HEK293 cells. HEK293 cells were maintained in DMEM (Sigma-Aldrich, D6429) with 10% foetal bovine serum and 1% Penicillin/streptomycin. The cells were cultured at 37°C, in a 5.0% CO_2 incubator. HEK293 cells were seeded at 800,000 cells per well in one 6-well plate and incubated at 37°C in a 5.0% CO_2 incubator overnight. 2 µg of *ENPP6* ORF cDNA was added into cells with lipofectamine 3000 and P3000 reagent in accordance with the manufacturer's instructions (Lipofectamine 3000, Thermo Fisher, L3000001). Untransfected cells were used as a negative control at the same time. After 48 hour-transfection, culture medium was replaced by using selective culture medium which contains 600 µg/mL G418 for the next 6-7 weeks. The culture medium was changed every 3-4 days. After 15 days, no live cells were visible in the untransfected group. Single colonies were picked using a P1000 pipette tip and then transferred to a new well of a 24-well plate with culture medium containing 600 µg/mL G418. 2-3 colonies were chosen and added to different wells. After 4-5 weeks cells were confluent enough to transfer into 6-well plate. The ENPP6 expression of each cell line was tested at this stage by qRT-PCR and ENPP6-TG-mPC activity cell-based assay. Figure 2.7 shows that schematic flowchart of the process of establishment of an *ENPP6*-overexpressing HEK293 cell line.

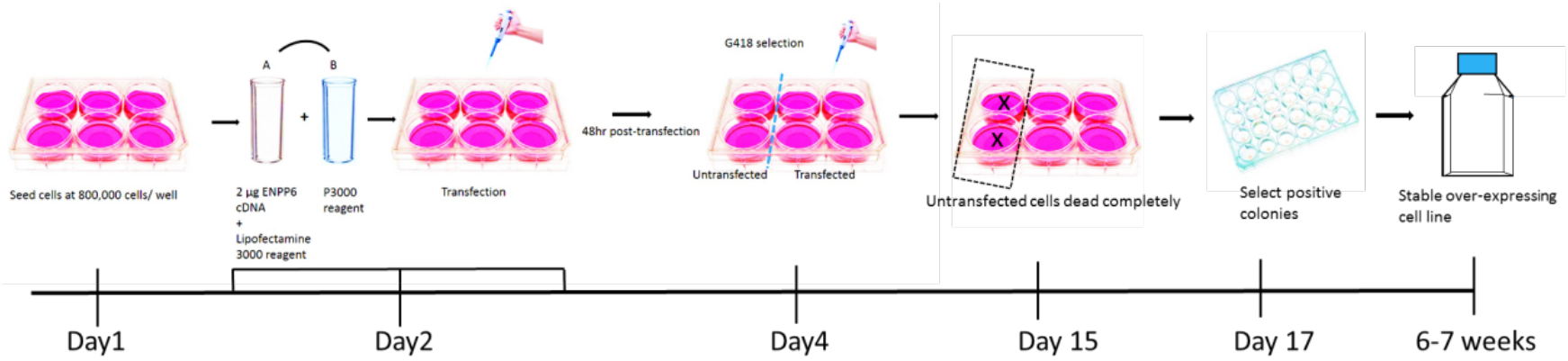

Figure 2.7 Schematic flowchart of developing an ENPP6 overexpressing stable HEK293 cell line. On Day 1, 800,000 cells per well were seeded. On Day 2, human ENPP6 cDNA was transfected into wide-type HEK293 cells with lipofectamine 3000 reagent for 48 hours. Untransfected cells were used as a negative control. From Day 4, culture medium was replaced by G418 selection medium (600 µg/mL) for the following 6-7 weeks. A single colony was picked up from the positive cells for sequential culture when no live cells were visible in the untransfected cells (after 15 days culture).

2.4 Quantification of gene expression at mRNA level

2.4.1 Total RNA extraction and quantification

For primary cell harvest, cells were separately collected after 0, 24, 48, 72 (rat only) and 144 hours (rat only) post-differentiation. For HEK293 wildtype (WT) and ENPP6 over-expressing HEK293 cells, cells were collected from 6-well plate or T75 flasks during passage (at least 3 different passage times). All RNA was extracted from cell/tissue lysis using the QIAGEN RNeasy Mini Kit (QIAGEN, 74104) in accordance with the manufacturer's instructions. RNA concentration and purity were assessed by UV spectroscopy (Nanodrop 1000 software). The A260/230 ratio was used to assess RNA purity.

2.5 cDNA synthesis

500 ng-1 µg of RNA (500 ng for primary cells; 1 µg for cell lines and tissues) was used to prepare cDNA using QuantiTect reverse transcription reaction kit (Qiagen, 205311) followed the manufacturer's instructions. In brief, firstly 2 µL of genomic DNA buffer and the proper volume of RNase-free water were added to RNA samples, to make up an overall volume of 14 µL. After that, the samples were incubated at 42°C for 2 minutes and immediately placed on ice. A mastermix was prepared including Reverse Transcriptase enzyme, RT buffer and Primer Mix, followed by incubating at 42°C for 15 minutes, then 3 minutes at 95°C.

2.5.1 Real-time polymerase chain reaction (RT-PCR)

Standards for each gene were prepared with 5 µL of each cDNA collected into a single tube followed by dilution of 1:4 with water. Then serial dilutions were prepared as follows: 1:8, 1:16, 1:32, 1:64, 1:128 and 1:256. 10 µL of PCR reaction included 2 µL of cDNA sample, 2X PerfeCTa FastMix II master mix, 20X TaqMan gene expression assay (primer/probe) and RNase-free water. TaqMan probes are listed in Table 2.2. Quantitatively Real-Time PCR was performed on a LightCycler 480 Real-time PCR system (Roche). The reactions were incubated in a 384-well PCR plate at 95°C for 5 minutes for polymerase

To obtain stable ENPP6-overexpressing HEK293 transfected cell line, the cDNA open reading frame (ORF) clone for the full-length human ENPP6 (Genscript®, untagged pcDNA3.1+ vector) was transfected into HEK293 cells. HEK293 cells were maintained in DMEM (Sigma-Aldrich, D6429) with 10% foetal bovine serum and 1% Penicillin/streptomycin. The cells were cultured at 37°C, in a 5.0% CO_2 incubator. HEK293 cells were seeded at 800,000 cells per well in one 6-well plate and incubated at 37°C in a 5.0% CO_2 incubator overnight. 2 µg of *ENPP6* ORF cDNA was added into cells with lipofectamine 3000 and P3000 reagent in accordance with the manufacturer's instructions (Lipofectamine 3000, Thermo Fisher, L3000001). Untransfected cells were used as a negative control at the same time. After 48 hour-transfection, culture medium was replaced by using selective culture medium which contains 600 µg/mL G418 for the next 6-7 weeks. The culture medium was changed every 3-4 days. After 15 days, no live cells were visible in the untransfected group. Single colonies were picked using a P1000 pipette tip and then transferred to a new well of a 24-well plate with culture medium containing 600 µg/mL G418. 2-3 colonies were chosen and added to different wells. After 4-5 weeks cells were confluent enough to transfer into 6-well plate. The ENPP6 expression of each cell line was tested at this stage by qRT-PCR and ENPP6-TG-mPC activity cell-based assay. Figure 2.7 shows that schematic flowchart of the process of establishment of an *ENPP6*-overexpressing HEK293 cell line.

2.6 Quantification of gene expression at mRNA level

2.6.1 Total RNA extraction and quantification

For primary cell harvest, cells were separately collected after 0, 24, 48, 72 (rat only) and 144 hours (rat only) post-differentiation. For HEK293 wildtype (WT) and ENPP6 over-expressing HEK293 cells, cells were collected from 6-well plate or T75 flasks during passage (at least 3 different passage times). All RNA was extracted from cell/tissue lysis using the QIAGEN RNeasy Mini Kit (QIAGEN, 74104) in accordance with the manufacturer's instructions. RNA concentration and purity were assessed by UV spectroscopy (Nanodrop 1000 software). The A260/230 ratio was used to assess RNA purity.

2.7 cDNA synthesis

500 ng-1 µg of RNA (500 ng for primary cells; 1 µg for cell lines and tissues) was used to prepare cDNA using QuantiTect reverse transcription reaction kit (Qiagen, 205311) followed the manufacturer's instructions. In brief, firstly 2 µL of genomic DNA buffer and the proper volume of RNase-free water were added to RNA samples, to make up an overall volume of 14 µL. After that, the samples were incubated at 42°C for 2 minutes and immediately placed on ice. A mastermix was prepared including Reverse Transcriptase enzyme, RT buffer and Primer Mix, followed by incubating at 42°C for 15 minutes, then 3 minutes at 95°C.

2.7.1 Real-time polymerase chain reaction (RT-PCR)

Standards for each gene were prepared with 5 µL of each cDNA collected into a single tube followed by dilution of 1:4 with water. Then serial dilutions were prepared as follows: 1:8, 1:16, 1:32, 1:64, 1:128 and 1:256. 10 µL of PCR reaction included 2 µL of cDNA sample, 2X PerfeCTa FastMix II master mix, 20X TaqMan gene expression assay (primer/probe) and RNase-free water. TaqMan probes are listed in Table 2.2. Quantitatively Real-Time PCR was performed on a LightCycler 480 Real-time PCR system (Roche). The reactions were incubated in a 384-well PCR plate at 95°C for 5 minutes for polymerase activation followed by 50 cycles of 95°C for 10 seconds and 60°C for 30 seconds. Absolute quantitation of target genes was calculated by LightCycler480 software. The standard curve was created by plotting crossing point value in cycles against the log of the dilution factor. The concentration of the samples was extrapolated from the standard curve and normalised using endogenous housekeeping gene controls (*GAPDH, TBP/Tbp*).

Table 2.2 List of TaqMan gene expression primer probes (Thermo Fisher)

Catalog Number	Gene	Species
Hs02758991_g1	*GAPDH*	Human
Hs00608905_m1	*ENPP6*	Human
Rn01455646_m1	*Tbp*	Rat
Rn01487952_m1	*Enpp6*	Rat
Mm00446971_m1	*Tbp*	Mouse
Mm00624107_m1	*Enpp6*	Mouse
Mm00839436_m1	*Pemt*	Mouse
Mm00447774_m1	*Pcyt1a*	Mouse
Mm00770121_m1	*Cept1*	Mouse
Mm00499536_m1	*Dgat2*	Mouse

2.8 Cell-based ENPP6 enzymatic activity assay

This method of this assay was updated from the published paper (290). In brief, isolated OPCs were seeded in the PDL-coated 6-well plated. Cells were differentiated with medium change every day. OPCs or oligodendrocytes at different stages of differentiation are harvested. Cells were detached by adding Accutase solution (Sigma-Aldrich, A6964) and incubated for maximum 10 minutes at 37°C. Cells were centrifuged at 300 g for 5 minutes, and the supernatant was carefully removed. Cells were then re-suspended in 45 µL of PBS per 100,000 cells. HEK293 WT and HEK293 transfected cells were re-suspended in 45 µL per 8,000 cells. Next, the cell suspension was transferred into a clear-bottom black 96-well plate for the ENPP6 enzymatic activity assay. 5 µL of 50 µM ENPP6 substrate (probe) TG-mPC with or without 10 µM ENPP6 inhibitor T11 (290), was added into the cells. The plate was then incubated for 1 hour at 37°C in the Tecan Infinite M1000 plate reader. 490 nm of excitation wavelength and 510 nm of emission wavelength were set up for this assay. ENPP6 enzymatic activity was determined from the fluorescent intensity, and the slope of linear region for each cell type represents as the initial rate of reaction.

2.9 Flow cytometry

2.9.1 Sample preparation

Cells were harvested and washed with PBS once and re-suspended in 100 µL of PBS with primary antibody (oligodendrocyte marker O4 antibody, R&D system, MAB1326) at a concentration of 0.25 µg /1 x 10^6 cells in FACS tubes. Cells were incubated for 1 hour at 4°C, followed by washing with PBS for three times. The secondary antibody (goat anti-Mouse IgG (H+L) cross-adsorbed secondary antibody Alexa Fluor 488, Invitrogen, R37120) was diluted in 1:500 in 100 µL of PBS and added into cells for 45 minutes incubation at 4°C. After washing with PBS, cells were re-suspended in 250 µL of PBS and ready for analysing. Alternatively, cells were fixed in 100 µL of 10% formalin at room temperature for 5 minutes and kept overnight at 4°C. For each assay, the same method to prepare cells was applied. For the conjugated antibody (Alexa Fluor 647 anti-mouse/human A2B5, BioLegend), cells were re-suspended in 100 µL of PBS with 1 µL of antibodies, and then incubated at 4°C for 30 minutes and followed by washing with PBS. Unstained cells (neither stained with primary antibody nor the second antibody) and control cells (stained with the second antibody only) were prepared at the same time. The isotype control for conjugated antibody (Alexa Fluor 647-Mouse IgM, BioLegend) was included in the assay.

2.9.2 Flow cytometry analysis

100,000 cells per group were re-suspended in 250 µL of PBS before analysis. Flow cytometry was performed on a BD 5 lasers LSR Fortessa analyser (BD Biosciences). On average 10,000 cells were collected for analysis. Compensation and gating were performed using unstained cells, cells stained with isotype antibody (for unconjugated antibody, cells stained with the secondary antibodies only was used) and cells stained with target antibodies. Single cells were gated in through forward scatter (FSC), and then cell debris was gated out by both FSC and side scatter (SSC). Subsequently, the auto-fluorescent cells were ruled out by adding another channel (B670) to Alexa Fluor 488 (O4). In a similar fashion to the gating strategy used for the O4

expression analysis, Alexa Fluor 657 (A2B5) channel was added. Data were analysed by FlowJo software.

2.10 Immunocytochemistry

(150,000 cells per well) OPCs were seeded in 24-well plate after isolation from the mixed glial culture and differentiation for 24 to 48 hours with daily changed differentiation medium. Differentiated mouse NFOs were washed with PBS once, and fixed in 300 µL of fixation/permeabilisation solution (BD, 554714) per well for 20 minutes at 4°C. After that, cells were washed twice with 1× BD Perm/Wash™ buffer (BD, 554723) and then kept in PBS at 4°C. Next, fixed cells were blocked in 3% BSA for 30 minutes at room temperature and then incubated with the selected primary antibodies overnight at 4°C. The following primary antibodies were used: mouse anti-O4 (1:100) and rat anti-MBP (1:100). After washed triple times with PBS, cells were then incubated for 30 mins at room temperature with the secondary goat anti-mouse (Alexa Fluor 488) (1:500), goat anti-rabbit (Alexa Fluor 647) (1:500), and chicken anti-rat (Alexa Fluor 647) (1:500). Cells were washed three times with PBS and incubated with DAPI at 0.5 µM for 5 minutes at room temperature. Cells were then washed a further three times with PBS. Images were visualised using an EVOS FL Auto 2 cell imaging system (Thermo Fisher) with a 20X objective in the following 3 fluorescent channels: DAPI, GFP and Cy5. Six images per well were captured and analysed. Image J software was used for cell counting from each channel.

2.11 Statistical analysis

Power calculation was carried out estimate the sample size for animal work to be able to test the hypothesis. The calculation was based on the previous data from Schraut's PhD thesis (2017), where the study carried out the body weight, glucose tolerance, and visceral (epididymal) adipose tissue weight between the 8 weeks of HFD-fed WT and *Enpp6* KO mice on a mixed genetic background (B6129F1, described in detail in chapter 2.1.1). In order to confidently detect a 22% reduction in visceral (epididymal fat weight)

compared to WT group (Mean 1: 2.168; Mean 2: 1.474; Standard deviation: 0.58, Power: 1-β: 0.8, Type 1 error rate α: 0.05, a sample size of n=11 is required). Sample size calculation was done by using online tool: http://powerandsamplesize.com/Calculators/Compare-2-Means/2-Sample-Equality. Thus, in order to achieve confident statistical analysis, we planned to use n=11 per group based on the power calculation above.

In chapter 3, to test the hypothesis whether dietary choline intervention can alter the metabolic phenotype of *Enpp6* KO mice, we eventually applied WT (n=13) and KO (n=9) for choline supplementary cohort, and WT (n=6) and KO (n=8) for choline deficiency cohort due to technical, time, economic and animal health reasons. In chapter 4, given the same hypothesis and the same experimental design as the previous study, but based on the other genetic strain of mice, we planned to use the n=11 per group based on the power calculation above to perform the study. However, due to the time and economic reasons, we ended up at n=10 for each genotype for the C57BL/6J-*Enpp6* mice study. In chapter 5, at least biological replication n=3 was applied for *in vitro* work.

All statistical analyses and graphing were performed by GraphPad Prism 8.0 software. The values are represented as mean ± SE (standard error). A value of $p < 0.05$ was considered significant. Given the limitation of group size in both animal work and *in vitro* cell work, in reference to test the normality, all data were assumed that the outcome is approximately normally distributed. Parametric tests were used for assessing the significance of statistical comparison. Details including individual group size for each cohort and experiments are stated in the results chapters.

Chapter 3 The effects of *Enpp6* deficiency on the mouse metabolic phenotype

3.1 Introduction

3.1.1 Obesity is a worldwide health crisis

As covered in detail (chapter 1.1), the global prevalence of obesity and its associated metabolic diseases continues to rise. Approximately 3 million people in the world die each year as a result of excess body weight and related metabolic diseases, such as type 2 diabetes and cardiovascular disease (1). Moreover, it has become clear that excess body weight and obesity increase the severity of outcomes from emerging pandemic viral diseases such as COVID19 (291). Different from the abdominal fat (also named as subcutaneous fat), visceral fat is stored around the internal organs, and carries higher risk factors for cardiometabolic diseases. Although there are several approved anti-obesity drugs, none of them are specifically targeting to the visceral obesity (detailed described in chapter 1.4). Thus, a renewed effort is required to explore the complicated mechanisms modulating energy homeostasis, and to seek effective therapies.

3.1.2 Variants near the human *ENPP6* gene associated with reduced visceral adiposity

The anatomical location of stored fat is crucial in determining the metabolic consequences of obesity. In particular, visceral fat (fat around the internal organs) accumulation carries a higher risk for associated cardiometabolic diseases such as type 2 diabetes, cardiovascular disease and certain cancers (metabolic syndrome) than fat stored in peripheral (e.g. subcutaneous depots) (292). From previous genome wide association studies (GWAS) (142), potential regulatory variants in and around the human *ENPP6 gene* were found associated with reduced visceral fat accumulation in humans. The direction of the effect of *ENPP6* expression was unknown due to unavailable quantitative trait locus (QTL) expression data. To investigate the translational significance of ENPP6, we previously examined the metabolic phenotypes of mice lacking the *Enpp6* gene*: Enpp6* knockout (*Enpp6*$^{-/-}$) mice. *Enpp6*$^{-/-}$ mice exhibited

reduced visceral (epididymal) fat depots after high-fat-diet (HFD) exposure compared to the *Enpp6*$^{+/+}$ controls, predicting that directionality of the effects in humans likely involves reduced levels of ENPP6 driving the reduced visceral fat accumulation. Moreover, *Enpp6*$^{-/-}$ mice displayed improved glucose tolerance compared to the *ENPP6*$^{+/+}$ controls, without altered energy expenditure or food intake. These data suggest an improved metabolic profile is the result of tissue-specific effects of ENPP6 ablation. As ENPP6 is an enzyme with properties amenable to pharmacological inhibition (290), it was reasoned that ENPP6 inhibition represented a novel anti-visceral obesity and anti-diabetic therapeutic strategy. However, the mechanism of ENPP6-deficiency–mediated resistance to impaired glucose metabolism is still unclear.

3.1.3 ENPP6 is a choline-specific phospholipid enzyme

The ENPP family of enzymes, of which there are 7 members, act as key regulators of several physiological signalling pathways (as covered in detail in Chapter 1.6). ENPPs recently emerged as novel therapeutic targets in a range of diseases (143). ENPPs consist predominantly of extracellular protein structures embedded in the cell plasma membrane (293, 294) and as such, are attractive drug-targets due to their pharmacological accessibility. Among the ENPPs, ENPP1 (146, 147, 150) and ENPP2 (autotaxin) (154-156, 158, 159) regulate glucose–insulin homeostasis and changes in their activities are associated with obesity and metabolic conditions. ENPP3 (160) and ENPP4 (161, 162) modulate allergic inflammation and vascular coagulation, respectively. ENPP5 (163), ENPP6 (164, 165) and ENPP7 (167) have poorly characterised functions and their role, if any, in pathological conditions remains obscure. Notably, ENPP2 and ENPP6 share the same lipid substrate, lysophosphatidylcholine (LPC). ENPP2 generates lysophosphatidic acid (LPA) and choline with a lysophospholipase D activity, whereas ENPP6 generates monoacylglycerol (MAG) and phosphocholine (PhoC) through a lysophospholipase C activity (see Figure 1.3 of chapter 1.6).

ENPP6 was ascribed the function of a supplier of choline via its substrate α-glycerophosphatidylcholine (GPC) (19). This was hypothesised to support the rapid generation of phospholipids in the membranes of proliferating ENPP6-expressing-Neuro2a and -NIH3T3 cells (165). Morita *et al.* suggested that mice lacking the *Enpp6* gene exhibited hypomyelination in the neonatal and adult brain (165). In parallel, qualitative histological assessment of liver lipid in the *Enpp6*$^{-/-}$ mice suggested increased fat accumulation, which was also attributed to choline deficiency (165). Notably, choline is considered an essential dietary component, as choline deficiency causes liver and muscle damage, increased risk for heart disease, impaired foetal development and brain function (e.g. lifelong memory and learning defects) (295, 296). Exposure to a choline-deficient diet is a well-established intervention for modelling non-alcoholic fatty liver disease (NAFLD) in animals (297). However, the effects of choline-deficiency on energy metabolism are controversial and depend on multiple factors such as the duration of feeding choline-deficient-diet and animal models. On one hand, several studies have shown that choline deficiency protected diet- or genetic defect-induced obese mice from increased body fat and hyperglycaemia (209, 211, 298) (key information summarised in Table 3.1, with the detailed description in Chapter 1.7.2). On the other hand, choline deficiency has been linked to NAFLD and its-associated metabolic complications such as insulin resistance, hyperglycaemia and obesity in humans (299, 300) and rodent studies (301).

Whether the observed improved metabolic phenotype of *Enpp6*$^{-/-}$ mice was due to endogenous choline deficiency is unknown, but is a plausible mechanism given that *Enpp6*$^{-/-}$ mice are reportedly choline-deficient and that choline-deficiency improves glucose metabolism and reduces fat mass under certain experimental conditions (209-211, 298). This chapter addressed the hypothesis that endogenous choline-deficiency underlies the metabolic phenotype of *Enpp6*$^{-/-}$ mice.

Table 3.1 Summary of metabolic studies manipulating choline in rodents

Mouse model	Diet	Feeding period	Phenotype	Reference
C57BL/6J mice	HFD (45% fat)	12 weeks	Obesity, hyperglycemia, hepatic steatosis; High choline levels in liver	Rubio-Aliaga I *et al.,* 2011
Pemt $^{-/-}$ mice	HFD (60% fat)	10 weeks	Reduced body weight, visceral fat, normal insulin sensitivity	Jacobs *et al.,* 2010
	HFD (60% fat) + CSD		Reversed phenotype HFD-induced C57BL/6J mice	
	HFD (60% fat) *or* HFD (60% fat)+ CSD	1 week	**HFD:** Normal	Wu *et al.,* 2013
			HFD+CSD: Impaired glucose and insulin tolerance	
C57BL/6J mice	HFD (45% fat), followed by CSD	HFD: 8 weeks CSD/CDD: 4 weeks	**HFD, HFD+CDD:** Weight gain, elevated liver triglycerides, hyperinsulinemia, glucose intolerance.	Raubenheimer,P.J *et al.,* 2015
	HFD (45% fat), followed by CDD		**HFD, HFD+CDD:** No altered body and adipose depot weights, but improved glucose tolerance	
ob/ob mice	CSD or CDD	2 months	**CDD:** Reduced fat mass, improved glucose and insulin intolerance, exacerbated fatty liver	Wu *et al.,* 2012

HFD: high fat diet; CSD: choline supplement diet; CDD: choline deficiency diet.

3.1.4 Hypothesis and aims

Hypothesis: *Enpp6*$^{-/-}$ mice protects from diet-induced obesity and diabetes via altering of endogenous choline levels.

Aims:

1. To test whether B6129F1-*Enpp6*$^{-/-}$ mice displayed a reduction in choline level cross the ENPP6-enriched tissues including liver, kidney and brain,

2. To investigate whether choline supplementation reversed the protective metabolic phenotype of B6129F1-*Enpp6*$^{-/-}$ mice exposed to HFD.

3. To investigate whether removal of choline exaggerated the protective metabolic phenotype of B6129F1-*Enpp6*$^{-/-}$ mice exposed to HFD.

4. To determine the molecular basis of altered choline metabolism in B6129F1-*Enpp6*$^{-/-}$ mice under different choline exposures as in aim 1 and 2.

3.2 Experimental design

3.2.1 Assessment of metabolic responses in B6129F1-*Enpp6*$^{-/-}$ mice with choline supplemented or choline deficient HFD

The flowcharts of experimental design are shown in Figure 3.1. Glucose tolerance tests (GTT) were performed after 7 weeks of HFD, and after a further 2-week exposure to a choline supplemented HFD (CSHFD) or choline deficient HFD (CDHFD) feeding post-HFD and their metabolic phenotype and hepatic genes expression were also assessed.

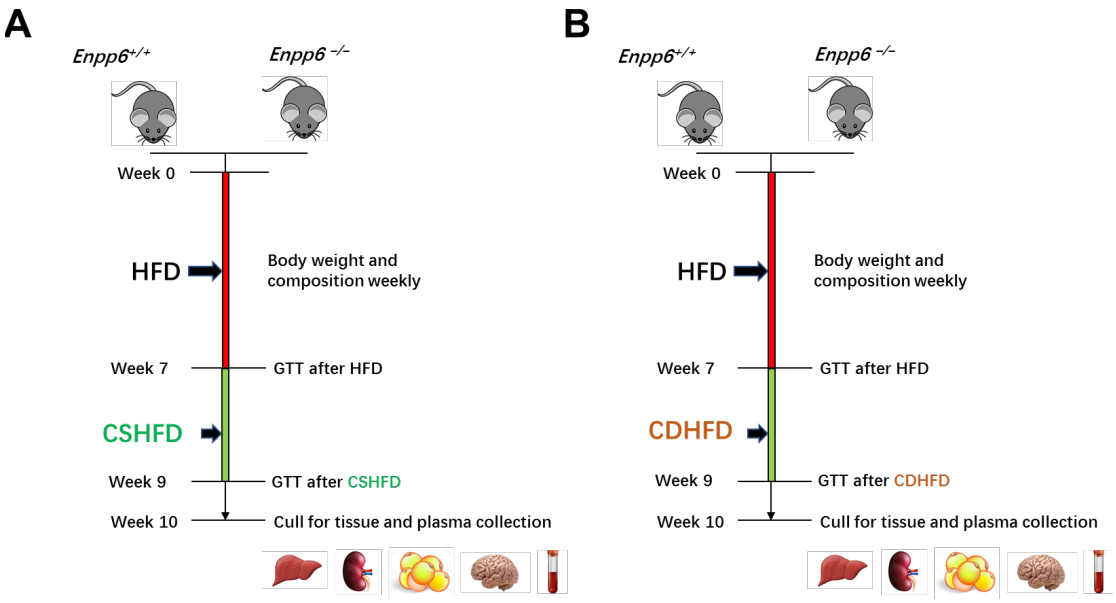

Figure 3.1 Investigations into the effects of choline supplementation or depletion on the metabolic consequences of HFD feeding in B6129F1-*Enpp6*$^{-/-}$ and *Enpp6*$^{+/+}$ mice. A 7-week HFD (0.08% choline) feeding regimen, matched to the previous work performed in *Enpp6*$^{-/-}$ mice was performed with a choline-supplemented HFD (CSHFD) (2.08% choline) or choline-deficient HFD (CDHFD) (0% choline) provided for a further 2-week of feeding post-HFD. During both feeding periods, mice were given *ad libitum* access to diets. The regular HFD contains 0.2% choline bitartrate, which comes to 0.08% choline.

3.3 Results

3.3.1 HFD-fed *Enpp6*$^{-/-}$ mice are selectively protected from visceral obesity

In our previous study, Schraut showed that *Enpp6* deletion did not affect the total body weight, fat or lean mass (142). However, *Enpp6*$^{-/-}$ mice exhibited selectively reduced visceral (epididymal) fat mass and maintained comparable subcutaneous fat mass after HFD feeding compared to *Enpp6*$^{+/+}$ littermates (Figure 3.2A), without affecting body weight, body composition, energy expenditure, respiratory exchange ratio, or physical activity (142). To further investigate the fat depot-level effect of *Enpp6* deficiency, adipocyte size was assessed in the *Enpp6*$^{-/-}$ mice and *Enpp6*$^{+/+}$ after 8 weeks of HFD feeding. Reduction of visceral (epididymal) adiposity in the *Enpp6*$^{-/-}$ mice was associated with smaller average adipocyte area than the *Enpp6*$^{+/+}$ mice without gross effect on subcutaneous adipocytes (Figure 3.2B and D). This was consistent with the selective phenotype in reduced visceral (epididymal) adipose tissue depots weight. HFD-fed *Enpp6*$^{-/-}$ mice, which showed a higher number of smaller adipocytes per field (Figure 3.2C), with decreased frequency of large adipocytes and increased frequency of small adipocytes (Figure 3.2E-F). No significant effect of adipocyte distribution or average number on subcutaneous adiposity was observed (Figure 3.2G-H). These data confirmed that *Enpp6* deficiency selectively reduced visceral (epididymal) adipocyte hypertrophy and increased visceral (epididymal) adipocyte hyperplasia.

Furthermore, consistent with decreased liver weight after HFD, which was observed previously (Figure 3.2A), this study showed that *Enpp6*$^{-/-}$ mice were resistant to HFD-induced hepatic steatosis, displaying significantly lower levels of liver triglycerides (Figure 3.3A). In line with reduced liver triglycerides levels, this study also showed a reduction of liver lipid droplet accumulation in the *Enpp6*$^{-/-}$ mice (Figure 3.3B-C).

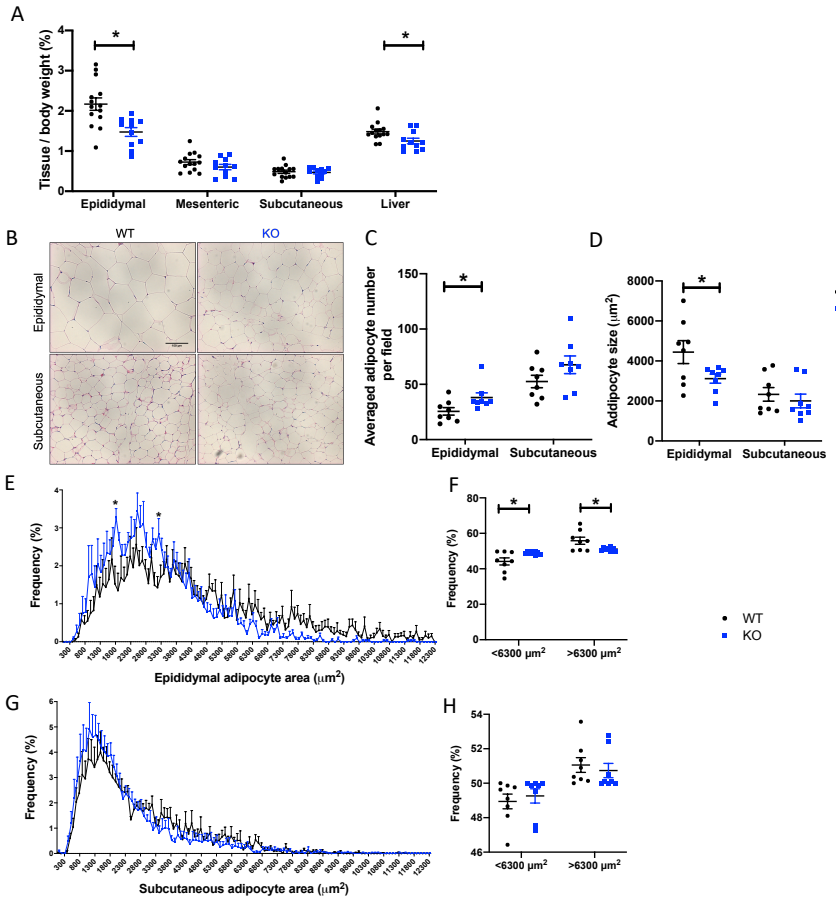

Figure 3.2 HFD-fed *Enpp6*$^{-/-}$ mice displayed selectively reduced visceral (epididymal) adiposity and visceral (epididymal) adipocyte hypertrophy. (A) Adipose tissue and liver weight (as a percentage of whole-body weight) of HFD-fed *Enpp6*$^{-/-}$ mice (n=11) and *Enpp6*$^{+/+}$ mice (n=14). Raw data were obtained from K. Schraut, PhD thesis in 2017 (142). **(B)** Representative micrographs of H&E stained epididymal and subcutaneous sections of HFD-fed *Enpp6*$^{-/-}$ and *Enpp6*$^{+/+}$ mice. Scale bar = 100 μm. Quantitative analysis of adipocytes in epididymal and subcutaneous sections (n=8 for each genotype): **(C)** average adipocyte number per field; **(D)** average adipocyte size; **(E)** visceral (epididymal) and **(G)** subcutaneous adipocyte area distribution; **(F)** frequency of large and small adipocyte. Large and small adipocyte were defined by using the median of the range of adipocyte size assessed. Large: a surface area greater than 6300 μm^2 and small: a surface area greater than 6300 μm^2).; **(H)** subcutaneous adipocyte. 2-way ANOVA with Bonferroni post-hoc testing was used for statistical analysis in **(E)** and **(G)**. *Unpaired student t-test* was used for statistical analysis in **(A)**, **(C-D)**, **(F)** and **(H)**. The values are represented as mean ± SE, *$p < 0.05$.

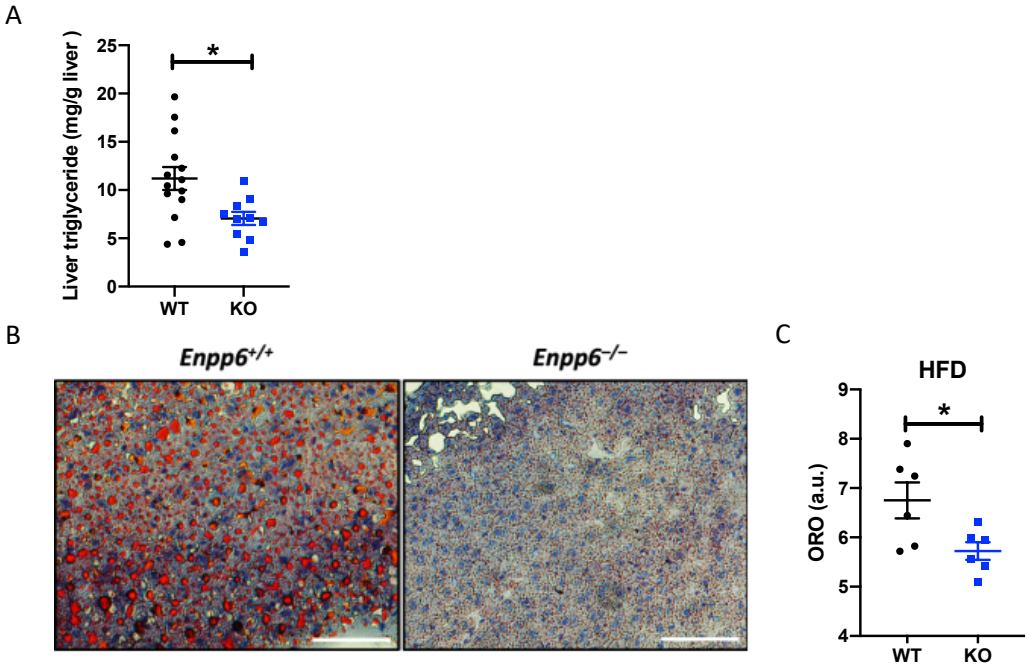

Figure 3.3 *Enpp6*$^{-/-}$ mice were protected from HFD-induced fatty liver. (A) Liver triglycerides levels after HFD feeding in *Enpp6*$^{-/-}$ (n=10) and *Enpp6*$^{+/+}$ mice (n=14). **(B)** Representative micrographs of oil red O-stained liver (left lobe) of sections of HFD-fed *Enpp6*$^{-/-}$ (n=6) and *Enpp6*$^{+/+}$ mice (n=6). Scale bar = 100 μm. **(C)** Quantitative analysis of lipid accumulation (n=6 for each genotype). *Unpaired student t-test* was used for statistical analysis. The values are represented as mean ± SE, *$p < 0.05$.

3.3.2 The beneficial metabolic phenotype in B6129F1-*Enpp6*$^{-/-}$ mice is reversed by choline supplementation

It was hypothesized that *Enpp6*$^{-/-}$ mice displayed a choline-deficient-like phenotype. To answer whether the beneficial metabolic phenotype in the *Enpp6*$^{-/-}$ mice was due to altered choline production and availability, we firstly assessed the total choline levels. The baseline levels of endogenous total choline levels were comparable in the tissues of chow-fed B6129F1-*Enpp6*$^{-/-}$ and *Enpp6*$^{+/+}$ mice (Figure 3.4A), consistent with the previous study by Morita *et al.* (2016). However, we found that the total liver choline levels of HFD-fed B6129F1-*Enpp6*$^{-/-}$ mice were significantly lower than that of HFD-fed B6129F1-*Enpp6*$^{+/+}$ mice (Figure 3.4B). No difference was found in the choline levels from kidney or brain between genotypes (Figure 3.4B).

Next, we tested the hypothesis that the improved metabolic phenotype of HFD-fed B6129F1-*Enpp6*$^{-/-}$ mice could be reversed by dietary choline supplementation (CS). Thus, the metabolic consequences of B6129F1-*Enpp6*$^{-/-}$ and *Enpp6*$^{+/+}$ mice fed a 7-week of HFD, followed by a 2% CSHFD for a further 2-week of feeding were investigated. After CSHFD feeding, the total choline levels from HFD-fed B6129F1-*Enpp6*$^{-/-}$ and *Enpp6*$^{+/+}$ mice were significantly elevated compared to only the mice with HFD feeding (Figure 3.4G-H). B6129F1-*Enpp6*$^{-/-}$ and *Enpp6*$^{+/+}$ mice consumed similar amounts of CSHFD (Figure 3.4E) and exhibited similar body weight and total body fat mass during 7 weeks of HFD feedings and after the further 2 weeks of CSHFD feeding (Figure 3.4C-D). CS normalised the difference in epididymal visceral fat and liver weight between B6129F1-*Enpp6*$^{-/-}$ and *Enpp6*$^{+/+}$ mice (Figure 3.4F). Notably, although there was no difference in total fat mass gain between two genotypes (Figure 3.4D), CS increased mesenteric fat depot mass, another type of visceral adiposity, in HFD-fed B6129F1-*Enpp6*$^{-/-}$ compared to *Enpp6*$^{+/+}$ mice (Figure 3.4F). This data indicated a reversal of the protective phenotype of body visceral fat distribution in CSHFD-fed B6129F1-*Enpp6*$^{-/-}$ mice.

Given there was no significant difference of glucose tolerance performance (Figure 3.5A-B), and liver triglycerides (Figure 3.5E) between two genotypes after the CSHFD feeding (Figure 3.5A-B), it suggested that dietary CS also attenuated the improvement in glucose tolerance and plasma triglycerides levels in the B6129F1-*Enpp6*$^{-/-}$ mice. Moreover, the lower liver triglycerides levels were no longer significant in the B6129F1-*Enpp6*$^{-/-}$ mice (Figure 3.5E). Fasting insulin concentration during the GTT (Figure 3.5C), and plasma triglycerides level (Figure 3.5D) were comparable between two genotypes after the CSHFD feeding (Figure 3.5C).

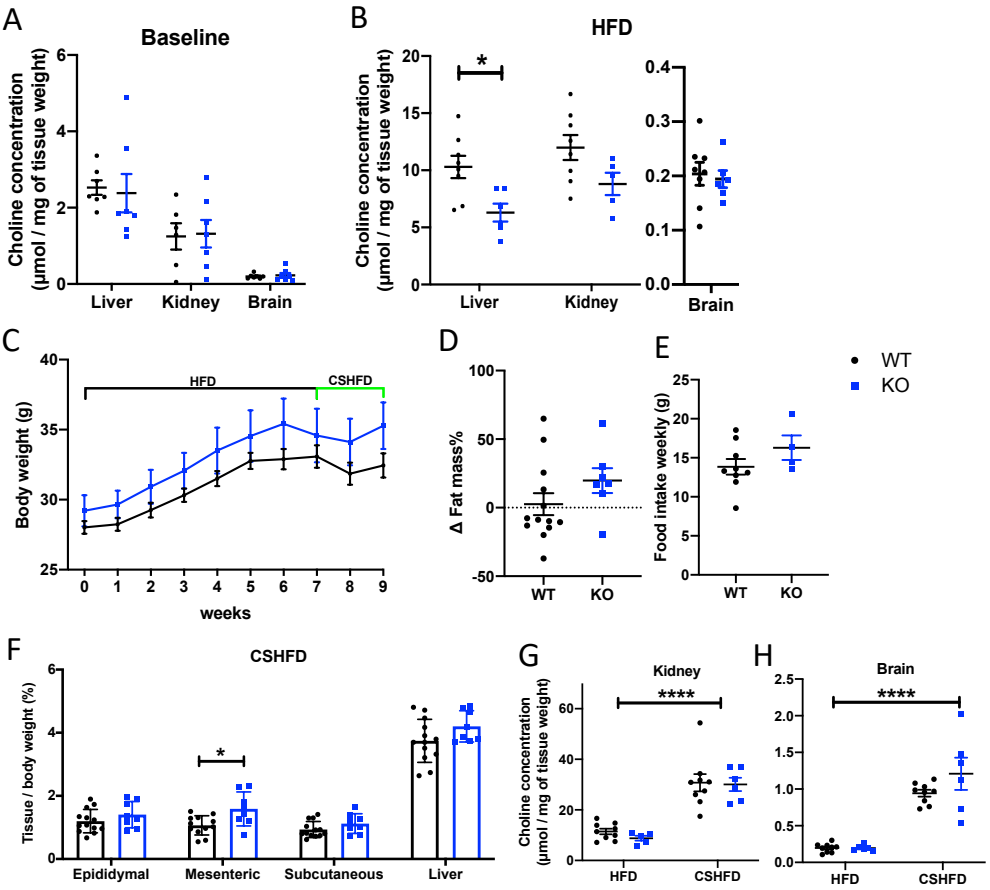

Figure 3.4 HFD-fed B6129F1-*Enpp6*$^{-/-}$ mice showed a hepatic choline deficient phenotype and reduced visceral fat and liver weight were reversed by dietary choline supplementation. (A) Total choline level in tissues from B6129F1-*Enpp6*$^{-/-}$ (KO) (n=7) and B6129F1-*Enpp6*$^{+/+}$ mice (WT) (liver and brain: n=7; kidney: n=6 for kidney) at the baseline level and **(B)** after HFD feeding in KO mice (liver and brain: n=6; kidney: n=5) and WT mice (n=8) **(C)** Body weight of KO and WT mice during 7 weeks of HFD and 2 weeks of choline supplemented HFD (CSHFD), KO (n=8) and WT mice (n=13). **(D)** Total fat mass gain during the CSHFD feeding in KO (n=7) and WT mice (n=13). **(E)** Food intake during the CSHFD feeding, KO (n=4) and WT mice (n=9). **(F)** Tissue weight (as a percentage of whole-body weight) after the CSHFD feeding, KO (n=8) and WT mice (n=13). **(G)** Total choline level in kidney and **(H)** brain from KO and WT mice after the CSHFD feeding, KO (n=6) and WT mice (n=9). Outlier data caused by technically error were removed from analysis after assessing by outlier test (GraphPad 8.0). 2-way ANOVA with Bonferroni post-hoc testing was used for statistical analysis in **(C)** and **(G-H)**. *Unpaired student t-test* was used for statistical analysis (**Figure A-B, D, E-F**). The values are represented as mean ± SE, *$p < 0.05$.****$p < 0.0001$.

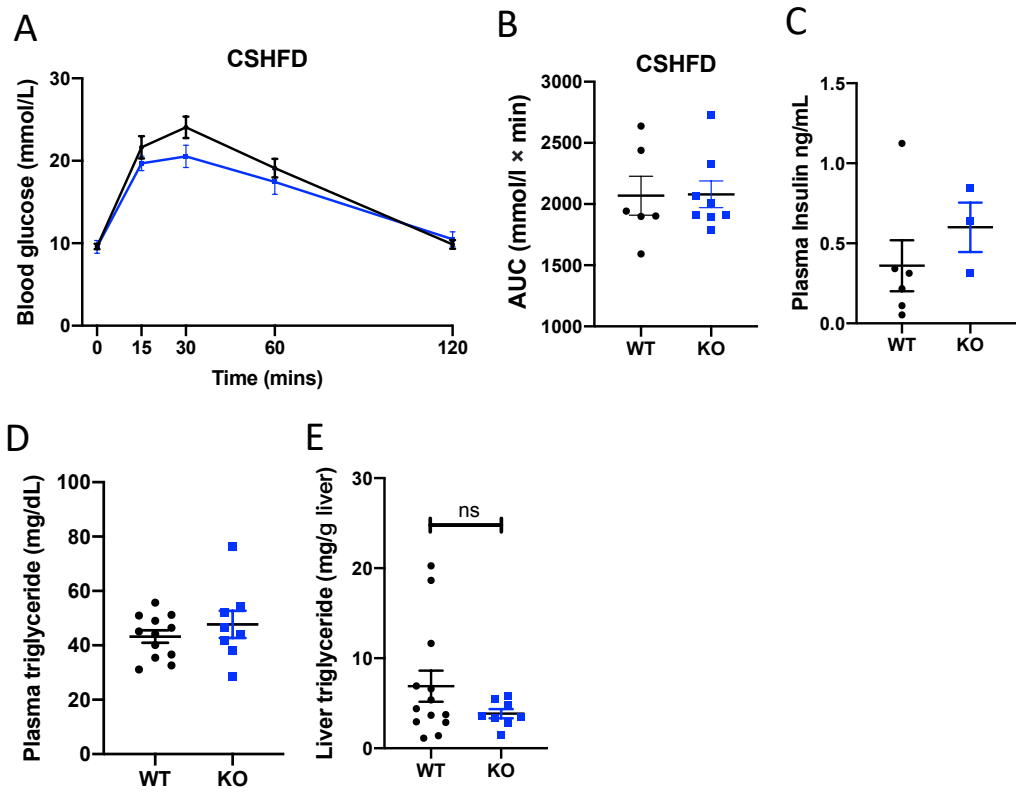

Figure 3.5 Choline supplementary reversed the metabolic phenotype of HFD-fed B6129F1-*Enpp6*$^{-/-}$ mice in glucose and liver triglycerides. Blood glucose during the GTT were measured in B6129F1-*Enpp6*$^{-/-}$ (KO) and *Enpp6*$^{+/+}$ (WT) mice after 7 weeks of HFD and a further 2-week of CSHFD feeding. **(A)** Blood glucose levels during the GTT after the CSHFD feeding and **(B)** area under the curve (AUC) of the GTT after the CSHFD, KO (n=8) and WT (n=13). Plasma fasting insulin, KO (n=3) and WT (n=6), fasting plasma and liver triglycerides levels, KO (n=8) and WT (plasma: n=12; liver: n=13) were measured after the CSHFD feeding: **(C)** plasma insulin levels; **(D)** circulating fasting triglycerides level and **(E)** liver triglycerides level. 2-way ANOVA with Bonferroni post-hoc testing was used for statistical analysis in **(A)**. *Unpaired student t-test* was used for statistical analysis (**B-E**). The values are represented as mean ± SE, **p <0.05. ns: not significant.*

3.3.3 Choline deficient diet feeding causes reduced body weight and fat mass gain but accelerates fatty liver in B6129F1-*Enpp6*$^{-/-}$ mice

To address the question that whether dietary choline deficiency might exaggerate the improved metabolic profile in the *Enpp6*$^{-/-}$ mice, the metabolic consequences of B6129F1-*Enpp6*$^{-/-}$ and *Enpp6*$^{+/+}$ mice fed 7 weeks of HFD, followed by a CDHFD (0% choline) for a further 2-week of feeding were then tested.

This study showed that two genotypes of mice consumed similar amount of CDHFD (Figure 3.6D). Although the B6129F1-*Enpp6*$^{-/-}$ mice exhibited comparable body weights with B6129F1-*Enpp6*$^{+/+}$ mice at the end of study (Figure 3.6A), body weight gain and fat mass gain were significantly blunted by CD in the B6129F1-*Enpp6*$^{-/-}$ mice relative to the B6129F1-*Enpp6*$^{+/+}$ mice (Figure 3.6B-C). The relative reduction in fat mass gain in CDHFD-fed B6129F1-*Enpp6*$^{-/-}$ mice was manifested in significantly reduced subcutaneous fat mass but maintained comparable intra-abdominal visceral fat mass compared to B6129F1-*Enpp6*$^{+/+}$ mice (Figure 3.6E). Short-term dietary choline deficiency resulted in significantly reduced total choline levels in the kidney and brain, and showed a trend for lower levels in liver *(p*=0.06) of B6129F1-*Enpp6*$^{-/-}$ mice compared to the B6129F1-*Enpp6*$^{+/+}$ mice (Figure 3.6F).

Unexpectedly, after HFD feeding, B6129F1-*Enpp6*$^{-/-}$ mice exhibited comparable blood glucose levels during the GTT relative to *Enpp6*$^{+/+}$ mice (Figure 3.7A), which is not consistent with our previous findings (Figure 3.5A). Glucose tolerance was not affected by short-term dietary choline deficiency in the HFD-fed B6129F1-*Enpp6*$^{-/-}$ mice (Figure 3.7B). In addition, HFD-fed B6129F1-*Enpp6*$^{-/-}$ and *Enpp6*$^{+/+}$ mice displayed comparable fasting insulin levels after short-term dietary CD (Figure 3.7C). However, after exposure to dietary CD, HFD-fed B6129F1-*Enpp6*$^{-/-}$ exhibited increased liver triglyceride levels (Figure 3.7E) with no gross alteration in circulating triglycerides levels

(Figure 3.7D), without histologically gross difference in liver lipid content accumulation (Figure 3.7F-G).

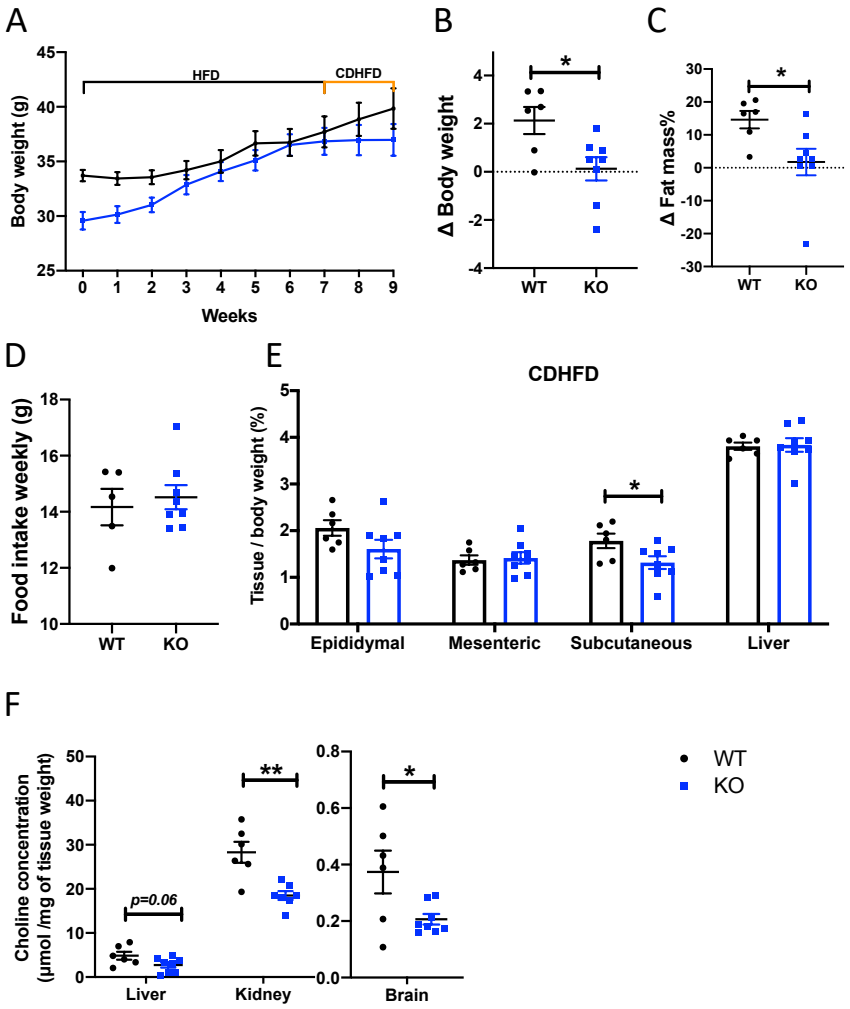

Figure 3.6 B6129F1-*Enpp6*$^{-/-}$ mice gain less and body fat and exhibited lower choline levels compared to *Enpp6*$^{+/+}$ mice. (A) Body weight of B6129F1-*Enpp6*$^{-/-}$ mice (KO) and *Enpp6*$^{+/+}$ (WT) mice during 7 weeks of HFD and 2 weeks of CDHFD, KO (n=8) and WT (n=6). **(B)** Total body weight and **(C)** fat mass gain during the CDHFD feeding KO (n=8) and WT (n=6). **(D)** Food intake during the CDHFD feeding KO (n=8) and WT (n=5). After 2 weeks of CDHFD feeding, **(E)** tissue weight (as a percentage of whole-body weight), KO (n=8) and WT (n=6) and **(F)** Total choline level in tissues, KO (liver and brain: n=8, kidney: n=7) and WT (n=6 for all tissues). Outlier data caused by technically error were removed from analysis after assessing by outlier test (GraphPad 8.0). 2-way ANOVA with Bonferroni post-hoc testing was used for statistical analysis in **(A)**. *Unpaired student t-test* was used for statistical analysis (**B-F**). The values are represented as mean ± SE, **p <0.05.**p <0.01.*

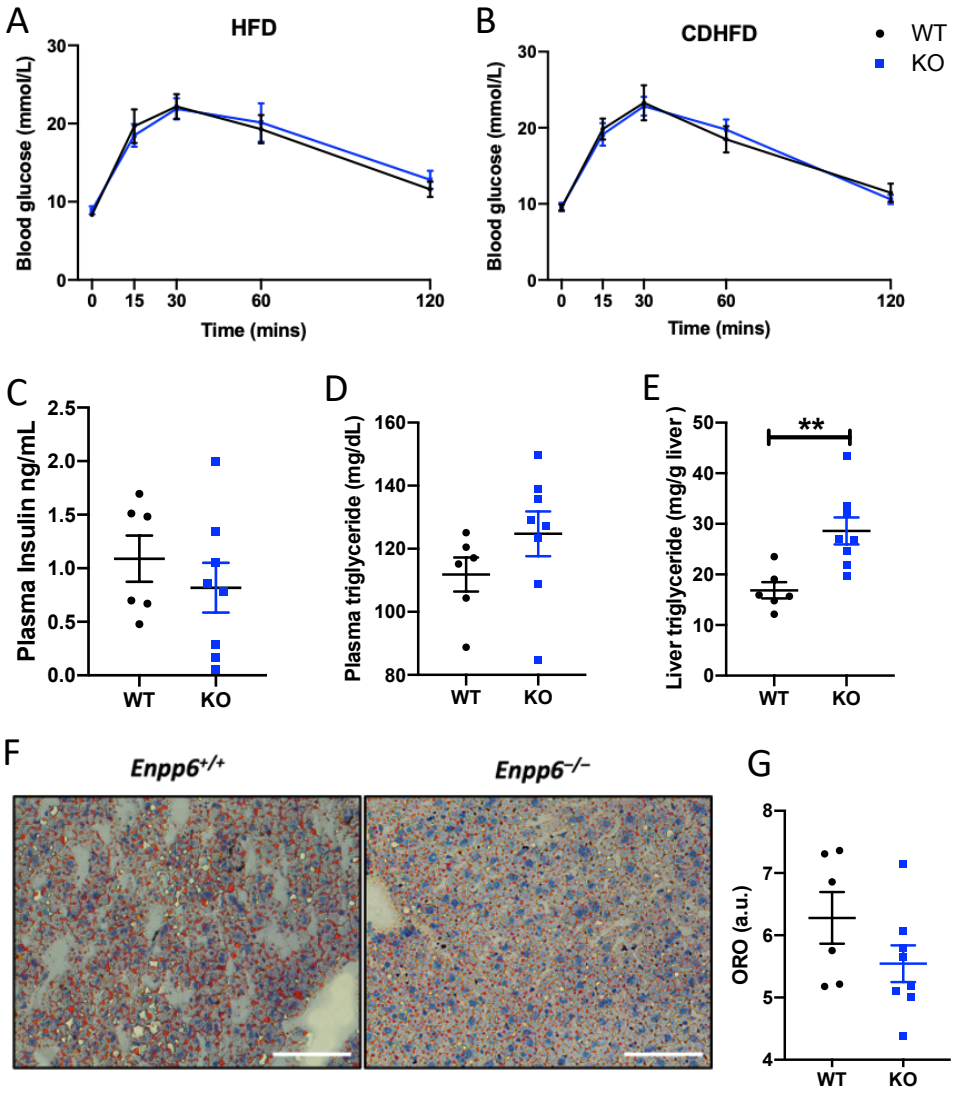

Figure 3.7 Choline deficiency did not further improve glucose tolerance but caused fatty liver in HFD-fed B6129F1-*Enpp6*$^{-/-}$ mice. Blood glucose during the GTT were measured in B6129F1-*Enpp6*$^{-/-}$ (KO) mice and *Enpp6*$^{+/+}$ (WT) mice after 7 weeks of HFD and a further 2-week of CDHFD feeding, KO (n=8) and WT (n=6). **(A)** Blood glucose level after HFD and **(B)** Blood glucose level after the CDHFD feeding. Plasma fasting insulin, fasting plasma and liver triglycerides levels were measured after the CDHFD feeding: **(C)** plasma insulin level; **(D)** circulating fasting triglycerides level and **(E)** liver triglycerides level; **(F)** Representative micrographs of oil red O-stained liver (left lobe). Scare bar= 100 µm. **(G)** Quantitative analysis of lipid accumulation. 2-way ANOVA with Bonferroni post-hoc testing was used for statistical analysis in **(A-B)**. *Unpaired student t-test* was used for statistical analysis (**C-E and G**). The values are represented as mean ± SE, ***p <0.01.*

3.3.4 Reduced hepatic choline levels in *Enpp6*$^{-/-}$ mice are associated with lower phosphatidyletholamine N-methyltransferase (PEMT) expression in *de novo* phosphatidyl choline biosynthesis pathway

We have shown ENPP6 deficiency results in reduced hepatic choline levels after HFD feeding. This led us to explore whether ENPP6 deficiency suppresses hepatic phosphatidylcholine (PC) biosynthesis, the major source of choline (182). Thus, gene expression profiles of two hepatic PC biosynthesis pathways, *de novo* PC biosynthesis and the CDP-choline pathway were compared (Figure 3.8A), between B6129F1-*Enpp6*$^{-/-}$ and *Enpp6*$^{+/+}$ mice. Our previous data showed that ENPP6 deficiency resulted in downregulated mRNA level of *Pemt* (Figure 3.8B, data obtained from Katharina Schraut, PhD thesis in 2017) (142), that encodes the key enzyme of PC *de novo* biosynthesis via methylation of phosphatidylethanolamine (PE). It was shown that this expression profile was maintained after HFD intervention (Figure 3.8C). However, reduced *Pemt* mRNA level in B6129F1-*Enpp6*$^{-/-}$ mice was reversed by dietary choline supplementation (Figure 3.8D). ENPP6 deficiency also caused a significant decrease in hepatic expression of choline/ethanolamine phosphotransferase 1 (CEPT1) mRNA, the enzyme responsible for the final step of CDP-choline pathway, in parallel with the CDP-ethanolamine pathway, for PC and PE synthesis, respectively (Figure 3.8B). However, the difference in hepatic *Cept1* mRNA level between B6129F1-*Enpp6*$^{-/-}$ mice and *Enpp6*$^{+/+}$ mice was eliminated by HFD intervention (Figure 3.8C). ENPP6 deficiency did not change the mRNA level of choline phosphate cytidylyltransferase 1A (PCYT1A), the gene encoding the diacylglycerol choline phosphotransferase (CPT) enzyme which converts the phosphocholine to CDP-choline at the baseline (Figure 3.8B) and after HFD intervention (Figure 3.8C). However, choline supplementation caused a significant increase in hepatic expression of *Pcyt1a* mRNA in HFD-fed B6129F1-*Enpp6*$^{-/-}$ mice compared to *Enpp6*$^{+/+}$ mice (Figure 3.8D), the rate-limiting enzyme of PC biosynthesis by the CDP-choline pathway. ENPP6 deficiency did not alter the mRNA level of diacylglycerol O-Acyltransferase 2 (*Dgat2*) (Figure 3.8C-E), an enzyme

responsible for the final esterification step of diacylglycerol (DAG) to triglycerides (TAG) under HFD, or CSHFD, or CDHFD intervention. Furthermore, although it was shown that CDHFD-fed B6129F1-*Enpp6*$^{-/-}$ mice exhibited a phenotype of fatty liver, evidenced by the significantly increased liver triglycerides level with a comparable circulating triglycerides level compared to *Enpp6*$^{+/+}$ mice (Figure 3.7D-E), there were no significant effect of short-term dietary choline deficiency on hepatic mRNA levels of PC biosynthesis pathways between the two genotypes (Figure 3.8E). Taken together, the data suggests that ENPP6 deficiency impaired the PC *de novo* biosynthesis pathway by downregulating the *Pemt* mRNA level, and resulted in the decreased hepatic choline level. This is also evidenced by the fact that downregulated *Pemt* mRNA level caused by ENPP6 deficiency, was compensated by dietary choline supplementation.

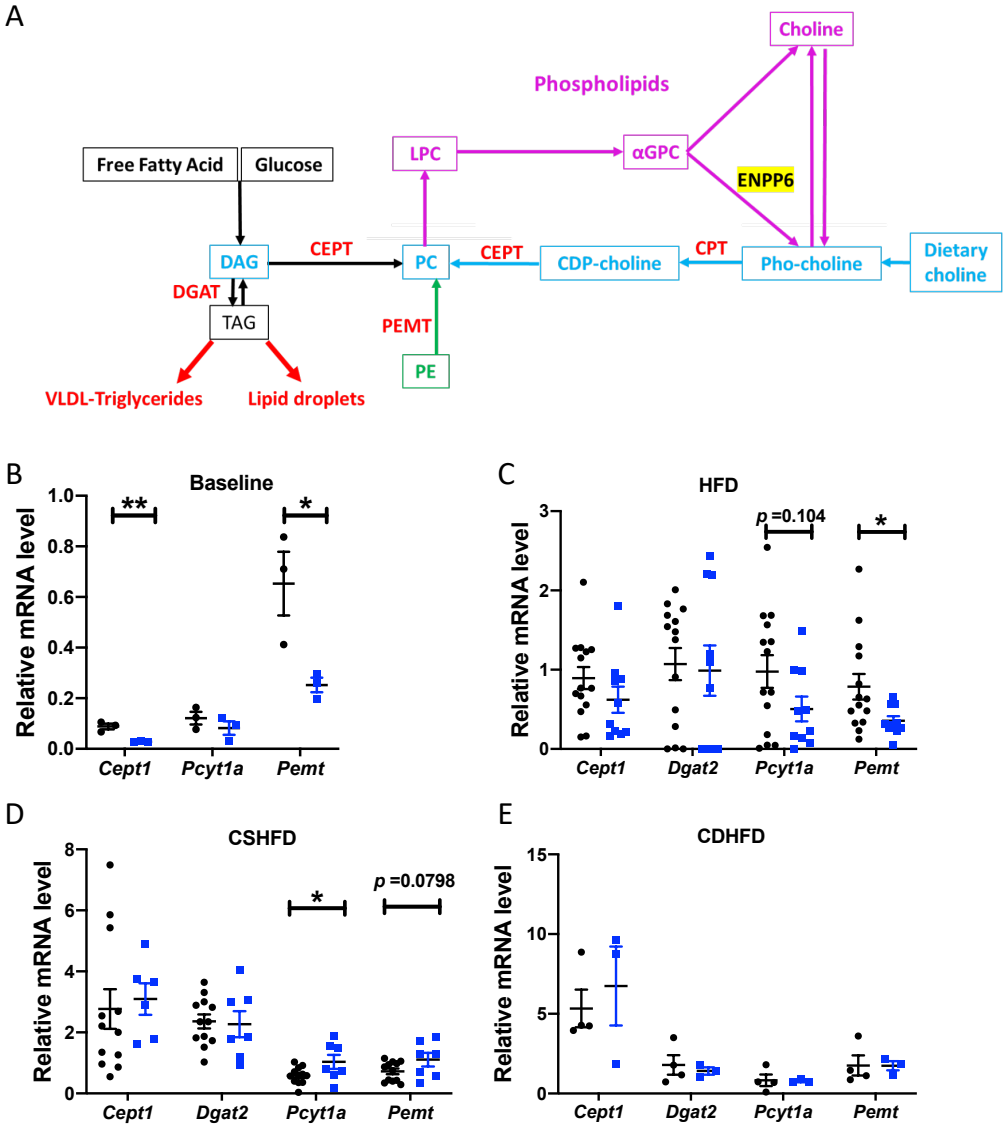

Figure 3.8 ENPP6 deficiency affects hepatic gene expression of fatty acid and phosphatidylcholine (PC) metabolism. (A) Simplified schematic pathway of ENPP6-choline-involved PC biosynthesis metabolism. The mRNA levels (normalised by the house-keeping gene *Tbp*) of hepatic enzymes in triglycerides and PC synthesis between B6129F1-*Enpp6*$^{-/-}$ mice and *Enpp6*$^{+/+}$ mice in different feeding interventions: **(B)** baseline (n=3 for each genotype), data obtained from K. Schraut PhD thesis 2017 (142); **(C)** HFD, KO (n=10) and WT (n=14); HFD with short-term **(D)** CSHFD, KO (n=12) and WT (except from *Cept1*: n=6, others: n=7) or **(E)** CDHFD, KO (n=3) and WT (n=4). Hepatic genes expression: *Pcyt1a*, *Dgat2, Pemt and Cept1*. The expression of housekeeping gene *Tbp* does not significantly change among individual samples and two genotype groups. *Unpaired student t-test* was used for statistical analysis. The values are represented as mean ± SE, **p<0.05, **p <0.01.*

3.4 Discussion

This chapter focused on mapping the metabolic profile of mice lacking *Enpp6*, on a mixed strain background (C57BL/6J and 129S6) and investigating its underlying mechanisms.

Combined with the previous data (Katharina Schraut, PhD thesis in 2017) (142), this study firstly reported an improved metabolic phenotype of B6129F1-*Enpp6*$^{-/-}$ mice when exposed to HFD. These mice displayed selectively reduced visceral adiposity and visceral adipose hypertrophy, improved glucose tolerance and were protected from hepatic steatosis. Furthermore, the data support the initial hypothesis of this study: *Enpp6*$^{-/-}$ mice had a choline-deficient-like phenotype, which protected them from diet-induced obesity and diabetes. This study showed that ENPP6 deficiency impaired phosphatidylcholine *de novo* biosynthesis by downregulating the *Pemt* expression, and decreased hepatic choline levels, suggesting the improved phenotype of *Enpp6*$^{-/-}$ mice associates with reduced hepatic choline levels. This conclusion is also evidenced by the fact that dietary choline supplementation reversed the improved metabolic phenotype of *Enpp6*$^{-/-}$ mice, in parallel with restored hepatic *Pemt* expression. Also, we found dietary CD did not augment the improved phenotype of HFD-fed *Enpp6*$^{-/-}$ mice, instead it induced an increase on liver fat accumulation to a greater extent in *Enpp6*$^{-/-}$ mice. To conclude, ENPP6 deficiency prevents the HFD-induced metabolic diseases by reducing the endogenous hepatic choline level.

3.4.1 *Enpp6*$^{-/-}$ mice are selectively protected from HFD-induced visceral obesity and fatty liver

ENPP6 was recently identified as a marker of newly formed oligodendrocytes (169, 170, 302). Although there have been some investigations of its function in the central nervous system (Chapter 5), the roles of ENPP6 in other organs and specifically those involved in metabolism, are largely unexplored. Building upon evidence from the preliminary human genetics data on visceral adiposity associations in our group and other recently identified metabolic roles for

ENPP6 in hepatic lipid accumulation (165), we aimed to understand its precise functions in the context of obesity and related metabolic diseases.

In this chapter, to support the evidence for reduction in the visceral adiposity, the visceral adipocyte size and number were further investigated from HFD-fed B6129F1-*Enpp6*$^{-/-}$ mice and *Enpp6*$^{+/+}$ littermates. In the obese state, adipose tissue significantly increases triacylglycerol content to enlarge the lipid droplet size, resulting in adipose tissue expansion; also known as adipose hypertrophy (170). Increasing adipocyte size is associated with a wide range of metabolic conditions including insulin resistance (303, 304) and adipose tissue lipolysis (305-307). The present study showed a selective reduction of visceral adiposity and visceral adipose hypertrophy in *Enpp6*$^{-/-}$ mice, suggesting ENPP6 deficiency results in the alteration of fat distribution. Reduced visceral but not subcutaneous adipocyte hypertrophy suggests a specific effect of *Enpp6* deficiency to alter fat distribution. Indeed, we have shown that there is evidence for white fat browning, the conversion of white adipocytes to lipid burning brown adipocytes, in B6129F1-*Enpp6*$^{-/-}$ mice (142). This is consistent with altered sympathetic drive from the brain to increase fat depot innervation and activation through the adrenergic beta3-adrenoreceptor (308-310), potentially linking brain ENPP6 activity and peripheral adipose tissue effects. Inhibition of visceral fat hypertrophy in HFD-fed *Enpp6*$^{-/-}$ mice is also consistent with improved glucose homeostasis. Several studies over the years have demonstrated that glucose homeostasis is highly associated with visceral obesity (21, 80, 85, 86, 92, 93). Regarding the influence of regional deposition of adipocyte hypertrophy, Fang *et al.* reported that visceral (omentum or mesentery) adipocytes are smaller than those from subcutaneous fat depots and are strongly associated with the presence of type 2 diabetes (311). Other studies reported that in obese humans and animals, hypertrophic visceral adipocytes, rather than subcutaneous adipocytes, act as a critical predictor of insulin resistance (306, 312). In summary, the present data support a depot-selective effect of ENPP6 deficiency in obesity and lacking ENPP6 is beneficial from visceral obesity-induced glucose intolerance. However, the lack of visceral fat gain in the HFD-fed B6129F1-*Enpp6*$^{-/-}$ mice

is not due to increased energy expenditure or food intake (142). In the adipose tissue, glucose uptake is insulin dependent. When insulin level drops or is absent, the adipocyte generates free fatty acid as an alternative energy source (ATP) through multiple hormone-regulated lipolytic action. Although we did not see any difference in insulin levels between the B6129F1-*Enpp6*$^{-/-}$ mice and their controls, we cannot exclude the effects of ENPP6 on lipolysis. ENPP6 deficiency might promote lipolysis by differentially affecting lipolytic stimuli such as adrenergic innervation by either activating this selectively through its effects on the brain-adipose nervous system or by altering systemic factors that predominantly affect visceral adipocytes.

Apart from reduced visceral adiposity and improved glucose tolerance, our data also showed that B6129F1-*Enpp6*$^{-/-}$ mice were protected from hepatic steatosis, evidenced by reduced liver triglycerides level, reduced liver weight, and decreased liver lipid accumulation by a qualitative histological assessment. Although the pathogenesis of hepatic steatosis or NAFLD, is not completely clear, growing evidence appears to suggest that obesity and diabetes are the critical contributors (313). As obesity causes the excess body fat, which progressively alters the lipid metabolism by delivering elevated fatty acid to the liver, and thus resulting in excess triglycerides (313, 314). Moreover, Thomas *et al.* used ^{1}H MRS (Proton magnetic resonance spectroscopy) to assess the relationship between IHCL accumulation and total body adipose tissue content/distribution. Their results suggest that hepatic steatosis appears to be closely related to body adiposity, especially central obesity (315). Therefore, the reduced visceral obesity and improved glucose tolerance by ENPP6 deficiency might also contribute to the protection from HFD-induced hepatic steatosis. However, this result is in contrast to Morita *et al.* who claimed an increasing liver lipid accumulation in the chow fed C57BL/6J mice lacking the *Enpp6* gene, which was attributed to choline deficiency symptom. Notably, Morita *et al*. did not quantify the liver lipid level, instead relying on restricted liver histological assessment and qualitative lipid staining upon which they based their claim. Our quantitative and qualitative results of reduced liver lipid

accumulation, liver weight and reduced hepatic choline level together, strongly support ENPP6 deficiency as causal for fatty liver resistance. Even if we assume that the qualitative data of Morita *et al.* on the liver histology of the C57BL/6J-*Enpp6*$^{-/-}$ mice was applicable to the whole liver and consistently across the cohort of mice (n numbers were not specified in the study), then we would find a discrepancy with our study. There could be an explanation for this discrepancy: differences in the genetic strain used to study the *Enpp6* ablation. The *Enpp6*$^{-/-}$ mice used in our laboratory were based on a mixed genetic strain (C57BL/6J and 129S6), whereas the *Enpp6*$^{-/-}$ mice used in Morita's group were on the C57BL/6J background. Further investigation of the genetic strain effect on ENPP6-mediated metabolic profiles is described in detail in Chapter 4.

Moreover, ENPP6 deficiency in liver appears to contribute to beneficial metabolism. ENPP6 could possibly alter lipid export and selectively visceral fat depletion. As ENPP6 is also expressed in the liver sinusoidal endothelial cells aside from brain and kidney (165), further study can focus on the role of ENPP6 in this cell type and how this connects to metabolism.

3.4.2 ENPP6 deficiency reduces the endogenous choline level

This chapter also asked the question of whether the beneficial metabolic phenotype observed in HFD-induced B6129F1-*Enpp6*$^{-/-}$ mice was due to attenuated choline production and availability. Choline is considered an essential dietary component, but the effect of choline deficiency on energy metabolism is controversial. On one hand, choline deficiency causes liver and muscle damage, increased risks for heart diseases, impaired foetal development and brain function (e.g. lifelong memory and learning defects) (295, 296). On the other hand, several studies have shown that choline deficiency protected diet- or genetic defect-induced obese mice from increased body fat and hyperglycaemia (209, 211, 298, 316). Jacobs *et al.* showed that choline deficiency significantly attenuated HFD-induced increased body weight and visceral fat in mice lacking the *Pemt* gene (encoding the PEMT enzyme responsible for *de novo* biosynthesis of PC) (209). Wu *et al.* reported that dietary choline deficiency significant reduced fat mass in the *ob/ob* mice compared to choline-supplemented *ob/ob* mice (316). Moreover, Rubio-Aliago *et al.* found that HFD-fed C57BL/6J mice exhibited an increased hepatic choline level. Based on these observations, it was hypothesised that ENPP6 deficiency resulted in endogenous hepatic choline deficiency, and thus mice were protected from HFD-induced metabolic diseases. Indeed, our results confirmed it by clearly showing a significant decrease of hepatic choline level in HFD-fed B6129F1-*Enpp6*$^{-/-}$ mice, with the lack of difference between chow-fed B6129F1-*Enpp6*$^{-/-}$ mice and *Enpp6*$^{+/+}$ mice. The comparable choline level between chow-fed B6129F1-*Enpp6*$^{-/-}$ mice and *Enpp6*$^{+/+}$ mice is also consistent with the previous finding (165). This could be explained by the internal compensation of choline balance by multiple choline providers and routes such as PC biosynthesis via CDP-choline or *de novo* PEMT pathway, PE biosynthesis via CDP-ethanolamine pathway. For example, our data showed that a significant decrease of *Pemt* mRNA level in the HFD-fed B6129F1-*Enpp6*$^{-/-}$ mice, suggesting that ENPP6 deficiency impaired *de no* PC synthesis, thus inhibiting the hepatic choline production. This result is in line with a previous study from Jacobs *et al*. who reported an

anti-obesity phenotype of *Pemt* knockout mice after HFD feeding. They suggest that impaired choline availability is responsible for the phenotype *Pemt* $^{-/-}$ mice, indicating the PEMT deficiency results in the reduced choline production. Moreover, the current study showed chow-fed B6129F1-*Enpp6*$^{-/-}$ mice had decreased *Pemt* mRNA levels but exhibited a comparable phenotype compared to the controls. This result can also be supported by the findings from Jacob *et al.* According to their study, the improved metabolic phenotype *Pemt*$^{-/-}$ mice was only observed after HFD feeding but not under the chow feeding circumstance.

Together, it suggests that ENPP6 deficiency does not alter the endogenous choline level, in parallel with no alteration of metabolism under the normal feeding circumstance (chow-diet feeding). However, ENPP6 deficiency resulted in the reduction of hepatic choline level when local choline availability is affected by the pathological condition (HFD-induced obesity). Rubio-Aliaga *et al.* found that HFD feeding resulted in an elevated hepatic choline level in C57BL/6J mice. Thus, excessive hepatic choline level might be the contributor to HFD-induced impaired metabolic phenotypes. This could possibly explain why the feature of hepatic choline-deficiency in *Enpp6*$^{-/-}$ mice can defend themselves against HFD challenging. The feature of choline-deficient-phenotype of HFD-fed B6129F1-*Enpp6*$^{-/-}$ mice can also be evidenced by the fact that short-term dietary choline supplementation reversed the reduction in epididymal visceral fat and liver weight gain in HFD-fed B6129F1-*Enpp6*$^{-/-}$ mice.

Moreover, apart from the reduced hepatic choline levels in HFD-fed B6129F1-*Enpp6*$^{-/-}$ mice, there was a weak effect of reduction in kidney choline levels in HFD-fed B6129F1-*Enpp6*$^{-/-}$ mice (Figure 3.4B). This could be due to the lower statistical power that reduces the chance of detecting a true effect. As mentioned in the power calculation (Chapter 2.11), a group size of n=11 is required to achieve a confident statistical analysis. Given the cost limitation, the choline level measurement in kidney was only achieved biological

replication of 5 mice for KO group. In the future, increasing the power for this measurement should be considered.

To better understand the impact of ENPP6 deficiency in liver lipid metabolism, measuring the levels of phospholipids and their metabolites such as PC, LPC, PE, CDP-choline, and PhoC using mass spectrometry would be useful for future studies.

3.4.3 Short-term dietary choline deficiency reduces body fat gain but causes fatty liver

To further investigate whether the improved metabolic profile of B6129F1-*Enpp6*$^{-/-}$ mice was due to the choline-deficiency-like phenotype, both genotypes of *Enpp6* mice were fed on HFD and followed by a short-term dietary choline-free HFD. It was hypothesised that choline deficiency would exaggerate the beneficial phenotype of HFD-fed B6129F1-*Enpp6*$^{-/-}$ mice.

In contrast to endogenous choline deficiency caused by *Enpp6* ablation, dietary choline deficiency appears to play a different anti-obesity role with a risk of hepatic steatosis. Instead of reducing selectively visceral adiposity without affecting the whole-body weight, dietary choline deficiency resulted in a significant decrease in HFD-induced whole-body gain. We excluded the possibility that blunted weight gain could have been associated with alterations in food consumption. Elsewhere it has been demonstrated that choline deficiency did not influence food consumption (210, 317). There are the possibilities that choline deficiency might enhance energy expenditure, or upregulated the UCP1 in brown adipose tissue (318), or enhance the expression of other browning markers in WAT, which can potentially result in reduced body weight gain and total body fat mass gain in B6129F1*Enpp6*$^{-/-}$ mice. In particular, reduction of subcutaneous adiposity rather than visceral adiposity in the B6129F1-*Enpp6*$^{-/-}$ mice relative to *Enpp6*$^{+/+}$ mice, suggesting that subcutaneous adiposity is the ‘first-to-go’ fat reduction by dietary choline deficiency and the visceral adiposity is more preserved than subcutaneous in CDHFD-fed *Enpp6*$^{-/-}$ mice. These ‘more preserved’ visceral adipocytes are more proinflammatory (319) and less affected by short-term dietary choline deficiency. This result also highlights the significant difference in the reduction in the type of adiposity (visceral *verse* subcutaneous) between ENPP6 ablation-induced endogenous choline deficiency and diet-induced choline deficiency. Thus, without improving the reduction of proinflammatory visceral adiposity, along with no external supply of choline, we showed that B6129F1-*Enpp6*$^{-/-}$ mice did not perform improved glucose tolerance but suffered more

from hepatic steatosis. Notably, although we reported the hepatic steatosis phenotype of CDHFD-fed B6129F1-*Enpp6*$^{-/-}$ mice as a result of a significant decrease in liver triglycerides levels without alteration in circulating triglycerides. There was no difference between two genotypes in the histological assessment of liver lipid accumulation. In parallel, we observed the significant reduction of the total choline levels in kidney and brain in CDHFD-fed B6129F1-*Enpp6*$^{-/-}$ mice compared to *Enpp6*$^{+/+}$ mice, but not in the liver (p = 0.06). This could potentially match the lack of difference in histological fatty liver.

The other explanations for no further improvement in metabolism of HFD-induced B6129F1-*Enpp6*$^{-/-}$ mice might be the difference in feeding duration of CDHFD and animal models. Several *in vivo* studies have demonstrated that choline deficiency is beneficial to energy metabolism (209, 211, 298, 316). However, Raubenheimer. P.J *et al.* reported that dietary choline deficiency did not affect body or adipose depots weights in HFD-fed C57BL/6J mice (211). The difference may be explained by the different feeding periods and animal models. In Raubenheimer's study, a relatively short-term dietary choline deficiency (4 weeks) did not cause a significant alteration in body weight or body fat. However, in Wu's study, long-term study (8 weeks) dietary choline deficiency caused reduced body fat gain in the *ob/ob* mice compared to choline supplemented dietary. In the present study, mice lacking *Enpp6* gene were fed a short-term (2 weeks) dietary choline-free HFD. Short-term dietary choline deficiency might not be sufficient to trigger the alteration of metabolism. Moreover, mouse models with genetic defects were used in Jacobs's and Wu's studies whereas wild-type C57BL/6J mice were used in Raubenheimer's study. Thus, we suggest that the specific gene that was mutated may impact choline metabolism independently of diet, thus resulting in the different outcomes.

Chapter 4 The metabolic profile of mice lacking *Enpp6* gene is strain dependent

4.1 Introduction

In Chapter 3, an improved metabolic profile of B6129F1-*Enpp6*$^{-/-}$ mice in response to high fat diet (HFD)-induced obesity, hyperglycaemia and hepatic steatosis was described. Notably, B6129F1-*Enpp6*$^{-/-}$ mice were generated and maintained as a mixed strain background (C57BL/6J and 129S6) in our laboratory. To better understand functions and mechanisms of ENPP6, we aimed to produce a robust and reproducible *Enpp6*$^{-/-}$ mouse model with metabolic characteristics more widely comparable to parameters described by the wider scientific community. We thus backcrossed our initial mixed strain (B6129F1-*Enpp6*$^{-/-}$) to the C57BL/6J strain. The C57BL6J strain is commonly used as a mouse model for diet-induced obesity (320, 321). These mice are prone to exhibit obesity, glucose intolerance (322, 323), insulin resistance (324) and hypertension (320, 325) when exposed to HFD compared to many other commonly used mouse strains such as C57BLKS/J (326, 327), DBA (328-330), FVB/N (330), and 129T2 (328).

By ruling out the potential effect of genetic background, *Enpp6*$^{-/-}$ mice and their *Enpp6*$^{+/+}$ controls will essentially differ only with respect to the *Enpp6* gene, removing the influence of confounding, strain dependent, genetic modifiers. Thus, in this chapter, HFD-induced metabolic response of global *Enpp6*$^{-/-}$ mice on an enriched C57BL/6J strain context was assessed.

Additionally, ENPP6 was shown to be highly expressed in the brain in newly formed oligodendrocytes (NFOs) (165, 169, 172). However, whether brain ENPP6 is involved in metabolic regulation is unknown. This chapter also addressed this question by assessing the metabolic consequence of a brain (oligodendrocyte precursor cell, OPC)-specific *Enpp6* knockdown mouse model: *Pdgfrα-Cre*$^{+}$*Enpp6*$^{fl/fl}$, in response to HFD.

4.1.1 The brain regulates metabolism

Brain is recognised as the 'master control centre' of metabolism. Hypothalamus, in particular, is an essential site for regulating the metabolic control of energy expenditure, food intake and food preference behaviours (212-214). Moreover, several genes in the hypothalamus have been found to be strongly associated with obesity (213). In the arcuate nucleus of the hypothalamus, genes encoding the hunger signalling (orexigenic) neuropeptides: neuropeptide Y (NPY)/Agouti-related peptide (AgRP), and satiety signalling (anorexigenic) neuropeptide pro-opiomelanocortin (POMC), play important roles in the control of food intake and energy homeostasis. For example, POMC is processed to numerous bioactive peptide hormones including adrenocorticotropin releasing hormone (ACTH) which controls adrenal growth and function (215, 331, 332). POMC produces several peptides including the melanocortin α-Melanocyte-stimulating-hormone (α-MSH). α-MSH can bind to the melanocortin 3 and 4 receptors (MCR3 and MCR4), resulting in the inhibition of food intake and increase of energy expenditure (216, 217, 333), whereas NPY/AgRP acts as endogenous MCR3/MCR4 antagonists, stimulating food intake and decreasing energy expenditure (334).

Another example of a recently discovered mechanism of hypothalamic energy balance regulation is the transcription factor SIM1, which is highly expressed in the paraventricular nucleus of the hypothalamus (133). Lack of *Sim1* neurons reduced energy expenditure and causes obesity (335); Michaud JL *et al.* showed that *Sim1* heterozygous mice developed early-onset obesity with increased linear growth, hyperinsulinaemia and hyperleptinaemia (133). Activation of FOXO1 in the hypothalamus led to increased food intake and body weight (218). All these pieces of evidence suggest a direct genetic link between the brain and metabolic control.

4.1.2 Oligodendrocyte-involved regulation in metabolism

The central nervous system (CNS) plays a cruial role in energy homeostasis. The arcuate nucleus in the hypothalamus is a key region for regulating food intake and energy expenditure (336, 337). Several studies have shown that non-neuronal cells such as glial cells also regulate mechanisms of appetite and energy balance (see Chapter 1.7.4). However, whether oligodendrocytes are involved in energy homeostasis has not been fully explored. Djogo *et al.* showed that ablation of NG2-glial cells (also referred to as OPCs) in the hypothalamus (particularly in the median eminence region) led to obesity related to a reduced leptin responsiveness, suggesting adult OPCs are required for normal leptin sensitivity and body weight control (279). Furthermore, Chang *et al.* showed that NG2-null mice exhibited an obese phenotype due to disruption of brown fat (which burns energy and produces heat) dependent energy homeostasis (278). Ou *et al.* showed that oligodendrocytes regulate energy metabolism through G-protein-coupled receptor (GPR17)-cyclic adenosine monophosphate (cAMP)-lactate signalling (271). However, more evidence is required to better understand the mechanism and roles of OPCs and oligodendrocytes on energy homeostasis.

ENPP6 is not in expressed fat cells where genes that influence fat distribition have been predoiminantly identified (338). Given the clear selective reduction in visceral fat, and improved metaboic profile (Chapter 3), it was reasoned that ENPP6 activity in the NFOs might influence metabolic parameters through its effects on brain/hypothalamic pathways that regulate energy balance. Deletion of the *Enpp6* gene in the NFO would provide a more targeted way to assess this possibility. Therefore, an OPC-specific *Enpp6* knockdown mouse model: *Pdgfrα-Cre*$^{+}$*Enpp6*$^{fl/fl}$, on a mixed C57BL/6N (*Enpp6*$^{fl/fl}$) and C57BL/6J (*Pdgfrα-Cre*) genetic background (details described in Chapter 2) was generated and the metabolic consequences in these mice characterised in response to HFD.

4.1.3 Hypothesis and aims

Hypothesis: OPC-specific *Enpp6* gene deletion protects against visceral obesity and diabetes in mice.

Assumption: The improved metabolic profile of B6129F1-*Enpp6*$^{-/-}$ mice would be replicated in the standardised congenic C57BL/6J strain.

Aims:

1. To assess the metabolic phenotype of C57BL/6J-*Enpp6*$^{-/-}$ mice fed on a 7-week of HFD.

2. To determine whether OPC-specific *Enpp6* gene knockdown mediates the protection in mice from HFD-induced visceral obesity and diabetes.

4.2 Experimental design

4.2.1 Assessment of metabolic responses in HFD-fed C57BL/6J-*Enpp6*$^{-/-}$ and HFD-fed *Pdgfrα-Cre*$^{+}$*Enpp6*$^{fl/fl}$ mice

The flowchart of the experimental design for C57BL/6J-*Enpp6*$^{-/-}$ mice and their control littermates *Enpp6*$^{+/+}$ mice is shown in Figure 4.1A, and *Pdgfrα-Cre*$^{+}$*Enpp6*$^{fl/fl}$ (OPC-*Enpp6*$^{-/-}$) mice and their control littermates *Pdgfrα-Cre*$^{-}$ *Enpp6*$^{fl/fl}$ (control) mice in Figure 4.1B. Body weight, body composition (fat and lean mass) and food intake were recorded weekly. GTTs were performed at the baseline and after 7 weeks of HFD. All animals were given one week to recover before being culled. Animals were culled after a 4 hour-fasting. Adipose tissues, brain, liver, and kidney were dissected and weighed at the end of experiment.

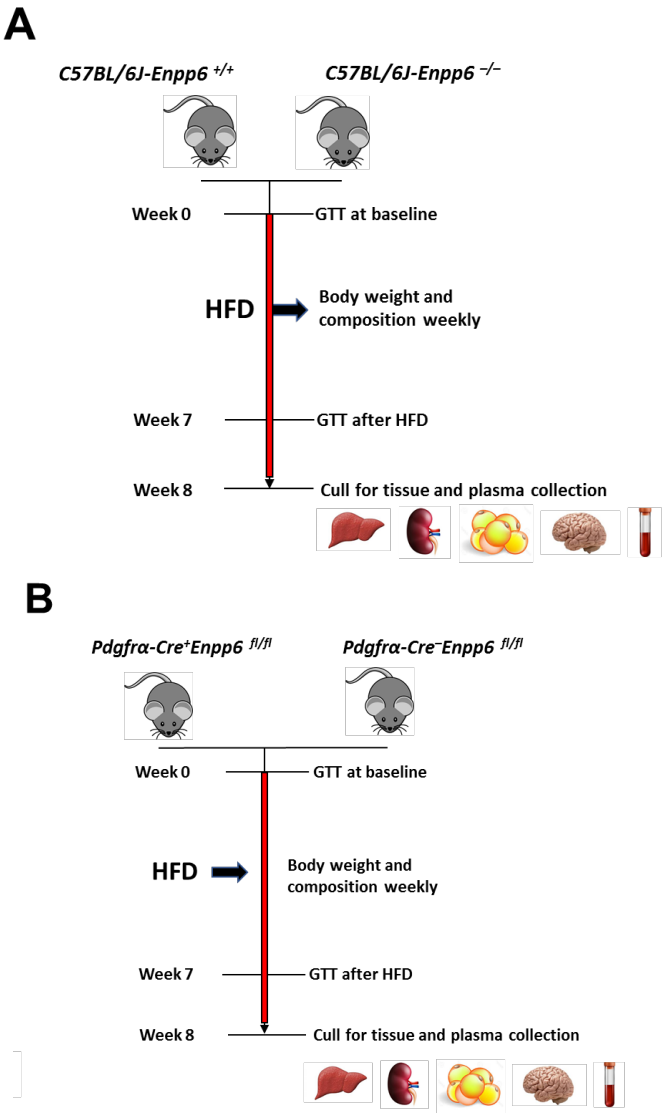

Figure 4.1 Experimental design of investigations into the metabolic profile of C57BL/6J-*Enpp6*$^{-/-}$ and *Pdgfrα-Cre*$^{+}$*Enpp6*$^{fl/fl}$ (CKO) mice. A 7-week HFD feeding regimen was matched to the previous work performed in B6129F1-*Enpp6*$^{-/-}$ mice. Mice were given *ad libitum* access to diets. **(A)** C57BL/6J-*Enpp6*$^{+/+}$: n=10 and *Enpp6*$^{-/-}$: n=10. **(B)** CKO: n=4 and control *Pdgfrα-Cre*$^{-}$*Enpp6*$^{fl/fl}$ mice: n=4 per genotype. *2-way ANOVA with Bonferroni post-hoc testing* was used for statistical analysis in body weight, fat and lean mass, glucose tolerance and insulin levels. *Unpaired student t-test* was used in tissue weight; percentage of body weight gain; fasting circulating insulin levels; liver and plasma triglycerides assessment between the genotypes.

4.3 Results

4.3.1 C57BL/6J-*Enpp6*$^{-/-}$ mice exhibit HFD-induced obesity and hyperinsulinaemia

During HFD feeding, C57BL6J-*Enpp6*$^{-/-}$ mice exhibited significantly increased body weight (Figure 4.2A). After HFD feeding, C57BL6J-*Enpp6*$^{-/-}$ and *Enpp6*$^{+/+}$ mice gained 41.53±1.598% and 28.79±1.443% of total body weight, respectively (Figure 4.2B). HFD-fed C57BL6J-*Enpp6*$^{-/-}$ mice also had significantly larger amount of fat mass (Figure 4.2C) without any difference in lean mass (Figure 4.2D) compared to *Enpp6*$^{+/+}$ controls at the baseline and throughout the HFD feeding period. The two groups of mice consumed similar amounts of food (Figure 4.2E). HFD-fed C57BL6J-*Enpp6*$^{-/-}$ mice exhibited significantly reduced the brain weight compared to the *Enpp6*$^{+/+}$ controls (Figure 4.3A), without altering other tissue weights (Figure 4.3A). When looked into the whether the tissue weights changed as a percentage of the individual total body weight, our data showed that HFD-fed C57BL6J-*Enpp6*$^{-/-}$ mice exhibited reduced brown adipose depots weight percentage and increased subcutaneous and mesenteric fat mass percentage, but maintained comparable epididymal fat mass percentage compared to the *Enpp6*$^{+/+}$ mice; HFD-fed C57BL6J-*Enpp6*$^{-/-}$ mice also displayed slightly reduced brain and liver weight percentage but comparable kidney weight percentage relative to their controls (Figure 4.3B). To assess whether *Enpp6* deficiency in the C57BL/6J strain improved HFD-induced glucose intolerance and insulin resistance, A GTT was performed in C57BL/6J- *Enpp6*$^{-/-}$ and *Enpp6*$^{+/+}$ controls. There was no difference in blood glucose levels during GTT between chow-fed C57BL/6J-*Enpp6*$^{-/-}$ and *Enpp6*$^{+/+}$ mice at baseline (Figure 4.4A). Although C57BL/6J-*Enpp6*$^{-/-}$ mice were more obese, no significant difference was observed in glucose homeostasis after HFD between C57BL/6J-*Enpp6*$^{-/-}$ and *Enpp6*$^{+/+}$ controls (Figure 4.4B). Interestingly, the insulin levels at the baseline, during GTT were significantly higher in C57BL/6J-*Enpp6*$^{-/-}$ mice compared to *Enpp6*$^{+/+}$ controls; fasting insulin concentration was 44.73% higher than in controls (Figure 4.4C). After HFD, the fasting insulin level markedly increased in C57BL/6J- *Enpp6*$^{-/-}$ mice and was 124.07% higher than in *Enpp6*$^{+/+}$ controls

(Figure 4.4D). Furthermore, there was a trend of increased liver triglycerides levels in HFD-fed C57BL/6J-*Enpp6*$^{-/-}$ mice (p=0.0551; Figure 4.5A), with comparable levels of circulating plasma triglycerides (Figure 4.5B) compared to *Enpp6*$^{+/+}$ mice.

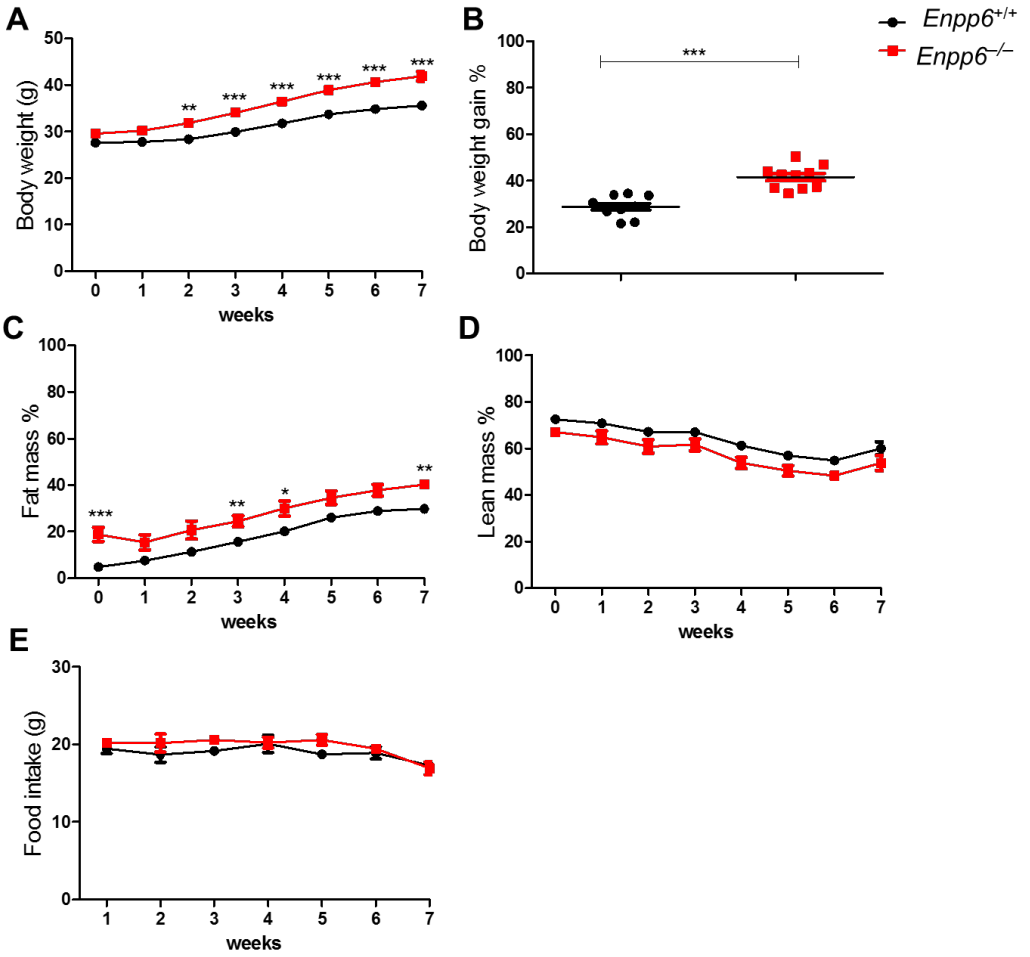

Figure 4.2 C57BL/6J-*Enpp6*$^{-/-}$ mice are more prone to HFD-induced obesity. (A) Whole body weight change during 7 weeks of HFD feeding. **(B)** Body weight gain percentages after HFD. **(C)** Fat mass as a percentage of total body weight during 7 weeks of HFD feeding. **(D)** Lean mass as a percentage of total body weight during 7 weeks of HFD. **(E)** Weekly food intake during 7 weeks of HFD feeding. n=10 per genotype. *2-way ANOVA with Bonferroni post-hoc testing* was used for statistical analysis in body weight, fat and lean mass and food intake. *Unpaired student t-test* was used in the percentage of body weight gain. Fat and lean mass percentage (n=10 per genotype for measurements in week 1, 3 and 7; n=6 per genotype for measurements in else weeks). The values are represented as mean ± SE, **p<0.05, **p<0.01, and ***p<0.001.*

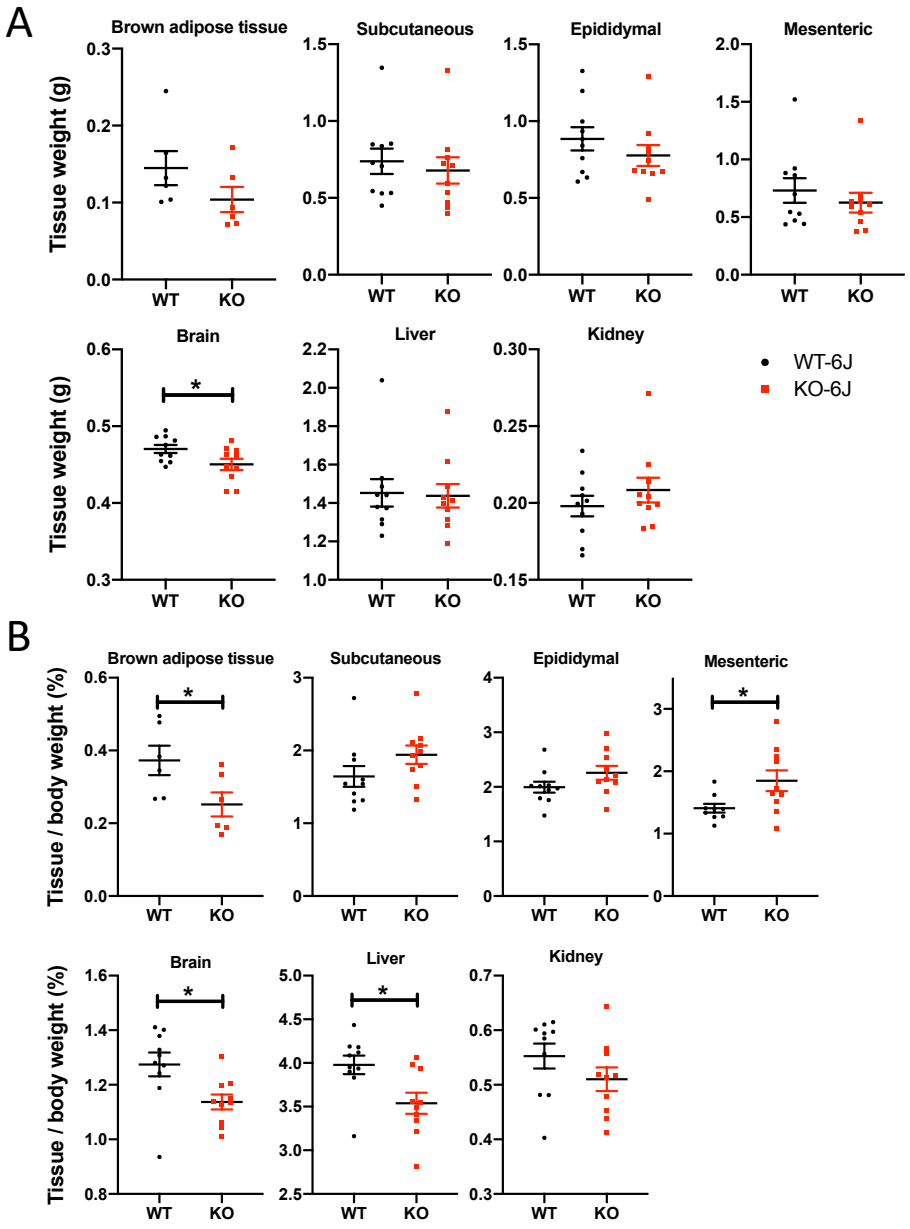

Figure 4.3 C57BL/6J-*Enpp6*$^{-/-}$ mice display increased adipose depots after HFD. Tissue weight expressed as absolute weight (A) and a percentage of total body weight **(B)** in the C57BL6J-*Enpp6*$^{-/-}$ (KO-6J) mice and *Enpp6*$^{+/+}$ (WT-6J) mice after 7 weeks of HFD: brown adipose tissue, n=6 per genotype; subcutaneous fat; visceral (epididymal) fat; visceral (mesenteric) fat, n=9 for WT-6J mice; brain; liver and kidney. n=10 per genotype for the statistical analysis (except from brown adipose tissue and WT-6J kidney). *Unpaired student t-test* was used for statistical analysis. The values are represented as mean ± SE, **p<0.05.*

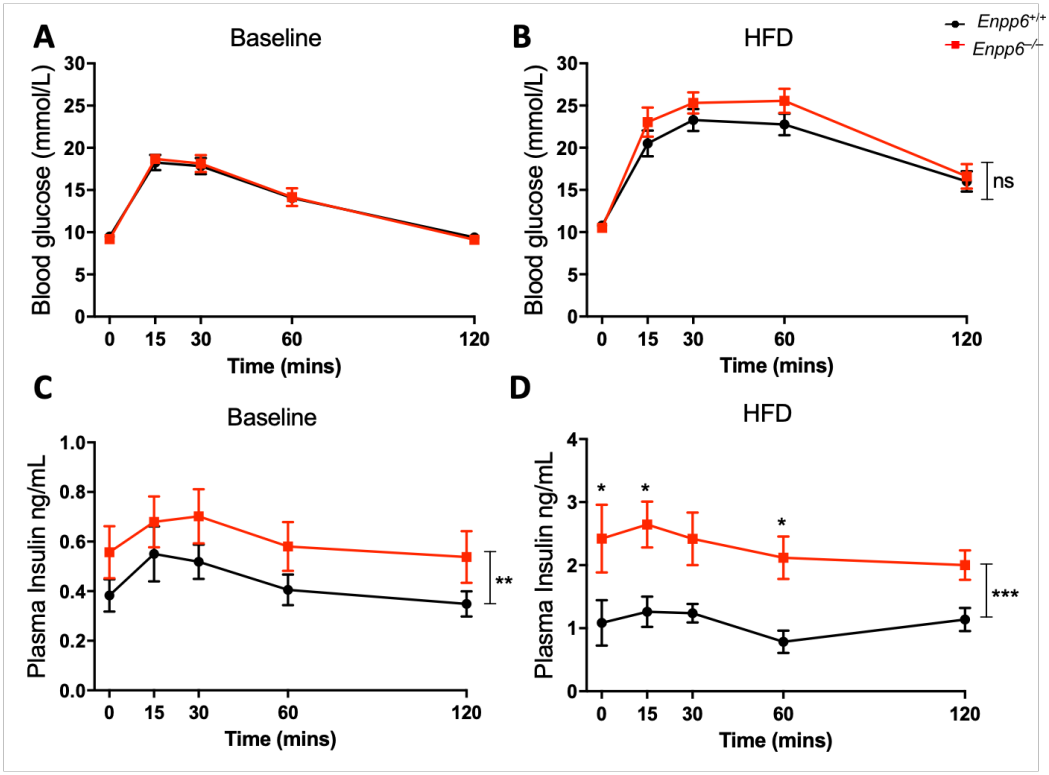

Figure 4.4 C57BL/6J-*Enpp6*$^{-/-}$ mice exhibit hyperinsulinaemia at baseline and after HFD. An i.p.GTT was performed by injecting glucose. Levels of circulating insulin during the GTT were analyzed by mouse insulin ELISA. **(A)** Baseline glucose level. **(B)** Glucose level after HFD feeding. **(C)** Baseline circulating insulin level. **(D)** Circulating insulin level after HFD feeding. n=10 per genotype. *2-way ANOVA with Bonferroni post-hoc testing* was used for statistical analysis in glucose and insulin levels. The values are represented as mean ± SE, **p<0.05, **p<0.01, and ***p<0.001.*

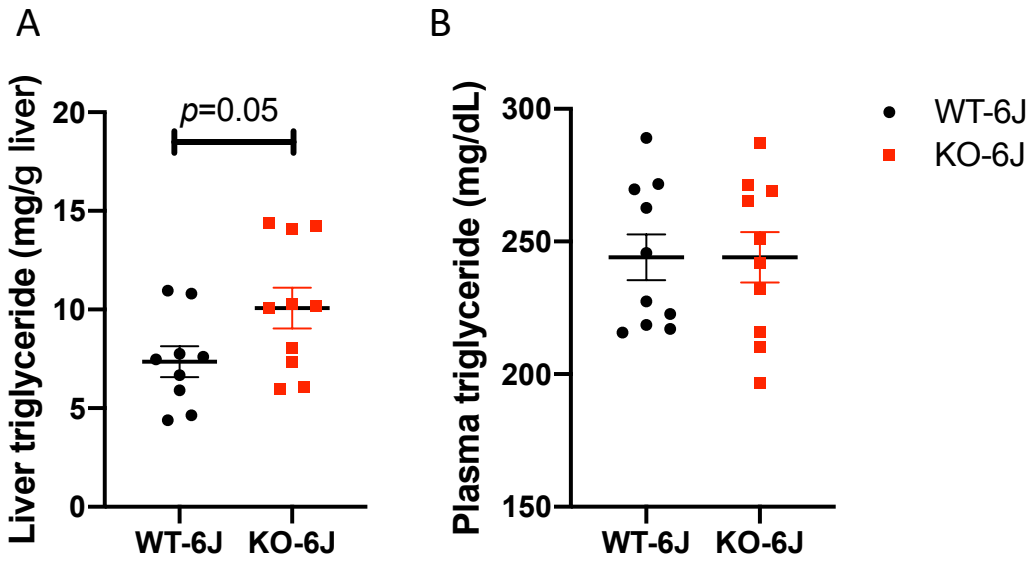

Figure 4.5 HFD-fed C57BL/6J-*Enpp6*$^{-/-}$ mice exhibit a trend in hepatic steatosis. Liver and plasma triglycerides levels were measured in C57BL6J-*Enpp6*$^{-/-}$ (KO-6J) mice and *Enpp6*$^{+/+}$ (WT-6J) mice after 7 weeks of HFD. **(A)** Liver triglycerides level, KO-6J (n=9) and WT-6J (n=10); **(B)** plasma triglycerides level, n=10 for each genotype. Outlier data caused by technical error were removed from analysis after assessing by outlier test (GraphPad 8.0). *Unpaired student t-test* was used for statistical analysis. The values are represented as mean ± SE, **p <0.05.*

4.3.2 *Enpp6* mRNA level varies from three mouse strains: 129S6, C57BL/6J and B6129F1

Previously observed phenotypes from the B6129F1-*Enpp6*$^{-/-}$ mice (mixed strain) were not replicated in the C57BL/6J-*Enpp6*$^{-/-}$ mice when exposed to HFD. Indeed, HFD-fed C57BL/6J-*Enpp6*$^{-/-}$ mice exhibited worsened metabolic phenotypes: greater adiposity and more exaggerated hyperinsulinaemia relative to the C57BL/6J-*Enpp6*$^{+/+}$ mice. Based on this, the *Enpp6*$^{-/-}$ metabolic phenotype is likely strain dependent and can be reversed due to the genetic modifiers present in each strain background. One explanation is that *Enpp6* expression may vary among different mouse strains, causing the strain dependent phenotype of *Enpp6*$^{-/-}$ mice. To address this question, two parental strains from the B6129F1-*Enpp6*$^{-/-}$ mice: C57BL/6J and 129S6, together with B6129F1 wildtype mice, were used to compare the *Enpp6* expression in the brain and kidney, because ENPP6 is highly expressed in brain and kidney.

In the brain, there was no difference in the *Enpp6* mRNA level among the three groups (Figure 4.6A). However, *Enpp6* expression in kidney was different across the three groups. *Enpp6* expression in kidney was significantly higher in C57BL/6J than in 129S6 or B6129F1 mice, but there was no difference betweeen129S6 and B6129F1 mice (Figure 4.6B).

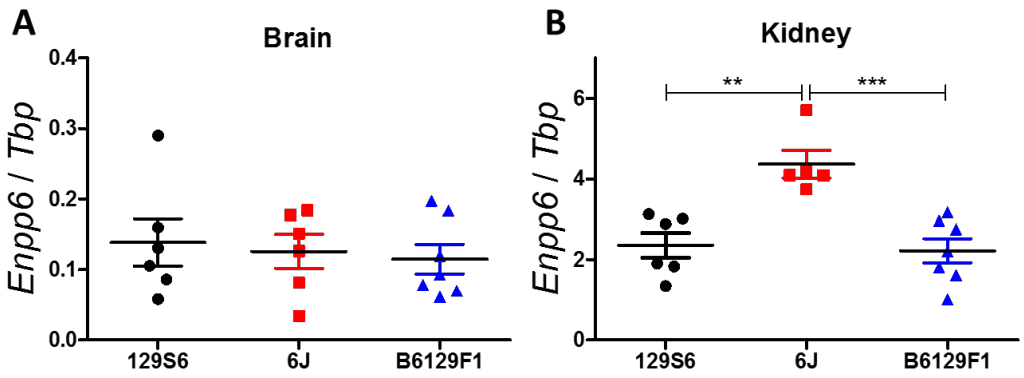

Figure 4.6 *Enpp6* mRNA level differs from 129S6, C57BL/6J and B6129F1 mouse strains. (A) *Enpp6* mRNA levels in the brain. **(B)** *Enpp6* mRNA levels in the kidney. Technical replicate: n=3. Biological replicate: 129S6: n=6; C57BL/6J (6J): n=5 (kidney, one of the 6J mice only had one kidney which was fixed for further investigation) and n=6 (brain) and B6129F1: n=7. *One-way ANOVA with Bonferroni's multiple comparison test* was used for statistical analysis. The values are represented as mean ± SE, ***p<0.01; ***p<0.001.*

4.3.3 Reduced brain *Enpp6* mRNA level is validated in *Pdgfrα-Cre*$^{+}$*Enpp6*$^{fl/fl}$ mice

To test the original hypothesis that ENPP6 deletion in oligodendrocytes improves the metabolic profile, an OPC-*Enpp6* knockout model was generated. Both OPC-*Enpp6*$^{-/-}$ and control mice were fertile and viable. Note that this experiment was already underway in parallel with the studies on the effects of HFD on C57BL/6J-*Enpp6*$^{-/-}$ mice above. *Enpp6* mRNA level was effectively knocked down in the brain (OPCs) in OPC-*Enpp6*$^{-/-}$ mice (Figure 4.7A) compared to controls, with no difference of *Enpp6* expression in the kidney (Figure 4.7B). *Enpp6 flox/flox* alleles did not affect endogenous ENPP6 expression in mice (Schraut et al., unpublished data).

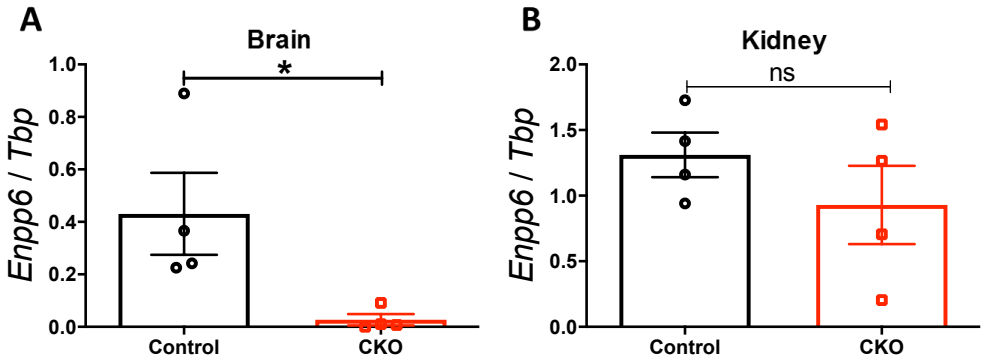

Figure 4.7 *Enpp6* mRNA level in the brain is reduced in OPC-*Enpp6*$^{-/-}$ (CKO) mice. (A) *Enpp6* mRNA levels in the brain. **(B)** *Enpp6* mRNA levels in the kidney. Control: *Pdgfrα-Cre*$^{-}$*Enpp6*$^{fl/fl}$; CKO: *Pdgfrα-Cre*$^{+}$*Enpp6*$^{fl/fl}$ (OPC-*Enpp6*$^{-/-}$). n=4 per genotype; technical replicate: n=3. *Unpaired student t-test* was used for statistical analysis. The values are represented as mean ± SE. **p<0.05, ns: not significant.*

4.3.4 HFD-fed OPC-*Enpp6*$^{-/-}$ mice do not exhibit an overtly altered metabolic phenotype compared to *Enpp6*$^{fl/fl}$ controls

To address the hypothesis that OPC-specific *Enpp6* ablation in mice causes reduced visceral adiposity and protects from diabetes after HFD feeding, we challenged OPC-*Enpp6*$^{-/-}$ mice with HFD as before. Metabolic responses of OPC-*Enpp6*$^{-/-}$ mice were assessed on 7 weeks of HFD. During HFD feeding, there was no difference in body weight or body composition between the two genotypes (Figure 4.8A-C). Gross tissue weights (adipose depots, kidney, liver and brain) were also similar (Figure 4.9). The two groups of mice consumed similar food weekly (Figure 4.8D). At the baseline, chow-diet fed OPC-*Enpp6*$^{-/-}$ exhibited comparable glucose tolerance and insulin levels as controls during the GTT (Figure 4.10A and C). Both genotypes of mice showed comparable susceptibility to HFD-induced hyperglycaemia (Figure 4.10B) and hyperinsulinaemia (Figure 4.10D). Moreover, there was no significant difference of triglycerides levels in either liver or circulating plasma between the two genotypes after HFD (Figure 4.11).

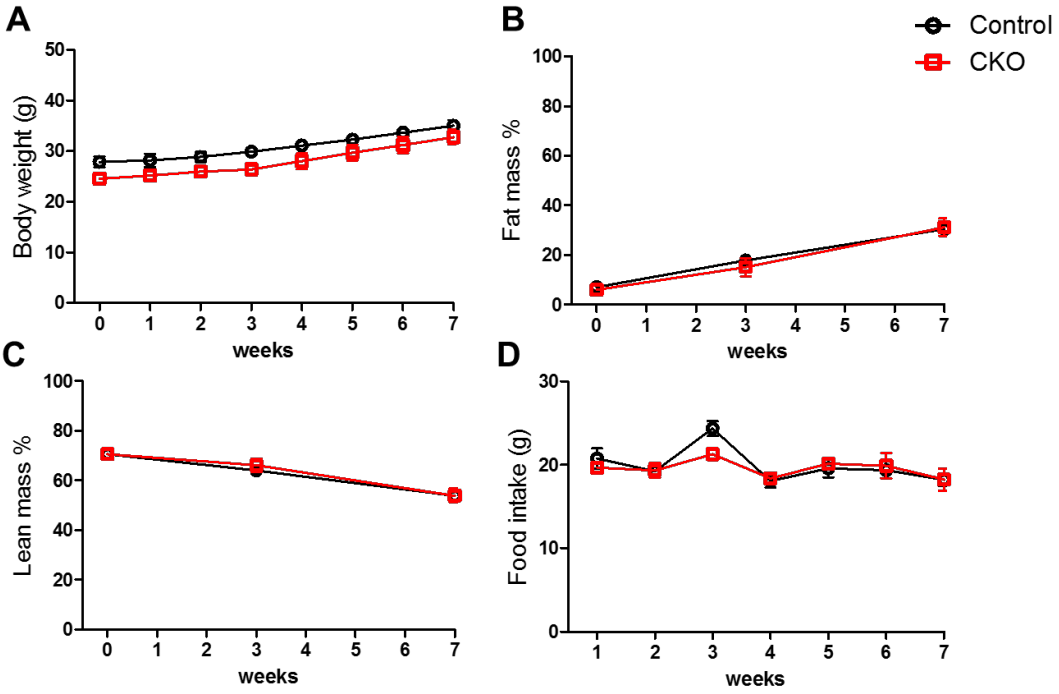

Figure 4.8 HFD-fed OPC-*Enpp6*$^{-/-}$ mice exhibited comparable body weight and fat mass from their control mice. (A) Whole body weight change during 7 weeks of HFD feeding. **(B)** Fat mass as a percentage of total body weight at baseline, after 3 and 7 weeks of HFD feeding. **(C)** Lean mass as a percentage of total body weight at baseline, after 3 and 7 weeks of HFD feeding. **(D)** Weekly food intake during 7 weeks of HFD feeding. CKO: conditional knockout: OPC-*Enpp6*$^{-/-}$. For all analyses, n=4 per genotype. *2-way ANOVA with Bonferroni post-hoc testing* was used for statistical analysis in body weight, fat and lean mass, food intake. The values are represented as mean ± SE.

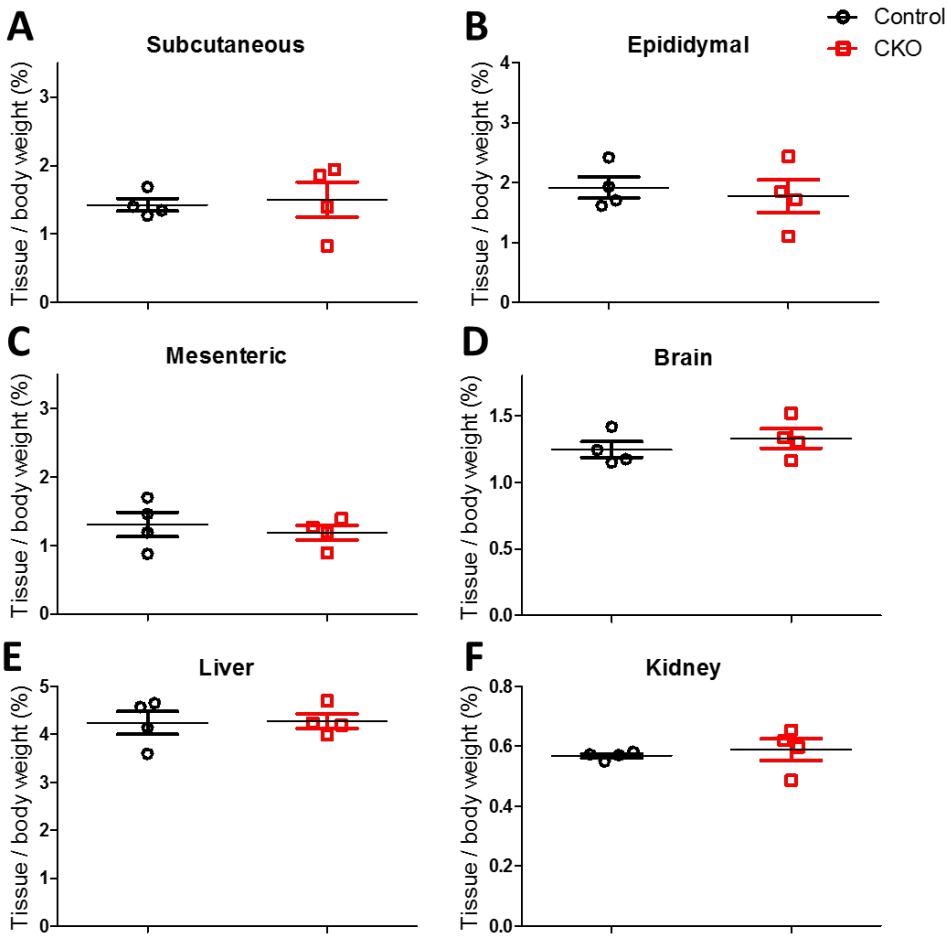

Figure 4.9 HFD-fed OPC-*Enpp6*$^{-/-}$ mice exhibited comparable tissue weights from their control mice. Tissue weight expressed as a percentage of total body weight. **(A)** Subcutaneous fat. **(B)** Visceral fat: epididymal fat. **(C)** Visceral fat: mesenteric fat. **(D)** Brain. **(E)** Liver. **(F)** Kidney. CKO: conditional knockout: OPC-*Enpp6*$^{-/-}$. For all analyses, n=4 per genotype. *Unpaired student t-test* was used for statistical analysis. The values are represented as mean ± SE. **p<0.05.*

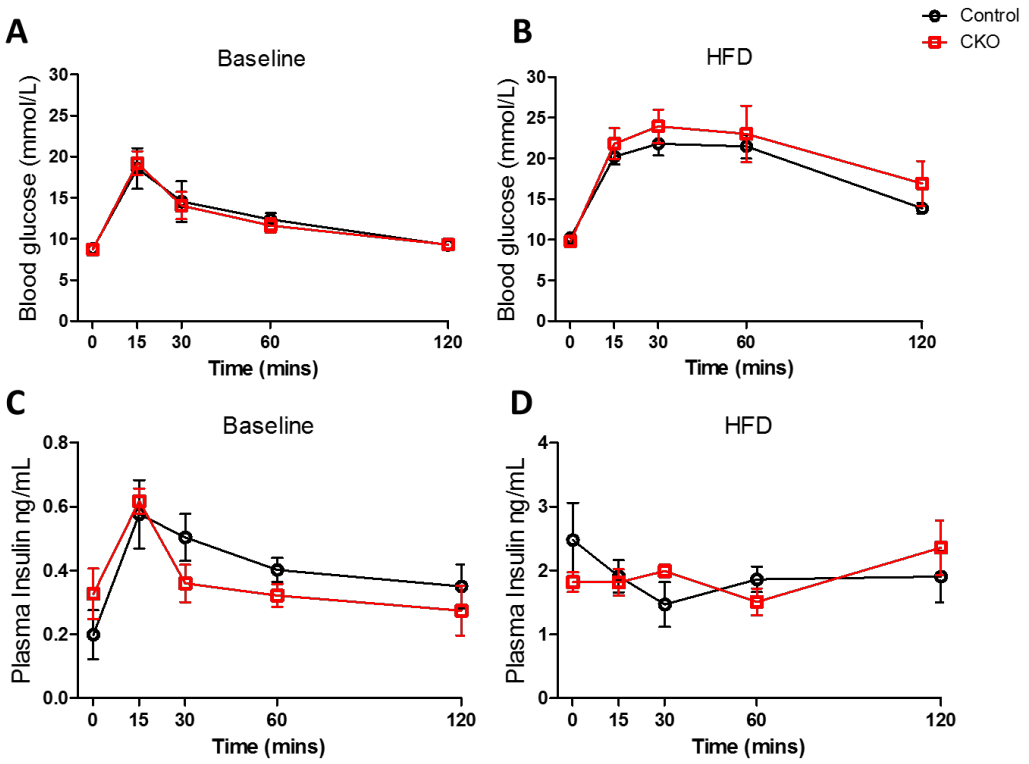

Figure 4.10 The OPC-*Enpp6*$^{-/-}$ mice exhibit comparable glucose and insulin homeostasis from their controls. (A) Baseline glucose level. **(B)** Glucose level after HFD feeding. **(C)** Baseline circulating insulin level. **(D)** Circulating insulin level after HFD feeding. CKO: conditional knockout: OPC-*Enpp6*$^{-/-}$. n=4 per genotype. *2-way ANOVA with Bonferroni post-hoc testing* was used for statistical analysis in glucose and insulin levels. The values are represented as mean ± SE. *$p<0.05$.

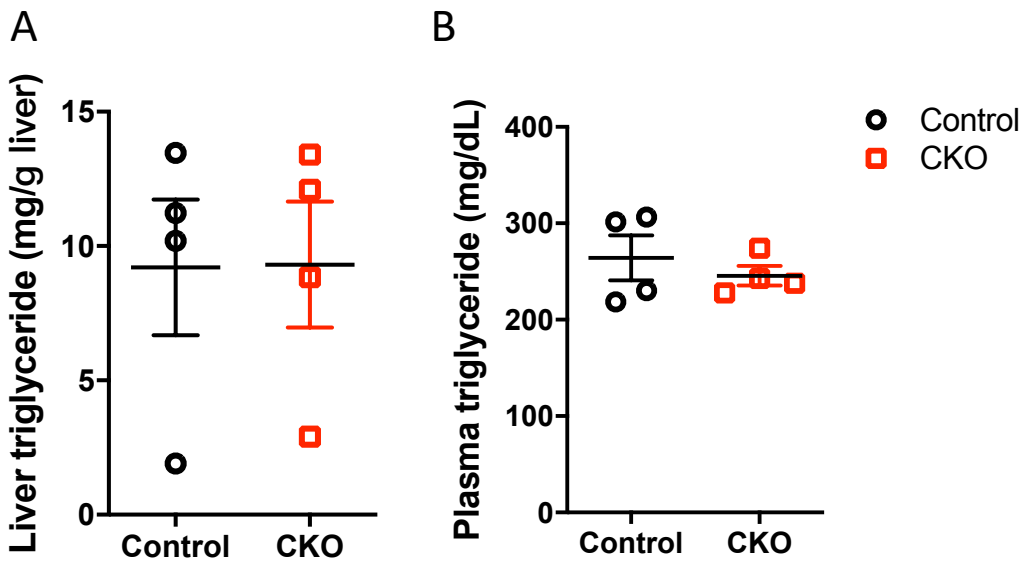

Figure 4.11 HFD-fed OPC-*Enpp6*$^{-/-}$ mice exhibit comparable liver and circulating plasma triglycerides. (A) Liver and plasma triglycerides levels were measured in HFD-fed OPC-*Enpp6*$^{-/-}$ mice (CKO) mice and control mice after 7 weeks of HFD. **(A)** Liver triglycerides level; **(B)** plasma triglycerides level, n=4 for each genotype. *Unpaired student t-test* was used for statistical analysis. The values are represented as mean ± SE, **p <0.05.*

4.4 Discussion

In this chapter, the metabolic profile of mice lacking *Enpp6* on a C57BL/6J strain background and OPC-specific *Enpp6*$^{-/-}$ mice were assessed. The prevailing assumption underpinning this hypothesis was that the improved metabolic phenotype observed in the mixed strain of *Enpp6*$^{-/-}$ mice (Chapter 3) would be replicated in the C57BL/6J strain of global *Enpp6*$^{-/-}$ mice. However, *Enpp6* ablation in C57BL/6J background presented with a worsened, not improved, metabolic profile than *Enpp6* ablation in the mixed strain B6129F1 mice. Therefore, with respect to the C57BL/6J-*Enpp6*$^{-/-}$ mice we have to reject the original hypothesis that *Enpp6* deletion protects against visceral obesity and diabetes. Clearly, the metabolic impact of *Enpp6* deficiency is strain dependent. This may be partially due to the differences in *Enpp6* gene expression in tissues distinct to mouse strains, such as, but not limited to, kidney where ENPP6 is highly expressed. Notably, *Enpp6* mRNA expression in brain is comparable across 129S6, B6129F1(mixed) and C57BL/6J mice. This indicates ENPP6 in brain (and by inference oligodendrocyte-*Enpp6* expression) is not the cause of this strain difference in metabolic response. In support of this, mice specifically lacking *Enpp6* in oligodendrocytes present with a comparable metabolic phenotype to mice with endogenous levels of ENPP6 on the C57BL/6J strain background.

4.4.1 Genetic background influences the metabolic phenotype of *Enpp6* ablation in mice

As described in chapter 3, B6129F1-*Enpp6*$^{-/-}$ mice, on a mixed strain, are protected from HFD-induced visceral obesity, hyperglycaemia and hepatic steatosis. This line was generated by using a 129S6-derived mouse embryonic stem cell line for introducing the *Enpp6* mutant into the mouse genome and crossed with C57BL/6J as the background line. This approach for generating transgenic mouse is commonly used and cost effective (321, 339). However, it can cause heterogeneous phenotypes and result in unpredictable genetic strains (340). This complex mixed strain can lead to low reproducibility for research: e.g. the effects observed from one group cannot always be repeated

and validated by the other groups or using other strains (341-343). Thus, standardisation of strain context is very important and necessary when understanding the role of *Enpp6* gene in translational animal study.

In the past 30 years, many studies focused on the impact of strain background on rodents' metabolic parameters in response to HFD feeding (344). Interestingly, not all strains of mice are susceptible to HFD-induced obesity and glucose intolerance (345). In particular, the C57BL/6J strain is a well-known obese mouse model mimicking human metabolic derangements. These mice exhibited obesity, hyperinsulinaemia, hyperglycaemia, and hypertension when exposed to HFD feeding, and without metabolic abnormalities when fed with normal chow diet (320, 325). However, Biddinger *et al.* suggested that this C57BL/6J strain developed features of metabolic syndrome even on a low-fat diet (LFD) due to high-fold increase in serum glucose during fasting and glucose tolerance test when fed with HFD (346). Moreover, when exposed to HFD or LFD feeding, strain-specific metabolic phenotypes have been observed in several studies. Fearnside *et al.* found increased obesity-prone and insulin resistant predisposition of C57BL/6J and 129S6 strain, whereas BALB/c and DBA/2 strains are relative resistance to HFD-induced obesity and glucose intolerance. Interestingly, under chow diet feeding, significantly cumulative glycaemia only occurred in the C57BL/6J strain, but not in 129S6, BALB/c DBA/2, or C3H strains (347). Similarly, Biddinger *et al.* found that 129S6 was susceptible to impaired glucose tolerance, obesity and NAFLD only under HFD feeding, whereas C57BL/6J developed these features on both LFD and HFD (346). This is also consistent with and supported by Dumas and his colleagues' study (348). They found that HFD-induced 129S6 mice exhibited impaired glucose homeostasis, NAFLD, and notably obesity, whereas BALB/c strain displayed improved glucose tolerance as reflected by significantly lower plasma glucose and higher plasma insulin. Nonetheless, when under LFD feeding, there was no evidence provided of these features in 129S6 and BALB/c strain (348). Together, these studies suggested the interaction

between strain background and diet-induced challenges plays a key role in metabolic phenotypes.

The B6129F1 line in our study (chapter 3), is a mixed background strain from two parental strains: C57BL/6J and 129S6. These two inbred mouse strains are both commonly used for modelling obesity and diabetes. 129S6 is also a widely used mouse model in biomedical research, though it is commonly characterized as rather idle and susceptible to anxiety (349). Despite similarities in their responses to HFD feeding, C57BL/6J mice were more obese and exhibited severe hyperglycaemia and milder hyperinsulinaemia compared to 129S6 mice (346, 348). Thus, for the purpose of this study, we only chose the C57BL/6J as the backcross strain to produce a reproducible line of *Enpp6*$^{-/-}$ mice. However, in the furfure, the 129S6-*Enpp6*$^{-/-}$ line should also be assessed for its metabolic profile in comparisons with C57BL/6J-*Enpp6*$^{-/-}$ and B6129F1-*Enpp6*$^{-/-}$ mice.

We have shown that *Enpp6*$^{-/-}$ mice from two genetic backgrounds: B6129F1 and C57BL/6J, displayed different metabolic parameters. It seems that the role of the *Enpp6* gene can be affected by different strain backgrounds. On the mixed background, *Enpp6* gene acts as a 'visceral-fat gene', and knockout of *Enpp6* gene prevents mice from HFD-induced selectively visceral obesity. However, on the C57BL/6J background, *Enpp6* gene seems to play the opposite role, acting as a 'lean gene'. The results showed a clear worsened phenotype in the HFD-fed C57BL/6J-*Enpp6*$^{-/-}$ mice compared with the C57BL/6J-*Enpp6*$^{+/+}$ mice, including significantly increased body weight and body fat, insulin resistance and a trend of hepatic steatosis. This suggests a strong insulin resistant-phenotype in C57BL/6J-*Enpp6*$^{-/-}$ mice. Thus, the insulin tolerance tests, and investigation of pancreatic beta-cells function in the C57BL/6J-*Enpp6*$^{-/-}$ mice can be considered for future study.

Regarding the in-consistent phenotype we observed in mice, targeted alleles in different strains have been reported to change the phenotype by others. *LEP*

is a monogenic gene for obesity and the *Lep* deficiency mouse (Lep$^{ob/ob}$) cannot produce leptin, which is widely used to study obesity and type 2 diabetes. However, even the same *ob* mutation but on the different strains, caused completely different phenotypes (350). B6.Cg-*Lep*^{ob}/J on this congenic background have transient hyperglycaemia but are revert to normal glycemia by 8 weeks of age. However, BTBR.Cg-*Lep*^{ob}/WiscJ, where the *ob* mutation is on a different genetic strain, exhibit severe hyperglycaemia, which is sustained and leads to worsened diabetic morbidity. Furthermore, Haluzik *et al*. showed that C57BL/6J$^{ob/ob}$ mice exhibited severer diabetes and insulin resistance than FVB/N$^{ob/ob}$ mice (351). Other than *ob/ob* mice, Carter *et al.* reported that *11β-HSD1*$^{-/-}$ mice on a mixed background (129/MF1), had reduced glucocorticoid negative feedback; whereas the opposite phenotype is observed in C57BL/6J-*11β-HSD1*$^{-/-}$ mice (352). Together, these pieces of evidence suggest that genetic background can lead to different phenotypes in genetically modified mice. Additionally, it is commonly accepted that different phenotypes might occur in human populations as well, based on gender, region, age, ethnicity etc.

The *Enpp6* gene association with visceral adiposity was initially discovered in a human population in the Orkney Islands by Genome-wide Association Study (GWAS) (142). However, this was not widely replicated in part due to very low allele frequency in other populations. When imputed into a theoretically large enough Icelandic cohort, the effect on visceral fat mass was not replicated (Schraut et al., unpublished data). This may be consistent with our observation in mice cohorts, that different phenotypes are displayed in different genetic contexts. Such an argument would need to be supported, but it is feasible if the Orkney effect was a founder effect from a gene enriched only on the islands that were effectively isolated from genetic admixture for approximately 1000 years. To date, hundreds of GWAS and other related studies have been performed to identify candidate loci associated with diseases (353, 354). GWAS can help understand the genetic susceptibility factors contributing to metabolic diseases and examine the polygenic obesity variants among human

populations (135). However, subsequent validation and functional investigation for the candidate loci are necessary. Despite limited successful characterisation, many variants identified by the GWAS approach are either at low frequency or have small effect size. GWAS performance suffers from limitations including sample size, incomplete genotyping and genetic background (355, 356). Therefore, even though the candidate genes have been identified, further validation, replication, and investigation are extremely crucial. In our case, the *Enpp6* gene-mediated metabolic phenotype is dependent upon the genetic background, suggesting that potential anti-visceral obesity and anti-diabetic therapy targeting ENPP6, may only benefit limited populations. This does not invalidate the approach as we move towards personalised medicine with tailored, genetically predictable drug responses. To put this in context, genetic susceptibility to adverse side effects of the most commonly used anti-diabetes drug, metformin has been described and a substantial proportion of patients do not respond to metformin (357). It will be crucial to explore more accurate therapeutic treatments for obesity and diabetes in patients in related to their region, gender, and age.

In summary, to investigate the underlying mechanisms of ENPP6 in further studies, it is worth generating another *Enpp6*$^{-/-}$ mouse model on the 129S6 strain, which is the other parental strain of the mixed background B6129F1-*Enpp6*$^{-/-}$ mice. Moreover, the *ENPP6* mRNA level in mice was different due to the genetic background. It is unclear how the confounding factors including genetic background, environmental factors and levels of target gene expression affect the metabolic consequences. The answers to these potential questions can provide us more evidence to understand the *Enpp6* gene and how genetic background affects *Enpp6*-mediated metabolic phenotype.

4.4.2 The metabolic role of oligodendrocyte ENPP6 remains to be determined

The initial hypothesis was that ENPP6 deficiency caused a beneficial metabolic phenotype through its effects on brain (NFOs). Excluding the unexpected strain divergence, the results suggested that oligodendrocyte

ENPP6-defiency contributed to protection from the HFD exposure exhibited by the C57BL/6J-*Enpp6*$^{-/-}$ mice, arguing that brain (oligodendrocyte) ENPP6 deficiency contributes to the metabolic consequences.

However, whether oligodendrocyte ENPP6 regulates metabolism still needs to be further investigated. For example, it is worth assessing the metabolic consequence of OPC-specific *Enpp6* knockdown mice on a different strain background (e.g., 129S6) and compare with those in the global *Enpp6*$^{-/-}$ mice on the same strain in the future.

Additionally, ENPP6 is also highly expressed in the liver sinusoidal endothelial cells and kidney proximal tubular cells apart from the brain NFOs (165), suggesting other organs (kidney and liver) may play roles in metabolism and may be responsible for HFD-induced altered metabolic phenotypes of *Enpp6*$^{-/-}$ mice. Morita *et al.* suggested that ENPP6 deficiency caused lipid accumulation in the liver in the C57BL/6J mouse (165). A similar phenotype was observed in our HFD-fed C57BL/6J-*Enpp6*$^{-/-}$ mice that displayed a nearly significant increase in liver triglycerides but no change in circulating plasma triglycerides. Despite this evidence, the function of ENPP6 in the kidney and liver is still largely unexplored. For the future studies, it may be worth assessing the metabolic consequences of kidney/liver specific *Enpp6*$^{-/-}$ mice when fed on HFD. This could provide more evidence on the mechanism of ENPP6 in the metabolic control.

Chapter 5 The effects of ENPP6 on oligodendrocytes

5.1 Introduction

ENPP6 is highly expressed in the newly formed oligodendrocytes (NFOs) and less strongly in the mature oligodendrocytes (MOs), but not in neurons or other glial cells (165, 170-172). The well-documented role of the oligodendrocyte in the central nervous system (CNS) is myelination, a process of membrane wrapping around neuronal axons that preserves signal transduction and other functions (173-175). However, whether ENPP6 is involved in the myelination process is not known. Morita *et al.* observed a reduction in myelin sheath layers in the C57BL/6J-*Enpp6*$^{-/-}$ mice, suggested ENPP6-deficiency results in hypomyelination (165). In Chapter 3, we showed that mixed strain HFD-fed global *Enpp6*$^{-/-}$ mice were protected from visceral obesity, impaired glucose tolerance and hepatic steatosis, suggesting ENPP6 inhibition may be a novel anti-visceral obesity and anti-diabetic therapeutic strategy. However, whether the *Enpp6*$^{-/-}$ mice generated for study in our laboratory (mixed 129S6 and C57BL/6J) mice (referred to as B6129F1) exhibit demyelination was unknown. Undoubtedly, it is crucial to determine whether demyelination is observed in *Enpp6*$^{-/-}$ mice. Indeed, it would be fatal for any therapeutic strategy targeting diabetes if that also resulted in brain dysfunction. Thus, in this chapter, the question of whether the Morton laboratory *Enpp6*$^{-/-}$ mice (B6129F1) suffered from the abnormal oligodendrocyte function and myelination was addressed.

Additionally, in Chapter 4, we showed that metabolic phenotypes of *Enpp6*$^{-/-}$ mice were strain dependent. In contrast to the beneficial phenotypes in B6129F1-*Enpp6*$^{-/-}$ mice, HFD-fed C57BL/6J-*Enpp6*$^{-/-}$ mice exhibited a worsened metabolic phenotype. These mice displayed increased body weight, glucose intolerance and a trend for hepatic steatosis. Excluding the strain divergence on the ENPP6-deficiency-mediated metabolism, this argues that ENPP6 deficiency oligodendrocyte contributes to the metabolic phenotype. However, the inhibition of ENPP6 in oligodendrocyte may theoretically cause

oligodendrocyte dysfunction. Therefore, this chapter will also study the effects of ENPP6 deficiency on oligodendrocyte functions based on the C57BL/6J strain.

5.1.1 ENPP6 in oligodendrocytes

Oligodendrocyte is a major cell population of brain glial cells (358). In the early postnatal period (~10 weeks age of mice; 5-10 years of humans), though myelination can still occur in the adult period (170, 172, 173, 175). Most oligodendrocyte precursor cells (OPCs) differentiate into myelinating oligodendrocytes and generate a lipid-rich myelin sheath. Oligodendrocytes participate in neurotransmission and play vital roles in supporting and protecting neurons structurally and metabolically (173, 175, 270).

In the brain, ENPP6 is predominantly and highly expressed in the NFOs, and less strongly expressed in the MOs (165, 170). However, ENPP6 is not expressed in neurons or other glial cells including the oligodendrocyte precursor cell (OPC), astrocyte and microglia (169). Moreover, ENPP6 is not expressed in the very earliest stage of differentiating oligodendrocytes. There is a time gap between the disappearance of *Pdgfrα* (OPC marker) and the expression and appearance of ENPP6 (170). In addition, *Enpp6* expression is not detected in any foetal tissues, only in neonatal and adult animals, as evidenced by the single-cell RNA sequencing(359) (359). More evidence from single-cell RNA sequencing studies confirmed that *Enpp6* is highly expressed in the NFO (171) . Morita *et al.* showed that young *Enpp6*$^{-/-}$ mice (post-partum day 14) developed myelin sheath abnormalities, therefore suggesting that ENPP6 affects oligodendrocyte development and myelination (165, 172). Due to the limited studies on ENPP6 reported in the literature, more research is needed to further investigate the effects of ENPP6 in OPC development and differentiation.

5.1.2 Development of a fluorescent reporter for ENPP6 activity

To study the biological function of ENPP6 enzyme in cells and tissues, an enzyme activity assay was developed. A synthetic substrate, Tokyo Green-methyleneoxy phosphocholine (TG-mPC), was used as a surrogate fluorescent substrate to assess ENPP6 enzymatic activity (290) with two potent ENPP6 inhibitors: dimaprit and 3-(Carbamimidoylsulfanyl)-N,N,N,-trimethyl-1-propanaminium (T11) (290). To validate the assay, TG-mPC was used to measure ENPP6 enzymatic activity in the kidney and brain of wild-type mice, and the *Enpp6*$^{-/-}$ mice. We confirmed that ENPP6 enzymatic activity was detected in the wild-type mice but not the *Enpp6*$^{-/-}$ mice. Furthermore, addition of dimaprit confirmed inhibition of ENPP6 activity in brain and kidney (Felici *et al.,* unpublished data).

TG-mPC-based assay was expected to be suitable to detect ENPP6 activity in ENPP6-expressing cells such as NFOs. However, neither dimaprit nor T11 had been validated in a cell-based ENPP6 enzymatic assay. Theoretically, based on molecular strutures, T11 was predicted to be more competitive against the substrate for the active sites on the ENPP6 enzyme than dimaprit. T11 possesses a charged trimethylamine, which mimics the choline moiety of ENPP6 substrates such as lysophosphatidylcholine (LPC) and α-glycerophosphorylcholine (αGPC) (165), whereas dimaprit has an uncharged dimethylamine structure (Figure 5.1). The inhibition of ENPP6 activity by T11 had previously not been demonstrated in ENPP6-expressing oligodendrocytes or in *in vivo* tests. Here, T11 was tested on rat OPCs *in vitro* to validate that T11 is a potent ENPP6 inhibitor. Moreover, this assay would be beneficial for screening small molecular inhibitors for ENPP6 in the future.

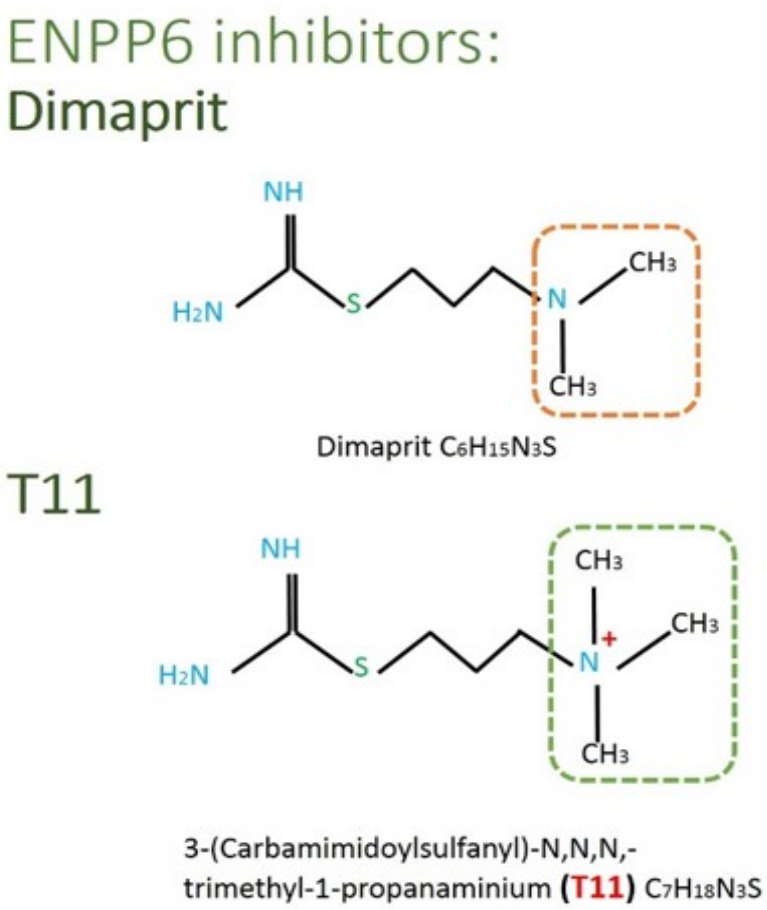

Figure 5.1 Chemical structure of ENPP6 inhibitors. ENPP6 has phosphodiesterase activities. ENPP6 recognizes the choline moiety (charged trimethylamine) as its substrate to produce phosphocholine. Two ENPP6 inhibitors: Dimaprit and T11, share a similar choline moiety (Dimaprit: Dimethylamine and T11: trimethylamine), which are considered as competitive enzyme inhibitors.

5.1.3 Hypothesis and aims

Hypothesis: Genetic loss or pharmacological inhibition of ENPP6 activity impairs oligodendrocyte development.

Aims:

1. To generate an ENPP6 over-expressing cell line as a positive control for cellular ENPP6 enzymatic activity assay.

2. To determine *Enpp6* mRNA expression and ENPP6 enzyme activity during OPC differentiation in rodents.

3. To validate the pharmacological inhibitory effect of T11 on ENPP6 in primary oligodendrocytes.

4. To investigate the effect of genetic deletion and pharmacological inhibition of ENPP6 on oligodendrocyte differentiation *in vitro*.

5.2 Experimental design

5.2.1 Validation of ENPP6 enzymatic activity in ENPP6 overexpressing HEK293 cells

The original method to assess ENPP6 activity was described using protein lysates (290). Here, ENPP6 enzymatic activity was measured at the intact whole cellular level in real-time. To validate the cell-based assay, an ENPP6 overexpressing HEK293 cell line was generated (details described in Chapter 2) and *Enpp6* mRNA expression was validated by qRT-PCR. Using TG-mPC assay, ENPP6 enzymatic activity was assessed in ENPP6 overexpressing HEK293 cells. Cells were harvested and re-suspended in PBS buffer containing pre-mixed 10 μM of TG-mPC before transferring into a 96-well plate (final volume: 50 μL per well). Cells were incubated at 37°C in a Tecan Infinite M1000 plate reader. ENPP6 activity was determined from the fluorescent intensity over time and the initial rate of reaction calculated from the slope of the linear region.

5.2.2 Assessment of real-time ENPP6 enzyme activity in rodent oligodendrocytes

Primary rodent OPCs were cultured and differentiated on poly-D-lysine (PDL)-coated 6-well plates. Oligodendrocytes were harvested at the different time points of differentiation for experiments. The pelleted oligodendrocytes were then re-suspended in PBS buffer containing pre-mixed 10 μM of TG-mPC in the presence or absence of T11 (10 μM) before transferring into a 96-well plate (final volume: 50 μL per well) for analysis.

5.2.3 Assessment of the effect of ENPP6 on OPC differentiation *in vitro*

5.2.3.1 The effect of pharmacological inhibition of ENPP6 activity by a putative ENPP6 inhibitor (T11) on primary rat NFOs

Primary rat OPCs were treated with 10 μM of T11 or 0.1% DMSO vehicle in culture medium over a differentiation time course of 72 hours with daily medium change. Two groups of cells were harvested and stained with an antibody to the oligodendrocyte-specific differentiation marker, O4. Cells were

analysed on flow cytometry (details described in chapter 2) (Figure 5.2). To assess the effect of ENPP6 inhibition on OPC differentiation, $O4^+$ cells (as a percentage of oligodendrocytes) were compared between the T11 treatment and vehicle control group. Anti-O4 antibody used in this project specifically targeted O4 in NFOs, evidenced by the comparison with unstained, second antibody stained and fully stained cell populations on flow cytometry (Figure 5.3).

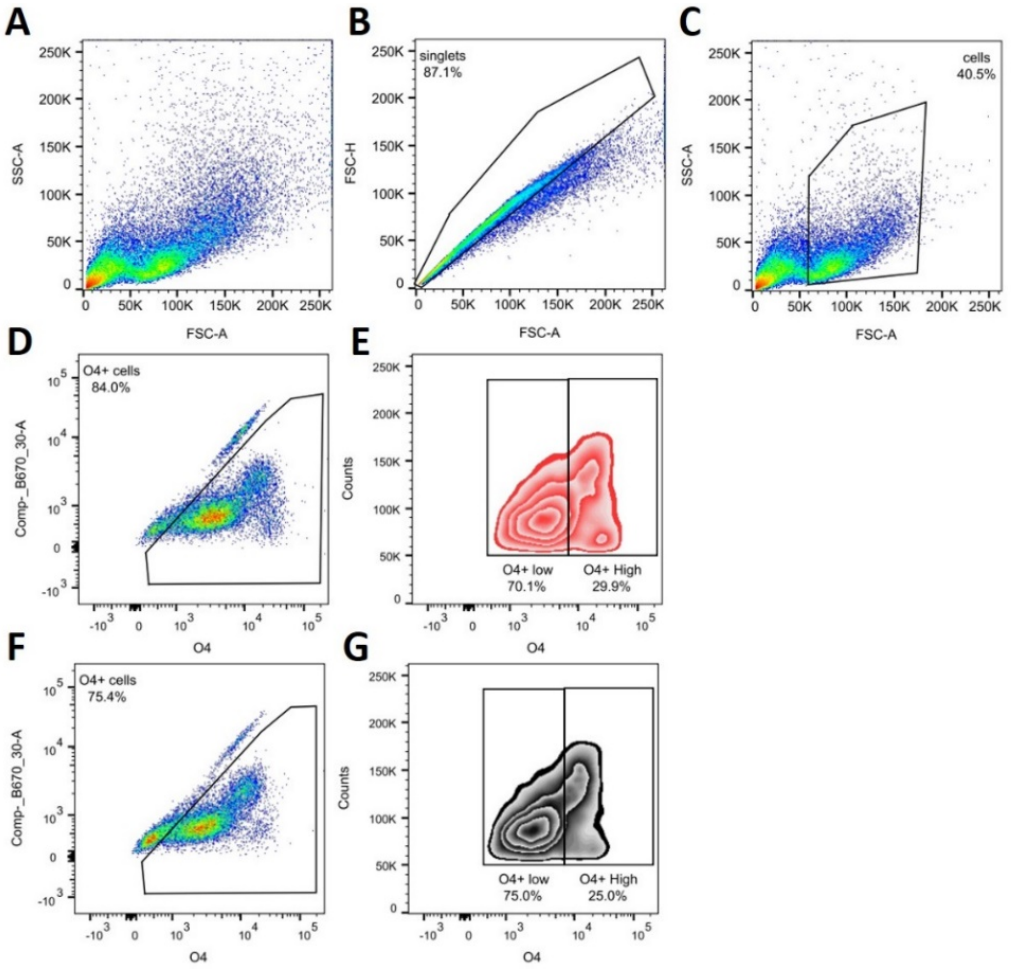

Figure 5.2 The gating strategy to quantify O4^{+} NFOs after T11 treatment in NFOs. Cells were gated using FSC (forward scatter) and SSC (Side scatter). Single cells were gated by FSC-A (area) and FSC-H (height) (**A-C**). O4-negative and auto-fluorescent cells were gated out using unstained and the secondary antibody stained only control cells through the blue laser (488nm and 670nm). NFOs with 0.1% DMSO vehicle control **(D)** and 10 μM of T11 treatment **(F)** were analysed. O4^{low} NFOs and O4^{high} NFOs were distinguished based on the level of O4 expression (**E and G**).

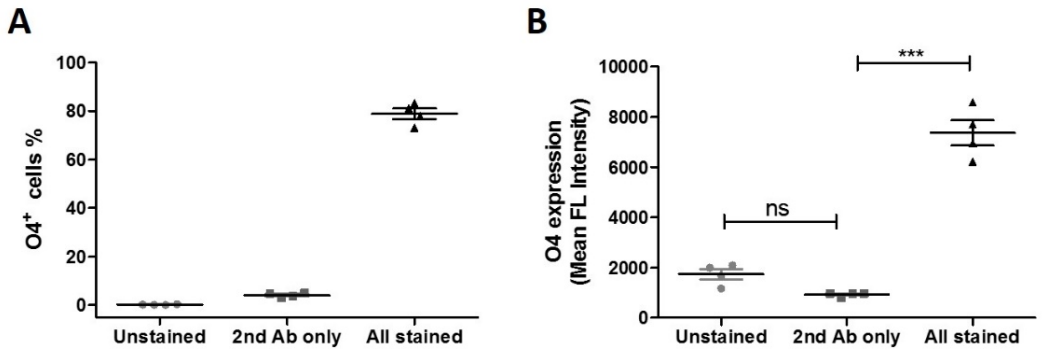

Figure 5.3 Validation of anti-O4 antibody in mouse NFOs. Cells were grouped as unstained, secondary antibody (2^{nd} Ab) stained only and all stained. $O4^+$ cells are shown as a percentage of the total cell number (**A**) and O4 expression (mean fluorescent intensity) (**B**). Biological replicate: n=4, The values are represented as mean ± SE. ****$p<0.0001$, ns: not significant. Statistical significance was tested by *One-way ANOVA* followed by a *Tukey's Multiple Comparison test*.

5.2.3.2 The effect of *Enpp6* knockout on primary mouse OPC and NFO differentiation

Primary mouse OPCs were obtained from C57BL/6J-*Enpp6*$^{-/-}$ and C57BL/6J-*Enpp6*$^{+/+}$ mice (P0-2). Firstly, the effect of *Enpp6* gene deletion on OPC population was tested. OPCs from C57BL/6J-*Enpp6*$^{-/-}$ and C57BL/6J-*Enpp6*$^{+/+}$ mice were processed and analysed by flow cytometry. Compensation and gating were performed using unstained and isotype controls (gating strategy is shown in Figure 5.2A-D). To assess the effect of *Enpp6* gene knockout on OPC population, the percentage of A2B5^{+} cells was compared between the two genotypes (A2B5: an OPC marker). Next, we investigated the effect of *Enpp6* gene knockout on NFOs by immunocytochemistry. 150,000 cells per well of OPCs were seeded and differentiated in a 24-well plate, followed by staining with anti-O4 and anti-MBP antibodies. Image J software was used for cell counting from each channel (details described in chapter 2). To give a more complete context for the differentiation state of the OPCs, the mRNA levels of *Mog* (Myelin oligodendrocyte glycoprotein), *Mbp* and the OPC differentiation marker *Gpr17* (G-coupled protein receptor 17) were also measured.

5.3 Results

5.3.1 ENPP6 is highly expressed in NFOs

To understand the physiological roles of ENPP6, as a first step, *Enpp6* mRNA expression was analysed from cultured primary rat OPCs during the differentiation *in vitro*. *ENPP6* mRNA was expressed at low levels in OPCs (0h), and increased, reaching a peak level around 48-72h. There was a slight decline in *ENPP6* mRNA after 144h (Figure 5.5C). The *Enpp6* mRNA level in cultured OPCs from C57BL/6J mice displayed a similar pattern. During the process of mouse OPC differentiation, the expression of *Enpp6* mRNA increased progressively (after 24h and 48h differentiation) and was significantly higher after 48h compared to OPCs (0h) (Figure 5.5B). Thus, these data confirmed that the mRNA of *Enpp6* is highly expressed in NFOs and MOs but rarely in OPCs. Morphological changes during the differentiation in rodent oligodendrocytes were shown (Figure 5.5A). OPCs showed a shape of simple bipolar and tripolar processes and ramified into a network of increasing processes after differentiation (Figure 5.5A).

Next, the protein level of ENPP6 was analysed by assessing oligodendrocyte ENPP6 enzymatic activity in real-time. This cell-based ENPP6 enzymatic assay was firstly validated in the ENPP6-overexpressing HEK293 ($ENPP6^+$ HEK293) cells. *Enpp6* mRNA expression was confirmed in the $ENPP6^+$ HEK293 cells but not detected in the wild-type (WT) HEK293 cells (Figure 5.4A). ENPP6 enzymatic activity (fluorescent intensity) was detected in the $ENPP6^+$ HEK293 cells but not WT HEK293 cells (Figure 5.4B). Furthermore, the effect of cell number on ENPP6 activity in the $ENPP6^+$ HEK293 cells was investigated. To understand the relationship between cell number and ENPP6 enzymatic activity, substrate TG-mPC was added to a range of cell numbers of $ENPP6^+$ HEK293 cells. WT HEK293 cell was performed as the negative control. Within the 20 min incubation (at 37°C), $ENPP6^+$ HEK293 cells showed a good linear relationship to their fluorescent intensity (Figure 5.4C). The rate of reaction in the linear region was plotted to represent ENPP6 activity (Figure 5.4D). Cell number and rate of the reaction showed a linear relationship (R^2=

0.9989) (Figure 5.4D), indicating that ENPP6 activity is proportional to the cell number (0.5-8 x 10^3 cells).

ENPP6 enzymatic activity was also detected in cultured primary rat NFOs (72h post differentiation) and MOs (144h post differentiation), but not in OPCs (0h) (Figure 5.5E). The initial rate of reaction was significantly higher in NFOs and MOs compared to OPCs (Figure 5.5G). For cultured primary mouse OPCs, ENPP6 enzyme was detected in NFOs (after 24h and 48h differentiation), but not detected in OPCs or NFOs from C57BL/6J-*Enpp6*$^{-/-}$ mice (Figure 5.5D). The initial rate of reaction was significantly higher in NFOs and MOs compared to OPCs (Figure 5.5F).

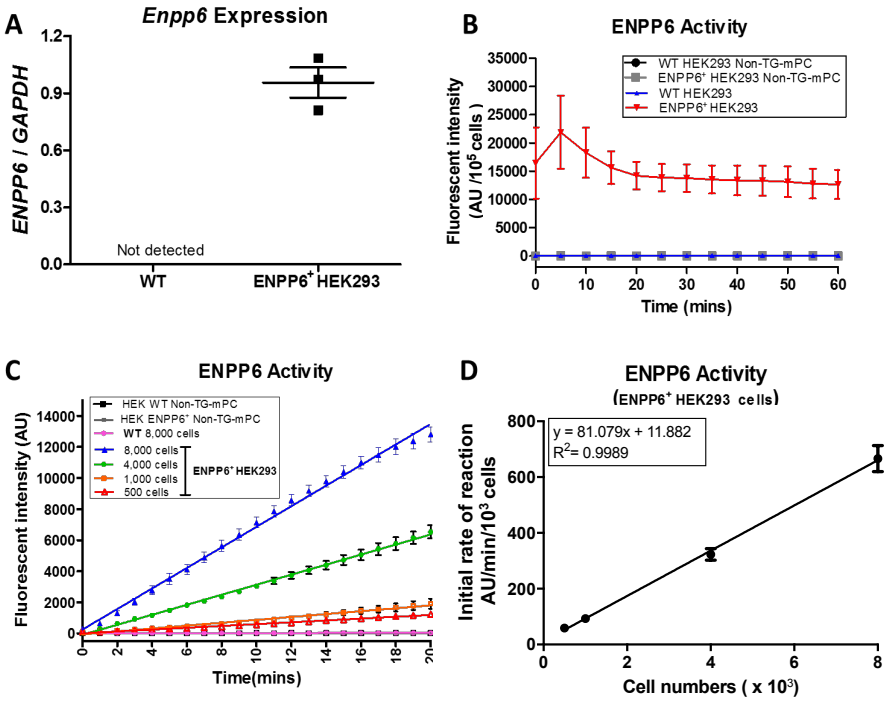

Figure 5.4 ENPP6 enzymatic activity is proportional to the cell number in ENPP6$^+$ HEK293 cells. (**A**) Levels of *ENPP6* mRNA expression in WT and ENPP6$^+$ HEK293 cells. (**B**) The fluorescent intensity of product produced from ENPP6 and its substrate TG-mPC in WT HEK293 cells (100,000 cells) and ENPP6$^+$ HEK293 cells (100,000 cells). Cells without TG-mPC were used as the negative control. Biological replicates n=3. (**C**) The fluorescent intensity of product produced from ENPP6 and its substrate TG-mPC in WT HEK293 cells (8,000 cells) and ENPP6$^+$ HEK293 cells (0.5–8 x 10^3 cells) in the liner region phase. WT HEK293 and cells without TG-mPC added were used as the negative controls. (**D**) The linear relationship between cell number and the rate of ENPP6 activity reaction (the reaction was fixed into the linear reaction region: 20 minutes). The units of rates of activity of ENPP6 are expressed in AU, since a pure standard of the product was not available for calibration. Biological replicates: n=3. The values are represented as mean ± SE.

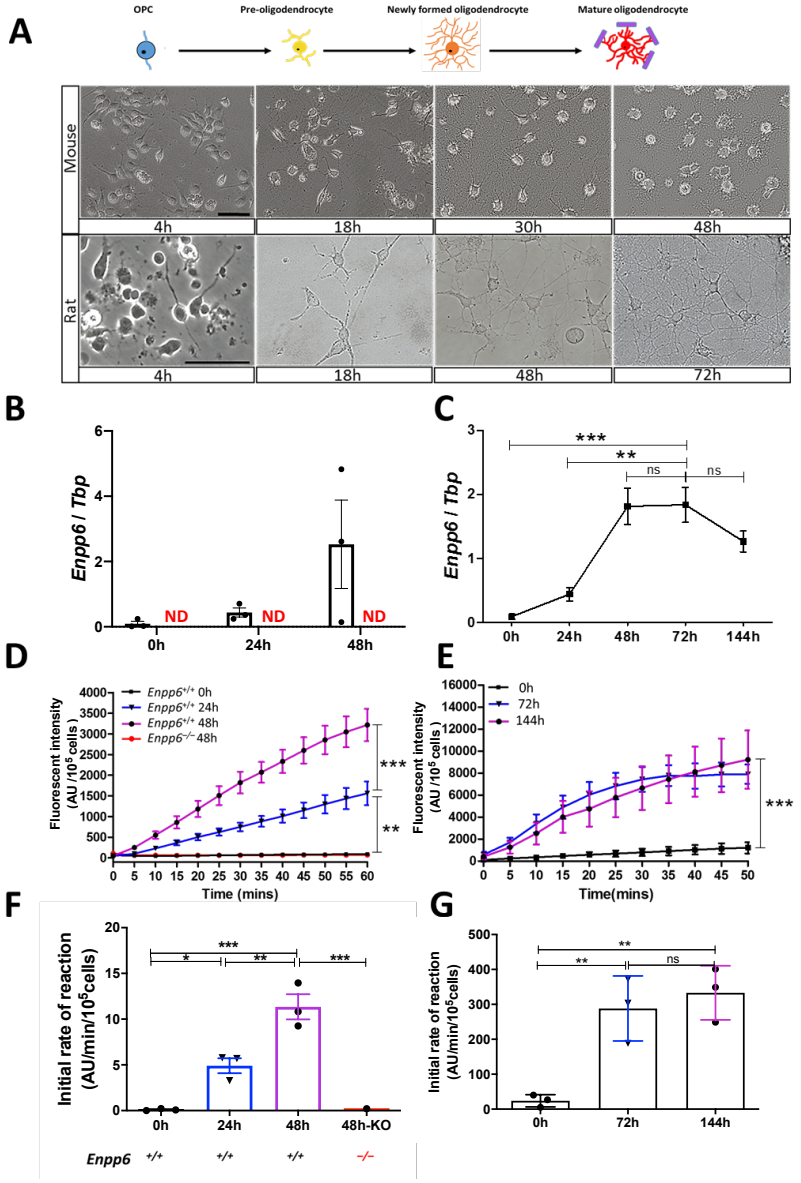

Figure 5.5 ENPP6 expression pattern during rodent OPC differentiation. (A) Morphology changes of OPC differentiation from P0-P2 C57BL/6J mouse and Sprague-Dawley rat. Scale bar = 200 µm. Level of *Enpp6* mRNA in oligodendrocytes from C57BL/6J mouse **(B)** and rat **(C)**. The fluorescent intensity of ENPP6 activity during mouse **(D)** and rat **(E)** OPC differentiation. The initial rate of ENPP6 enzyme reaction per min per 100,000 cells mouse **(F)** and rat **(G).** The reaction was fixed in the linear region (mouse: 45 min; rat: 15 min). n=3 for each group. Statistical significance was tested by *One-way ANOVA* followed by a *Tukey's multiple comparison test.* The values are represented as mean ± SE, **p<0.05; **p<0.01; ***p<0.001, ns: not significant; ND: not detected*. Images were captured by EVOS microscope.

5.3.2 Pharmacological inhibition of ENPP6 reduces OPC differentiation

To investigate the impact of inhibition of ENPP6 on OPC maturation *in vitro*, purified primary rat NFOs were treated with a putative pharmacological ENPP6 inhibitor T11. These NFOs were pre-treated with 10 μM of T11 or 0.1% DMSO as the vehicle control for 72h. ENPP6 enzymatic activity produced by NFOs was measured in real-time. After adding the substrate probe TG-mPC, ENPP6 enzymatic activity gradually increased and then entered the plateau phase (Figure 5.6A). The initial reaction rate of ENPP6 enzyme activity significantly reduced by T11 treatment (Figure 5.6B), resulting in on average 56.62% inhibition of ENPP6 enzyme activity. The data indicate the inhibitory function of T11 in ENPP6 enzymatic activity in rat NFOs.

Next, we aimed to determine the extent of differentiation of oligodendrocytes in NFOs in the presence or absence of T11 pre-treatment. An immature oligodendrocyte cell surface marker O4 was used as the marker of oligodendrocyte differentiation. We showed that total $O4^+$ NFOs (as a percentage of all NFOs) was significantly reduced after T11 treatment (Figure 5.6C). Furthermore, given two distinct populations was observed from the gating based on the level of O4 expression (Figure 5.6D), $O4^+$ NFOs were categorised as: $O4^{low}$ and $O4^{high}$ NFOs (assessed as a percentage of all $O4^+$ NFOs). There was no difference in $O4^{low}$ and $O4^{high}$ NFOs between T11 treatment and control group (Figure 5.6E-F). Our data suggests that pharmacological inhibition of ENPP6 in NFOs impairs or delays the OPC differentiation process.

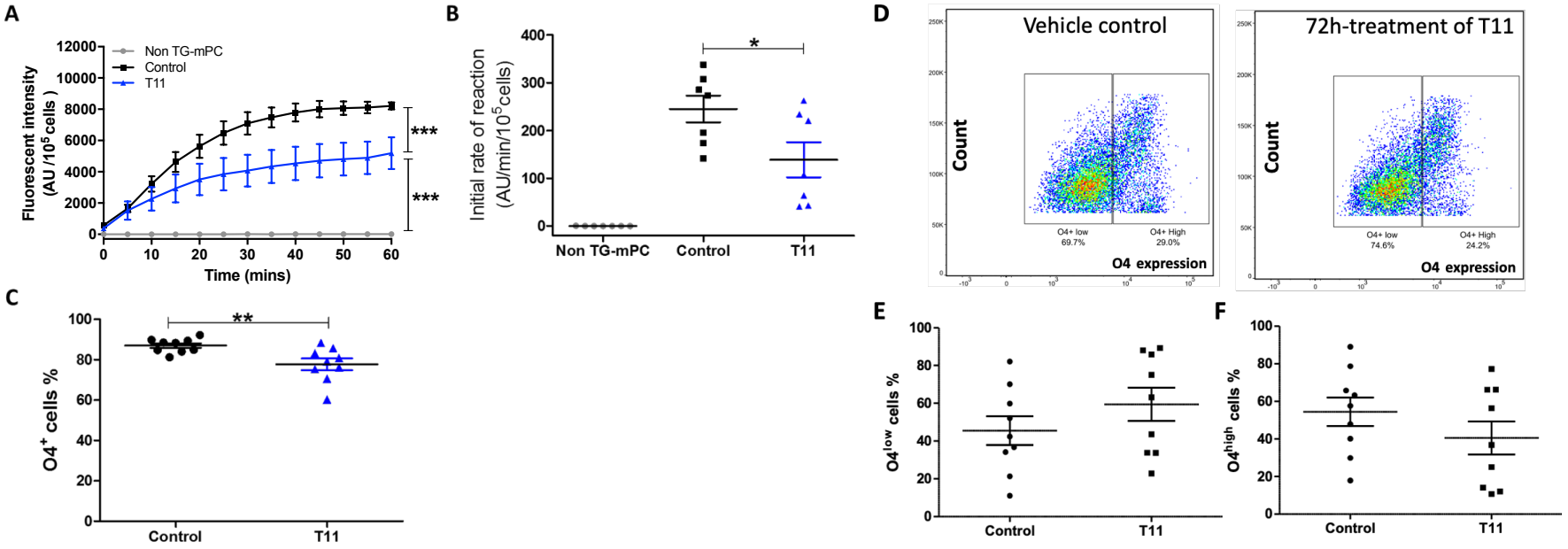

Figure 5.6 The effect of inhibition of ENPP6 on OPC differentiation. (A) The fluorescent intensity of ENPP6 activity in rat NFOs in the presence or absence of T11. Cells without the addition of TG-mPC were used as negative controls. The initial rate of ENPP6 reaction per min per 100,000 cells. n=7 for each group. **(B)** The initial rate of reaction was tested by *One-way ANOVA* followed by *a Tukey's multiple comparison test*. **(C)** $O4^+$ NFOs cell percentage of the total NFOs in the presence or absence of T11 treatment. n=9 for each group. *Unpaired student t-test* was used for statistical analysis. **(D)** Gating strategy for two subpopulations of $O4^+$ NFOs: $O4^+$ low and $O4^+$high, determined by the level of O4 expression. Quantification of $O4^+$ low **(E)** and $O4^+$ high **(F)** NFOs cell percentage of total $O4^+$ NFOs in the presence or absence of T11. The values are represented as mean ± SE, **p<0.05; **p<0.01; ***p<0.001*.

5.3.3 Genetic ablation of *Enpp6* suppresses OPC differentiation without affecting MBP expression

Pharmacological inhibition of ENPP6 suppressed OPC differentiation by reducing $O4^+$ NFOs. Here, NFOs from C57BL/6J-*Enpp6*$^{-/-}$ mice and their littermate controls C57BL/6J-*Enpp6*$^{+/+}$ were used to determine the impact of ENPP6 deficiency on OPC maturation *in vitro*. On average, 98% $A2B5^+$-OPCs (as a percentage of the total OPCs) were identified from mouse cerebral cortex by flow cytometry analysis (Figure 5.7G). $A2B5^+$-OPC cells as a percentage of total cell population was comparable between *Enpp6*$^{-/-}$ mice and their controls (Figure 5.7G). Immature oligodendrocyte lineage marker O4 and mature myelinating oligodendrocyte marker MBP were used for the characterisation of differentiated NFOs by immunocytochemistry. During differentiation, more complex morphology of cell processes and MBP positive staining were observed in after 48 hour-differentiation NFOs compared to after 24 hour-differentiation (Figure 5.8A). Total $O4^+$ NFOs (as a percentage of total NFOs) was significantly reduced in C57BL/6J-*Enpp6*$^{-/-}$ mice after 48h differentiation, compared with controls (Figure 5.8B). However, no difference was observed in MBP protein expression from either total NFOs or $O4^+$ NFOs (Figure 5.8B). To further define the effect of ENPP6 deficiency on the morphology of NFOs, the complexity of the processes of NFOs was quantified. Thus, $O4^+$ NFOs were distinguished by two categories: $O4^{low}$ NFOs and $O4^{high}$ NFOs (Figure 5.8C). $O4^{low}$ NFOs (at earlier stage of differentiation) with simple and intermediate morphology with abundant processes; whereas $O4^{high}$ NFOs (at later stage of differentiation) with a complex morphology with network of ramification (the method was adapted from Marin-Husstege *et al.* (360) and Gomez O *et al.* (361)). Increased $O4^{low}$ NFOs % and decreased $O4^{high}$ NFOs % were found in C57BL/6J-*Enpp6*$^{-/-}$ mice (Figure 5.8D). Importantly, this suggested ENPP6 deficiency suppressed or delayed OPC differentiation without affecting myelination at the later stage of OPC maturation *in vitro*.

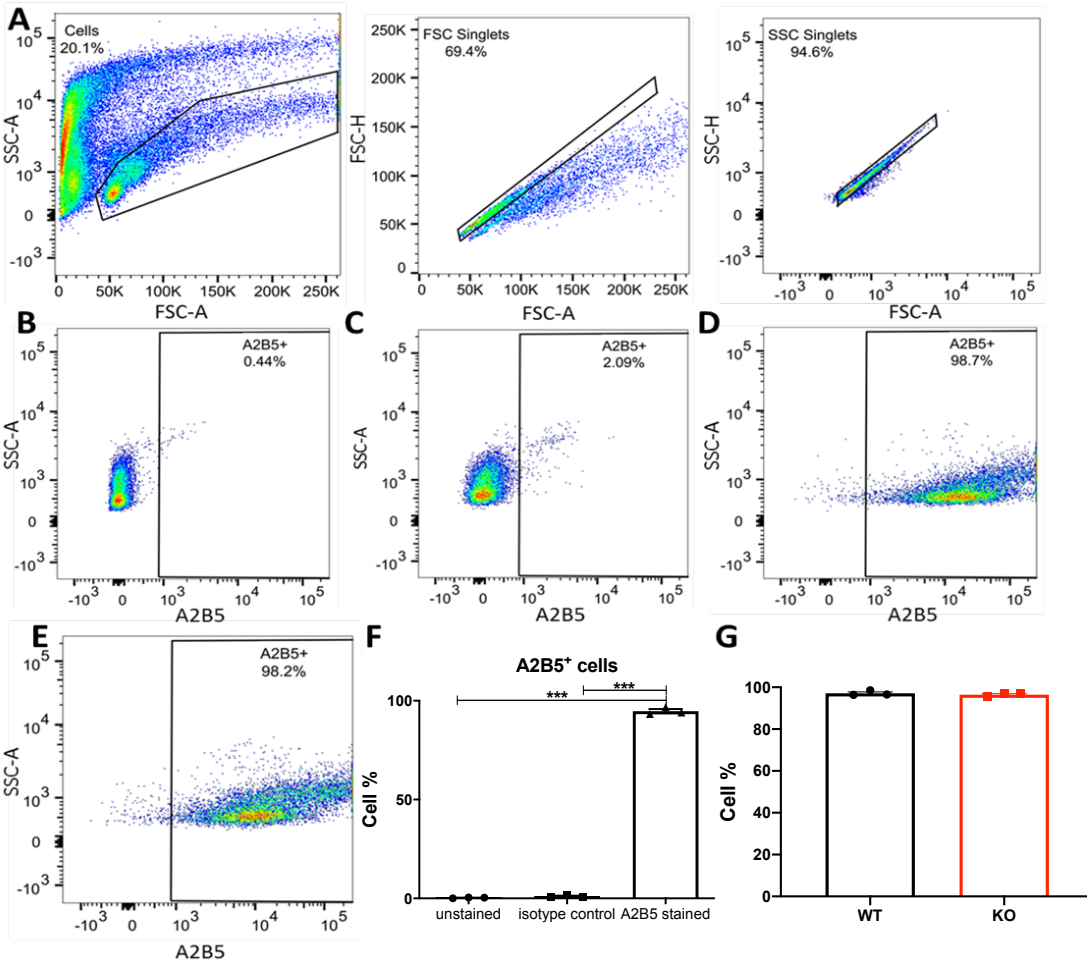

Figure 5.7 Characterisation of OPCs from *Enpp6*$^{+/+}$ and *Enpp6*$^{-/-}$ mice. (A) Cells were gated by forward scatter (FSC) and side scatter (SSC), followed by singlet gating. A2B5^{+} OPCs were distinguished from unstained cells **(B)** and isotype controls **(C)**. Singlet A2B5^{+} OPC were gated from **(D)** C57BL/6J-*Enpp6*$^{+/+}$ mice and **(E)** C57BL/6J-*Enpp6*$^{-/-}$ mice. **(F)** The percentage of A2B5^{+}-OPCs in unstained, isotype and A2B5 stained groups (unstained: n=6; isotype: n=4; A2B5 stained: n=6). Statistical significance was tested by One-way ANOVA followed by a Tukey's multiple comparison test. **(G)** The percentages of A2B5^{+} OPCs from *Enpp6*$^{+/+}$ and *Enpp6*$^{-/-}$ mice. n=3 for each group. *Unpaired student t-test* was used for statistical analysis. The values are represented as mean ± SE*, *p<0.05; **p<0.01.*

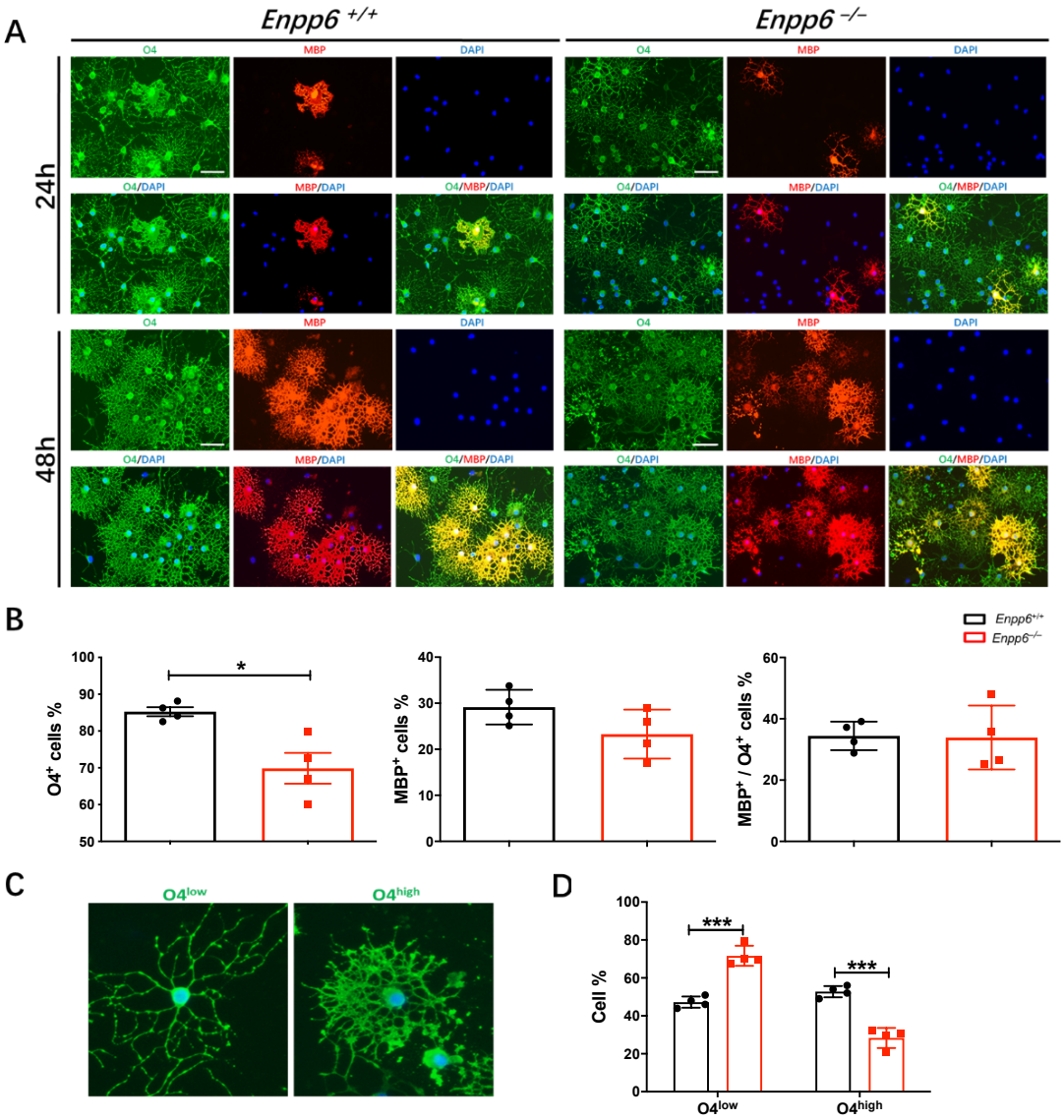

Figure 5.8 The effect of genetic deletion of *Enpp6* on OPC maturation. Primary mouse OPC cultures differentiated for 24h and 48h from C57BL/6J-*Enpp6*$^{+/+}$ mice and C57BL/6J-*Enpp6*$^{-/-}$ mice. **(A)** O4 (green) and MBP (red) staining showed significant NFOs cell processes. Nuclei was stained with DAPI (blue). Scale bar = 50 µm. Minimum 6 images were captured for analyzing one biological repeat. n=4 for each genotype. **(B)** Quantification of O4 positive and MBP positive cell proportions in 48-hour differentiated NFOs. *Unpaired student t-test* was used for statistical analysis. **(C)** Representative images of O4^{low} NFO and O4^{high} NFO based on the complexity of morphology. **(D)** Quantification of 2 types of O4^{+} NFOs as a percentage of the total NFOs. *2-way ANOVA with Bonferroni post-hoc testing* was used for statistical analysis. The values are represented as mean ± SE, **p<0.05; ***p<0.001*; *ns: not significant.* Images were captured by EOS FL2 microscope.

5.3.4 ENPP6 deficiency induced increased G-coupled protein receptor 17 (GPR17) mRNA level in NFOs

To further study the effect of ENPP6-deficiency on the expression pattern of other oligodendrocyte markers, Gi-coupled GPCR 17 (GPR17), which was emerged as a new marker for differentiation (362), was shown to down-regulate the differentiation of OPCs (362). Thus, we firstly measured the expression of GPR17 in NFOs from C57BL/6J-*Enpp6*$^{+/+}$ mice and C57BL/6J-*Enpp6*$^{-/-}$ mice. Consistent with the previous study, *Gpr17* mRNA was found at low levels at the beginning of differentiation in *Enpp6*-expressing or non-*Enpp6*-expressing OPCs. After 24 hour-differentiation, the mRNA levels of *Gpr17* increased as a fold change of 11.97 and 10.70 in non-*Enpp6*-expressing and *Enpp6*-expressing OPCs, respectively. However, there was no significant difference of *Gpr17* mRNA level in NFOs (after 24 hour differentiation) between two genotypes. After 48 hour-differentiation, the mRNA levels of *Gpr17* increased sharply in non-*Enpp6*-expressing OPCs as a fold change of 31.94, and was significantly higher than the control *Enpp6*-expressing OPCs (Figure 5.9B). Notably, for those non-*Enpp6*-expressing NFOs (after 48 hour differentiation), the mRNA levels of *Gpr17* slightly decreased compared to 24 hour-post differentiation group but without significant difference, suggesting the 48 hour-post differentiated OPCs were more likely mature. This was also confirmed by using two further markers of mature oligodendrocytes: *Mog* and *Mbp.* The mRNA levels of *Mog* and *Mbp* progressively increased from 24–48 hour differentiation (Figure 5.9B), but no difference of *Mog* or *Mbp* mRNA expression in NFOs was observed between genotypes (Figure 5.9B).

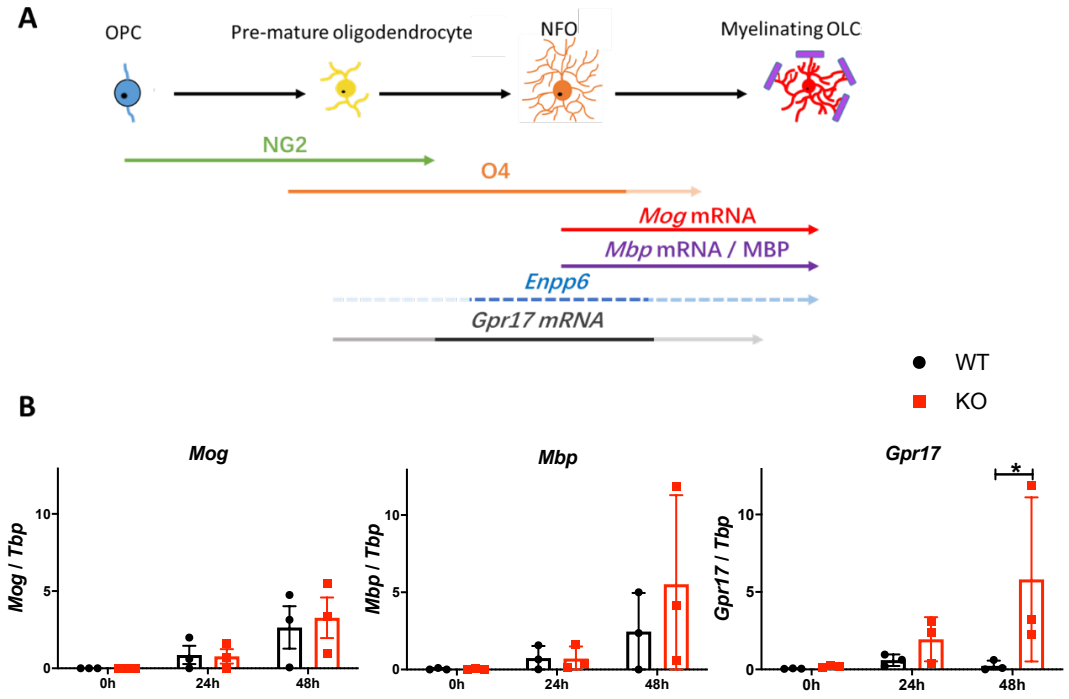

Figure 5.9 Oligodendrocyte differentiation marker expression profile across differentiation in OPCs from *Enpp6*$^{-/-}$ and *Enpp6*$^{+/+}$ mice. (A) Schematic of mRNA and protein expression for *Enpp6* and other known markers identifying specific stages of OPC differentiation. The figures represent the typical morphology of oligodendrocytes at the different specific steps of differentiation, from OPC to pre-mature oligodendrocyte; NFO and myelinating oligodendrocyte (mature oligodendrocyte). **(B)** The mRNA expression of myelin oligodendrocyte glycoprotein (*Mog*), myelin basic protein (*Mbp*), and G-protein receptor 17 (*Gpr17*) in primary mouse OPC cultures differentiated for 24 and 48 hours from C57BL/6J-*Enpp6*$^{+/+}$ mice and C57BL/6J-*Enpp6*$^{-/-}$ mice. *2-way ANOVA with Bonferroni post-hoc testing* was used for statistical analysis. n=3 for each genotype. n=3 for technical repeat. The values are represented as mean ± SE, **p<0.05; ns: not significant.*

5.3.5 *Enpp6* deletion does not affect myelination

To further explore the role of ENPP6 in OPC development, we investigated whether *Enpp6* deficiency affects myelination *in vivo*. No significant effect on total myelin was observed in *Enpp6*$^{-/-}$ mice compared to control *Enpp6*$^{+/+}$ mice (note that these mice were on the mixed genetic strain. Thus, ENPP6 deficiency did not affect myelination in the cortex (grey matter) and corpus callosum (white matter) as judged by the number of Oligo2^{+}oligodendrocytes (Figure 5.10B and C). Moreover, no gross difference in MBP and Luxol Fast Blue (LFB) staining was observed (Figure 5.10A). The result was consistent with our *in vitro* data that *Enpp6* deficiency did not affect the MBP expression in NFOs (Figure 5.8B). Increases in percentage of mature CC1^{+}Oligo2^{+} and CNPase^{+}Oligo2^{+} oligodendrocytes were observed in the *Enpp6*$^{-/-}$ mice (Figure 5.11A-C). Morphologically, the number of process per CNPase^{+} oligodendrocyte was fewer in *Enpp6*$^{-/-}$ compared to their controls (*Enpp6*$^{+/+}$) (Figure 5.11D and E). These data suggest that myelination was not affected in in *Enpp6*$^{-/-}$ mice, but these mice exhibited reduced development of oligodendrocyte processes and increased numbers of MOs.

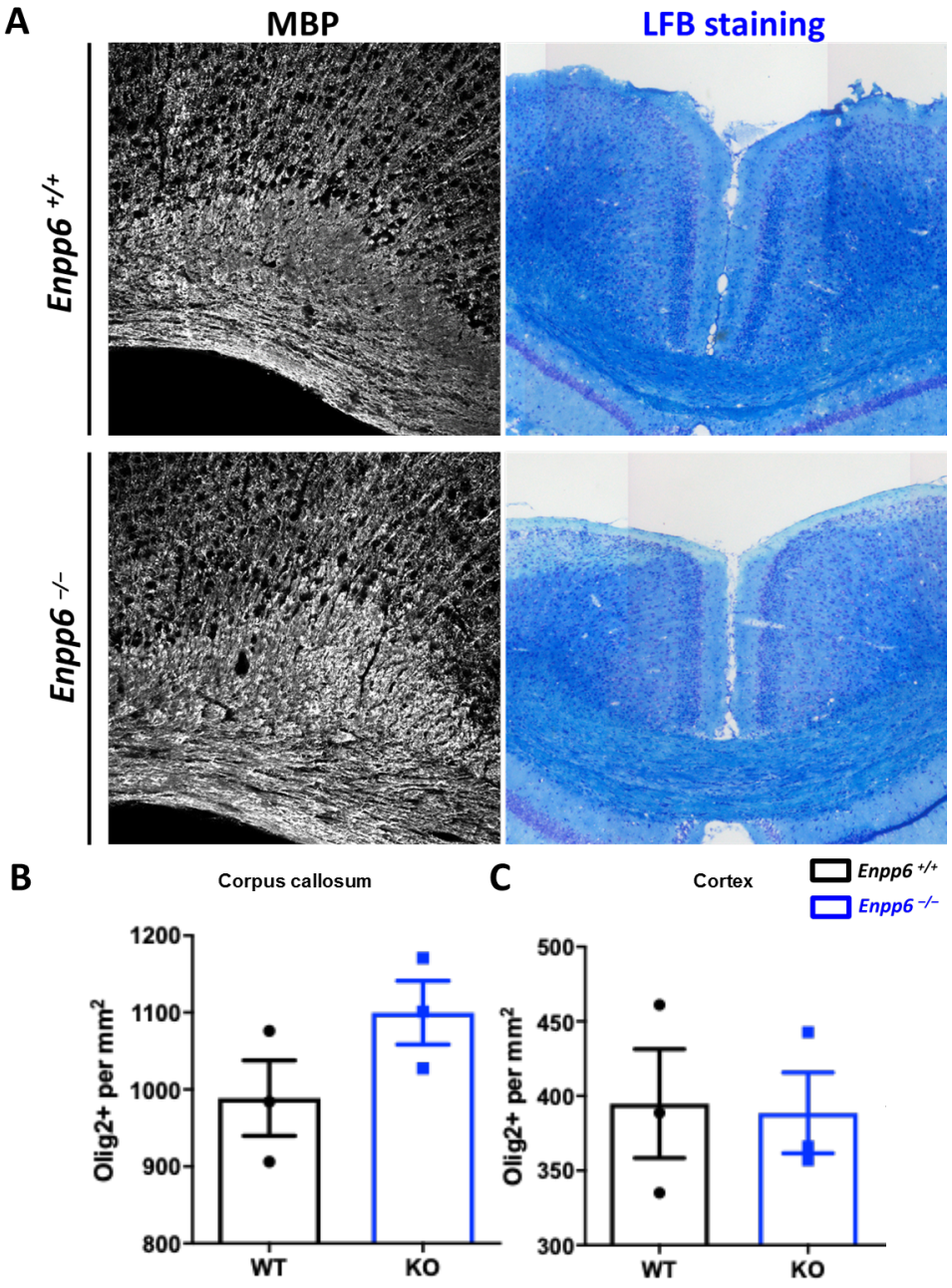

Figure 5.10 Effect of *Enpp6* depletion on myelination *in vivo*. (A) Images of MBP and LFB staining in the corpus callosum from P90 *Enpp6*$^{+/+}$ and *Enpp6*$^{-/-}$ mice. Quantification of Oligo2+ oligodendrocyte cell number in the corpus callosum **(B)** and the cortex **(C)** between *Enpp6*$^{+/+}$ and *Enpp6*$^{-/-}$ mice. n=3 for each genotype. This work was performed with Dr. Steffen Mayerl. *Unpaired student t-test* was used for statistical analysis. The values are represented as mean ± SE, *$p<0.05$. Images were captured by confocal.

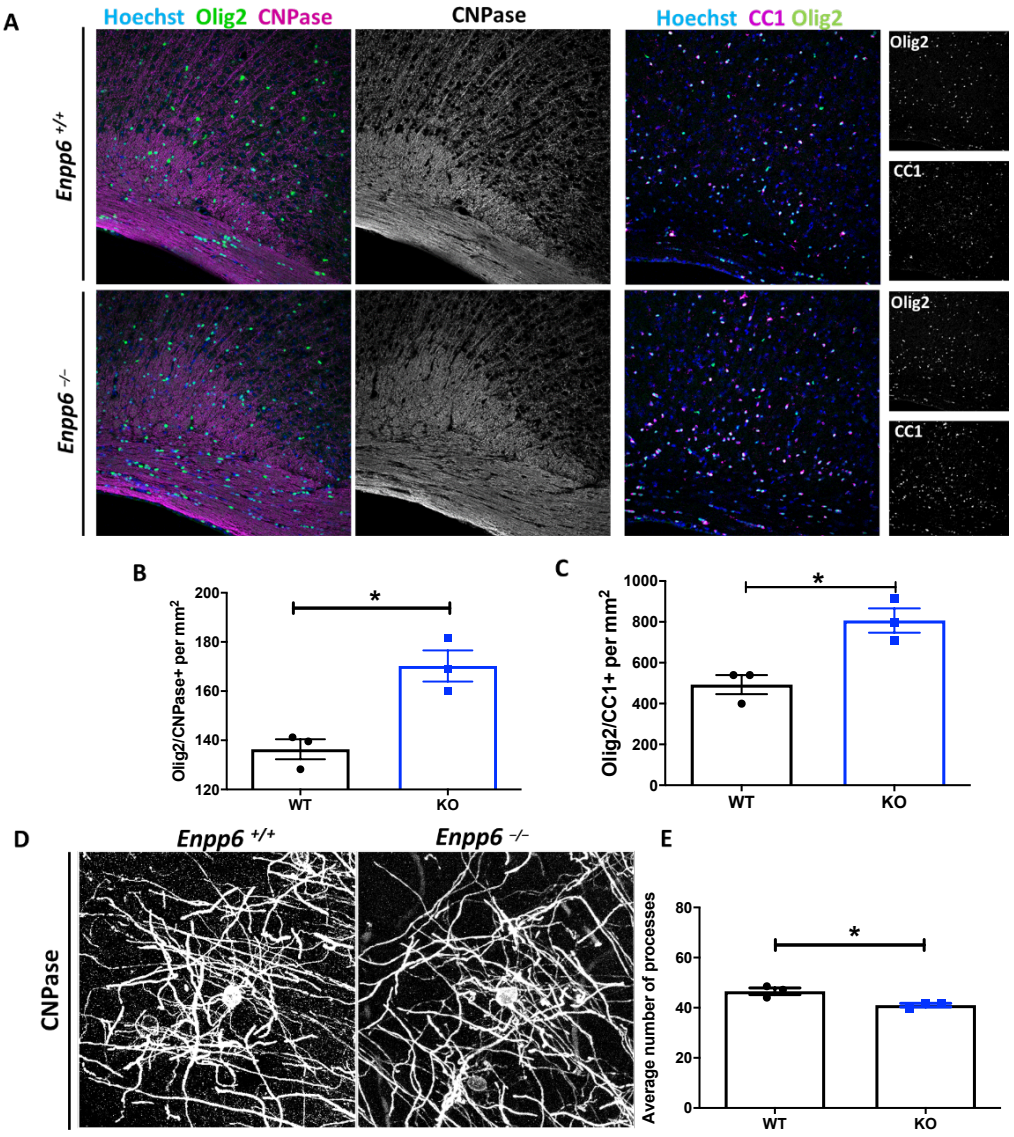

Figure 5.11 Effect of *Enpp6* depletion on CNPase and CC1 expression *in vivo*. **(A)** Images and quantification of CNPase^{+}Oligo2^{+} cells in the cortex **(B)**. CC1^{+}Oligo2^{+} cells in the corpus callosum **(C)** from the *Enpp6*$^{-/-}$ and *Enpp6*$^{+/+}$ mice. These mice were on the mixed genetic background. n=3 for each genotype. *Unpaired student t-test* was used for statistical analysis. Images were captured by confocal. **(D)** Images of cell process per cell. **(E)** Quantification of average of number of processes per cell. The values are represented as mean ± SE, *$p<0.05$.

5.4 Discussion

In this chapter, I studied the expression of ENPP6 and their enzymatic activity during the oligodendrocyte development. Moreover, the impact of ENPP6 deletion and pharmacological inhibition was tested in NFOs, in part through the development of a novel cell-based assay for ENPP6 enzymatic activity. It was hypothesised that ENPP6 deficiency caused dysfunction in oligodendrocyte development. The data support this hypothesis but reveal a complexity in its interpretation. Mainly, a delay or impairment of oligodendrocyte differentiation was observed *in vitro* but did not lead to discernible effects on total myelin protein expression *in vitro* or myelination *in vivo*. There was a subtle change in the nature of how comparable myelination was achieved in *Enpp6*$^{-/-}$ brain: more OPCs with fewer processes compared to *Enpp6*$^{+/+}$ mice and restored normal overall myelination. The ENPP6 expression pattern during oligodendrocyte differentiation was determined at the mRNA levels and functional protein (enzymatic activity) levels. We showed that ENPP6 deficiency delayed or suppressed oligodendrocyte differentiation and the molecular effect of this on for example GPR17 signalling. It warrants further investigation to assess any potential impact on neuronal function. Moreover, *Enpp6* deficiency did not affect myelination, and so there is no obvious contra-indication for the use of ENPP6 inhibitors as anti-diabetic drugs with respect to brain side effects.

5.4.1 ENPP6 enzymatic assay as a useful tool for future small molecular inhibitor screening

The method of ENPP6 activity assay was firstly described by Kawaguchi *et al.* in 2011 using protein/tissue lysates. In this chapter, we assessed the ENPP6 enzymatic activity in rodent oligodendrocytes based on this assay. Significantly greater ENPP6 activity was detected in NFOs and MOs. The data were consistent with *Enpp6* mRNA expression. We also showed that ENPP6 activity was decreased after T11 treatment (Figure 5.6A and B), confirming T11 can be employed as an inhibitor of ENPP6. Notably, ENPP6 activity was not completely inhibited by T11. The main reason might be that T11 is not a very

potent inhibitor, thus a higher concentration is needed to achieve the full inhibition (10 μM was used in this project). However, overdose of inhibitor may cause other problems such as toxicity. Thereby, with this assay, screening small molecules with low half maximal inhibitory concentration (IC_{50}) value is worth exploring in the future. This assay can be used to screen small candidate molecules as potent ENPP6 inhibitors.

5.4.2 Inhibition of ENPP6 compromised OPC differentiation without affecting the myelination

The monoclonal antibody to A2B5 was used to identify a biopotential O2A progenitor (oligodendrocytes-type 2 astrocytes progenitor, also called OPC). The O2A progenitors modulate their survival and proliferation mainly depends on a number of growth factors including platelet derived growth factor A (PDGFA) through PDGFα receptors (PDGFRα) (281, 363-365). Therefore, OPCs can be identified by the expression of A2B5, PDGFRα and also the cell surface marker NG2 (a sulphated proteoglycan) (366). Baracskay *et al.* demonstrated that $NG2^+$ cells and $A2B5^+$ cells appear from overlapping cell populations; Additionally, $NG2^+$ cells arise prior to the $A2B5^+$ cells. Therefore, $NG2^+A2B5^-$ cells are identified as pre-OPCs, whereas $A2B5^+$ cells are considered as OPCs (366). As very little expression of ENPP6 was detected at the earliest stages of OPC differentiation in this study, it suggests that ENPP6 deficiency is unlikely to affect OPC population.

This study disagreed with a previously published research where P14 young C57BL/6J-*Enpp6*$^{-/-}$ mice were described as a hypomyelination phenotype (8). Our data showed that no gross effect on myelin sheath area was observed in neither young nor adult *Enpp6*$^{-/-}$ mice. This is also evidenced by the results from the *in vitro* study, where pharmacological inhibition of ENPP6 activity and genetic ablation of *Enpp6* did not affect the myelin protein expression (Figure 5.10). Although future studies are needed to clarify the effects of ENPP6 on myelination, the difference from two studies could be explained by the different

genetic strain of mouse model used in two studies (details discussed in chapter 4).

Given that ENPP6 deficiency caused delayed differentiation without affecting myelination, the morphology of single oligodendrocyte and myelin sheaths were assessed in the prefrontal cortex of 3-month-old *Enpp6*$^{-/-}$ and *Enpp6*$^{+/+}$ mice. It was found that oligodendrocytes from *Enpp6*$^{-/-}$ mice had fewer processes compared to their controls (*Enpp6*$^{+/+}$) (Figure 5.11D and E). This might imply that ENPP6 deficiency compromised oligodendrocyte differentiation and caused impaired development of cell processes. However, increased numbers of mature oligodendrocyte compensated for impaired processes development in the *Enpp6*$^{-/-}$ mice. Hence, this does not result in a change in the myelination as the final stage of OPC maturation.

5.4.3 The potential link between ENPP6 and GPR17

NFOs from *Enpp6*$^{-/-}$ mice unusually expressed high levels of GPR17, a negative regulator of NFO differentiation (362). Previous research showed that overexpression of GPR17 inhibited oligodendrocyte maturation, whereas mice lacking *Gpr17* exhibited precocious onset of myelination (367). GPR17 is a 7 transmembrane receptor (7TR) with two putative endogenous lipid ligands; uracil nucleotides and cysteinyl leukotrienes (LTD4 and LTE4) (368). 7TR expression is regulated by ligand activation, with classical down-regulation of expression occurring when ligand is persistently high, and up-regulation when ligand is low. Therefore, high level of *Gpr17* mRNA in NFOs from *Enpp6*$^{-/-}$ mice, suggests that the expression of GPR17 ligands may be low. Notably, GPR17 ligands LTD4/LTE4 are produced from the sequential conversion of arachidonic acid (AA), which derives from phospholipase A2 (PLA2) activity on phosphatidylcholine (PC). The ENPP6 substrate LPC is also formed from this PLA2 activity. Moreover, LPC (20:4) is a preferred substrate for ENPP6. AA can therefore, theoretically, derive from sequential activity of ENPP6 (LPC 20:4 to 2-AG) and then action of monoacylglycerol lipase (MAGL) (164). Figure 5.12 shows the putative schematic signalling pathway of ENPP6-mediated

GPR17 activation in oligodendrocytes. ENPP6 is likely to mediates its effects on NFOs through upregulation of GPR17 signalling and NFO lipid metabolism. Thus, future studies can focus on investigating whether ENPP6 deficiency affects GPR17 signalling in NFOs and leads to the delayed differentiation of oligodendrocytes we observed in this chapter.

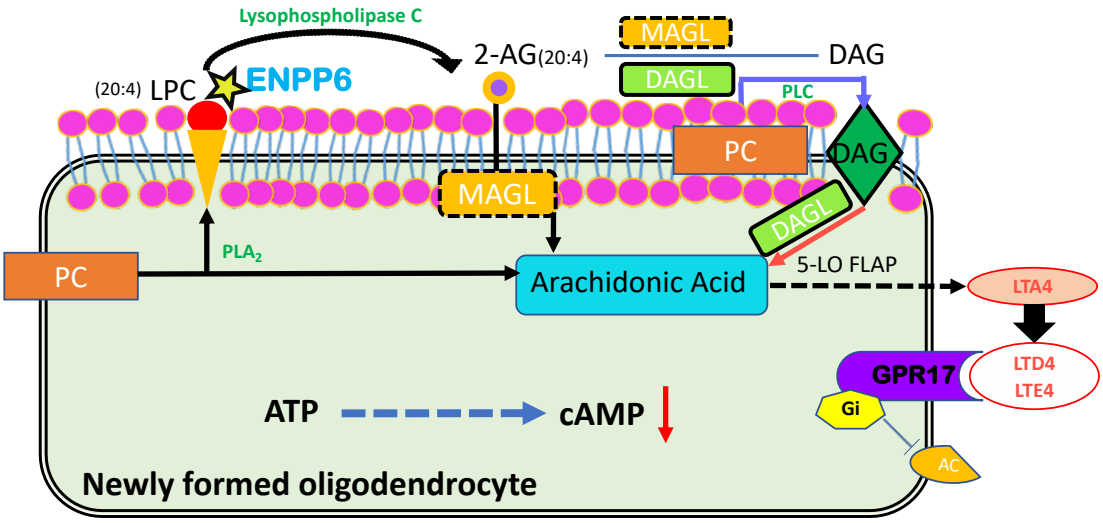

Figure 5.12 The putative signalling pathway of ENPP6-mediated GPR17 activation in NFOs. Phosphatidylcholine (PC) (20:4) hydrolysed by phospholipase A2 (PLA2) activity to produce LPC (20:4). ENPP6 has a preference to hydrolyse LPC (20:4) to produce 2-AG (details is described in chapter 1.8.2.1). Troughing a series reaction including: (1) 2-AG is metabolised to arachidonic acid (AA) by MAG lipase (MAGL) hydrolysis; or DAG converts to AA by DAG lipase (DAGL) hydrolysis; (2) AA is metabolised by 5-lipoxygenase (LO) and 5-LO activating protein (FLAP) to produce the GPR17 ligands LTD4 and LTE4. The activation of GPR17 trigger the activation of Gi protein thus inhibits the adenylyl cyclase (AC), which is a cAMP-dependent protein kinase that induce the reduction of cAMP production. Together, ENPP6 may be involved in the above pathway to contribute the cAMP-related metabolism in NFOs.

5.4.4 ENPP6-mediated 2-AG synthesis in NFOs

ENPP6 hydrolyses LPC to synthesise 2-AG via lysophospholipase C activity (164), and 2-AG is a specific ligand for the central and peripheral cannabinoid

receptors (CBRs) (details described in chapter 1.8.2). Thus, it is likely that ENPP6 may be associated with CBRs activation. Previous studies showed that OPCs and MOs express functional CBRs, suggesting OPCs and MOs are the potential targets for endocannabinoids (267-269). Interestingly, Gomez *et al.* reported that 2-AG synthesis and the activation of CBRs were required for oligodendrocyte maturation (361, 369), highlighting the role of 2-AG and activation of CBRs in oligodendrocyte maturation. Therefore, ENPP6 deficiency-induced impaired OPC differentiation may be caused by the interruption of the 2-AG synthesis in OPCs. Future studies can investigate whether the inhibition of ENPP6 activity reduces the 2-AG levels and downregulates CBRs activation in NFOs.

5.4.5 ENPP6-mediated cholinergic signalling in NFOs

Apart from LPC, ENPP6 also shows catalytic activity with other phospholipids such as GPC to produce phosphocholine, as a source of choline, suggesting its ability to supply endogenous choline (165). Choline plays an important role in supporting multiple organs, including liver and brain. Regarding its role in the brain development, choline acts as a precursor to the neurotransmitter acetylcholine. Although the function of acetylcholine in myelination has been investigated for decades (370), the precise roles of the acetylcholine signalling in oligodendrocyte maturation and myelination remains unclear. Future studies can also address the question if ENPP6 participates in choline-acetylcholine metabolism in oligodendrocytes, and therefore affecting the OPC development via regulating endogenous choline levels in the brain.

5.4.6 Oligodendrocyte plays a role in the metabolic control

Recently, Ou *et al.* showed that lack of GPR17 increased glycolysis and lactate production in oligodendrocytes (271). This suggests GPR17 plays a metabolic role in the oligodendrocytes. Although how this links to its functions in oligodendrocyte development is unknown, the interaction between ENPP6 and GPR17 is more likely to contribute to ENPP6 deficiency-induced impaired/delayed oligodendrocyte differentiation. Moreover, apart from

affecting oligodendrocyte development, ENPP6 may play other roles in oligodendrocytes, such as in lipid metabolism. Furthermore, our data suggest that ENPP6-expressing oligodendrocytes are more likely responsible for other functions such as lipid metabolism (through GPR17-involved pathway), but not the myelination (the primary role of oligodendrocyte). However, it is largely unexplored how oligodendrocytes regulate their own metabolism and, crucially affect that in those neighbouring neurons. Djogo *et al.* showed that the ablation of NG2-glial (also referred to as OPCs) in the hypothalamus (particularly in median eminence region) led to obesity, and associated with reduced responsiveness to the anorectic hormone leptin. This suggested that adult OPCs are required for leptin sensitivity and body weight control (279). Furthermore, Chang *et al.* showed that NG2-null mice exhibited an obese phenotype due to disruption of brown fat (burns energy and produces heat) dependent energy homeostasis (278), suggesting the control of the sympathetic outflow system by OPC-derived cells. More importantly, mice lacking oligodendrocyte *Gpr17* were reported to be resistant to high-fat-diet (HFD)-induced obesity and diabetes (271). This study highlights that oligodendrocyte GPR17 regulates body weight and glucose/insulin homeostasis through the cAMP and protein-kinase A signalling pathway (271). Particularly, this study is reminiscent of the involvement of ENPP6 in modulating obesity and diabetes risk, as ENPP6 is also predominantly expressed in the NFOs. These earlier studies gave us a clue that not merely neurons but their assocaited oligodendrocytes also regulate mechanisms of appetite and energy balance apart from being responsible for myelination. More studies are required to better understand the mechanism of effect of OPC and oligodendrocytes on energy homeostasis.

Chapter 6 Final discussion

6.1 Main findings

During my PhD, I investigated the role of ENPP6 in metabolism and addressed its function in oligodendrocyte differentiation. Figure 6.1 shows an overall schematic overview of my PhD work, including the background, experimental design and main findings.

Firstly, my work provided further evidence to support preliminary analysis on the phenotype of 'global' (whole body gene knockout) *Enpp6*$^{-/-}$ mice: an improved metabolic profile in mice lacking the *Enpp6* gene on the mixed genetic strain background. This included reduced visceral (epididymal) adiposity in parallel with reduced visceral (epididymal) adipocyte hypertrophy, improved glucose tolerance, and reduced liver fat accumulation. I demonstrated that ENPP6 deficiency-induced hepatic choline reduction represents an underlying mechanism contributing to their phenotype. this result suggests that ENPP6 is a novel anti-visceral obesity target, and ENPP6-regulated endogenous choline production plays a role in body-fat distribution distinct to dietary choline.

The second finding was the metabolic profile of mice lacking the *Enpp6* gene is strain dependent. In contrast to the phenotype of global *Enpp6*$^{-/-}$ mice in the mixed strain, *Enpp6* gene ablation in the C57BL/6J strain (5 generations of backcross) presented with a worsened metabolic profile. C57BL/6J global *Enpp6*$^{-/-}$ mice were prone to diet-induced obesity, insulin resistance and hepatic steatosis. This could partially be explained by the differences in *Enpp6* gene expression in distinct mouse strains, although this would formally require confirmation in similarly back-crossed 129S6 global *Enpp6*$^{-/-}$ mice.

The third finding was that the mice specifically lacking the *Enpp6* gene in oligodendrocytes presented a comparable metabolic phenotype to the control mice on the C57BL/6J strain. Given the unexpected strain divergence, the role

of ENPP6 in regulation of metabolic control via the oligodendrocyte is not conclusive and needs to be further investigated.

The final finding focused on the effect of ENPP6 on oligodendrocyte differentiation. I showed that ENPP6 deficiency by pharmacological inhibition and gene ablation resulted in a delay or impairment of OPC differentiation. Interestingly, ENPP6 deficiency did not affect the overall myelination content in global *Enpp6*$^{-/-}$ mice. Furthermore, I proposed a putative link between ENPP6 and G-protein coupled receptor 17 (GPR17) in newly formed oligodendrocytes (NFOs). The interaction between GPR17 and ENPP7 requires further investigation to assess any potential impact on mature oligodendrocyte function or related neuronal function.

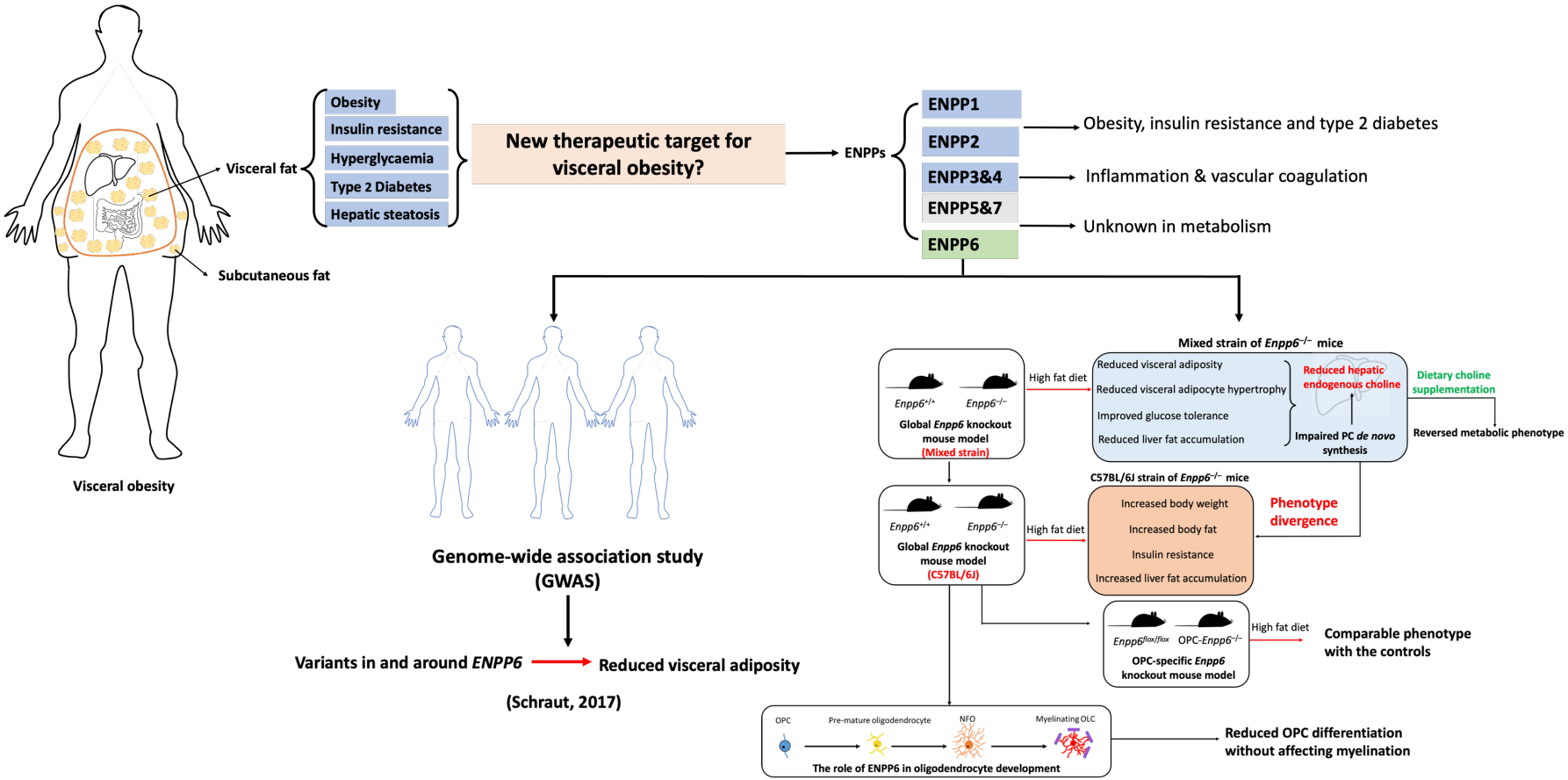

Figure 6.1 The schematic overview of research. OPC: oligodendrocyte precursor cell. PC: Phosphotidylcholine.

6.2 Implications

6.2.1 Therapeutic targetting of visceral obesity

Given that the currently approved anti-obesity drugs rely heavily on the overall weight loss either via reducing food intake or increasing energy expenditure, along with existing side-effects, exploring new pharmaceutical therapies and preventative strategies targeting adverse body fat distribution is warranted. My PhD research presents ENPP6 as a potential anti-visceral obesity pharmacotherapeutic target, and suggests the endogenous hepatic-choline-deficiency as the underlying mechanism. Lacking ENPP6 facilitates the metabolic profile in mice. Due to tractable cell surface location of ENPP6, it also represents a potentially more easily druggable target than compounds that require cell access.

The current knowledge of ENPP6 is limited to its structure and a few putative biological functions. Recently, Dillon *et al.*, reported that deletion of ENPP6 resulted in transient bone hypomineralisation (166). ENPP6 is described as a choline-specific glycerophosphodiester-phosphodiesterase which participates in choline metabolism (165), and a phospholipid enzyme which breakdowns the lysophosphotidylcholine (LPC) into phosphocholine (PhoC) and monoacylglycerol (MAG) (164). *Enpp6* gene knockout (*Enpp6*$^{-/-}$) mice were firstly reported by Morita *et al.* (165) where *Enpp6*$^{-/-}$ mice were described as exhibiting 'choline-deficiency'. It is plausible that this cell-level choline deficiency caused the phenotype of hypomyelination in the brain and fatty liver. Notably, the phenotype of fatty liver described in Morita *et al*., was subjective and non-quantitative (details described in chapter 3.4.1). However, Morita *et al.* did not provide direct evidence indicating that *Enpp6*$^{-/-}$ mice lacks choline, as the choline levels and its metabolites in plasma, liver, brain, and kidney were comparable to the wild-type mice (165). Our study identified a functional role of ENPP6 in metabolism, in particular, body fat distribution (visceral-epididymal adiposity). Similar to Morita *et al.*, we demonstrated that *Enpp6*$^{-/-}$ mice were apparently choline-deficient, but notably, the 'choline-deficiency' phenotype was only observed when exposed to high fat diet (HFD). These

HFD-fed *Enpp6*$^{-/-}$ mice exhibited lower level of liver choline compared to the wild-type mice. However, the choline levels of *Enpp6*$^{-/-}$ mice were comparable to the wile-type mice under normal diet circumstances (chow diet feeding). This results was consistent with Morita's findings (165). Furthermore, in contrast to Morita's study, *Enpp6*$^{-/-}$ mice in our lab did not display the phenotype of hypomyelination. Intriguingly, the HFD-fed *Enpp6*$^{-/-}$ mice were protected from fatty liver compared to the HFD-fed wild-type mice. Our data suggest this 'choline-deficiency' phenotype results in an improved metabolic phenotype including reduced visceral adiposity, improved glucose tolerance and reduced liver fat accumulation, without affecting overall oligodendrocyte myelination.

The model of 'choline-deficiency' in mouse, either achieved by altering dietary choline supply, or genetic deletion of *Pemt* (responsible for *de novo* biosynthesis of phosphatidylcholine from phosphatidylethanolamine) has been linked to altered metabolism including body weight, glucose homeostasis and visceral fat deposition. For example, HFD-fed *Pemt*$^{-/-}$ mice exhibited reduced body weight gain, a smaller amount of visceral fat and improved glucose tolerance compared to the wild-type mice (209). Dietary choline deficiency-fed *ob/ob* mice exhibited reduced total fat mass compared to the dietary choline supplemented diet-fed *ob/ob* mice (316). Thus, *Enpp6* gene deletion-induced reduced visceral (epididymal) adiposity and improved glucose tolerance is consistent with endogenous 'choline-deficiency'.

In contrast to other 'choline-deficiency' models where HFD-fed *Pemt*$^{-/-}$ mice were described to exhibit hepatic steatosis (209), choline deficient diet-fed *ob/ob* mice were described to exhibit exaggerated fatty liver (316). Consistent with that observation, C57BL/6J *Enpp6*$^{-/-}$ mice used in Morita's study were reported to display fatty liver – although this was on the basis of purely qualitative visualisation liver lipid content (165). In contrast, we found that HFD-fed *Enpp6*$^{-/-}$ mice were protected from the fatty liver. There are several potential reasons for this discrepancy. Firstly, the effect of endogenous choline

deficiency caused by *Enpp6* gene deletion was different from dietary choline deficiency. As ENPP6 is a cell surface enzyme, it may affect the choline content through controlling local plasma and membrane lipid, whereas dietary choline may go through metabolic routes and incorporation into membranes.

Dietary choline deficiency appears to trigger hepatic steatosis, although it may protect against the diet-induced obesity and its associated metabolic dysfunction. This is evidenced by the choline deficient-HFD (CDHFD)-fed *Enpp6*$^{-/-}$ mice that exhibited increased liver lipid accumulation compared to the wild-type mice, although they had a lower overall body fat gain, in particular subcutaneous fat. Similarly, Wu *et al.* showed that dietary choline deficiency-fed *ob/ob* mice exhibited fatty liver although these mice had lower fat mass compared to choline supplemented diet-fed *ob/ob* mice (316). Secondly, we found a discrepancy with Morita's study with regard to the opposite phenotype of fatty liver in *Enpp6*$^{-/-}$ mice. This could be due to differences in the genetic strain used to study the *Enpp6* gene deletion. The *Enpp6*$^{-/-}$ mice used in our laboratory were based on a mixed genetic strain (C57BL/6J and 129S6), whereas the *Enpp6*$^{-/-}$ mice used in Morita's group were exclusively generated on the C57BL/6J background.

The potential genetic strain effects on metabolic profile led this study to further investigate the relationship between the genetic strain background and metabolic parameters. The initial observation of *Enpp6*$^{-/-}$ mice in our lab was generated by using a 129S6-derived mouse embryonic stem cell line and crossed with C57BL/6J as the background line. This approach for generating transgenic mouse model is commonly used (321, 339) due to cost-effectiveness. However, the complex mixed strain can cause low reproducibility of research. Therefore, standardisation of strain background is important and necessary in translational animal studies.

We found that *Enpp6*$^{-/-}$ mice from two genetic strains: mixed background and C57BL/6J, displayed different metabolic parameters. In contrast to mixed stain

of *Enpp6*$^{-/-}$ mice, C57BL/6J strain of *Enpp6*$^{-/-}$ mice exhibited a worsened metabolic profile. Thus, the role of the *Enpp6* gene appears to be affected by different strain backgrounds. In the past decades, the relationship between the strain background and metabolic parameters in rodent study has been widely discussed. Indeed, rodents under the different strains exhibited various phenotypes. Apart from the strain *per se*, targeted alleles in different strains have also been reported to display different phenotype, e.g., *ob/ob* mice (350, 351). Therefore, the choice of the genetic background to generate and analyse the mutant mice models in the translational study is important as any other factors such as the environmental, age, sex, which can cause variability of phenotypic results.

The different phenotype of *Enpp6*$^{-/-}$ mice under two strains also have implications for one assumption: the anti-visceral obesity potential of inhibiting ENPP6 may only benefit a limited population on a genetic susceptibility basis. This does not invalidate the approach as we move towards personalised medicine with tailored and genetically predictable drug responses. To put this in context, for example, metformin, the most commonly used first-line drugs for type 2 diabetes has a genetic susceptibility-dependent efficacy; a substantial proportion of patients do not respond to metformin, or respond adversely (357). Given ENPP6 is predominantly and highly expressed in the brain NFOs, and because the brain plays a central role in metabolic control, we initially hypothesised that ENPP6 deficiency-regulated metabolism through its effects on the NFO ENPP6. Excluding the unexpected strain divergence, we rejected this hypothesis, as mice lacking oligodendrocyte-*Enpp6* gene in the C57BL/6J strain exhibited a comparable phenotype relative to the control mice. However, whether oligodendrocyte ENPP6 regulates metabolism still needs further investigation regarding discrepancy in genetic background. As ENPP6 is also highly expressed in the liver sinusoidal endothelial cells and kidney proximal tubular cells (165). ENPP6-regulated metabolism might also be achieved through its effects on liver or kidney. The functional roles of ENPP6 in the liver or kidney is largely unexplored and thus needs to address in the future, which

could benefit the understanding of metabolic role of ENPP6. Notably, ENPP6 is undetectable in adipose tissue (142), indicating an indirect adipose-independent effect of ENPP6 deficiency to regulate fat distribution.

6.2.2 ENPP6-expressing oligodendrocyte in metabolism

Our *in vitro* study suggests ENPP6-expressing oligodendrocyte is likely responsible for other functions such as lipid metabolism (via GPR17-involved signalling pathway), but ultimately not the myelination function of oligodendrocytes. Current knowledge in the biological and physiological function of oligodendrocytes suggests they form the insulating myelin sheath to wrap the neuronal axons in the central nervous system (CNS). The dysfunction and apoptosis of oligodendrocytes can result in pathological process, such as demyelination (e.g., multiple sclerosis, a chronic demyelination diseases of the CNS), and neurodegeneration. However, little is known about whether oligodendrocytes, or their intermediate precursors, participate in metabolic control – for example by modulating neuronal function – in the context of obesity. In other words, whether the dysfunction of oligodendrocyte can lead to obesity pathogenesis is poorly understood. Only two studies so far have identified that undifferentiated OPCs participate in regulating brown adipose tissue-involved energy expenditure (278), or control body weight via modulation of leptin signalling (279). Only one recent study reported the metabolic role of differentiated oligodendrocytes (NFOs) in the context of diet-induced obesity via oligodendrocyte-neuronal crosstalk in the CNS (271). Given that ENPP6 is not expressed in the neurons or other types of glial cells including OPCs, and its metabolic role in regulating visceral adiposity and glucose homeostasis, our study provides more evidence for a role for oligodendrocytes in the regulation of energy metabolism. Further investigation on how ENPP6-expressing oligodendrocytes regulate metabolic control, including visceral adiposity (that we show is predominantly peripheral organ-dependent) and glucose homeostasis is thus needed.

6.3 Limitations and future work

The main limitation of this PhD project is the mouse model with respect to four aspects: sex, genetic strain background, pharmacological inhibition and target tissues.

Firstly, in this study, only male mice were used for two main reasons: 1. Female mice may face the effects of hormone cycling (oestrus) on their metabolic profiles. 2. Time and funding limitations. An increasing body of studies have argued that sex should be taken into account in preclinical studies as sex indeed affects the control of metabolic homeostasis (371). A great number of studies have shown sex differences in metabolic alterations in different mouse models (372-377). Similar for humans, a fundamental sex difference exists in glucose homeostasis (378), energy balance related to food intake (379) and energy expenditure (380). Regarding the research of sex divergence in visceral obesity, a recent genome-wide association study (GWAS) of body fat distribution identified 98 independent loci among 362,499 individuals from the UK biobank, in which a high degree of sex-heterogeneity was observed (140). Together, in the future, it is worth studying female mice lacking the *Enpp6* gene to better understand the effect of sex on the functional role of ENPP6.

Secondly, our data showed that the metabolic profile of mice lacking the *Enpp6* gene is strain dependent. Our initial mouse model of *Enpp6* deletion was performed on a mixed genetic strain: 129S6:C57BL/6J. The heterozygous x heterozygous breeding strategy to produce the experimental mice maintained a roughly 50:50 strain content, and so heterogeneity in the individual mice for strain background also generates variability in their metabolic responses. Nevertheless, effects of gene knockout that persist in mixed backgrounds may be more relevant to the mixed genetic background found in humans – and could even predict greater efficacy across populations for inhibitor drugs. As we only backcrossed the mixed strain of *Enpp6*$^{-/-}$ mice with C57BL/6J and assessed their phenotype, it the metabolic phenotype of *Enpp6*$^{-/-}$ mice on the pure 129S6 strain is unknown. The mixed strain of *Enpp6*$^{-/-}$ mice might be

more metabolically similar to a theoretically pure 129S6 strain of *Enpp6*$^{-/-}$ mice. This is also evidenced by a comparable *Enpp6* mRNA level between 129S6 mice and mixed strain mice. Study of a 129S6 line of *Enpp6*$^{-/-}$ mice with a predicted protected metabolic phenotype would benefit future studies related to drug inhibition and tissue-specific gene deletion.

Thirdly, this study lacks the study of pharmacological inhibition of ENPP6 in mice. According to *in vitro* study, we tested the effect of a potential ENPP6 inhibitor T11 in rat NFO differentiation. We showed that T11 did not completely inhibit ENPP6 activity, resulting in on average 56.62% inhibition of ENPP6 enzyme activity in rat NFOs at a concentration of 10μM. Given T11 is not a very potent inhibitor, which requires a very high concentration to achieve the full inhibition, we have not applied T11 in *Enpp6*$^{-/-}$ mice yet. The pharmacokinetics of T11 are also unknown *in vivo*. Screening higher-potency small molecule inhibitors for ENPP6 inhibition is indeed worth exploring before conducting the drug inhibition study *in vivo*. Thus, we generated a workable ENPP6-expressing cell line which can facilitate the small molecular drug screening for ENPP6.

The last aspect of limitation is the mouse model for tissue specific *Enpp6* deletion. This PhD project generated and assessed the metabolic profile of brain (OPC)-specific *Enpp6* deletion mouse model. Excluding the issue of genetic background, we did not see a distinct metabolic phenotype in this mouse model. As ENPP6 is also highly expressed in the liver sinusoidal endothelial cells and kidney proximal tubular cells, it is worth investigating the metabolic profile of mice lacking the *Enpp6* gene in liver and kidney, respectively.

For the future work, apart from using different mouse models described above, further investigation regarding understanding the cellular mechanisms that mediate the beneficial effects of ENPP6 in NFOs can be considered.

Firstly, we showed that NFOs from *Enpp6*$^{-/-}$ mice expressed unusually high levels of GPR17, a negative regulator of OPC differentiation. GPR17 is a target for endogenous lipid signalling molecules such as leukotrienes. A recently published study showed NFO GPR17 contributes to whole-body metabolism including body weight, glucose homeostasis and energy expenditure, through the cyclic Adenosine Monophosphate (cAMP) and protein-kinase A signalling pathway, reminiscent of the involvement of ENPP6 in modulating visceral obesity and diabetes risks. Thus, future investigations should assess GPR17 and leukotrienes signalling and include analysis of NFO metabolic signalling (e.g. lactate production) and cellular metabolic profile of NFOs and measurement of the cAMP levels in NFOs from *Enpp6*$^{-/-}$ mice or after small molecular ENPP6 inhibitors-treatment of NFOs.

Secondly, ENPP6 activity may associate with the cannabinoid receptor activation (CBRs) as it hydrolyses LPC to synthesise 2-arachidonoyglycerol (2-AG), which is a specific ligand for the CBRs (details described in chapter 1.8.2). The metabolic roles of CBRs in the CNS include control of appetite, energy intake, and energy expenditure (263). Moreover, previous studies suggested the oligodendrocytes are the targets for CBRs (267-269). Thus, another opportunity for future work is investigation of whether NFO ENPP6 is involved in the activation of CBRs via 2-AG production and thus contributes to its beneficial metabolic effects.

Thirdly, we reported that hepatic choline deficiency is a plausible underlying mechanism of ENPP6-regulated metabolism. Given choline plays important roles in multiple organs including the brain, where choline acts as a precursor to the neurotransmitter acetylcholine, it is worth investigating the functions of ENPP6-regulated choline metabolism in NFOs.

6.4 Conclusions

Overall, this PhD work demonstrated that ENPP6 is a novel anti-visceral obesity and anti-diabetic target, and highlights ENPP6-regulated endogenous hepatic choline production plays a novel role in body fat distribution distinct to dietary choline. Given the existence of strain differences in metabolic profile of mice lacking *Enpp6* gene, screening small molecular inhibitor for ENPP6 needs to consider the population-heterogeneity of response for any future clinical development. Moreover, this study suggests the potential contribution of NFOs in energy metabolism, highlighting an unexpected role of NFOs apart from the myelination in the CNS.

References

1. Organization WH. Obesity and overweight 2016 [updated 2021 June 9]. Available from: https://www.who.int/mediacentre/factsheets/fs311/en/.
2. Organization WH. Noncommnicable dieases progress monitor 2017 [updated 2021 October 26]. Available from: https://www.who.int/nmh/publications/ncd-progress-monitor-2017/en/.
3. Pi-Sunyer X. The medical risks of obesity. Postgraduate Medicine. 2009;121(6):21-33.
4. Finucane MM, Stevens GA, Cowan MJ, Danaei G, Lin JK, Paciorek CJ, et al. National, regional, and global trends in body-mass index since 1980: systematic analysis of health examination surveys and epidemiological studies with 960 country-years and 9.1 million participants. The Lancet. 2011;377(9765):557-67.
5. Colditz GA, Willett WC, Rotnitzky A, Manson JE. Weight gain as a risk factor for clinical diabetes mellitus in women. Annals of Internal Medicine. 1995;122(7):481-6.
6. Willett WC, Manson JE, Stampfer MJ, Colditz GA, Rosner B, Speizer FE, et al. Weight, weight change, and coronary heart-disease in women - risk within the normal-weight range. Journal of the American Medical Association. 1995;273(6):461-5.
7. Calle EE, Rodriguez C, Walker-Thurmond K, Thun MJ. Overweight, obesity, and mortality from cancer in a prospectively studied cohort of US adults. New England Journal of Medicine. 2003;348(17):1625-38.
8. Collaboration ERF. Separate and combined associations of body-mass index and abdominal adiposity with cardiovascular disease: collaborative analysis of 58 prospective studies. The Lancet. 2011;377(9771):1085-95.
9. Lapidus L, Bengtsson C, Larsson B, Pennert K, Rybo E, Sjöström L. Distribution of adipose tissue and risk of cardiovascular disease and death: a 12 year follow up of participants in the population study of women in Gothenburg, Sweden. British Medical Journal (Clinical Research Ed). 1984;289(6454):1257-61.
10. Larsson B, Svärdsudd K, Welin L, Wilhelmsen L, Björntorp P, Tibblin G. Abdominal adipose tissue distribution, obesity, and risk of cardiovascular disease and death: 13 year follow up of participants in the study of men born in 1913. British Medical Journal (Clinical Research Ed). 1984;288(6428):1401-4.
11. Stevens J, Cai J, Pamuk ER, Williamson DF, Thun MJ, Wood JL. The effect of age on the association between body-mass index and mortality. New England Journal of Medicine. 1998;338(1):1-7.
12. Wannamethee SG, Shaper AG, Walker M, Ebrahim S. Lifestyle and 15-year survival free of heart attack, stroke, and diabetes in middle-aged British men. Archives of Internal Medicine. 1998;158(22):2433-40.
13. Wilson PW, D'Agostino RB, Sullivan L, Parise H, Kannel WB. Overweight and obesity as determinants of cardiovascular risk: the Framingham experience. Archives of Internal Medicine. 2002;162(16):1867-72.

14. Odamaki M, Furuya R, Ohkawa S, Yoneyama T, Nishikino M, Hishida A, et al. Altered abdominal fat distribution and its association with the serum lipid profile in non-diabetic haemodialysis patients. Nephrology Dialysis Transplantation. 1999;14(10):2427-32.
15. Brunzell JD, Hokanson JE. Dyslipidemia of central obesity and insulin resistance. Diabetes Care. 1999;22:C10-3.
16. Björntorp P. Visceral obesity: a “civilization syndrome”. Obesity Research. 1993;1(3):206-22.
17. Després J-P, Lemieux I. Abdominal obesity and metabolic syndrome. Nature. 2006;444(7121):881-7.
18. Browning LM, Hsieh SD, Ashwell M. A systematic review of waist-to-height ratio as a screening tool for the prediction of cardiovascular disease and diabetes: 0· 5 could be a suitable global boundary value. Nutrition Research Reviews. 2010;23(2):247-69.
19. Vague J. Sexual differentiation, a factor affecting the forms of obesity. La Presse médicale. 1947;30:339-40.
20. Krotkiewski M, Björntorp P, Sjöström L, Smith U. Impact of obesity on metabolism in men and women. Importance of regional adipose tissue distribution. Journal of Clinical Investigation. 1983;72(3):1150-62.
21. Ohlson L-O, Larsson B, Svärdsudd K, Welin L, Eriksson H, Wilhelmsen L, et al. The influence of body fat distribution on the incidence of diabetes mellitus: 13.5 years of follow-up of the participants in the study of men born in 1913. Diabetes. 1985;34(10):1055-8.
22. Ruderman N, Berchtold P, Schneider S. Obesity-associated disorders in normal-weight individuals: some speculations. International Journal of Obesity. 1982;6:151-7.
23. Ruderman N, Chisholm D, Pi-Sunyer X, Schneider S. The metabolically obese, normal-weight individual revisited. Diabetes. 1998;47(5):699-713.
24. St-Onge M-P, Janssen I, Heymsfield SB. Metabolic syndrome in normal-weight Americans: new definition of the metabolically obese, normal-weight individual. Diabetes Care. 2004;27(9):2222-8.
25. Ferrannini E, Natali A, Bell P, Cavallo-Perin P, Lalic N, Mingrone G. Insulin resistance and hypersecretion in obesity. European Group for the Study of Insulin Resistance (EGIR). Journal of Clinical Investigation. 1997;100(5):1166-73.
26. Bonora E, Kiechl S, Willeit J, Oberhollenzer F, Egger G, Targher G, et al. Prevalence of insulin resistance in metabolic disorders: the Bruneck Study. Diabetes. 1998;47(10):1643-9.
27. Bosello O, Zamboni M. Visceral obesity and metabolic syndrome. Obesity Reviews. 2000;1(1):47-56.
28. Silver HJ, Welch EB, Avison MJ, Niswender KD. Imaging body composition in obesity and weight loss: challenges and opportunities. Diabetes, Metabolic Syndrome and Obesity: Targets and Therapy. 2010;3:337-47.
29. Sjostrom L, Kvist H, Cederblad A, Tylen U. Determination of total adipose tissue and body fat in women by computed tomography, 40K, and tritium. American Journal of Physiology-Endocrinology And Metabolism. 1986;250(6):E736-E45.

30. Ferland M, DesprÉS J-p, Tremblay A, Pinault S, Nadeau A, Moorjani S, et al. Assessment of adipose tissue distribution by computed axial tomography in obese women: association with body density and anthropometric measurements. British Journal of Nutrition. 1989;61(2):139-48.
31. Chowdhury B, Sjöström L, Alpsten M, Kostanty J, Kvist H, Löfgren R. A multicompartment body composition technique based on computerized tomography. International Journal of Obesity and Related Metabolic Disorders: Journal of the International Association for the Study of Obesity. 1994;18(4):219-34.
32. Björntorp P, Sjöström L. Carbohydrate storage in man: speculations and some quantitative considerations. Metabolism. 1978;27(12):1853-65.
33. Reshef L, Olswang Y, Cassuto H, Blum B, Croniger CM, Kalhan SC, et al. Glyceroneogenesis and the triglyceride/fatty acid cycle. Journal of Biological Chemistry. 2003;278(33):30413-6.
34. Strålfors P P, Honnor RC. Insulin‐induced dephosphorylation of hormone‐sensitive lipase: Correlation with lipolysis and cAMP‐dependent protein kinase activity. European Journal of Biochemistry. 1989;182(2):379-85.
35. Björntorp P, Bergman H, Varnauskas E. Plasma free fatty acid turnover rate in obesity. Acta Medica Scandinavica. 1969;185(1‐6):351-6.
36. Jensen MD, Haymond MW, Rizza RA, Cryer PE, Miles J. Influence of body fat distribution on free fatty acid metabolism in obesity. Journal of Clinical Investigation. 1989;83(4):1168-73.
37. Smith U, Hammersten J, Björntorp P, Kral J. Regional differences and effect of weight reduction on human fat cell metabolism. European Journal of Clinical Investigation. 1979;9(5):327-32.
38. Björntorp P. Metabolic implications of body fat distribution. Diabetes Care. 1991;14(12):1132-43.
39. Arner P. Differences in lipolysis between human subcutaneous and omental adipose tissues. Annals of Medicine. 1995;27(4):435-8.
40. Bonadonna R, Bonora E. Glucose and free fatty acid metabolism in human obesity-Relationships to insulin resistance. Diabetes Reviews. 1997;5(1):21-51.
41. Shepherd PR, Kahn BB. Glucose transporters and insulin action—implications for insulin resistance and diabetes mellitus. New England Journal of Medicine. 1999;341(4):248-57.
42. Bryant NJ, Govers R, James DE. Regulated transport of the glucose transporter GLUT4. Nature Reviews Molecular Cell Biology. 2002;3(4):267-77.
43. Reaven GM. Role of insulin resistance in human disease. Diabetes. 1988;37(12):1595-607.
44. Preis SR, Massaro JM, Robins SJ, Hoffmann U, Vasan RS, Irlbeck T, et al. Abdominal subcutaneous and visceral adipose tissue and insulin resistance in the Framingham heart study. Obesity. 2010;18(11):2191-8.
45. McLaughlin T, Lamendola C, Liu A, Abbasi F. Preferential fat deposition in subcutaneous versus visceral depots is associated with insulin sensitivity. Journal of Clinical Endocrinology & Metabolism. 2011;96(11):E1756-E60.

46. Bergstrom RW, Newell-Morris LL, Leonetti DL, Shuman WP, Wahl PW, Fujimoto WY. Association of elevated fasting C-peptide level and increased intra-abdominal fat distribution with development of NIDDM in Japanese-American men. Diabetes. 1990;39(1):104-11.
47. Hayashi T, Boyko EJ, Leonetti DL, McNeely MJ, Newell-Morris L, Kahn SE, et al. Visceral adiposity and the risk of impaired glucose tolerance: a prospective study among Japanese Americans. Diabetes Care. 2003;26(3):650-5.
48. Sparrow D, Borkan GA, Gerzof SG, Wisniewski C, Silbert CK. Relationship of fat distribution to glucose tolerance: results of computed tomography in male participants of the normative aging study. Diabetes. 1986;35(4):411-5.
49. Group D-DS, Group EDE. Age, body mass index and type 2 diabetes—associations modified by ethnicity. Diabetologia. 2003;46(8):1063-70.
50. Verboven K, Wouters K, Gaens K, Hansen D, Bijnen M, Wetzels S, et al. Abdominal subcutaneous and visceral adipocyte size, lipolysis and inflammation relate to insulin resistance in male obese humans. Scientific Reports. 2018;8(1):1-8.
51. Boden G, Chen X, Ruiz J, White JV, Rossetti L. Mechanisms of fatty acid-induced inhibition of glucose uptake. Journal of Clinical Investigation. 1994;93(6):2438-46.
52. Santomauro A, Boden G, Silva M, Rocha DM, Santos RF, Ursich M, et al. Overnight lowering of free fatty acids with Acipimox improves insulin resistance and glucose tolerance in obese diabetic and nondiabetic subjects. Diabetes. 1999;48(9):1836-41.
53. Strissel KJ, Stancheva Z, Miyoshi H, Perfield JW, DeFuria J, Jick Z, et al. Adipocyte death, adipose tissue remodeling, and obesity complications. Diabetes. 2007;56(12):2910-8.
54. Murano I, Barbatelli G, Parisani V, Latini C, Muzzonigro G, Castellucci M, et al. Dead adipocytes, detected as crown-like structures, are prevalent in visceral fat depots of genetically obese mice. Journal of Lipid Research. 2008;49(7):1562-8.
55. Hardy OT, Czech MP, Corvera S. What causes the insulin resistance underlying obesity? Current Opinion in Endocrinology, Diabetes, and Obesity. 2012;19(2):81-7.
56. Zhang Y, Proenca R, Maffei M, Barone M, Leopold L, Friedman JM. Positional cloning of the mouse obese gene and its human homologue. Nature. 1994;372(6505):425-32.
57. Arita Y, Kihara S, Ouchi N, Takahashi M, Maeda K, Miyagawa J-i, et al. Paradoxical decrease of an adipose-specific protein, adiponectin, in obesity. Biochemical and Biophysical Research Communications. 1999;257(1):79-83.
58. Trayhurn P, Wood IS. Adipokines: inflammation and the pleiotropic role of white adipose tissue. British Journal of Nutrition. 2004;92(3):347-55.
59. Fried SK, Bunkin DA, Greenberg AS. Omental and subcutaneous adipose tissues of obese subjects release interleukin-6: depot difference and regulation by glucocorticoid. Journal of Clinical Endocrinology & Metabolism. 1998;83(3):847-50.

60. Bruun JM, Pedersen SB, Richelsen B. Regulation of interleukin 8 production and gene expression in human adipose tissue in vitro. Journal of Clinical Endocrinology & Metabolism. 2001;86(3):1267-73.
61. Fain JN, Madan AK, Hiler ML, Cheema P, Bahouth SW. Comparison of the release of adipokines by adipose tissue, adipose tissue matrix, and adipocytes from visceral and subcutaneous abdominal adipose tissues of obese humans. Endocrinology. 2004;145(5):2273-82.
62. Fruhbeck G, Gómez-Ambrosi J, Muruzábal FJ, Burrell MA. The adipocyte: a model for integration of endocrine and metabolic signaling in energy metabolism regulation. American Journal of Physiology-Endocrinology And Metabolism. 2001;280(6):E827-E47.
63. Trayhurn P, Beattie JH. Physiological role of adipose tissue: white adipose tissue as an endocrine and secretory organ. Proceedings of the Nutrition Society. 2001;60(3):329-39.
64. Fernández-Real JM, Ricart W. Insulin resistance and chronic cardiovascular inflammatory syndrome. Endocrine Reviews. 2003;24(3):278-301.
65. Rajala MW, Scherer PE. Minireview: the adipocyte—at the crossroads of energy homeostasis, inflammation, and atherosclerosis. Endocrinology. 2003;144(9):3765-73.
66. Sethi JK, Hotamisligil GS, editors. The role of TNFα in adipocyte metabolism. Seminars in Cell & Developmental Biology; 1999: Elsevier.
67. Hotamisligil G. Inflammatory pathways and insulin action. International Journal of Obesity. 2003;27(3):S53-S5.
68. Hotamisligil GS, Shargill NS, Spiegelman BM. Adipose expression of tumor necrosis factor-alpha: direct role in obesity-linked insulin resistance. Science. 1993;259(5091):87-91.
69. Kern PA, Saghizadeh M, Ong JM, Bosch RJ, Deem R, Simsolo RB. The expression of tumor necrosis factor in human adipose tissue. Regulation by obesity, weight loss, and relationship to lipoprotein lipase. Journal of Clinical Investigation. 1995;95(5):2111-9.
70. Kern PA, Ranganathan S, Li C, Wood L, Ranganathan G. Adipose tissue tumor necrosis factor and interleukin-6 expression in human obesity and insulin resistance. American Journal of Physiology-Endocrinology and Metabolism. 2001;280(5):E745-E51.
71. Esposito K, Pontillo A, Giugliano F, Giugliano G, Marfella R, Nicoletti G, et al. Association of low interleukin-10 levels with the metabolic syndrome in obese women. Journal of Clinical Endocrinology & Metabolism. 2003;88(3):1055-8.
72. Rytka JM, Wueest S, Schoenle EJ, Konrad D. The portal theory supported by venous drainage–selective fat transplantation. Diabetes. 2011;60(1):56-63.
73. Hardy OT, Perugini RA, Nicoloro SM, Gallagher-Dorval K, Puri V, Straubhaar J, et al. Body mass index-independent inflammation in omental adipose tissue associated with insulin resistance in morbid obesity. Surgery for Obesity and Related Diseases. 2011;7(1):60-7.
74. Stienstra R, Joosten LA, Koenen T, Van Tits B, Van Diepen JA, Van Den Berg SA, et al. The inflammasome-mediated caspase-1 activation

controls adipocyte differentiation and insulin sensitivity. Cell Metabolism. 2010;12(6):593-605.
75. Yang Y, Wang H, Kouadir M, Song H, Shi F. Recent advances in the mechanisms of NLRP3 inflammasome activation and its inhibitors. Cell Death & Disease. 2019;10(2):1-11.
76. Schroder K, Zhou R, Tschopp J. The NLRP3 inflammasome: a sensor for metabolic danger? Science. 2010;327(5963):296-300.
77. Vandanmagsar B, Youm Y-H, Ravussin A, Galgani JE, Stadler K, Mynatt RL, et al. The NLRP3 inflammasome instigates obesity-induced inflammation and insulin resistance. Nature Medicine. 2011;17(2):179.
78. Holman RR, Paul SK, Bethel MA, Matthews DR, Neil HAW. 10-year follow-up of intensive glucose control in type 2 diabetes. New England Journal of Medicine. 2008;359(15):1577-89.
79. Chatterjee S, Khunti K, Davies MJ. Type 2 diabetes. The Lancet. 2017;389(10085):2239-51.
80. Björntorp P, Rosmond R. Visceral obesity and diabetes. Drugs. 1999;58(1):13-8.
81. Federation ID. IDF Diabetes Atlas, 7th edn 2015 [updated 2021 December 6]. Available from: https://diabetesatlas.org/en/.
82. Fujioka S, Matsuzawa Y, Tokunaga K, Tarui S. Contribution of intra-abdominal fat accumulation to the impairment of glucose and lipid metabolism in human obesity. Metabolism-Clinical and Experimental. 1987;36(1):54-9.
83. Kissebah AH. Intra-abdominal fat: is it a major factor in developing diabetes and coronary artery disease? Diabetes Research and Clinical Practice. 1996;30:S25-S30.
84. Rönnemaa T, Koskenvuo M, Marniemi J, Koivunen T, Sajantila A, Rissanen A, et al. Glucose metabolism in identical twins discordant for obesity. The critical role of visceral fat. Journal of Clinical Endocrinology & Metabolism. 1997;82(2):383-7.
85. Pascot A, Despres J, Lemieux I, Bergeron J, Nadeau A, Prud'Homme D, et al. Contribution of visceral obesity to the deterioration of the metabolic risk profile in men with impaired glucose tolerance. Diabetologia. 2000;43(9):1126-35.
86. Wajchenberg BL. Subcutaneous and visceral adipose tissue: their relation to the metabolic syndrome. Endocrine Reviews. 2000;21(6):697-738.
87. Fujioka S, Matsuzawa Y, Tokunaga K, Tarui S. Contribution of intra-abdominal fat accumulation to the impairment of glucose and lipid metabolism in human obesity. Metabolism. 1987;36(1):54-9.
88. Després J-P, Nadeau A, Tremblay A, Ferland M, Moorjani S, Lupien PJ, et al. Role of deep abdominal fat in the association between regional adipose tissue distribution and glucose tolerance in obese women. Diabetes. 1989;38(3):304-9.
89. Despres J-P, Moorjani S, Lupien PJ, Tremblay A, Nadeau A, Bouchard C. Regional distribution of body fat, plasma lipoproteins, and cardiovascular disease. Arteriosclerosis. 1990;10(4):497-511.
90. Ross R, Aru J, Freeman J, Hudson R, Janssen I. Abdominal adiposity and insulin resistance in obese men. American Journal of Physiology-Endocrinology and Metabolism. 2002;282(3):E657-E63.

91. Ross R, Freeman J, Hudson R, Janssen I. Abdominal obesity, muscle composition, and insulin resistance in premenopausal women. The Journal of Clinical Endocrinology & Metabolism. 2002;87(11):5044-51.
92. Wang Y, Rimm EB, Stampfer MJ, Willett WC, Hu FB. Comparison of abdominal adiposity and overall obesity in predicting risk of type 2 diabetes among men. The American Journal of Clinical Nutrition. 2005;81(3):555-63.
93. Balkau B, Deanfield JE, Després J-P, Bassand J-P, Fox KA, Smith Jr SC, et al. Clinical perspective. Circulation. 2007;116(17):1942-51.
94. Boyko EJ, Fujimoto WY, Leonetti DL, Newell-Morris L. Visceral adiposity and risk of type 2 diabetes: a prospective study among Japanese Americans. Diabetes Care. 2000;23(4):465-71.
95. Tchernof A, Després J-P. Pathophysiology of human visceral obesity: an update. Physiological Reviews. 2013;93(1):359-404.
96. Lamarche B, Uffelman KD, Carpentier A, Cohn JS, Steiner G, Barrett PH, et al. Triglyceride enrichment of HDL enhances in vivo metabolic clearance of HDL apo AI in healthy men. Journal of Clinical Investigation. 1999;103(8):1191-9.
97. Steinberg D. Lewis A. Conner memorial lecture: oxidative modification of LDL and atherogenesis. Circulation. 1997;95(4):1062-71.
98. Després J-P, Lemieux I, Prud'Homme D. Treatment of obesity: need to focus on high risk abdominally obese patients. British Medical Journal 2001;322(7288):716-20.
99. Grundy SM, Cleeman JI, Daniels SR, Donato KA, Eckel RH, Franklin BA, et al. Diagnosis and management of the metabolic syndrome: an American heart association/national heart, Lung, and blood institute scientific statement. Circulation. 2005;112(17):2735-52.
100. Despres J-P, Moorjani S, Lupien PJ, Tremblay A, Nadeau A, Bouchard C. Regional distribution of body fat, plasma lipoproteins, and cardiovascular disease. Arteriosclerosis: An Official Journal of the American Heart Association, Inc. 1990;10(4):497-511.
101. Matsushita Y, Nakagawa T, Yamamoto S, Takahashi Y, Yokoyama T, Mizoue T, et al. Effect of longitudinal changes in visceral fat area and other anthropometric indices to the changes in metabolic risk factors in Japanese men: the Hitachi health study. Diabetes Care. 2012;35(5):1139-43.
102. Castelli W. Epidemiology of coronary heart disease: the Framingham study. The American Journal of Medicine. 1984;76(2):4-12.
103. Lemieux I, Pascot As, Couillard C, Lamarche Bt, Tchernof A, Alméras N, et al. Hypertriglyceridemic waist: a marker of the atherogenic metabolic triad (hyperinsulinemia; hyperapolipoprotein B; small, dense LDL) in men? Circulation. 2000;102(2):179-84.
104. Neeland IJ, Ayers CR, Rohatgi AK, Turer AT, Berry JD, Das SR, et al. Associations of visceral and abdominal subcutaneous adipose tissue with markers of cardiac and metabolic risk in obese adults. Obesity. 2013;21(9):E439-E47.
105. Pascot A, Lemieux I, Prud'homme D, Tremblay A, Nadeau A, Couillard C, et al. Reduced HDL particle size as an additional feature of the atherogenic dyslipidemia of abdominal obesity. Journal of Lipid Research. 2001;42(12):2007-14.

106. Tchernof A, Lamarche B, Prud'homme D, Nadeau A, Moorjani S, Labrie F, et al. The dense LDL phenotype: association with plasma lipoprotein levels, visceral obesity, and hyperinsulinemia in men. Diabetes Care. 1996;19(6):629-37.
107. Irlbeck T, Massaro J, Bamberg F, O'donnell C, Hoffmann U, Fox C. Association between single-slice measurements of visceral and abdominal subcutaneous adipose tissue with volumetric measurements: the Framingham Heart Study. International Journal of Obesity. 2010;34(4):781-7.
108. Oka R, Miura K, Sakurai M, Nakamura K, Yagi K, Miyamoto S, et al. Impacts of visceral adipose tissue and subcutaneous adipose tissue on metabolic risk factors in middle‐aged Japanese. Obesity. 2010;18(1):153-60.
109. Rock CL, Flatt SW, Pakiz B, Quintana EL, Heath DD, Rana BK, et al. Effects of diet composition on weight loss, metabolic factors and biomarkers in a 1-year weight loss intervention in obese women examined by baseline insulin resistance status. Metabolism. 2016;65(11):1605-13.
110. Smith Jr S, Benjamin E, Bonow R, Braun L, Creager M, Franklin B, et al. World Heart Federation and the Preventive Cardiovascular Nurses Association. AHA/ACCF secondary prevention and risk reduction therapy for patients with coronary and other atherosclerotic vascular disease: 2011 update: a guideline from the American Heart Association and American College of Cardiology Foundation. Circulation. 2011;124(22):2458-73.
111. Abdeen G, Le Roux C. Mechanism underlying the weight loss and complications of Roux-en-Y gastric bypass. Review. Obesity Surgery. 2016;26(2):410-21.
112. Arterburn DE, Bogart A, Sherwood NE, Sidney S, Coleman KJ, Haneuse S, et al. A multisite study of long-term remission and relapse of type 2 diabetes mellitus following gastric bypass. Obesity Surgery. 2013;23(1):93-102.
113. Patel D. Pharmacotherapy for the management of obesity. Metabolism. 2015;64(11):1376-85.
114. FDA. Guidance for Industry Developing Products for Weight Management. 2007 [updated 2017 January 31]. Available from: https://www.fda.gov/downloads/Drugs/.../Guidances/ucm071612.pdf.
115. Narayanaswami V, Dwoskin LP. Obesity: Current and potential pharmacotherapeutics and targets. Pharmacology & Therapeutics. 2017;170:116-47.
116. Yanovski SZ, Yanovski JA. Long-term drug treatment for obesity: a systematic and clinical review. Journal of the American Medical Association. 2014;311(1):74-86.
117. Sweeting AN, Tabet E, Caterson ID, Markovic TP. Management of obesity and cardiometabolic risk–role of phentermine/extended release topiramate. Diabetes, Metabolic Syndrome and Obesity: Targets and Therapy. 2014;7:35-44.
118. Garvey WT, Ryan DH, Look M, Gadde KM, Allison DB, Peterson CA, et al. Two-year sustained weight loss and metabolic benefits with controlled-release phentermine/topiramate in obese and overweight adults (SEQUEL): a randomized, placebo-controlled, phase 3 extension study. The American Journal of Clinical Nutrition. 2012;95(2):297-308.

119. Brown TM, Skop BP, Mareth TR. Pathophysiology and management of the serotonin syndrome. Annals of Pharmacotherapy. 1996;30(5):527-33.
120. Siebenhofer A, Jeitler K, Horvath K, Berghold A, Siering U, Semlitsch T. Long‐term effects of weight‐reducing drugs in hypertensive patients. Cochrane Database of Systematic Reviews. 2013(3):CD007654.
121. Comuzzie AG, Allison DB. The search for human obesity genes. Science. 1998;280(5368):1374-7.
122. Saltiel AR, Kahn CR. Insulin signalling and the regulation of glucose and lipid metabolism. Nature. 2001;414(6865):799-806.
123. Pennington AW. A reorientation on obesity. New England Journal of Medicine. 1953;248(23):959-64.
124. Singh RK, Kumar P, Mahalingam K. Molecular genetics of human obesity: A comprehensive review. Comptes Rendus Biologies. 2017;340(2):87-108.
125. Thaker VV. Genetic and epigenetic causes of obesity. Adolescent Medicine: State of the Art Reviews. 2017;28(2):379-405.
126. Silventoinen K, Rokholm B, Kaprio J, Sørensen TI. The genetic and environmental influences on childhood obesity: a systematic review of twin and adoption studies. International Journal of Obesity. 2010;34(1):29-40.
127. Frayling TM, Timpson NJ, Weedon MN, Zeggini E, Freathy RM, Lindgren CM, et al. A common variant in the FTO gene is associated with body mass index and predisposes to childhood and adult obesity. Science. 2007;316(5826):889-94.
128. Tartaglia LA, Dembski M, Weng X, Deng N, Culpepper J, Devos R, et al. Identification and expression cloning of a leptin receptor, OB-R. Cell. 1995;83(7):1263-71.
129. Challis BG, Pritchard LE, Creemers JW, Delplanque J, Keogh JM, Luan Ja, et al. A missense mutation disrupting a dibasic prohormone processing site in pro-opiomelanocortin (POMC) increases susceptibility to early-onset obesity through a novel molecular mechanism. Human Molecular Genetics. 2002;11(17):1997-2004.
130. Jackson RS, Creemers JW, Ohagi S, Raffin-Sanson M-L, Sanders L, Montague CT, et al. Obesity and impaired prohormone processing associated with mutations in the human prohormone convertase 1 gene. Nature Genetics. 1997;16(3):303-6.
131. Farooqi IS, Yeo GS, Keogh JM, Aminian S, Jebb SA, Butler G, et al. Dominant and recessive inheritance of morbid obesity associated with melanocortin 4 receptor deficiency. Journal of Clinical Investigation. 2000;106(2):271-9.
132. Holder Jr JL, Butte NF, Zinn AR. Profound obesity associated with a balanced translocation that disrupts the SIM1 gene. Human Molecular Genetics. 2000;9(1):101-8.
133. Michaud JL, Boucher F, Melnyk A, Gauthier F, Goshu E, Lévy E, et al. Sim1 haploinsufficiency causes hyperphagia, obesity and reduction of the paraventricular nucleus of the hypothalamus. Human Molecular Genetics. 2001;10(14):1465-73.

134. Hinney A, Vogel CI, Hebebrand J. From monogenic to polygenic obesity: recent advances. European Child & Adolescent Psychiatry. 2010;19(3):297-310.
135. Witte JS. Genome-wide association studies and beyond. Annual Review of Public Health. 2010;31:9-20.
136. Locke AE, Kahali B, Berndt SI, Justice AE, Pers TH, Day FR, et al. Genetic studies of body mass index yield new insights for obesity biology. Nature. 2015;518(7538):197-206.
137. Lu Y, Day FR, Gustafsson S, Buchkovich ML, Na J, Bataille V, et al. New loci for body fat percentage reveal link between adiposity and cardiometabolic disease risk. Nature Communications. 2016;7(1):1-15.
138. Heid IM, Jackson AU, Randall JC, Winkler TW, Qi L, Steinthorsdottir V, et al. Meta-analysis identifies 13 new loci associated with waist-hip ratio and reveals sexual dimorphism in the genetic basis of fat distribution. Nature Genetics. 2010;42(11):949-60.
139. Wen W, Kato N, Hwang J-Y, Guo X, Tabara Y, Li H, et al. Genome-wide association studies in East Asians identify new loci for waist-hip ratio and waist circumference. Scientific Reports. 2016;6(1):1-9.
140. Rask-Andersen M, Karlsson T, Ek WE, Johansson Å. Genome-wide association study of body fat distribution identifies adiposity loci and sex-specific genetic effects. Nature Communications. 2019;10(1):1-10.
141. Fox CS, Liu Y, White CC, Feitosa M, Smith AV, Heard-Costa N, et al. Genome-wide association for abdominal subcutaneous and visceral adipose reveals a novel locus for visceral fat in women. PLOS Genetics. 2012;8(5):e1002695.
142. Schraut KE. Exploration of genetic contributions to body composition and their role in metabolic health [PhD thesis]: The University of Edinburgh; 2017.
143. Massé K, Bhamra S, Allsop G, Dale N, Jones EA. Ectophosphodiesterase/nucleotide phosphohydrolase (Enpp) nucleotidases: cloning, conservation and developmental restriction. International Journal of Developmental Biology. 2009;54(1):181-93.
144. Grigoriadis DE, Hoare SR, Lechner SM, Slee DH, Williams JA. Drugability of extracellular targets: discovery of small molecule drugs targeting allosteric, functional, and subunit-selective sites on GPCRs and ion channels. Neuropsychopharmacology. 2009;34(1):106-25.
145. Johnson K, Hessle L, Vaingankar S, Wennberg C, Mauro S, Narisawa S, et al. Osteoblast tissue-nonspecific alkaline phosphatase antagonizes and regulates PC-1. American Journal of Physiology-Regulatory, Integrative and Comparative Physiology. 2000;279(4):R1365-R77.
146. Meyre D, Bouatia-Naji N, Tounian A, Samson C, Lecoeur C, Vatin V, et al. Variants of ENPP1 are associated with childhood and adult obesity and increase the risk of glucose intolerance and type 2 diabetes. Nature Genetics. 2005;37(8):863-7.
147. Maddux BA, Chang Y-N, Accili D, McGuinness OP, Youngren JF, Goldfine ID. Overexpression of the insulin receptor inhibitor PC-1/ENPP1 induces insulin resistance and hyperglycemia. American Journal of Physiology-Endocrinology and Metabolism. 2006;290(4):E746-E9.

148. Goldfine ID, Maddux BA, Youngren JF, Reaven G, Accili D, Trischitta V, et al. The role of membrane glycoprotein plasma cell antigen 1/ectonucleotide pyrophosphatase phosphodiesterase 1 in the pathogenesis of insulin resistance and related abnormalities. Endocrine Reviews. 2008;29(1):62-75.
149. Prudente S, Morini E, Trischitta V. Insulin signaling regulating genes: effect on T2DM and cardiovascular risk. Nature Reviews Endocrinology. 2009;5(12):682-93.
150. Huesa C, Zhu D, Glover JD, Ferron M, Karsenty G, Milne EM, et al. Deficiency of the bone mineralization inhibitor NPP1 protects mice against obesity and diabetes. Disease Models & Mechanisms. 2014;7(12):1341-50.
151. Liu S, Murph M, Panupinthu N, Mills GB. ATX-LPA receptor axis in inflammation and cancer. Cell Cycle. 2009;8(22):3695-701.
152. Ferry G, Tellier E, Try A, Grés S, Naime I, Simon MF, et al. Autotaxin is released from adipocytes, catalyzes lysophosphatidic acid synthesis, and activates preadipocyte proliferation: up-regulated expression with adipocyte differentiation and obesity. Journal of Biological Chemistry. 2003;278(20):18162-9.
153. Boucher J, Quilliot D, Praderes J, Simon M-F, Grès S, Guigné C, et al. Potential involvement of adipocyte insulin resistance in obesity-associated up-regulation of adipocyte lysophospholipase D/autotaxin expression. Diabetologia. 2005;48(3):569-77.
154. Federico L, Ren H, Mueller PA, Wu T, Liu S, Popovic J, et al. Autotaxin and its product lysophosphatidic acid suppress brown adipose differentiation and promote diet-induced obesity in mice. Molecular Endocrinology. 2012;26(5):786-97.
155. Nishimura S, Nagasaki M, Okudaira S, Aoki J, Ohmori T, Ohkawa R, et al. ENPP2 contributes to adipose tissue expansion and insulin resistance in diet-induced obesity. Diabetes. 2014;63(12):4154-64.
156. Brandon JA, Kraemer M, Vandra J, Halder S, Ubele M, Morris AJ, et al. Adipose-derived autotaxin regulates inflammation and steatosis associated with diet-induced obesity. PLOS One. 2019;14(2):e0208099.
157. Gesta S, Simon M-F, Rey A, Sibrac D, Girard A, Lafontan M, et al. Secretion of a lysophospholipase D activity by adipocytes: involvement in lysophosphatidic acid synthesis. Journal of Lipid Research. 2002;43(6):904-10.
158. Dusaulcy R, Rancoule C, Grès S, Wanecq E, Colom A, Guigné C, et al. Adipose-specific disruption of autotaxin enhances nutritional fattening and reduces plasma lysophosphatidic acid. Journal of Lipid Research. 2011;52(6):1247-55.
159. Bain G, Shannon KE, Huang F, Darlington J, Goulet L, Prodanovich P, et al. Selective inhibition of autotaxin is efficacious in mouse models of liver fibrosis. Journal of Pharmacology and Experimental Therapeutics. 2017;360(1):1-13.
160. Tsai SH, Kinoshita M, Kusu T, Kayama H, Okumura R, Ikeda K, et al. The ectoenzyme E-NPP3 negatively regulates ATP-dependent chronic allergic responses by basophils and mast cells. Immunity. 2015;42(2):279-93.

161. Albright RA, Ornstein DL, Cao W, Chang WC, Robert D, Tehan M, et al. Molecular basis of purinergic signal metabolism by ectonucleotide pyrophosphatase/phosphodiesterases 4 and 1 and implications in stroke. Journal of Biological Chemistry. 2014;289(6):3294-306.
162. Agis-Torres Á, Recio P, López-Oliva ME, Martínez MP, Barahona MV, Benedito S, et al. Phosphodiesterase type 4 inhibition enhances nitric oxide- and hydrogen sulfide-mediated bladder neck inhibitory neurotransmission. Scientific Reports. 2018;8(1):1-11.
163. Gorelik A, Randriamihaja A, Illes K, Nagar B. A key tyrosine substitution restricts nucleotide hydrolysis by the ectoenzyme NPP 5. The FEBS Journal. 2017;284(21):3718-26.
164. Sakagami H, Aoki J, Natori Y, Nishikawa K, Kakehi Y, Natori Y, et al. Biochemical and molecular characterization of a novel choline-specific glycerophosphodiester phosphodiesterase belonging to the nucleotide pyrophosphatase/phosphodiesterase family. Journal of Biological Chemistry. 2005;280(24):23084-93.
165. Morita J, Kano K, Kato K, Takita H, Sakagami H, Yamamoto Y, et al. Structure and biological function of ENPP6, a choline-specific glycerophosphodiester-phosphodiesterase. Scientific Reports. 2016;6(1):20995.
166. Dillon S, Suchacki K, Hsu SN, Stephen LA, Wang R, Cawthorn WP, et al. Ablation of Enpp6 results in transient bone hypomineralization. Journal of Bone and Mineral Research Plus. 2021;5(2):e10439.
167. Zhang Y, Cheng Y, Hansen GH, Niels-Christiansen L-L, Koentgen F, Ohlsson L, et al. Crucial role of alkaline sphingomyelinase in sphingomyelin digestion: a study on enzyme knockout mice. Journal of Lipid Research. 2011;52(4):771-81.
168. Tokumura A, Majima E, Kariya Y, Tominaga K, Kogure K, Yasuda K, et al. Identification of human plasma lysophospholipase D, a lysophosphatidic acid-producing enzyme, as autotaxin, a multifunctional phosphodiesterase. Journal of Biological Chemistry. 2002;277(42):39436-42.
169. Zhang Y, Chen K, Sloan SA, Bennett ML, Scholze AR, O'Keeffe S, et al. An RNA-sequencing transcriptome and splicing database of glia, neurons, and vascular cells of the cerebral cortex. Journal of Neuroscience. 2014;34(36):11929-47.
170. Xiao L, Ohayon D, McKenzie IA, Sinclair-Wilson A, Wright JL, Fudge AD, et al. Rapid production of new oligodendrocytes is required in the earliest stages of motor-skill learning. Nature Neuroscience. 2016;19(9):1210-7.
171. Marques S, van Bruggen D, Vanichkina DP, Floriddia EM, Munguba H, Väremo L, et al. Transcriptional convergence of oligodendrocyte lineage progenitors during development. Developmental Cell. 2018;46(4):504-17. e7.
172. Chen R, Wu X, Jiang L, Zhang Y. Single-cell RNA-seq reveals hypothalamic cell diversity. Cell Reports. 2017;18(13):3227-41.
173. Sturrock R. Myelination of the mouse corpus callosum. Neuropathology and Applied Neurobiology. 1980;6(6):415-20.
174. Johns TG, Bernard CC. The structure and function of myelin oligodendrocyte glycoprotein. Journal of Neurochemistry. 1999;72(1):1-9.

175. Yeung MS, Zdunek S, Bergmann O, Bernard S, Salehpour M, Alkass K, et al. Dynamics of oligodendrocyte generation and myelination in the human brain. Cell. 2014;159(4):766-74.
176. Duncan ID, Radcliff AB, Heidari M, Kidd G, August BK, Wierenga LA. The adult oligodendrocyte can participate in remyelination. Proceedings of the National Academy of Sciences. 2018;115(50):E11807-E16.
177. Pitkin RM, Allen L, Bailey L, Bernfield M, editors. Dietary Reference Intakes for Thiamin, riboflavin, niacin, vitamin B6, folate, vitamin B12, Pantothenic acid, biotin and choline. Washington, DC: National Academies Press (US); 2000.
178. Penry JT, Manore MM. Choline: an important micronutrient for maximal endurance-exercise performance? International Journal of Sport Nutrition and Exercise Metabolism. 2008;18(2):191-203.
179. Zeisel SH, Da Costa K-A. Choline: an essential nutrient for public health. Nutrition Reviews. 2009;67(11):615-23.
180. DeLong CJ, Shen Y-J, Thomas MJ, Cui Z. Molecular distinction of phosphatidylcholine synthesis between the CDP-choline pathway and phosphatidylethanolamine methylation pathway. Journal of Biological Chemistry. 1999;274(42):29683-8.
181. van der Veen JN, Kennelly JP, Wan S, Vance JE, Vance DE, Jacobs RL. The critical role of phosphatidylcholine and phosphatidylethanolamine metabolism in health and disease. Biochimica et Biophysica Acta (BBA)-Biomembranes. 2017;1859(9):1558-72.
182. Zeisel SH. Choline: critical role during fetal development and dietary requirements in adults. Annual Review of Nutrition. 2006;26:229-50.
183. Li Z, Vance DE. Thematic review series: glycerolipids. Phosphatidylcholine and choline homeostasis. Journal of Lipid Research. 2008;49(6):1187-94.
184. Zeisel SH, Da Costa KA, Franklin PD, Alexander EA, Lamont JT, Sheard NF, et al. Choline, an essential nutrient for humans. The FASEB Journal. 1991;5(7):2093-8.
185. Zeisel SH, Blusztajn JK. Choline and human nutrition. Annual Review of Nutrition. 1994;14(1):269-96.
186. Zeisel SH, Mar M-H, Howe JC, Holden JM. Concentrations of choline-containing compounds and betaine in common foods. Journal of Nutrition. 2003;133(5):1302-7.
187. Craig SA. Betaine in human nutrition. The American Journal of Clinical Nutrition. 2004;80(3):539-49.
188. Shaw GM, Carmichael SL, Yang W, Selvin S, Schaffer DM. Periconceptional dietary intake of choline and betaine and neural tube defects in offspring. American Journal of Epidemiology. 2004;160(2):102-9.
189. Zeisel SH. Choline: needed for normal development of memory. Journal of the American College of Nutrition. 2000;19(sup5):528S-31S.
190. Zeisel SH. Nutritional importance of choline for brain development. Journal of the American College of Nutrition. 2004;23(sup6):621S-6S.
191. Zeisel SH, Niculescu MD. Perinatal choline influences brain structure and function. Nutrition Reviews. 2006;64(4):197-203.

192. Collaboration HS. Homocysteine and risk of ischemic heart disease and stroke. Journal of the American Medical Association. 2002;288(16):2015-22.
193. Rajaie S, Esmaillzadeh A. Dietary choline and betaine intakes and risk of cardiovascular diseases: review of epidemiological evidence. ARYA Atherosclerosis. 2011;7(2):78-86.
194. Wu LL, Wu JT. Hyperhomocysteinemia is a risk factor for cancer and a new potential tumor marker. Clinica Chimica Acta. 2002;322(1-2):21-8.
195. Nitter M, Norgård B, De Vogel S, Eussen S, Meyer K, Ulvik A, et al. Plasma methionine, choline, betaine, and dimethylglycine in relation to colorectal cancer risk in the european prospective investigation into cancer and nutrition (EPIC). Annals of Oncology. 2014;25(8):1609-15.
196. Fischer LM, DaCosta KA, Kwock L, Stewart PW, Lu T-S, Stabler SP, et al. Sex and menopausal status influence human dietary requirements for the nutrient choline. The American Journal of Clinical Nutrition. 2007;85(5):1275-85.
197. Konstantinova SV, Tell GS, Vollset SE, Nygard O, Bleie Ø, Ueland PM. Divergent associations of plasma choline and betaine with components of metabolic syndrome in middle age and elderly men and women. Journal of Nutrition. 2008;138(5):914-20.
198. Kohlmeier M, da Costa K-A, Fischer LM, Zeisel SH. Genetic variation of folate-mediated one-carbon transfer pathway predicts susceptibility to choline deficiency in humans. Proceedings of the National Academy of Sciences. 2005;102(44):16025-30.
199. da Costa K-A, Kozyreva OG, Song J, Galanko JA, Fischer LM, Zeisel SH. Common genetic polymorphisms affect the human requirement for the nutrient choline. The FASEB Journal. 2006;20(9):1336-44.
200. Xu X, Gammon MD, Zeisel SH, Lee YL, Wetmur JG, Teitelbaum SL, et al. Choline metabolism and risk of breast cancer in a population‐based study. The FASEB Journal. 2008;22(6):2045-52.
201. Song J, Da Costa KA, Fischer LM, Kohlmeier M, Kwock L, Wang S, et al. Polymorphism of the PEMT gene and susceptibility to nonalcoholic fatty liver disease (NAFLD). The FASEB Journal. 2005;19(10):1266-71.
202. Resseguie M, Song J, Niculescu MD, da Costa K-A, Randall TA, Zeisel SH. Phosphatidylethanolamine N‐methyltransferase (PEMT) gene expression is induced by estrogen in human and mouse primary hepatocytes. The FASEB Journal. 2007;21(10):2622-32.
203. Resseguie ME, Da Costa K-A, Galanko JA, Patel M, Davis IJ, Zeisel SH. Aberrant estrogen regulation of PEMT results in choline deficiency-associated liver dysfunction. Journal of Biological Chemistry. 2011;286(2):1649-58.
204. Saunderson CL, Mackinlay J. Changes in body-weight, composition and hepatic enzyme activities in response to dietary methionine, betaine and choline levels in growing chicks. British Journal of Nutrition. 1990;63(2):339-49.
205. Daily III JW, Hongu N, Mynatt RL, Sachan DS. Choline supplementation increases tissue concentrations of carnitine and lowers body fat in guinea pigs. The Journal of Nutritional Biochemistry. 1998;9(8):464-70.

206. Hongu N, Sachan DS. Caffeine, carnitine and choline supplementation of rats decreases body fat and serum leptin concentration as does exercise. Journal of Nutrition. 2000;130(2):152-7.
207. Gao X, Randell E, Zhou H, Sun G. Higher serum choline and betaine levels are associated with better body composition in male but not female population. PLOS One. 2018;13(2):e0193114.
208. Chen Y, Liu Y, Liu Y, Wang X, Guan K, Zhu H. Higher serum concentrations of betaine rather than choline is associated with better profiles of DXA-derived body fat and fat distribution in Chinese adults. International Journal of Obesity. 2015;39(3):465-71.
209. Jacobs RL, Zhao Y, Koonen DP, Sletten T, Su B, Lingrell S, et al. Impaired de novo choline synthesis explains why phosphatidylethanolamine N-methyltransferase-deficient mice are protected from diet-induced obesity. Journal of Biological Chemistry. 2010;285(29):22403-13.
210. Wu G, Zhang L, Li T, Lopaschuk G, Vance DE, Jacobs RL. Choline deficiency attenuates body weight gain and improves glucose tolerance in ob/ob mice. Journal of Obesity. 2012;2012:319172.
211. Raubenheimer PJ, Nyirenda MJ, Walker BR. A choline-deficient diet exacerbates fatty liver but attenuates insulin resistance and glucose intolerance in mice fed a high-fat diet. Diabetes. 2006;55(7):2015-20.
212. Schwartz MW, Woods SC, Porte D, Seeley RJ, Baskin DG. Central nervous system control of food intake. Nature. 2000;404(6778):661-71.
213. Lee EB, Mattson MP. The neuropathology of obesity: insights from human disease. Acta Neuropathologica. 2014;127(1):3-28.
214. Brobeck JR. Mechanism of the development of obesity in animals with hypothalamic lesions. Physiological Reviews. 1946;26(4):541-59.
215. Cowley MA, Smart JL, Rubinstein M, Cerdán MG, Diano S, Horvath TL, et al. Leptin activates anorexigenic POMC neurons through a neural network in the arcuate nucleus. Nature. 2001;411(6836):480.
216. Huszar D, Lynch CA, Fairchild-Huntress V, Dunmore JH, Fang Q, Berkemeier LR, et al. Targeted disruption of the melanocortin-4 receptor results in obesity in mice. Cell. 1997;88(1):131-41.
217. Samama P, Rumennik L, Grippo JF. The melanocortin receptor MCR4 controls fat consumption. Regulatory Peptides. 2003;113(1-3):85-8.
218. Kim M-S, Pak YK, Jang P-G, Namkoong C, Choi Y-S, Won J-C, et al. Role of hypothalamic Foxo1 in the regulation of food intake and energy homeostasis. Nature Neuroscience. 2006;9(7):901-6.
219. Meye F, Trezza V, Vanderschuren LJ, Ramakers G, Adan R. Neutral antagonism at the cannabinoid 1 receptor: a safer treatment for obesity. Molecular Psychiatry. 2013;18(12):1294-301.
220. Blüher M, Engeli S, Klöting N, Berndt J, Fasshauer M, Bátkai S, et al. Dysregulation of the peripheral and adipose tissue endocannabinoid system in human abdominal obesity. Diabetes. 2006;55(11):3053-60.
221. Zhang X, van den Pol AN. Hypothalamic arcuate nucleus tyrosine hydroxylase neurons play orexigenic role in energy homeostasis. Nature Neuroscience. 2016;19(10):1341-7.

222. Güemes A, Georgiou P. Review of the role of the nervous system in glucose homoeostasis and future perspectives towards the management of diabetes. Bioelectronic Medicine. 2018;4(1):9.
223. Broberger C, Hökfelt T. Hypothalamic and vagal neuropeptide circuitries regulating food intake. Physiology & Behavior. 2001;74(4-5):669-82.
224. Williams G, Bing C, Cai XJ, Harrold JA, King PJ, Liu XH. The hypothalamus and the control of energy homeostasis: different circuits, different purposes. Physiology & Behavior. 2001;74(4-5):683-701.
225. Bray GA, Gallagher Jr TF. Manifestations of hypothalamic obesity in man: a comprehensive investigation of eight patients and a reveiw of the literature. Medicine. 1975;54(4):301-30.
226. Ferguson AV, Latchford KJ, Samson WK. The paraventricular nucleus of the hypothalamus–a potential target for integrative treatment of autonomic dysfunction. Expert Opinion On Therapeutic Targets. 2008;12(6):717-27.
227. Hervey G. The effects of lesions in the hypothalamus in parabiotic rats. Journal of Physiology. 1959;145(2):336-52.
228. Billington CJ, Levine AS. Hypothalamic neuropeptide Y regulation of feeding and energy metabolism. Current Opinion In Neurobiology. 1992;2(6):847-51.
229. Kang L, Routh VH, Kuzhikandathil EV, Gaspers LD, Levin BE. Physiological and molecular characteristics of rat hypothalamic ventromedial nucleus glucosensing neurons. Diabetes. 2004;53(3):549-59.
230. Wang R, Liu X, Hentges S, Dunn-Meynell A, Levin B, Wang W, et al. The regulation of glucose-excited neurons in the hypothalamic arcuate nucleus by glucose and feeding-relevant peptides. Diabetes. 2004;53(8):1959-65.
231. Krashes MJ, Koda S, Ye C, Rogan SC, Adams AC, Cusher DS, et al. Rapid, reversible activation of AgRP neurons drives feeding behavior in mice. Journal of Clinical Investigation. 2011;121(4):1424-8.
232. Shin AC, Filatova N, Lindtner C, Chi T, Degann S, Oberlin D, et al. Insulin receptor signaling in POMC, but not AgRP, neurons controls adipose tissue insulin action. Diabetes. 2017;66(6):1560-71.
233. Gropp E, Shanabrough M, Borok E, Xu AW, Janoschek R, Buch T, et al. Agouti-related peptide–expressing neurons are mandatory for feeding. Nature Neuroscience. 2005;8(10):1289-91.
234. Luquet S, Perez FA, Hnasko TS, Palmiter RD. NPY/AgRP neurons are essential for feeding in adult mice but can be ablated in neonates. Science. 2005;310(5748):683-5.
235. Ahima RS, Antwi DA. Brain regulation of appetite and satiety. Endocrinology and Metabolism Clinics of North America. 2008;37(4):811-23.
236. Garfield AS, Lam DD, Marston OJ, Przydzial MJ, Heisler LK. Role of central melanocortin pathways in energy homeostasis. Trends in Endocrinology & Metabolism. 2009;20(5):203-15.
237. Broadwell RD, Brightman MW. Entry of peroxidase into neurons of the central and peripheral nervous systems from extracerebral and cerebral blood. Journal of Comparative Neurology. 1976;166(3):257-83.
238. Van Houten M, Posner BI, Kopriwa BM. Insulin binding sites localized to nerve terminals in rat median eminence and arcuate nucleus. Science. 1980;207(4435):1081-3.

239. Cheung CC, Clifton DK, Steiner RA. Proopiomelanocortin neurons are direct targets for leptin in the hypothalamus. Endocrinology. 1997;138(10):4489-92.
240. Schwartz MW, Seeley RJ, Woods SC, Weigle DS, Campfield LA, Burn P, et al. Leptin increases hypothalamic pro-opiomelanocortin mRNA expression in the rostral arcuate nucleus. Diabetes. 1997;46(12):2119-23.
241. Elmquist JK, Bjørbæk C, Ahima RS, Flier JS, Saper CB. Distributions of leptin receptor mRNA isoforms in the rat brain. Journal of Comparative Neurology. 1998;395(4):535-47.
242. Ahima RS, Saper CB, Flier JS, Elmquist JK. Leptin regulation of neuroendocrine systems. Frontiers in Neuroendocrinology. 2000;21(3):263-307.
243. Ganong WF. Circumventricular organs: definition and role in the regulation of endocrine and autonomic function. Clinical and Experimental Pharmacology and Physiology. 2000;27(5‐6):422-7.
244. Katsuki A, Sumida Y, Murashima S, Furuta M, Araki-Sasaki R, Tsuchihashi K, et al. Elevated plasma levels of α-melanocyte stimulating hormone (α-MSH) are correlated with insulin resistance in obese men. International Journal of Obesity. 2000;24(10):1260-4.
245. Costa JL, Hochgeschwender U, Brennan M. The role of melanocyte-stimulating hormone in insulin resistance and type 2 diabetes mellitus. Treatments in Endocrinology. 2006;5(1):7-13.
246. Marie LS, Miura GI, Marsh DJ, Yagaloff K, Palmiter RD. A metabolic defect promotes obesity in mice lacking melanocortin-4 receptors. Proceedings of the National Academy of Sciences. 2000;97(22):12339-44.
247. Vaisse C, Clement K, Guy-Grand B, Froguel P. A frameshift mutation in human MC4R is associated with a dominant form of obesity. Nature Genetics. 1998;20(2):113-4.
248. Yeo GS, Farooqi IS, Aminian S, Halsall DJ, Stanhope RG, O'Rahilly S. A frameshift mutation in MC4R associated with dominantly inherited human obesity. Nature Genetics. 1998;20(2):111-2.
249. Fan W, Dinulescu DM, Butler AA, Zhou J, Marks DL, Cone RD. The central melanocortin system can directly regulate serum insulin levels. Endocrinology. 2000;141(9):3072-9.
250. Obici S, Feng Z, Tan J, Liu L, Karkanias G, Rossetti L. Central melanocortin receptors regulate insulin action. Journal of Clinical Investigation. 2001;108(7):1079-85.
251. Farooqi IS, Keogh JM, Yeo GS, Lank EJ, Cheetham T, O'Rahilly S. Clinical spectrum of obesity and mutations in the melanocortin 4 receptor gene. New England Journal of Medicine. 2003;348(12):1085-95.
252. Piomelli D. The molecular logic of endocannabinoid signalling. Nature Reviews Neuroscience. 2003;4(11):873-84.
253. Devane WA, Hanus L, Breuer A, Pertwee RG, Stevenson LA, Griffin G, et al. Isolation and structure of a brain constituent that binds to the cannabinoid receptor. Science. 1992;258(5090):1946-9.
254. Mechoulam R, Ben-Shabat S, Hanus L, Ligumsky M, Kaminski NE, Schatz AR, et al. Identification of an endogenous 2-monoglyceride, present in

canine gut, that binds to cannabinoid receptors. Biochemical Pharmacology. 1995;50(1):83-90.
255. Matsuda LA, Lolait SJ, Brownstein MJ, Young AC, Bonner TI. Structure of a cannabinoid receptor and functional expression of the cloned cDNA. Nature. 1990;346(6284):561-4.
256. Munro S, Thomas KL, Abu-Shaar M. Molecular characterization of a peripheral receptor for cannabinoids. Nature. 1993;365(6441):61-5.
257. Devane WA, Dysarz Fr, Johnson MR, Melvin LS, Howlett AC. Determination and characterization of a cannabinoid receptor in rat brain. Molecular Pharmacology. 1988;34(5):605-13.
258. Van Sickle MD, Duncan M, Kingsley PJ, Mouihate A, Urbani P, Mackie K, et al. Identification and functional characterization of brainstem cannabinoid CB2 receptors. Science. 2005;310(5746):329-32.
259. Klein TW. Cannabinoid-based drugs as anti-inflammatory therapeutics. Nature Reviews Immunology. 2005;5(5):400-11.
260. Marsicano G, Lutz B. Neuromodulatory functions of the endocannabinoid system. Journal of Endocrinological Investigation. 2006;29(3):27-46.
261. Kano M, Ohno-Shosaku T, Hashimotodani Y, Uchigashima M, Watanabe M. Endocannabinoid-mediated control of synaptic transmission. Physiological Reviews. 2009;89(1):309-80.
262. Bénard G, Massa F, Puente N, Lourenço J, Bellocchio L, Soria-Gómez E, et al. Mitochondrial CB 1 receptors regulate neuronal energy metabolism. Nature Neuroscience. 2012;15(4):558-64.
263. Bellocchio L, Cervino C, Pasquali R, Pagotto U. The endocannabinoid system and energy metabolism. Journal of Neuroendocrinology. 2008;20(6):850-7.
264. Hanuš Lr, Avraham Y, Ben-Shushan D, Zolotarev O, Berry EM, Mechoulam R. Short-term fasting and prolonged semistarvation have opposite effects on 2-AG levels in mouse brain. Brain Research. 2003;983(1-2):144-51.
265. Di Marzo V, Goparaju SK, Wang L, Liu J, Bátkai S, Járai Z, et al. Leptin-regulated endocannabinoids are involved in maintaining food intake. Nature. 2001;410(6830):822-5.
266. Kola B, Hubina E, Tucci SA, Kirkham TC, Garcia EA, Mitchell SE, et al. Cannabinoids and ghrelin have both central and peripheral metabolic and cardiac effects via AMP-activated protein kinase. Journal of Biological Chemistry. 2005;280(26):25196-201.
267. Mato S, Alberdi E, Ledent C, Watanabe M, Matute C. CB1 cannabinoid receptor‐dependent and‐independent inhibition of depolarization‐induced calcium influx in oligodendrocytes. Glia. 2009;57(3):295-306.
268. Molina-Holgado E, Vela JM, Arévalo-Martín A, Almazán G, Molina-Holgado F, Borrell J, et al. Cannabinoids promote oligodendrocyte progenitor survival: involvement of cannabinoid receptors and phosphatidylinositol-3 kinase/Akt signaling. Journal of Neuroscience. 2002;22(22):9742-53.
269. Sim FJ, Lang JK, Waldau B, Roy NS, Schwartz TE, Pilcher WH, et al. Complementary patterns of gene expression by human oligodendrocyte progenitors and their environment predict determinants of progenitor maintenance and differentiation. Annals of Neurology: Official Journal of the

American Neurological Association and the Child Neurology Society. 2006;59(5):763-79.
270. Tsacopoulos M, Magistretti PJ. Metabolic coupling between glia and neurons. Journal of Neuroscience. 1996;16(3):877-85.
271. Ou Z, Ma Y, Sun Y, Zheng G, Wang S, Xing R, et al. A GPR17-cAMP-Lactate Signaling Axis in Oligodendrocytes Regulates Whole-Body Metabolism. Cell Reports. 2019;26(11):2984-97 e4.
272. De Souza CT, Araujo EP, Bordin S, Ashimine R, Zollner RL, Boschero AC, et al. Consumption of a fat-rich diet activates a proinflammatory response and induces insulin resistance in the hypothalamus. Endocrinology. 2005;146(10):4192-9.
273. Thaler JP, Yi CX, Schur EA, Guyenet SJ, Hwang BH, Dietrich MO, et al. Obesity is associated with hypothalamic injury in rodents and humans. Journal of Clinical Investigation. 2012;122(1):153-62.
274. Valdearcos M, Robblee MM, Benjamin DI, Nomura DK, Xu AW, Koliwad SK. Microglia dictate the impact of saturated fat consumption on hypothalamic inflammation and neuronal function. Cell Reports. 2014;9(6):2124-38.
275. García-Cáceres C, Fuente-Martín E, Burgos-Ramos E, Granado M, Frago LM, Barrios V, et al. Differential acute and chronic effects of leptin on hypothalamic astrocyte morphology and synaptic protein levels. Endocrinology. 2011;152(5):1809-18.
276. Hsuchou H, He Y, Kastin AJ, Tu H, Markadakis EN, Rogers RC, et al. Obesity induces functional astrocytic leptin receptors in hypothalamus. Brain : a journal of neurology. 2009;132(Pt 4):889-902.
277. Gao Y, Ottaway N, Schriever SC, Legutko B, Garcia-Caceres C, de la Fuente E, et al. Hormones and diet, but not body weight, control hypothalamic microglial activity. Glia. 2014;62(1):17-25.
278. Chang Y, She ZG, Sakimura K, Roberts A, Kucharova K, Rowitch DH, et al. Ablation of NG2 proteoglycan leads to deficits in brown fat function and to adult onset obesity. PLOS One. 2012;7(1):e30637.
279. Djogo T, Robins SC, Schneider S, Kryzskaya D, Liu X, Mingay A, et al. Adult NG2-glia are required for median eminence-mediated leptin sensing and body weight control. Cell Metabolism. 2016;23(5):797-810.
280. Bozón MV, Yunis EJ, editors. Congenic mice. Encyclopedia of Immunology (Second Edition): Elsevier; 1998.
281. Pringle N, Collarini E, Mosley M, Heldin C, Westermark B, Richardson W. PDGF A chain homodimers drive proliferation of bipotential (O‐2A) glial progenitor cells in the developing rat optic nerve. The EMBO Journal. 1989;8(4):1049-56.
282. Richardson WD, Pringle N, Mosley MJ, Westermark B, Dubois-Dalcg M. A role for platelet-derived growth factor in normal gliogenesis in the central nervous system. Cell. 1988;53(2):309-19.
283. McCarthy KD, De Vellis J. Preparation of separate astroglial and oligodendroglial cell cultures from rat cerebral tissue. Journal of Cell Biology. 1980;85(3):890-902.
284. Chen Y, Balasubramaniyan V, Peng J, Hurlock EC, Tallquist M, Li J, et al. Isolation and culture of rat and mouse oligodendrocyte precursor cells. Nature Protocol. 2007;2(5):1044-51.

285. Mecha M, Iñigo PM, Mestre L, Hernangómez M, Borrell J, Guaza C. An easy and fast way to obtain a high number of glial cells from rat cerebral tissue: a beginners approach. Protocol Exchange. 2011;218:1038.
286. O'Meara RW, Ryan SD, Colognato H, Kothary R. Derivation of enriched oligodendrocyte cultures and oligodendrocyte/neuron myelinating co-cultures from post-natal murine tissues. Journal of Visualized Experiments. 2011(54).
287. Lenhard T, Hulsermann U, Martinez-Torres F, Fricker G, Meyding-Lamade U. A simple method to quickly and simultaneously purify and enrich intact rat brain microcapillaries and endothelial and glial cells for ex vivo studies and cell culture. Brain Research. 2013;1519:9-18.
288. Bechler ME, Byrne L, Ffrench-Constant C. CNS myelin sheath lengths are an intrinsic property of oligodendrocytes. Current Biology. 2015;25(18):2411-6.
289. Bottenstein JE, Sato GH. Growth of a rat neuroblastoma cell line in serum-free supplemented medium. Proceedings of the National Academy of Sciences. 1979;76(1):514-7.
290. Kawaguchi M, Okabe T, Okudaira S, Hanaoka K, Fujikawa Y, Terai T, et al. Fluorescence probe for lysophospholipase C/NPP6 activity and a potent NPP6 inhibitor. Journal of the American Chemical Society. 2011;133(31):12021-30.
291. Lockhart SM, O'Rahilly S. When two pandemics meet: Why is obesity associated with increased COVID-19 mortality? Med: Cell Press. 2020.
292. Kissebah A. Central obesity: measurement and metabolic effects. Current Diabetes Reviews. 1997;5(1):13-23.
293. Bollen M, Gijsbers R, Ceulemans H, Stalmans W, Stefan C. Nucleotide pyrophosphatases/phosphodiesterases on the move. Critical Reviews In Biochemistry and Molecular Biology. 2000;35(6):393-432.
294. Stefan C, Jansen S, Bollen M. NPP-type ectophosphodiesterases: unity in diversity. Trends in Biochemical Sciences. 2005;30(10):542-50.
295. Lombardi B, Pani P, Schlunk F. Choline-deficiency fatty liver: impaired release of hepatic triglycerides. Journal of Lipid Research. 1968;9(4):437-46.
296. Sanders LM, Zeisel SH. Choline: dietary requirements and role in brain development. Nutrition Today. 2007;42(4):181-6.
297. Sherriff JL, O'Sullivan TA, Properzi C, Oddo J-L, Adams LA. Choline, its potential role in nonalcoholic fatty liver disease, and the case for human and bacterial genes. Advances In Nutrition. 2016;7(1):5-13.
298. Wu G, Zhang L, Li T, Zuniga A, Lopaschuk GD, Li L, et al. Choline supplementation promotes hepatic insulin resistance in phosphatidylethanolamine N-methyltransferase-deficient mice via increased glucagon action. Journal of Biological Chemistry. 2013;288(2):837-47.
299. Samuel VT, Petersen KF, Shulman GI. Lipid-induced insulin resistance: unravelling the mechanism. The Lancet. 2010;375(9733):2267-77.
300. Kumashiro N, Erion DM, Zhang D, Kahn M, Beddow SA, Chu X, et al. Cellular mechanism of insulin resistance in nonalcoholic fatty liver disease. Proceedings of the National Academy of Sciences. 2011;108(39):16381-5.
301. Liu J, Han L, Zhu L, Yu Y. Free fatty acids, not triglycerides, are associated with non-alcoholic liver injury progression in high fat diet induced obese rats. Lipids In Health and Disease. 2016;15(1):1-9.

302. McKenzie IA, Ohayon D, Li H, De Faria JP, Emery B, Tohyama K, et al. Motor skill learning requires active central myelination. Science. 2014;346(6207):318-22.
303. Jocken JW, Langin D, Smit E, Saris WH, Valle C, Hul GB, et al. Adipose triglyceride lipase and hormone-sensitive lipase protein expression is decreased in the obese insulin-resistant state. Journal of Clinical Endocrinology & Metabolism. 2007;92(6):2292-9.
304. Bickerton A, Roberts R, Fielding B, Tornqvist H, Blaak E, Wagenmakers A, et al. Adipose tissue fatty acid metabolism in insulin-resistant men. Diabetologia. 2008;51(8):1466-74.
305. Ryden M, Bäckdahl J, Petrus P, Thorell A, Gao H, Coue M, et al. Impaired atrial natriuretic peptide-mediated lipolysis in obesity. International Journal of Obesity. 2016;40(4):714-20.
306. Verboven K, Hansen D, Moro C, Eijnde BO, Hoebers N, Knol J, et al. Attenuated atrial natriuretic peptide-mediated lipolysis in subcutaneous adipocytes of obese type 2 diabetic men. Clinical Science. 2016;130(13):1105-14.
307. Nielsen TS, Jessen N, Jørgensen JOL, Møller N, Lund S. Dissecting adipose tissue lipolysis: molecular regulation and implications for metabolic disease. Journal of Molecular Endocrinology. 2014;52(3):R199-R222.
308. Lee Y-H, Mottillo EP, Granneman JG. Adipose tissue plasticity from WAT to BAT and in between. Biochimica et Biophysica Acta (BBA)-Molecular Basis of Disease. 2014;1842(3):358-69.
309. Lee Y-H, Petkova AP, Mottillo EP, Granneman JG. In vivo identification of bipotential adipocyte progenitors recruited by β3-adrenoceptor activation and high-fat feeding. Cell Metabolism. 2012;15(4):480-91.
310. Wang QA, Tao C, Gupta RK, Scherer PE. Tracking adipogenesis during white adipose tissue development, expansion and regeneration. Nature Medicine. 2013;19(10):1338-44.
311. Fang L, Guo F, Zhou L, Stahl R, Grams J. The cell size and distribution of adipocytes from subcutaneous and visceral fat is associated with type 2 diabetes mellitus in humans. Adipocyte. 2015;4(4):273-9.
312. Kabir M, Stefanovski D, Hsu IR, Iyer M, Woolcott OO, Zheng D, et al. Large size cells in the visceral adipose depot predict insulin resistance in the canine model. Obesity. 2011;19(11):2121-9.
313. Birkenfeld AL, Shulman GI. Nonalcoholic fatty liver disease, hepatic insulin resistance, and type 2 diabetes. Hepatology. 2014;59(2):713-23.
314. Bhatt HB, Smith RJ. Fatty liver disease in diabetes mellitus. Hepatobiliary Surgery and Nutrition. 2015;4(2):101-8.
315. Thomas EL, Hamilton G, Patel N, O'Dwyer R, Doré CJ, Goldin RD, et al. Hepatic triglyceride content and its relation to body adiposity: a magnetic resonance imaging and proton magnetic resonance spectroscopy study. Gut. 2005;54(1):122-7.
316. Wu G, Zhang L, Li T, Lopaschuk G, Vance DE, Jacobs RL. Choline Deficiency Attenuates Body Weight Gain and Improves Glucose Tolerance in ob/ob Mice. Journal of obesity. 2012;2012:319172.

317. Rinella ME, Elias MS, Smolak RR, Fu T, Borensztajn J, Green RM. Mechanisms of hepatic steatosis in mice fed a lipogenic methionine choline-deficient diet. Journal of Lipid Research. 2008;49(5):1068-76.
318. Feldmann HM, Golozoubova V, Cannon B, Nedergaard J. UCP1 ablation induces obesity and abolishes diet-induced thermogenesis in mice exempt from thermal stress by living at thermoneutrality. Cell Metabolism. 2009;9(2):203-9.
319. Schäffler A, Schölmerich J, Büchler C. Mechanisms of disease: adipocytokines and visceral adipose tissue—emerging role in nonalcoholic fatty liver disease. Nature Clinical Practice Gastroenterology & Hepatology. 2005;2(6):273-80.
320. Surwit RS, Kuhn CM, Cochrane C, McCubbin JA, Feinglos MN. Diet-induced type II diabetes in C57BL/6J mice. Diabetes. 1988;37(9):1163-7.
321. Hedrich H. The laboratory mouse. San Diego, United States: Academic Press, 2nd Ed; 2004.
322. Kaku K, Fiedorek FT, Province M, Permutt MA. Genetic analysis of glucose tolerance in inbred mouse strains: evidence for polygenic control. Diabetes. 1988;37(6):707-13.
323. Toye A, Lippiat J, Proks P, Shimomura K, Bentley L, Hugill A, et al. A genetic and physiological study of impaired glucose homeostasis control in C57BL/6J mice. Diabetologia. 2005;48(4):675-86.
324. Surwit RS, Seldin MF, Kuhn CM, Cochrane C, Feinglos MN. Control of expression of insulin resistance and hyperglycemia by different genetic factors in diabetic C57BL/6J mice. Diabetes. 1991;40(1):82-7.
325. Collins S, Martin TL, Surwit RS, Robidoux J. Genetic vulnerability to diet-induced obesity in the C57BL/6J mouse: physiological and molecular characteristics. Physiology & Behavior. 2004;81(2):243-8.
326. Wencel HE, Smothers C, Opara EC, Kuhn CM, Feinglos MN, Surwit RS. Impaired second phase insulin response of diabetes-prone C57BL/6J mouse islets. Physiology & Behavior. 1995;57(6):1215-20.
327. Anderson AA, Helmering J, Juan T, Li C-M, McCormick J, Graham M, et al. Pancreatic islet expression profiling in diabetes-prone C57BLKS/J mice reveals transcriptional differences contributed by DBA loci, including Plagl1 and Nnt. PathoGenetics. 2009;2(1):1-17.
328. Andrikopoulos S, Massa CM, Aston-Mourney K, Funkat A, Fam BC, Hull RL, et al. Differential effect of inbred mouse strain (C57BL/6, DBA/2, 129T2) on insulin secretory function in response to a high fat diet. Journal of Endocrinology. 2005;187(1):45-53.
329. Aston-Mourney K, Wong N, Kebede M, Zraika S, Balmer L, McMahon JM, et al. Increased nicotinamide nucleotide transhydrogenase levels predispose to insulin hypersecretion in a mouse strain susceptible to diabetes. Diabetologia. 2007;50(12):2476-85.
330. Berglund ED, Li CY, Poffenberger G, Ayala JE, Fueger PT, Willis SE, et al. Glucose metabolism in vivo in four commonly used inbred mouse strains. Diabetes. 2008;57(7):1790-9.
331. Bertagna X. Proopiomelanocortin-derived peptides. Endocrinology and Metabolism Clinics of North America. 1994;23(3):467-85.

332. Cone RD. Anatomy and regulation of the central melanocortin system. Nature Neuroscience. 2005;8(5):571-8.
333. Elias CF, Kelly JF, Lee CE, Ahima RS, Drucker DJ, Saper CB, et al. Chemical characterization of leptin‐activated neurons in the rat brain. Journal of Comparative Neurology. 2000;423(2):261-81.
334. Morton G, Schwartz M. The NPY/AgRP neuron and energy homeostasis. International Journal of Obesity. 2001;25(5):S56-S62.
335. Xi D, Gandhi N, Lai M, Kublaoui BM. Ablation of Sim1 neurons causes obesity through hyperphagia and reduced energy expenditure. PLOS One. 2012;7(4):e36453.
336. Bouret SG, Draper SJ, Simerly RB. Formation of projection pathways from the arcuate nucleus of the hypothalamus to hypothalamic regions implicated in the neural control of feeding behavior in mice. Journal of Neuroscience. 2004;24(11):2797-805.
337. Coppari R, Ichinose M, Lee CE, Pullen AE, Kenny CD, McGovern RA, et al. The hypothalamic arcuate nucleus: a key site for mediating leptin's effects on glucose homeostasis and locomotor activity. Cell Metabolism. 2005;1(1):63-72.
338. Shungin D, Winkler TW, Croteau-Chonka DC, Ferreira T, Locke AE, Mägi R, et al. New genetic loci link adipose and insulin biology to body fat distribution. Nature. 2015;518(7538):187-96.
339. Yoshiki A, Moriwaki K. Mouse phenome research: implications of genetic background. ILAR Journal. 2006;47(2):94-102.
340. Heinla I, Leidmaa E, Visnapuu T, Philips M-A, Vasar E. Enrichment and individual housing reinforce the differences in aggressiveness and amphetamine response in 129S6/SvEv and C57BL/6 strains. Behavioural Brain Research. 2014;267:66-73.
341. Crabbe JC, Wahlsten D, Dudek BC. Genetics of mouse behavior: interactions with laboratory environment. Science. 1999;284(5420):1670-2.
342. Wahlsten D, Metten P, Phillips TJ, Boehm SL, Burkhart‐Kasch S, Dorow J, et al. Different data from different labs: lessons from studies of gene–environment interaction. Journal of Neurobiology. 2003;54(1):283-311.
343. Mandillo S, Tucci V, Holter SM, Meziane H, Banchaabouchi MA, Kallnik M, et al. Reliability, robustness, and reproducibility in mouse behavioral phenotyping: a cross-laboratory study. Physiological Genomics. 2008;34(3):243-55.
344. Zhang D, Christianson J, Liu Z-X, Tian L, Choi CS, Neschen S, et al. Resistance to high-fat diet-induced obesity and insulin resistance in mice with very long-chain acyl-CoA dehydrogenase deficiency. Cell Metabolism. 2010;11(5):402-11.
345. Johnson PR, Greenwood M, Horwitz BA, Stern JS. Animal models of obesity: genetic aspects. Annual Review of Nutrition. 1991;11(1):325-53.
346. Biddinger SB, Almind K, Miyazaki M, Kokkotou E, Ntambi JM, Kahn CR. Effects of diet and genetic background on sterol regulatory element-binding protein-1c, stearoyl-CoA desaturase 1, and the development of the metabolic syndrome. Diabetes. 2005;54(5):1314-23.

347. Fearnside JF, Dumas M-E, Rothwell AR, Wilder SP, Cloarec O, Toye A, et al. Phylometabonomic patterns of adaptation to high fat diet feeding in inbred mice. PLOS One. 2008;3(2):e1668.
348. Dumas M-E, Barton RH, Toye A, Cloarec O, Blancher C, Rothwell A, et al. Metabolic profiling reveals a contribution of gut microbiota to fatty liver phenotype in insulin-resistant mice. Proceedings of the National Academy of Sciences. 2006;103(33):12511-6.
349. Abramov U, Puussaar T, Raud S, Kurrikoff K, Vasar E. Behavioural differences between C57BL/6 and 129S6/SvEv strains are reinforced by environmental enrichment. Neuroscience Letters. 2008;443(3):223-7.
350. Montagutelli X. Effect of the genetic background on the phenotype of mouse mutations. Journal of the American Society of Nephrology. 2000;11(suppl 2):S101-S5.
351. Haluzik M, Colombo C, Gavrilova O, Chua S, Wolf N, Chen M, et al. Genetic background (C57BL/6J versus FVB/N) strongly influences the severity of diabetes and insulin resistance in ob/ob mice. Endocrinology. 2004;145(7):3258-64.
352. Carter R, Paterson J, Tworowska U, Stenvers D, Mullins J, Seckl J, et al. Hypothalamic‐pituitary‐adrenal axis abnormalities in response to deletion of 11β-HSD1 is strain‐dependent. Journal of Neuroendocrinology. 2009;21(11):879-87.
353. Hindorff LA, Sethupathy P, Junkins HA, Ramos EM, Mehta JP, Collins FS, et al. Potential etiologic and functional implications of genome-wide association loci for human diseases and traits. Proceedings of the National Academy of Sciences. 2009;106(23):9362-7.
354. Feero WG, Guttmacher AE, Collins FS. Genomic medicine—an updated primer. New England Journal of Medicine. 2010;362(21):2001-11.
355. Korte A, Farlow A. The advantages and limitations of trait analysis with GWAS: a review. Plant Methods. 2013;9(1):29.
356. Boyle EA, Li YI, Pritchard JK. An expanded view of complex traits: from polygenic to omnigenic. Cell. 2017;169(7):1177-86.
357. Zhou K, Bellenguez C, Spencer CC, Bennett AJ, Coleman RL, Tavendale R, et al. Common variants near ATM are associated with glycemic response to metformin in type 2 diabetes. Nature Genetics. 2011;43(2):117.
358. Kandel ER, Schwartz JH, Jessell TM, Siegelbaum SA, Hudspeth AJ. Principles of neural science: McGraw-hill New York; 2000.
359. Han X, Wang R, Zhou Y, Fei L, Sun H, Lai S, et al. Mapping the mouse cell atlas by Microwell-seq. Cell. 2018;172(5):1091-107. e17.
360. Marin-Husstege M, Muggironi M, Liu A, Casaccia-Bonnefil P. Histone deacetylase activity is necessary for oligodendrocyte lineage progression. Journal of Neuroscience. 2002;22(23):10333-45.
361. Gomez O, Sanchez‐Rodriguez A, Le M, Sanchez‐Caro C, Molina‐Holgado F, Molina‐Holgado E. Cannabinoid receptor agonists modulate oligodendrocyte differentiation by activating PI3K/Akt and the mammalian target of rapamycin (mTOR) pathways. British Journal of Pharmacology. 2011;163(7):1520-32.

362. Fumagalli M, Daniele S, Lecca D, Lee PR, Parravicini C, Fields RD, et al. Phenotypic changes, signaling pathway, and functional correlates of GPR17-expressing neural precursor cells during oligodendrocyte differentiation. Journal of Biological Chemistry. 2011;286(12):10593-604.
363. Raff MC, Miller RH, Noble M. A glial progenitor cell that develops in vitro into an astrocyte or an oligodendrocyte depending on culture medium. Nature. 1983;303(5916):390-6.
364. Noble M, Murray K, Stroobant P, Waterfield MD, Riddle P. Platelet-derived growth factor promotes division and motility and inhibits premature differentiation of the oligodendrocyte/type-2 astrocyte progenitor cell. Nature. 1988;333(6173):560-2.
365. Richardson JS, Richardson DC. Amino acid preferences for specific locations at the ends of alpha helices. Science. 1988;240(4859):1648-52.
366. Baracskay KL, Kidd GJ, Miller RH, Trapp BD. NG2-positive cells generate A2B5-positive oligodendrocyte precursor cells. Glia. 2007;55(10):1001-10.
367. Chen Y, Wu H, Wang S, Koito H, Li J, Ye F, et al. The oligodendrocyte-specific G protein–coupled receptor GPR17 is a cell-intrinsic timer of myelination. Nature Neuroscience. 2009;12(11):1398.
368. Ciana P, Fumagalli M, Trincavelli ML, Verderio C, Rosa P, Lecca D, et al. The orphan receptor GPR17 identified as a new dual uracil nucleotides/cysteinyl ‐ leukotrienes receptor. The EMBO Journal. 2006;25(19):4615-27.
369. Gomez O, Arevalo ‐ Martin A, Garcia ‐ Ovejero D, Ortega ‐ Gutierrez S, Cisneros JA, Almazan G, et al. The constitutive production of the endocannabinoid 2 ‐ arachidonoylglycerol participates in oligodendrocyte differentiation. Glia. 2010;58(16):1913-27.
370. Fields RD, Dutta DJ, Belgrad J, Robnett M. Cholinergic signaling in myelination. Glia. 2017;65(5):687-98.
371. Mauvais-Jarvis F. Sex differences in metabolic homeostasis, diabetes, and obesity. Biology of Sex Differences. 2015;6(1):1-9.
372. Hwang LL, Wang CH, Li TL, Chang SD, Lin LC, Chen CP, et al. Sex differences in high ‐ fat diet ‐ induced obesity, metabolic alterations and learning, and synaptic plasticity deficits in mice. Obesity. 2010;18(3):463-9.
373. Ingvorsen C, Karp N, Lelliott C. The role of sex and body weight on the metabolic effects of high-fat diet in C57BL/6N mice. Nutrition & Diabetes. 2017;7(4):e261-e.
374. Hong J, Stubbins RE, Smith RR, Harvey AE, Núñez NP. Differential susceptibility to obesity between male, female and ovariectomized female mice. Nutrition Journal. 2009;8(1):1-5.
375. Pettersson US, Waldén TB, Carlsson P-O, Jansson L, Phillipson M. Female mice are protected against high-fat diet induced metabolic syndrome and increase the regulatory T cell population in adipose tissue. PLOS One. 2012;7(9):e46057.
376. Dakin RS, Walker BR, Seckl JR, Hadoke PW, Drake AJ. Estrogens protect male mice from obesity complications and influence glucocorticoid metabolism. International Journal of Obesity. 2015;39(10):1539-47.

377. Salomäki-Myftari H, Vähätalo LH, Ailanen L, Pietilä S, Laiho A, Hänninen A, et al. Neuropeptide Y overexpressing female and male mice show divergent metabolic but not gut microbial responses to prenatal metformin exposure. PLOS One. 2016;11(9):e0163805.
378. Frias JP, Macaraeg GB, Ofrecio J, Joseph GY, Olefsky JM, Kruszynska YT. Decreased susceptibility to fatty acid–induced peripheral tissue insulin resistance in women. Diabetes. 2001;50(6):1344-50.
379. Wade GN. Gonadal hormones and behavioral regulation of body weight. Physiology & Behavior. 1972;8(3):523-34.
380. Shi H, Strader AD, Woods SC, Seeley RJ. Sexually dimorphic responses to fat loss after caloric restriction or surgical lipectomy. American Journal of Physiology-Endocrinology and Metabolism. 2007;293(1):E316-E26.